Chromatographic Separation of Metals

by

John David Emmott

A thesis submitted in partial fulfilment for the requirements for the degree of Doctor of Philosophy, via MPhil at the University of Central Lancashire

March 2016

Student Declaration

Concurrent registration for two or more academic awards

Either *I declare that while registered as a candidate for the research degree, I have not been a registered candidate or enrolled student for another award of the University or other academic or professional institution

or ~~*I declare that while registered for the research degree, I was with the University's specific permission, a *registered candidate/*enrolled student for the following award:~~

Material submitted for another award

Either *I declare that no material contained in the thesis has been used in any other submission for an academic award and is solely my own work

or ~~*I declare that the following material contained in the thesis formed part of a submission for the award of~~

Collaboration

Where a candidate's research programme is part of a collaborative project, the thesis must indicate in addition clearly the candidate's individual contribution and the extent of the collaboration. Please state below:

Signature of Candidate _____

Type of Award _____

School _____

Abstract

In nuclear reprocessing, PUREX, a solvent extraction process, has long been the separation method employed for the separation of the bulk components of irradiated nuclear fuel (namely uranium and plutonium) from the fission products and other minor actinides produced during the fuel use. The uranium and plutonium constitutes approximately 96 % by mass of the irradiated fuel and for this to be removed, requires large volumes of extractant and equipment with large surface area contactors and therefore floor space requirements.

The PUREX process has for nearly 60 years been the largely unchallenged separation technology for the reprocessing of irradiated fuel, for both nuclear weapon production and commercial nuclear power generation. The merits and ability of this process are unquestionable since it achieves the objectives of highly purified plutonium and uranium which both can be eventually recycled.

Although well proven and predictable, the PUREX process is not without its challenges: the generation of significant quantities of highly active aqueous liquid containing fission products (FPs) and minor actinides (MAs), and the degradation of the solvent phase reagents and non-specific nature of the extractant TriButylPhosphate (TBP) may have contributed to only a fraction of the total annual output of irradiated fuel being reprocessed.

Fission products are elements which are produced in a nuclear reactor and are the atomic fragments left after a large atomic nucleus (typically uranium-235) undergoes nuclear fission, splitting into two smaller nuclei, along with a few neutrons, the release of heat energy (kinetic energy of the nuclei), and gamma rays (1).

Minor actinides such as neptunium, americium, curium, berkelium, californium, einsteinium, and fermium are the actinide elements in irradiated nuclear fuel other than uranium and plutonium; they are minor as they represent a very small proportion of actinides in comparison to U and Pu (2).

This thesis explores the possibility of using a continuous chromatographic method to extract the lesser components of the irradiated fuel. One of the major problems with the use of chromatography as an industrial process is the expansion from the batch separations on the bench top to a continuous efficient process, capable of processing large volumes. This thesis, through existing concepts, will describe a proof of concept chromatographic separation of surrogates and isotopes of the components of irradiated fuels which can be readily scaled up to a continuous chromatographic separation.

The project is a radical departure from PUREX and will offer many advantages over PUREX. It is based on the separation of FPs and MAs **from** uranium and plutonium isotopes using continuous chromatographic separation.

This thesis assesses a number of commercial resins for their suitability for the proposed continuous chromatography reprocessing method. The experiments were all undertaken at elevated nitric acid concentrations and as such are describing interactions which are rarely required commercially and therefore seldom reported, with batch studies to assess separation factors between ions, uptake kinetics and isotherms over a range of nitric acid concentrations to more dynamic column breakthrough and eventually separations.

The research demonstrates that a separation can be achieved at an elevated HNO_3 concentration on a commercially available ion exchange resin.

Acknowledgments

My thanks and gratitude is expressed toward the Engineering and Physical Sciences Research Council and National Nuclear Laboratory for providing me with this opportunity within their industrial CASE scheme.

I’m indebted to H. Eccles, Professor of Nuclear Materials and G. Bond, Professor of Materials Science and Associate Head of School for their numerous and extremely valuable discussions, encouragement and input throughout this research project.

Many thanks are also expressed to James Donnelly and Tamar Garcia Sorribes for their help with all things analytical and to UCLan personnel at large for the use of their research facilities as well as Purolite for the supply of resins and adsorbents.

Finally, t’ ‘rents, wi’out whom, nowt coulda or woulda happened.

Arte et labore

Contents

List of Figures

List of Tables

List of Equations

Abbreviations

1/n	The reciprocal of n
A	Eddy diffusion
A_0	activity of known weight of resin
AHA	Acetohydroxamic acid
A_s	activity of known volume of solution
A_s	Asymmetry factor relating to peak shape on a chromatogram
b	Constant relating to free energy
B	longitudinal diffusion
B.V.	Bed volume
C	Mass transfer
C_0	Initial ion concentration
CAC	Continuous annular chromatography
CC	Continuous chromatography
C_e	Ion concentration after uptake
C_f	Cross sectional area
C_m	concentration of component in mobile phase
C_s	concentration of component in stationary phase
CSEX	Caesium extraction
D	Distribution ratio
DVB	Divinyl benzene
D_w	weight distribution ratio
ε	fraction of bed free space
FLUOEX	Fluorine extraction
FP	Fission products
FT-IR	Fourier Transform - Infra Red
ɣ	Gamma ray
GEN IV	Generation four
Gy	Gray is the SI derived term of adsorbed ionisation radiation and is equivalent to one joule per kilogram of matter
H	Height equivalent to theoretical plate
HLW	High level waste
IC	Ion chromatography
ICP-MS	Inductively Coupled Plasma - Mass Spectrometry
ILW	Intermediate level waste
k	Mass transfer co-efficient
k'	Free column volumes to peak maximum
K_A	Distribution constant for component A
k_A	retention factor
K_D	Distribution Co-efficient
K_{ex}	Equilibrium constant
K_f	Constant relating to adsorption capacity
LLW	Low level waste

m	Mass of adsorbent
MA	Minor actinides
MOX	Mixed oxide fuel
N	Number of theoretical plates
n_m	moles of ion in mobile phase
n_s	moles of ion in stationary phase
OK	Odourless kerosene
pK_a	Acid dissociation constant
ppb	Parts per billion
ppm	Parts per million
PUREX	Plutonium and uranium extraction
Q	Maximum capacity
q_e	Ion Uptake
Q_f	Feed flow rate
q_i	Component concentration in stationary phase
QI	Quantity of solute per cross-sectional area
Q_T	Fluid flow rate
q_{theo}	Theoretical uptake
R_L	Separation factor
R_s	Resolution
SMB	Simulated moving bed
SOP	Standard operating procedure
SREX	Strontium extraction
TBP	Tributylphosphate
t_m	retention time of a unretained component
t_r	retention time of a component
TRUEX	Trans uranium extraction
u	linear velocity
u, v, u	interstitial velocity
UCLan	University of Central Lancashire
UREX	Uranium extraction
V	Volume of Liquor
v_c	Velocity of component
V_m	Volume of mobile phase
V_R	Volume eluted when $C/C_0 = 0.5$
V_s	Volume of stationary phase
$w_{1/2}$	Width of peak at half height
w_b	width of peak at base
z	axial co-ordinate
α	Alpha particle (radiochemistry) or selectivity factor (chromatography)
α_R	elution angle
β	Beta particle
θ	Angle co-ordinate
σ	Standard deviation
ω	Rotational rate

1. Introduction

1.1 Aims of the Project

The project aims to evaluate the potential of continuous chromatography (CC) in the separation of fission products (FPs) and minor actinides (MAs) from uranium and plutonium in irradiated nuclear fuel. Current technology (the PUREX process) requires large amounts of equipment, and inflexibility within the flow-sheets and standard operating procedures (SOPs). It is considered that CC will achieve higher flexibility, process intensiveness and chemically distinct wastes for separate treatments and disposal routes. Further to this, the objectives of this project are:

- The demonstration of CC as a separator of FPs and MAs from uranium and plutonium (U and Pu).
- The reduction of the environmental impact of spent fuel in regard to solvent use, energy usage and volume of waste sent to geological disposal.
- The gain of greater flexibility in regard to current SOP parameters.
- The ability to re-categorise nuclear waste, again reducing the volume sent to geological disposal.

Although CC has been utilised within the pharmaceutical environment, the application to inorganic separations has been minimal and will require an evaluation of the aqueous chemistry and separation technology before it will gain favour.

As with all chromatographic systems, the key components of the aqueous phase, stationary phase, and equipment configuration will require extensive evaluation and optimisation. This preliminarily project will focus on the achievement of a static column separation of four surrogates and isotopes of ions found within irradiated nuclear fuel.

Initial studies will identify commercial stationary phases and their suitability for non-radioactive and surrogate cations in nitric acid media. Suitability will be decided by the selectivity, capacity and stability of the stationary phases to varying levels of HNO_3 within the aqueous medium.

Nitric is the acid of choice within the nuclear industry (especially with uranium refinery and spent fuel reprocessing solutions) because the extractant for uranium and plutonium is tri butyl phosphate (TBP) which forms an adduct with uranyl and/or plutonium nitrates ($MO_2(NO_3)_2 \cdot 2TBP$). Non-radioactive surrogates are employed in order to reduce exposure to radioactivity and help in the reduction of the project's environment impact.

The novelty of this project is found primarily in the use of chromatography for any kind for a nuclear reprocessing function. Solvent extraction via PUREX is the preferred method for the separation of U and Pu from spent nuclear fuels. This gives rise to a number of issues which are also described in detail below. There are a number of other factors which make this project unique and distinctive however: the continuous chromatographic separation of metals has only been attempted once before when separating zirconium from hafnium. This was performed on a continuous annular bed, however the option of a simulated moving bed technology is also of initial interest (3) (4). This project expects to take advantage of novel stationary phases to be developed within UCLan and eventually anticipates being able to separate spent fuel into similar elemental or fission product groups, if not individual elements (both of which would be much more discerning than current techniques). The approach itself is a departure from the current methods which remove the bulk mass from the "contaminants" formed during fuel use.

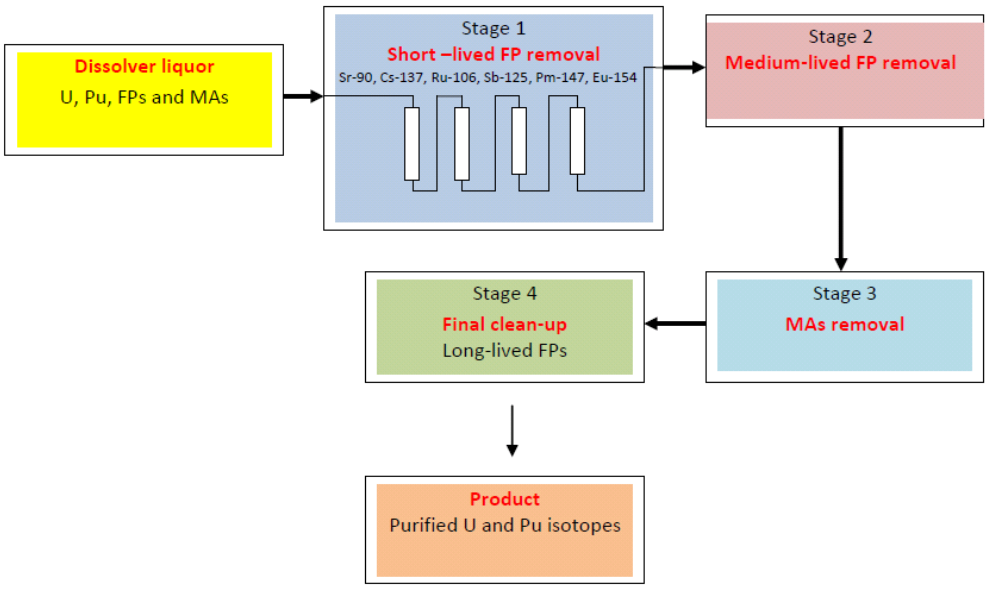

Figure 1.1 Proposed chromatographic separation stages (5)

1.2 The Nuclear Fuel Cycle and Reprocessing

The industrial processes associated with the production of electricity from uranium radioactivity are referred to as the uranium nuclear fuel cycle. The cycle starts with the mining of uranium ore and ends with the disposal of the irradiated fuel and/or associated nuclear waste. When reprocessing of the irradiated fuels is utilised as an option, the activities form a true cycle, i.e. closed fuel cycle.

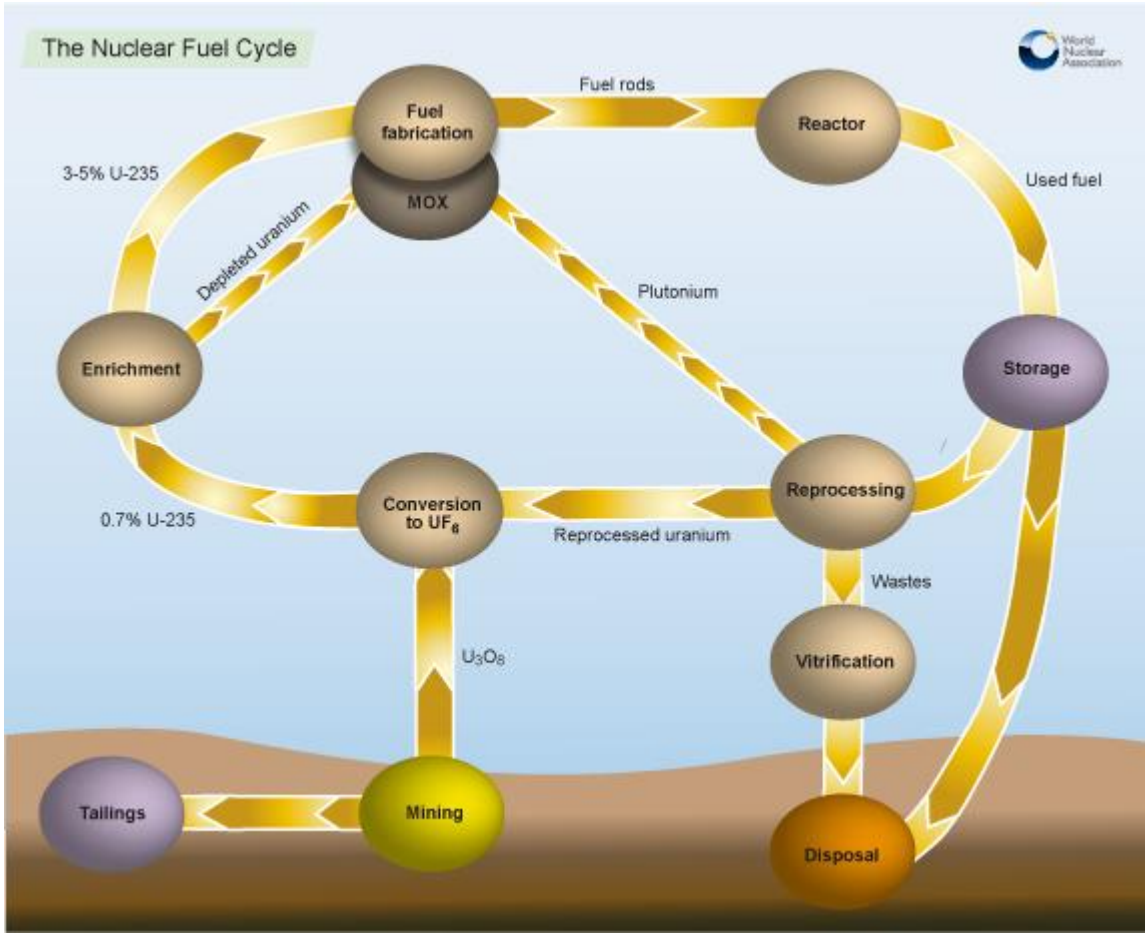

Figure 1.2 Uranium fuel cycle taken from (6)

The nuclear cycle is divided into two: the “front end” which involves all processes before the uranium enters the nuclear reactor and thus the mining and milling, conversion, enrichment and fuel fabrication and the “back end” which involves the fuel once it has been taken out of the reactor and comprises short term storage, reprocessing, and any recycling before the unwanted wastes are disposed of.

Uranium mining is generally similar to other types of mining in that it can be either open cast or underground. However, uranium also has a third method, in-situ leaching, in which oxygenated aqueous liquid is pumped through permeable ores to leach the uranium into the liquid which is then recovered and sent to the milling operation in the same way as the more traditional ore mining (6) (7).

Milling is the process where the uranium ion is extracted from the ore or leachate, into a product called yellowcake due to its colour; it is a uranium oxide with an approximate 80 % uranium concentration (7). The ore is crushed to a powder, and exposed to sulfuric acid which extracts the uranium from the ore body, the uranyl sulfate is purified using ion exchange or solvent extraction, and then the recovered ions from these procedures are

precipitated and dried to form the oxide (U_3O_8). The remaining rock and ore bodies are termed tailings and have to be disposed of with care, due to the latent long-lived radioactivity and toxicity for other heavy metals residues which are left after the acid extraction.

As natural uranium contains only 0.72 % of the U-235 isotope and the majority of nuclear reactors require a concentration of between 3.5 - 5%, the uranium must be enriched to the required concentration. The enrichment process, developed during World War Two, is performed by gas centrifugation and thus the uranium must be in gaseous form. To achieve this, at the refinery, U_3O_8 is further purified and converted to uranium dioxide and then reacted with anhydrous hydrogen fluoride and subsequently fluorine, to produce uranium hexafluoride; this is gaseous at relatively low temperatures. The UF_6 is transported to the enrichment plant where centrifugation is used to enriched the U-235 content and simultaneously produce a depleted stream; the enriched stream is used in fuel manufacture. Due to the low separation yields of the enrichment process, the process may have to be repeated 1500 times with a cascade between each of the steps, in order to achieve the levels of enrichment required. This is obviously quite an energy intensive method, estimated to consume about 10 % of the total energy produced by the uranium when in the reactor. At the fuel fabrication facility the uranium is converted back to the dioxide form and is then ready for fuel fabrication (7).

The second generation (GEN II) nuclear reactors in the UK use ceramic oxide pellets rather than the uranium metal used in the first fleet of nuclear reactors (Magnox, GEN I). The oxide pellets (UO_2) are contained within a stainless steel fuel pin, whereas for Magnox reactors the uranium metal rod was enclosed within a Magnox alloy fuel pin. The change from metal to ceramic oxide was based on reactor performance and process technology. GEN II reactors operate at higher temperatures, which is possible as the melting point of stainless steel is considerably higher than the Magnox alloy. In addition uranium dioxide melting point is more than twice that of uranium metal. The oxide fuel remains in GEN II reactors longer and undergoes higher burn-up largely as it contains enriched uranium.

GEN II reactors use enriched uranium (U-235 isotope greater than natural value of 0.71 %) which requires natural uranium hexafluoride undergoing enrichment to produce UF_6 of 2.5 to 3.5% U-235. The enriched UF_6 is converted to a ceramic oxide which is a relatively simple and one stage process. Converting UF_6 to uranium metal is far more complicated would require several stages and present significant challenges in controlling criticality. Burnable poisons such as gadolinium can also be incorporated into oxide fuels but this would not be the case for uranium metal, due their solubility in liquid metal.

When in the reactor, the U-235 undergoes fission. This produces energy in the form of heat, neutrons and ɣ radiation. This chain reaction is controlled or moderated by the presence of water or graphite in order that the reaction is a controlled use of the energy output. The neutrons released can follow a number of routes. Some go on to cause fission in other U-235 atoms, others are adsorbed by U-238, which transmutes the U to a Pu atom via two β emissions. Half of these Pu atoms will in turn undergo fission and will add to the energy output of the reactor. When the atoms fission, they produce daughter atoms or fission products; within a reactor a number of different elements may fission, leading to a wide range of elements being present within the irradiated nuclear fuels.

Once the U-235 percentage of the fuel has been reduced to approximately 1 % for water reactors, the concentration of fission products and actinides, some of which act as neutron poisons, will have become too high for the further economic use of that fuel, it is therefore removed from the reactor and placed into storage ponds in order to adsorb the radiation and heat until both have reduced enough (usually five years) so that the fuel can either by reprocessed or prepared for permanent safe disposal (8).

Nuclear reprocessing on the other hand is a chemical technology developed to separate and recover materials left from irradiated nuclear fuels. It does not eradicate any radioactivity, the heat the material radiates or the materials from which it arises; it merely separates it into three categories: uranium and plutonium, and the waste categories of FPs and MAs.

There are numerous purposes in the ambition for countries to reprocess their nuclear fuels, with the importance of each altering over time. In addition to the political factors, a large influence is the financial implication involved with storage or the final disposal of the materials, as well as the initial cost of mining uranium ore and manufacture into fuel. Originally, the political drive was for the manufacture and separation of plutonium for the use in nuclear armaments; this progressed toward a civil use with the rise of enriched fuels and reactors for mixed oxide fuels (MOX), where the unused fissionable uranium and plutonium isotopes are recycled for use within thermal reactors as a method of extending the earth's uranium reserves, which were at the time of the MOX fuel reactor development, during the 1960 and through the 1970s, felt to be much more limited and therefore more expensive, than is presently estimated meaning, that reprocessing became the more financially viable option (7) (9). With the discovery of new uranium deposits since the peak in the 1980s, the price of uranium has dropped and therefore become less of a consideration (9) (10).

Reprocessing has evolved further still and is now equally seen as a method to enable and facilitate geological disposal by reducing the volume of high level wastes (HLW) from

irradiated fuels by transmuting the FPs and MAs in GEN IV “fast breeder” reactors as well as a method in which to close the nuclear fuel cycle (7).

The UK classifies radioactive wastes on both the nature and quantity of the radioactivity which they contain. High level wastes are defined as those in which the temperature may rise significantly as a result of their radioactivity; therefore, this has to be taken into account in the design of their storage or disposal facilities. Intermediate level wastes (ILW) are those which exceed the upper boundaries of low level wastes but do not require heating to be taken into account with their storage and disposal facilities. Low level waste (LLW) is defined as wastes having a radioactivity which does not exceed 4 GBq per tonne for alpha activity or 12 GBq per tonne of beta/gamma activity (11).

Reprocessing first took place in the Manhattan project of the 1940s and initially employed a pyrochemical-precipitation process. However this was swiftly replaced by a solvent extraction method; this is more efficient for the continuous increase and large volumes of fuels to be reprocessed. A number of solvent extraction techniques were evaluated before the PUREX system was settled upon, this method will be discussed in detail in the next section (12).

The first commercial solvent extraction plant for spent nuclear fuel reprocessing was built in the 1960s in Dessel, Belgium and named EUROCHEMIC; reprocessing ran from 1966 until 1974 (13). Rapid growth of nuclear energy and therefore uranium demand, was forecast in the 1970s and consequently the operation of an industrial scale PUREX closed cycle was expanded to include fuels from the gas-cooled and light-water reactors; this was manifest in the introduction of the oxide fuels as standard practice. The forecast was proven to be too ambitious and during the 1980s the plans for fast breeder reactors was scaled back or postponed. PUREX continued to be employed and improved in the UK, France, Japan, Russia and India, helping to reduce the volume of irradiated fuels in temporary storage and meaning the volume of HLW is much lower than if a “once-through fuel cycle” had been employed in the last 40 years (9).

The management of irradiated and spent nuclear fuel is an issue for the nuclear industry as a whole. Currently there are approximately 10,500 tonnes of heavy metal irradiated fuel removed annually from nuclear power reactors globally, with a world reprocessing capacity of only approximately 5,500 tonnes per year. The reprocessing issue is further complicated by many of the current reactors reaching the end of their licensed life time in the year 2020; this will add a further 445,000 tonnes of heavy metal to the cumulative inventory of spent fuel and irradiated materials (14) (15).

There are three main strategies for the management of irradiated fuel:

- Once through the reactor with direct geological disposal,
- Postpone the decision by placing the materials in storage tanks for a number of years or
- Reprocess and recycle the isotopes post-treatment for use in a breeder reactor, making a closed fuel cycle.

The virtues of a closed fuel cycle are:

- The conservation of natural resources such as uranium, by using a greater amount of the energy emitted by the FPs and MAs. This in turn optimises waste management and disposal conditions, reducing the heat and volume to approximately one fifth of levels currently required,
- The volume of high level waste due for disposal in any long or short term storage solutions will be reduced.
- It will also help to minimise environmental impact, both in the original mining of the uranium and also in the storage pools and geological repository proposed in the UK and operated in several countries.
- Improved fuel cycle economics with MOX fuels potentially giving an extra 25 % of the energy from the fissile materials originally mined when compared to that of a once through fuel use.
- It will also reduce the possibility of nuclear proliferation by removing and using plutonium.
- The radioactivity of the wastes produced from reprocessing is lower and has a shorter half-life than the irradiated fuel itself, with radioactivity becoming significantly lower after 100 years (6) (7).

Spent irradiated fuel contains 96% uranium (approximately 1 % of this is the fissile U-235) and 1 % plutonium. The rest is FPs and MAs

It is therefore envisioned that this UCLan project will aid in achieving a more efficient and environmentally friendly closed fuel cycle.

Table 1.1 Components of nuclear waste (16)

Radionuclide	Approximate Concentration ($g\ l^{-1}$)	Percentage Comosition (%)
U	300	95.85
Y and lanthanides	3.5	1.12
Pu	3.2	1.02
Ru, Rh and Pd	1.3	0.42
Zr	1.2	0.38
Mo	1.1	0.35
Alkali metals (Cs, Rb)	1	0.32
Alkaline earth metals (Sr, Ba)	0.9	0.29
Tc	0.26	0.08
Am	0.2	0.06
Np	0.15	0.05
Se and Te	0.15	0.05
Ag, Cd, Sn, Sb	0.03	0.01
Cm	0.007	< 0.005

Options for the next generation of reactors (GEN IV) are focused on the transuranium elements (neptunium, plutonium, americium and curium). The use of the latent energy which is currently wasted when placed into the fuel cooling pools, once taken out of the reactor, and the advantage that the reduction of their half-lives can also be achieved by transmutation, within the GEN IV reactor, is achieved by bombarding the nuclei with neutrons, causing fission and transforming them into stable or short lived isotopes. It stands to reason that these elements will have to be either previous or subsequent to the transmutation have been separated from the other elements within the spent fuel, in particular the uranium, which if exposed to the neutron beam, will be likely to transmute to plutonium. Other arguments for partitioning and transmutation include:

- The reduction of the radio-toxic inventory of long lived high level wastes,
- the reduction of the heat load on geological repositories,
- the reduction of inter-generation liabilities of nuclear power,
- the start of fast spectrum GEN IV reactors and formation of a basis for the transition to more sustainable nuclear power.

1.3 PUREX and Current Technology

PUREX is the principal method for reprocessing spent nuclear fuel. It is an aqueous based chemical process utilising nitric acid and TBP. TBP extracts the bulk Uranium (U) and (Pu) from the other fission products and MAs, into odourless kerosene (OK). The major drawback of the process is the degeneration to the TBP and odourless kerosene extractant

by the radioactivity of the highly active fission products, and to a lesser extent the oxidation by nitric acid. (16) (17)

The PUREX process has for nearly 60 years been largely unopposed as the separation technology for the reprocessing of irradiated fuel from nuclear weapons production to commercial nuclear power generation. The advantages and effectiveness of this process are undeniable: it achieves the goals of highly purified plutonium and uranium, both of which can subsequently be recycled into MOX fuels. Although well established and predictable, the PUREX process is not without its difficulties. The generation of significant quantities of highly active aqueous liquid containing the FPs and MAs; the oxidative degradation by nitric acid and the radioactivity of the fuel components of the solvent phase reagents, (requiring a solvent scrubbing process to be introduced, as well as the inherent environmental issues of using two types of hydrocarbon and non-specific discrimination of the extractant TBP,) may have contributed to only a fraction of the total annual output of irradiated fuel being reprocessed.

The PUREX process, or really the inherent lack of specificity of TBP, also requires strict control of process conditions (flow sheet parameters) to ensure the decontamination levels of uranium and plutonium are achieved to the desired levels. The largest issue however is that for the bulk of the heavy metals (U and Pu isotopes) to be extracted from the aqueous phase into the organic phase requires appropriately sized, large, contactors. PUREX's intrinsic ability to produce highly purified, separated uranium and plutonium contributes to non-proliferation issues of concern in today's political climate (9).

The developments of alternative nuclear fuel reprocessing schemes are being evaluated as an add-on to PUREX, whilst others are investigating an updated PUREX process such as UREX, COEX and others discussed below. Many of these developments are targeting better waste management of high active waste for future Gen IV fuel cycles (9). The incorporation of the PUREX process, whether updated or not into future reprocessing, will still have the characteristic disadvantages of PUREX, and these may be further exacerbated with future fuels that will have significant higher burn ups and therefore differing compositions to that in Table 1.1 (18)

Although all commercial reprocessing uses the PUREX process, alternatives are available. These can roughly be split into aqueous and non-aqueous techniques. The aqueous processes include Uranium Extraction or UREX; this separates the uranium and technetium from the irradiated fuels. It uses a similar method to PUREX but with the addition of Acetohydroxamic Acid (AHA) which prevents the separation of plutonium and neptunium by TBP. UREX has had a couple of modifications itself: the first was adding a step for the

separation of the plutonium and neptunium; the second uses an ion exchange resin instead of concentrated nitric acid for the separation of uranium from technetium.

Combined Extraction or COEX was proposed as a simplified version of PUREX and as such did not separate uranium from plutonium as they would then be recombined to form the MOX fuels. It therefore avoided many of the steps involved in the manipulation of the U and Pu oxidation changes and consequently gave a more relaxed separation protocol. There have been many other methods which focus on specific components such as Cs or Sr (CSEX and SREX respectively), as well as groups of components such as the transuranic element or TRUEX. (19)

The non-aqueous processes are largely based on fluoride chemistry, however, some pyro methods have also been developed. The fluoride methods include fluoride volatility and FLUOREX, the former is a development of the fluorination of uranium in the enrichment stage of the nuclear fuel cycle, expanded to include plutonium and neptunium hexafluorides. These compounds are volatile and can be separated at relatively low pressure and temperatures from the other constituents of the irradiated fuel. The latter is a mixture of an oxidation technique (AIROX) The AIROX (Atomics International Reduction Oxidation) process can be used to recycle light water reactor fuel (LWR) in this process, the volatiles and the cladding from spent LWR fuel are separated from the fuel. The AIROX process involves exposing the fuel rods to high-temperature cycles of oxygen and hydrogen to produce a powder via the $UO_2 => U_3O_8$ reaction. The UO_2 is then mechanically separated from the cladding and subsequently blended with enriched uranium oxide to produce new fuel. This is therefore not a truly non-aqueous technique or indeed a replacement for PUREX and both methods still remove the bulk components from the fuels. (19)

The pyro-processing techniques utilise chemical extraction, volatilisation, precipitations and electrodeposition of metals and salts at high temperature. In these methods the oxide form of the fuel is reduced to the metal, using lithium chloride and calcium chloride molten salts, where the various chemical separation methods can then be performed to extract the uranium. Unfortunately the separation factors for this technique are not to the required standard. (19)

All these have similar issues associated with them as PUREX; it is the bulk component of the irradiated fuel which is being removed, not the purification process envisaged by UCLan to remove the minor components. Any new process must overcome the PUREX challenges as well as offering some distinct advantages, as both regulators and operators have become acclimatised to sixty year old technology. The concept developed at the University of Central

Lancashire (5) is a radical departure from PUREX; it is based on the separation of FPs and MAs from uranium and plutonium isotopes using a CC separation. It would be advantageous to develop a method to extract the much lower volumes of FPs and MAs from the nitric acid medium than the 96 % or more U and Pu that is present in the dissolved spent fuel as currently happens.

1.4 Chromatography

Chromatography is a physical separation technique and is one of the most relied upon analytical, separation and purification methods available. It has found uses in a wide range of applications where the separation of compounds would be inordinately difficult, prohibitively costly or, due to the chemistry involved, impossible by any other means. (20)

Table 1.2 Description of some Chromatographic Methods (20)

Classification	Method	Stationary Phase	Equilibrium
Gas Chromatography	Gas Liquid Chromatography	Liquid on a solid surface	Partition between liquid and solid phases
	Gas Solid	Solid	Adsorption
Liquid Chromatography	Liquid-Liquid (Distribution)	Liquid on a solid surface	Partition between liquid and solid phases
	Liquid-Solid (Adsorption)	Solid	Adsorption
	Ion Exchange	Ion Exchange Resin	Ion Exchange
	Size Exclusion	Liquid due to size of polymetric solid	Partition
	Affinity	Group specific on a solid surface	Partition
Supercritical fluid Chromatography		Organic species on a solid surface	Partition

In most types of liquid chromatography as displayed in Table 1.2, the sample to be separated is dissolved in the mobile phase which can be a liquid or super-critical fluid (CO_2). The dissolution of the sample is not the case with gas chromatography, where the gaseous sample is mixed with the carrier gas. This solution or mixture is then driven through an insoluble stationary phase with the addition of supplementary mobile phase. The mobile and stationary phases are chosen due to their distribution ratios for the components to be separated. Those components which are more highly retained by the stationary phase will travel down the column more slowly than that of the less retained components. Therefore, if allowed to travel far enough, a physical separation between components will be achieved. If this is undertaken with the stationary phase in a column, the components can be collected in separate collection vessels as they are eluted from the end of the column. This is essentially the proposal under investigation for this project, albeit with the addition of a continuous aspect.

To fully understand and have an ability to predict the interaction of the components with the stationary and mobile phases and therefore their ability to separate, a number of equations are available from basic principles, which can be expanded with other concepts to model the possibility of separations within a column.

One of the most basic concepts for chromatography is that of the distribution ratio. This is fundamental in affecting the distribution between the phases and therefore the separation achievable. At equilibrium this is given by the equation:

$$K_A = \frac{n_S/V_S}{n_M/V_M}$$

Equation 1.1 Distribution ratio for component "A" at equilibrium

where n_S and n_M are the amounts in moles of the analyte in the stationary and mobile phases respectively and V_S and V_M are the volumes of the stationary and mobile phases respectively. Although relatively simple to calculate experimentally, the distribution ratio is calculated at equilibrium whereas conditions within a column separation are dynamic, due to the constant addition of mobile phase forcing the analyte through the stationary phase, this continuously creates a high concentration gradient between the analyte and stationary phase, altering the distribution ratio. It is consequently important to take this into account and therefore a term called the retention factor is calculated and can be used more directly to compare movement within columns. This term is also useful in that it is not dependent on column dimensions or flow rate of the mobile phase. This is an IUPAC (International Union of Pure and Applied Chemistry) term and is given by the equation:

$$k_A = K_A \frac{V_S}{V_M} = \frac{t_r - t_m}{t_m}$$

Equation 1.2 Retention factor for component "A" from experimentation and a chromatogram (20)

where t_r is the retention time of the component and $t_m$is the time for an unretained component to reach the detector. This is derived from measurements from a chromatograph and therefore from a separation which is already fairly well understood. It is however useful as a confirmation tool.

The distribution constant can be used for other important constants for predicting separations; one of the easiest to describe is the selectivity factor, α, given by equation:

$$\alpha = \frac{K_B}{K_A}$$

Equation 1.3 Selectivity factor (20)

As can be seen from the equation this is a measure of the relative retention of the two components within a mixture upon a column, and for peak separation on a chromatograph, α must be greater than 1. However due to the proposed system for UCLan having no back pressure and various other variables advantageous to chromatographic separations, the required α will be greater than 2. As will be discussed within the Discussion this figure of 2 is generally double that which is considered sufficient within standard pressurised ion and liquid chromatographies. As this project will attempt not to use pressurised eluent or feed on the resin, the ability of the resin to separate the ions will be reduced and therefore a much larger selectivity factor will be required to compensate for the loss of the inherent separation power of the resin.

The objective of chromatography is to produce a distinct separation for the constituents of the initial mixture, objectively resolution is a measure of the two components retention times divided by the average peak width. This can only be achieved from a chromatograph:

$$R_s = \frac{t_{r2} - t_{r1}}{\left(\frac{w_{b1} + w_{b2}}{2}\right)}$$

Equation 1.4 Resolution from a chromatograph (20)

where R_s is the resolution of the two adjacent peaks and w_b is the width at the base of the peaks, t_{r2} is the retention time of the second peak and t_{r1} is the retention time of the first eluted peak. Peaks are considered to be fully resolved at the baseline once the resolution value is greater than 1.5.

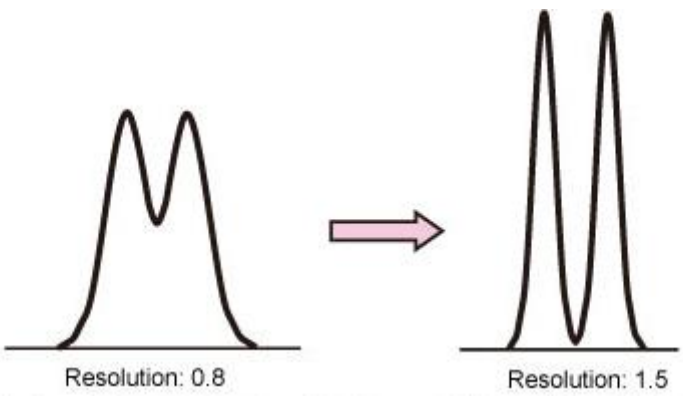

Figure 1.3 Two sets of chromatographic peaks displaying non-resolved and fully resolved peaks. (21)

Column efficiency is related to the number of “plates” within a column and will affect the sharpness or width of the peak on the chromatograph. The concept of a plate is a regression to the petrochemical distillation processes whence chromatography as a separation method was developed. Within these large columns were distinct plates where similar molecular weight compounds would equilibrate: the larger the column the more plates and the more separation efficiency could be achieved.

The number of these theoretical plates, N, is most easily calculated from a chromatograph with a Gaussian shaped peak:

$$N = 16\left(\frac{t_r}{w_b}\right)^2$$

Equation 1.5 Theoretical plates from a chromatograph at peak base width (20)

However, since the width at the base of a peak is quite difficult to measure accurately, the equation is usually modified to the width at half peak height, $w_{1/2}$. Giving equation:

$$N = 5.546\left(\frac{t_r}{w_{1/2}}\right)^2$$

Equation 1.6 Theoretical plates from a chromatograph width at half peak height (21)

Therefore, for a given column, the plate number will remain constant. Resolution can theoretically be calculated using the equation:

$$R_s = \left(\frac{k}{k+1}\right)\left(\frac{\alpha-1}{\alpha}\right)\left(\frac{\sqrt{N}}{4}\right)$$

Equation 1.7 Resolution from basic concepts (21)

The resolution is an aspect of two factors: the retention due to selectivity, and the efficiency of the column. As the number of theoretical plates or efficiency of the column can easily be improved by increasing the column length, assuming other physical dimensions remain constant, the most important factors during method development are the retention and selectivity. Therefore due to the importance of the selectivity in this particular separation is why the α requirement was set at 2 in this project.

Another important concept in assessing how well a column is working is in the shape of the peaks themselves. Under ideal conditions the peaks should exhibit a Gaussian shape. This is rarely the case and a measure of the symmetry of the peak will reveal how far from the ideal the peak has become by the use of the tailing factor.

$$A_s = {}^{b}/_{a}$$

Equation 1.8 Asymmetry factor from a chromatograph (21)

where A_s is the asymmetry factor, b is the width of the peak at 10 % height to the vertical at peak maximum to the end of the peak and a the peak width at 10 % height from the front of the peak to the maximum peak height. The closer this figure is to one, the more symmetric the peak. Values > 1 describe a "fronting" peak and figures <1 describe a "tailing" peak.

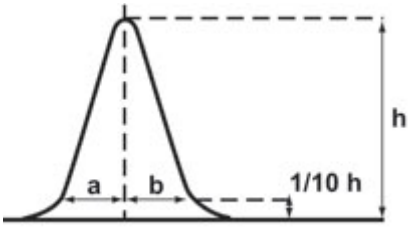

Figure 1.4 Ideal Gaussian peak with measurement of peak width at maximum height.

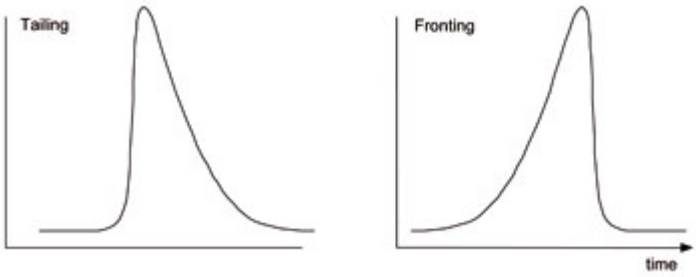

Figure 1.5 Tailing and fronting peak morphology.

Fronting of peaks occurs when the column is overloaded at those particular column conditions, so the concentration of the analyte is in excess of the capacity of the column, this means that the analyte peak reaches the maximum eluted concentration in a very short time but will retain a Gaussian shape after the peak maximum. Tailing peaks will display the opposite, where a Gaussian peak shape will be exhibited up to the peak maximum, after which the detector response does not follow a Gaussian shape but "tails" with a detector response for longer than expected. The explanation is more complicated than that of a fronting peak in that the analyte and stationary phase are reacting in a secondary way to that of the normal column chemistry. In liquid chromatography, it is usually due to the uncapped silanol groups of the silica used for the stationary phase (21), it can also be an aspect of the uptake isotherm, with a Langmuir isotherm especially influential in a tailing peak (22).

1.5 Continuous Chromatography Overview

The single biggest problem associated with chromatography has always been the inability of the technique to be satisfactorily scaled up from the analytical bench to an industrial scale separation process and applications remain limited in this regard. This is largely due to the batch nature of traditional chromatography separations performed within a column.

To counter this issue, a number of attempts have been made towards developing a continuous chromatographic system. These have included moving and simulated moving beds, counter flow, annular beds, radial flow, and disk chromatographic systems. However, widespread industrial use of these techniques is rare even within biological and organic applications and virtually non-existent in inorganic separations, in particular nuclear reprocessing. This thesis focuses on the potential use of SMB and CAC as potential separation techniques for metal ions focusing on irradiated nuclear fuels (23).

SMB are most easily understood by considering a two component mixture: one with a high affinity (A) for the stationary phase and one with a lesser affinity (B). As these are placed onto the top of a chromatographic column, the speed at which they travel in the direction of the mobile phase flow through the column will vary depending on their affinity for the stationary phase: the one with higher affinity will be held up more than the lower affinity component. Providing the chromatographic conditions are favourable, separation of components A and B will have occurred by the end of the column (23). Figures 1.6 and 1.7 display this in a single column and multiple columns respectively.

It should therefore be theoretically possible, if the stationary phase were to move in the opposite direction to that of the mobile phase flow and continually be replaced at the average rate that component A and B was moving, that component A would collect at one point within the column and component B at a point further up the column with the inlet point in-between. If these components were to be tapped at their points of collection and a continuous flow of mixed components applied to the stationary phase, a continuous separation could be achieved (23).

This is practically accomplished, by using a number of columns with a timed switching valve to achieve a simulated moving of the stationary phase.

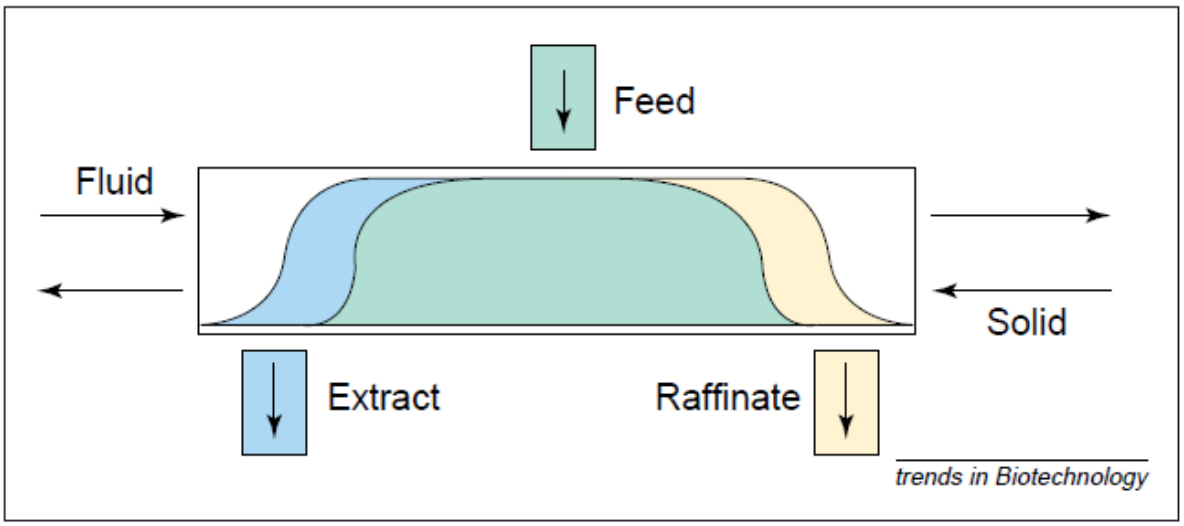

Figure 1.6 Continuous Moving Bed Column Metaphor. A stream of regenerated stationary phase flows against the flow of mobile phase. A mixture of componets A and B are fed into the centre and the two pure componets can be collected at either side. (24)

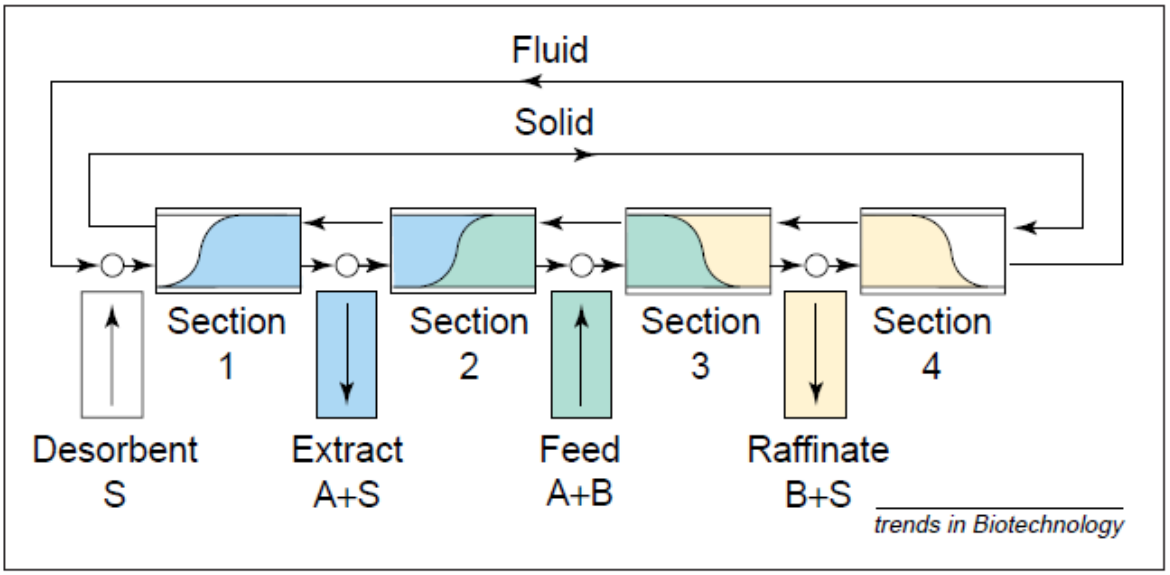

Figure 1.7 A Four Section Moving Bed System. Each of the sections contains a column and each provides a role in the separation of the components. Section one is regeneration of the stationary phase, two and three are where separation occurs and section four cleans the solvent. (24)

This has been achieved in the pharmaceutical and biotechnology industries with the development of continuous chromatography being employed to separate amino acids and enantiomeric forms of drugs, as well as the constituents of milk and it has proved successful for these biological applications (23). This instrumentation has not yet been applied to a wide range of hydrometallurgical problems and even less to the nuclear fuel cycle (3).

In a CAC instrument the stationary phase is sandwiched between two concentric cylinders with a “plough” utilised to keep the height of the bed and therefore flow resistance, constant.

As the annulus rotates, a continuous feed can achieve separation of several species simultaneously, this being a specific advantage of CAC over SMB. The innovation is embodied in equipment that permits continuous feed and separation of chemical species on an apparatus consisting of an annular bed of adsorbent particles. The apparatus is rotated slowly about its axis while eluent and a separate feed solution are fed into one end of the bed. Eluent is fed to the entire bed circumference while the feed mixture is introduced into a narrow sector of the circumference at a single point. Helixical component bands develop with the passage of time, extending from the feed point, with slopes dependent on eluent velocity, rotational speed, and the distribution coefficient of the component between the fluid and sorbent phases. The separated components are continuously recovered once steady state is attained as they emerge from the annular column, each at its unique position on the circumference of the annular bed opposite the feed end (Figure 1.8). Separations can be carried out with simple or gradient elution, wherein the eluent concentration is changed continuously (24).

The inlet feed is situated at a fixed position as the annulus is rotated. Eluent is introduced at all other positions, and flows through the chromatographic bed by gravity alone. The annulus apparatus is rotated at a fixed rate (angle per unit time) so that as the components within the feed travel down the column and are separated due to their differing interactions with the stationary and mobile phases. They will be eluted at different positions, as they reach the base of the column at different times. This method of separation is displayed in Figure 1.8.

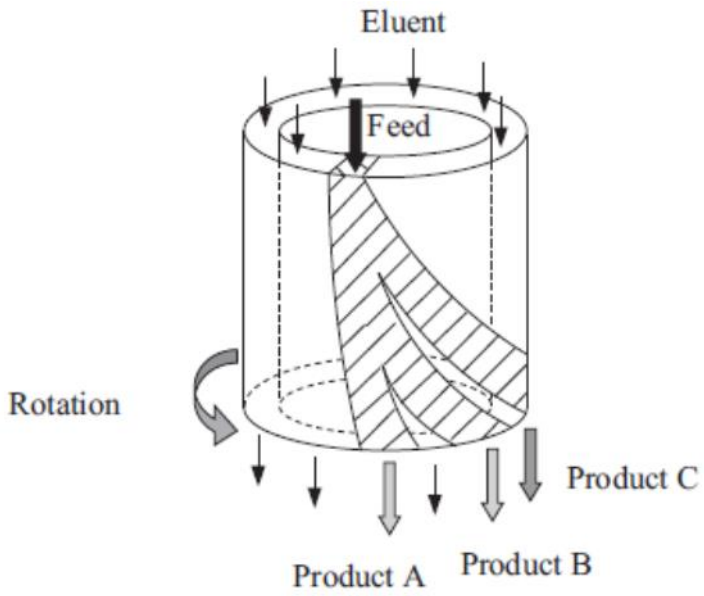

Figure 1.8: The principal of annular chromatography. Taken from (25)

Continuous chromatography would appear to be an ideal solution to the separation of metals arising from spent nuclear fuel. Application of this technique would solve all the above issues, by reducing solvent use, providing the required selectivity, minimising radiolytic degradation due to the relatively short retention time of the metals within the column and with the reduced solvent use, would therefore help to reduce the environment impact. Most importantly however is the overall reduction in cost that a transition from “batch” to “continuous” would produce (24).

The downside to CAC for the proposed UCLan reprocessing project is that the concentration of the ions will inevitably be reduced. With the use of a chromatographic method the volume of the actual waste streams containing either the U and Pu or the FPs and MAs will actually increase. However, the practice of evaporating excess water and therefore reducing the volume, in addition to the concentration of nitric acid, has been performed in nuclear reprocessing processes at Sellafield for over thirty years (26). In addition, from a chromatographic point of view, the introduction of the third dimension of a lateral separation may introduce an issue of peak broadening to the point of there being no separation; this potential problem was addressed in a study described below, with favourable results.

Therefore if a suitable chromatographic method for the separation of the ions can be found within the irradiated fuel, either CAC or SMB could be employed for a reprocessing separation protocol with the advantage of a smaller footprint, a continuous process and potentially the separation of individual ions. The transfer from a column separation to that of a CAC should be relatively simple with the *x*-axis time replaced by an axial coordinate around the annulus. The lack of applications to have achieved this however is concerning. The conversion to a SMB would possibly be a greater challenge with binary separations being predominant in the literature. However this may afford the possibility of utilising different adsorptive media for different separational steps and possibly be able to target single ions.

1.6 Continuous Chromatography History and Design

An excellent review detailing the history, development and use of continuous annular chromatography (CAC) was published by Hilbrig and Freitag (23). The major developments and a few applications are presented in a tabulated form (Table 1.3), with the addition of other continuous chromatography forms from the literature, to give context.

Table 1.3 Timeline of developments within continuous chromatography, metal ion separations are highlighted. Compiled from (23). References: (3, 25, 27 - 39)

Year	Author	Development or separation
1949	Martin	Concept of a rotating annular bed for continuous chromatography
1955	Solms	An array of columns with ion exchange materials
1955	Svensson	A circular array of 36 columns
1957	Freund	First reported moving bed by separating Acetylene from Methane
1958	Scott	Benzene from Coal gas
1959	Hall and Cole	Patent for a annular gas chromatographic system
1962	Luft	Patent for a annular gas chromatographic system
1962	Giddings	Theoretical work on resolution and throughput capabilities of GC CAC
1962	Dinelli	Construction of a preparative scale GC CC with one hundred columns
1963	Heaton	Patent for a annular gas chromatographic system
1963	Mosier	Rotating Annular gas chromatography, not constructed.
1964	Taramassoi and Dinelli	Separation of isomeric compounds
1969	Fox, Calhoun et al.	Separation of myoglobin from haemoglobin
1970	Tuthill	Rotating Annular gas chromatography, not constructed.
1972	Hurrel	Multi column simulated moving bed system proposed
1976	Scott	Pressurised CAC , Dowex 50 separation of nickel and cobalt
1978	Canon and Sisson	Modified Scott's instrument with gradient elution
1980	Canon, Begovich et al	Cannon and Sisson's instrument to separate copper, nickel and cobalt.
1981	Begovich and Sisson	Cannon and Sisson's instrument to separate iron and aluminium.
1983	Begovich, Byers et al	Cannon and Sisson's instrument to separate zirconium and hafnium.
1984	Begovich and Sisson	Cannon and Sisson's instrument to separate cobalt and blue dextran.
1987	Sisson, Begovich et al	Cannon and Sisson's instrument to separate cobalt and blue dextran.
1988	Howard, Carta et al	Cannon and Sisson's instrument to separate fructose, sucrose and glucose.
1988	Barker and Ganetsos	Simulated moving bed with a wheel concept
1989	Begovich, Sisson et al	Cannon and Sisson's instrument to separate fructose, sucrose and glucose.
1989	Carta and DeCarli	Iron and Chromium
1991	Takahashi and Goto	Amino Acids
1991	Bloomburg and Barker	Albumin, Haemoglobin and Cytochrome C
1992	Takahashi and Goto	Myoglobin and Haemoglobin
1993	Yohemoto, Kitakawa et al	Amino Acids
1994	Bloomburg and Carta	Bovine serum albumin and Haemoglobin
1995	Wolfgang, Prior et al	Fructose, mannitol and sorbitol
1995	Kitakawa, Yamanishi et al	Amino Acids
1996	Bart, Messenbocl	Fructose, mannitol and sorbitol
1996	Reissner, Prior et al	Desalting of Bovine serum albumin
1997	Paris	Modelling and simulation of a SMB system using 12-26 Separex
1997	Le Van, Carta et al	Waste gas treatment
1997	Kitakawa, Yamanishi et al	Amino Acids

The first mention of continuous chromatography in the literature is attributed to Martin (27). The author tries to envisage methods to move chromatography into the large scale or as an industrial separation technique. The author describes the two methods envisaged for use within the UCLan project and how this may be achieved, which generally persist today; the first is a moving bed configuration, although the exact arrangement for this was not configured and it was thought it too complicated for the contemporary technology. It goes on to describe a method where the stationary phase is forced against the flow of mobile phase

within a thin tube. If the balance between mobile and stationary phase flow rates were balanced correctly, the author theorised, components with higher affinity for the mobile phase would be carried further with this than the stationary phase. This would result in a separation of the components over the length of the tube. To be noted here is that the separations were for one component in a complex mixture; a criticism which still persists to some extent today with many of the described separations being binary mixtures of enantiomers or other similar biological applications. Another issue described by Martin was the ability to achieve uniform packing of the stationary phase into the tube and therefore uniform flow rates through the apparatus. It is however, the method described by Martin, often referred to as a true moving bed, which is effectively the method still in use today. The logistical difficultly of moving the solid and liquid phases in a continuous counter current is overcome as a simulated moving bed (SMB) from where a virtual infinite column length is produced through timings of feed and eluent over a number of columns arranged in series with multiple inlet and outlet points. This adaptation means that instead of both the solid and liquid phases moving counter-current to one another, the solid phase does remain stationary with the timing of the change in feeds from an input, to that of a stripping and then regeneration feed, giving the simulation of a continuously moving bed. The timing of the switching between the liquid media and the large number of columns allows separation to be performed continuously (24).

It would appear from the literature that SMBs have not been as widely developed as CAC which is the other idea described by Martin. Here two concentric tubes, with the adsorbent media held between, are slowly rotated, when feed solution is added to a specific point of the annulus and eluent to all other parts of the annulus. Specific helices of the separated components of the feed will develop which can be collected at points around the base of the annulus. Martin also mentions that a working version of this instrument had been demonstrated by Wadman, however he did not publish anything on the subject (23).

The few metal CAC applications which have been published by Begovich and Sisson in the early 1980s with a review and investigation performed by DeCarli, Carta *et al* published in 1989 (28). These focused on the separation of mixtures of Zirconium and Hafnium (29), Copper, Nickel and Cobalt (12) and latterly Iron and Chromium (28). The adsorbent employed for all of the investigations was Dowex 50W-X8 cation exchange resin.

Begovich and Sisson (29) used a CAC for a metal separation which was one of the few related to the nuclear industry, separating zirconium from hafnium (29). Zirconium ores contain 1 – 3 % w/w hafnium. The separation of these is difficult due to their similar chemical properties but the separation and purity of these metals is advantageous for the

nuclear industry in order to have very pure zirconium for the cladding of fuel, due to the low neutron capture cross sectional area, opposed to the high area of the hafnium which can be utilised for control rods.

In the experiment, an annulus of diameter 279 mm was employed, with a 600 mm bed depth and 12.7 mm width. The resin employed was Dowex 50W-X8 50-60 µm bead diameter. Eluent was sulfuric acid ranging from 0.9 – 1.6 M and flow rate of 15 litres per hour. The feed contained approximately 135 g l^{-1} and 4.1 g l^{-1} of Zr to Hf respectively at 1 ml min^{-1}. Rotation rate was 39˚ hr^{-1}.

Using the experimental conditions described above, a separation between the two peaks of 80˚was achieved at the exit of the CAC. 90 % of the Zr was eluted in a band from 20˚to approximately 100˚from the feed point, the Hf eluted from 170˚ to 220˚. There was a third peak which eluted before the two pure peaks, this contain both Zr and Hf and did not interact with the stationary phase. Due to the method of identification (neutron activation analysis) the sensitivity was very high for the Hf, but much lower for the Zr. This led to the composition of this first peak not being fully established, beyond that it contain approximately 10% of the Zr fed into the annulus and an unknown amount of Hf.

The zirconium peak contained less than 0.01 % (100ppm) hafnium; this, according to the authors, is pure enough to be used in the nuclear industry. The lack in sensitivity (less than 5 ppm for Zr) also led to the composition of the third peak not being quantified for Zr and no recovery calculations were performed for the two metals, however a material balance between the feed and elution did show that the hafnium peak contain less than 1 % zirconium.

The authors then go on to state that sufficient separation was provided at one fifth of the 60cm bed length, if this was to be introduced. This would mean a much lower dilution factor for the metals, reducing the amount of eluent needed, as well as reducing initial costs of the annulus bed. The authors also test the resolution of the peaks as the concentration of the feed is increased. This showed that although the dead space between the peaks is decreased as the feed and concentration is increased, the resolution does not drop below one until the feed is approximately 35 g l^{-1} min^{-1} of zirconium. However this figure may have been lower due to the low sensitivity and possibility of tailing which may be present at concentrations of less than 5ppm for Zr.

This journal article demonstrated that the continuous separation of metals can be achieved on a CAC instrument. Although some of the purity issues were hampered by the analytical methods employed to quantify the metals, the authors were able to ascertain that the

zirconium peak was pure enough to be employed in the nuclear industry. Unfortunately due to rigorous recovery calculations not being performed, the amount of Zr and Hf retained by the resin was not found, neither was an accurate value of Zr within the Hf peak established.

Begovich and Sisson also undertook an investigation of the separation of copper, nickel and cobalt (I) and (II). This too was performed on Dowex 50 X8 resin using ammonium carbonate as the eluent. This study was more focused upon the effect of increasing the size of the annulus in both the width and length of the bed and therefore the throughput of the system. This study also investigated the effect of annulus rotation rate upon the component separation, with and without compensated eluent flow rates (3), as opposed to the proof of theory undertaken in the previous investigation (29).

Table 1.4: Physical Characteristics of CACs used in Begovich and Sisson Study (3)

CAC Designation	Outer Diamer of Annulus (mm)	Annulus Width (mm)	Annular Bed Cross-Section (cm^2)	Bed Length (mm)	Bed Volume (l)	Pressure (kPa)
CAC-ME	89	6.4	16.5	600	1	275
-2	89	12.7	30.4	600	1.8	275
-3	89	22.2	46.6	600	2.8	275
CAC-II	279	12.7	106.4	600	6.4	275
-2	279	50.8	364.8	600	21.9	275
CAC III	445	31.8	411.7	1100	45.3	1135

The CAC designation is that given to the instruments within the study and differ from one another in the manner described in Table 1.4.

The results show that with equivalent or identical pressures and flow rates, the difference in the physical size of the CAC does not significantly affect the resolution of the peaks eluted. As the feed rate/eluent rate increases as a percentage, the peak resolution is reduced, with the trend demonstrated in all three of the instruments tested. The decrease exhibits quite a good linearity over all of the CACs and especially at the higher feed rates, the implication being that the separation performances are not affected by the bed length or the annulus size, so long as the relative feed and pressure applied are kept constant. This may not be directly applicable to this project due to the reluctance to use a pressurised eluent feed.

The effect of the annulus width showed a similar but less marked reduction in peak resolution (when pressure was held constant across the bed) but a better linearity being observed than with the change in annulus size. The authors also claim that there is very little effect due to radial flows on the separational effectiveness of the different size CACs. This is demonstrated by the similarity in the two graphs in which the only difference is the change in the width of the annulus. The authors also concede that the radial flow effects

are difficult to determine due to the exit tubes at the base of the bed being arranged in a single central ring. The author does not give any indication as to how the feed was applied to the bed or whether it was an “even” coverage over the whole bed or proportionally more was applied to the outside than the inside.

The final variable tested was that of the rotational rate and loading feed. This was achieved by keeping the feed rate constant and changing the rotational rate. A constant resolution was achieved above 45 $^{\circ}.hr^{-1}$, but this rapidly declined as the rotation rate dropped below 30 $^{\circ}.hr^{-1}$. This is explained in that the resin was being overloaded by the feed at the lower rotation rates, which would be analogous to fronting, on column chromatography. This was confirmed, as the next part of the experiment was to keep a constant ratio between the feed applied to the bed and the degrees through which the annulus turns. This experiment gave a constant resolution as the rotation rate and feed were altered.

The authors demonstrated that the scale-up of both the width and size of the annulus bed had little negative effect on the resolution between peaks. In addition to being able to have an effective throughput 60 times the original CAC-ME with only 45 times the bed volume, with the authors claiming that the principles used in the original scale-up of the instrument could be applied to even larger CACs with larger pressures.

As can be observed from Table 1.3, the vast majority of articles since the 1990s have been concerned with biological separations based on SMB. The application of CAC to practical separations has generally been limited to biotechnology and protein separations and has seen few uses in the separation of metal ions. The practical applications which have been reported, generally give very encouraging results with good separation and efficiencies equivalent to that of conventional batch chromatography (23).

Within the Hilbrig and Freitag review, the authors argue that CAC is a viable option for large volumes of complex feed streams, as well as being used to separate a wide range of analytes. Therefore a reduction in the capital investment in equipment and the physical footprint within a facility could be achieved.

This did not, though, consider the development issues connected with the transfer from column to annular chromatography or the purity of the product yielded. Indeed in one of the articles cited, the resolution between the two eluents, albumin and haemoglobin, remained below baseline resolution even at the most efficient of variables assessed, and remained less than 1.5 (un-resolved, peaks overlap) for most of the variables tested (31). This is also evident in a report published in 1988 with glucose and fructose as the eluent feed. In this study the comparison was made between the theoretical and observed resolution; the

observed resolution was consistently lower than that of the theoretical but was generally above one and a half. (32)

1.7 Continuous Chromatography Theory

The prediction of the elution patterns and degree of separation of components with differing elution profiles and other chromatographic variables is important for the optimisation of chromatographic separations (21). The two dimensional (angular and axial) separation observed in CAC is analogous to single dimensional, time dependent separations of column chromatography (23). This is because the space and time co-ordinates used in column chromatography are replaced by the space and annular (angular) displacement co-ordinates of the rotating bed.

Isocratic elution in column chromatography can be described by the equation;

$$v_c = \frac{v}{1 + \frac{1-\varepsilon}{\varepsilon} K_A}$$

Equation 1.9: Isocratic elution in column chromatography

where v_c is the velocity of a component, v is the interstitial velocity both measured in mm.s^{-1}, ε is the fraction of the bed free space and K_A is the distribution coefficient of the component at equilibrium. To be noted is that this equation applies only to gel particles and not those with macroporous properties.

This is not adequate to describe an annular chromatograph however, as it does not include any of the angular variables. The most common method for modelling this is given by Brozio and Bart describing a rigorous model for CAC (25). In this equation the dispersion is neglected or combined within a mass transfer coefficient for both annular and axial dispersion.

$$\omega \frac{\partial c_m}{\partial \theta} + \frac{(1-\varepsilon)}{\varepsilon} \frac{\partial q_i}{\partial \theta} + u \frac{\partial c_m}{\partial z} = 0$$

Equation 1.10: Mass balance of component i for the mobile and stationary phase from (25)

where ω is the rotational rate, c_m is the concentration of component i in the mobile phase (kg.m^{-3}), θ = the angle co-ordinate, q_i is the concentration of component i in the stationary phase (kg.m^{-3}), u is the interstitial velocity and z is the axial co-ordinate (m). The first term describes angular convection in the fluid phase, the second angular convection in the solid phase and the third the convection in the axial direction.

The mass balance for component i within the stationary phase is given by:

$$\omega \frac{\partial q_i}{\partial \theta} = k(c_i - c_i^*)$$

Equation 1.11: Mass balance of component i in stationary phase from (25).

where k is the mass transfer co-efficient and c_i^* is the fluid phase concentration at equilibrium.

This is complicated by the addition of other components within the mobile phase and the total adsorption equilibrium is calculated from;

$$q_i^* = f(c_1^*, c_2^* \ldots . etc)$$

Equation 1.12: Adsorption equilibrium for component i from (25).

When the band broadening due to dispersion and diffusion through the axial and angular planes is included, the following equation is used;

$$\omega \frac{\partial c_i}{\partial \theta} + \frac{(1-\varepsilon)\omega}{\varepsilon} \frac{\partial q_i}{\partial \theta} + u \frac{\partial c_i}{\partial z} = D_z \frac{\partial^2 c_i}{\partial z^2} + D_\theta \frac{\partial^2 c_i}{\partial \theta^2}$$

Equation 1.13: Rigorous mass transfer and dispersion model from (25).

This equation considers the dispersion in both axial (D_z) and angular directions (D_θ) in the two terms to the right of the equation.

This equation can be used to calculate the effect of D_θ on the peak shape and height (25).

If D_θ = 0 or assumed to be, then the retention time, t_R is equivalent to α_R/ω. With α_R the elution angle.

To calculate the chromatographic response Equation 1.13 is employed with the assumptions from Brozio and Bart that (25):

1. the feed arc is infinitely small,
2. the number of transfer units is less than five, ($n = k_o az/u$) where $k_o a$ is the interphase mass transfer co-efficient,
3. dispersion in axial and angular directions is negligible,
4. adsorption isotherm is linear,
5. concentration and fluid velocity gradients in the radial direction can be ignored
6. the elution is isocratic.

Transfer units in elution chromatography are equivalent to theoretical plates within analytical chromatography to the extent that:

$$N = NTU = \frac{1}{\sigma^2}$$

$$HETP = HTU = \sigma^2\, l$$

Equation 1.14 Equation showing equivalence of Theoretical Plates and Transfer Units

Where N is the number of theoretical plates, NTU is the number of transfer units, σ is the standard deviation, $HETP$ is the height equivalent to a theoretical plate, HTU is the height equivalent to a transfer unit and l is the length of the column.

Therefore as a very sharp peak on a chromatogram implies a large number of theoretical plates it would mean the same number of transfer units within the column (39).

$$c_i(z,\tau) = \frac{QI}{2\pi^{0.5}}\left\{\frac{(k_o a)^2}{u^3 z\tau[(1-\varepsilon)K]^3}\right\}^{0.25} * exp\left\{-\left[\sqrt{\frac{k_o a z}{u}} - \sqrt{\frac{k_o a \tau}{(1-\varepsilon)K}}\right]^2\right\}$$

Equation 1.15: Chromatographic Response for component i

$$\tau = \frac{\alpha_R}{\omega} - \frac{\varepsilon z}{u}$$

Equation 1.16: Derivation of τ

$$QI = \frac{c_F u Q_F}{Q_T} . \frac{360°}{\omega}$$

Equation 1.17: Derivation of QI

where K_A is the distribution co-efficient of a given substance, QI is the quantity of solute injected per cross sectional area (c_f), Q_F the feed flow rate, Q_T the total fluid flow rate through the annular bed and α_R is the elution angle.

1.8 Ion Chromatography Commercial Resins and Ion Exchange Materials

The phenomenon of ion exchange was discovered separately in 1850 by both Thompson and Way whilst working with natural zeolites within soils (40) (41). Development and exploration continued into the ion exchange process, but it was not until 1935 that Adams and Holmes (42) produced a synthetic organic exchanger of polymeric formaldehyde with

phenols and aryl amines. This original exchanger was advanced by Kressman and Kitchener (43) some 14 years later in 1949, using formaldehyde with phenol and sodium phenol sulfonate, however, these chains were highly cross-linked and contained two methylene bridges for each aromatic ring, meaning a relatively low number of exchangeable hydrogen ions.

Around the same time, resins were also being developed by D'Alelio in the USA, based on polystyrene and divinyl benzene. These were subsequently treated to produce a sulfonic cation exchanger (44) and a tertiary amine to produce an anion exchanger. These were later proven to be reproducible, stable and achieve a relatively high exchange capacity when commercially manufactured and have been available in this capacity since the 1950s (45) (46).

Indeed the "backbone" of most commercial resins to this day is the styrene and divinyl benzene copolymer. Depending on the ion exchange mechanism required, for sulfonic cationic resins, the copolymer is reacted with either concentrated sulfonic acid or chlorosulfonic acid at 100˚C in the presence of a catalyst. To prepare a quaternary amine anionic exchanger, the resin is first subjected to a chloromethylation with chloromethyl ether and an appropriate catalyst, the product of which is then reacted with trimethylamine to produce the exchanger. These types of resins exchange on the strength and charge of the ion in solution, limiting the ability to selectively exchange differing ions with similar properties. Although the exchange environment can be changed to optimise certain conditions such as pH or with the addition of complexing agents, it is not always possible or practical when considering downstream functions and processes. Therefore instead of the addition of complexing agents to the solution, these were incorporated onto the resins as chelates.

The use of chelates as a chromatographic stationary phase dates to the 1940s with Erlenmeyer and Dahn. Here a column containing powdered hydroxyl-quinoline was used in an attempt to separate various cations (47). This was developed by Skogseid, who attempted to produce resins with highly selective chelates in the hope that the polymerised forms would display similar selectivity to that of the monomers (48). This was achieved by Skogseid and others with O-hydroxy azo and α-diketone compounds but not for 1-hydroxy-4-vinylpyridinium, this was attempted by Heller et al who found that the geometry of forming appropriately directed covalent bonds with two adjacent aromatic rings or the N-hydroxy or N-oxide groups would not work (49).

The development of chelating resins subsequently moved toward compounds which formed specific and very strong complexes with a low number of ions, as an alternative to that of a

weaker complex but with a larger number of ions such as oxine or salicylic acid. This is borne out by the work by Kennedy *et al* who produced a resin utilising the strong complexes that phosphates and phosphonates formed with Th (IV), Fe (III) and UO_2 (II) (50). These resin compounds had the additional advantage that they actually increase the stability constants, (a phenomenon credited to the polymer entropy effect and the reduction in the dielectric constant in the resin phase).

Ion Chromatography (IC) has become a valuable tool in the separation of complex mixtures of positive and negative ions as well as their quantification (51). Separation of ions is achieved when the ion exchange resin interacts with a charged species dissolved within an acidic or basic mobile phase whilst this is eluted. These resins are synthetic cross-linked polymers which have had a functional group (such as a sulfonic or quaternary ammonium) bonded to the resin. These bonded ions are referred to as fixed ions, while the ions in the mobile phase of opposing charge are known as counter ions (52).The degree of cross-linking is due to the percentage of divinylbenzene added to the styrene to produce a co polymer at the manufacturing stage and affects the kinetics and capacity of the ion uptake onto the resin (52).

Ions diffuse through the pores created by the cross-linkage and the water within the polymer, incorporated during the manufacture of the resin. The more cross-linked the polymer, the smaller these pores, the less water that can be retained and therefore the less ion exchange will occur. If the cross-linkage becomes too low, too much moisture will be retained within the resin, which in turn will lead to facile diffusion of ions and problems with the physical strength of the resin. (52)

Water is absorbed, due to the hydration and osmotic pressure of the fixed ions on the functional groups which have been bonded to the resin. A compromise is therefore required between the adsorption capacity and elasticity of the matrix, as too high a cross-linkage would reduce water available for ion exchange and reduce the kinetics, but too little would result in an amorphous mass.

Resins which exchange positive ions are named cation exchange resins (anion exchange resins for negative ions) and can be further categorised as either weak or strongly acid or base, due to the strength of the functional group attached.

For example, on a cation exchange resin, Na^+ and K^+ ions would compete for the active sites on the resin with the H^+ ions of the acidic eluent. Assuming that there is some difference in the attraction and interaction of the ions with the resin, separation occurs through the column

as the eluent is continuously added to the top of the column (51). There is a plethora of commercial cation and anion resins available:

Table 1.5: Selection of commercial ion exchange resins. Data taken from (52)

Resin	Form Shipped	Moisture Content (%)	Bulk Density (apparent) ($g.ml^{-3}$)	Wet Exchange Capacity ($meq.g^{-1}$)	Cross Linking (%)	pH Range	Active Group
Amberlite IR 120	H^+ or Na^+	15 - 52	0.84 - 0.77	1.9	8	1 – 14	$-SO_3^-$
Dowex-50 X8	Na^+	45	0.85	1.9	8	1 – 14	$-SO_3^-$
Dowex-50W X8	H^+ or Na^+	53	0.8	1.7	8	1 – 14	$-SO_3^-$
Duolite C225	Na^+	14 - 52	0.85	2	8	1 – 14	$-SO_3^-$
Duolite C255	H^+	14 - 32	0.85	2	10	1 – 14	$-SO_3^-$
Amberlite IRC-50	H^+	43 - 53	0.69	3.5	N/A	5 – 14	$-COO^-$
Amberlite CG-50	H^+	10	0.7	3.5	N/A	5 – 14	$-COO^-$
DuoliteC436	H^+	52 - 57	0.77	3.7	2.5	6 – 9	$-COO^-$
Amberlite IRA-400	Cl^-	42 - 52	0.7	1.4	8	1 – 12	Quarternary Ammonium
Amberlite IRA-401	Cl^-	59 - 65	0.69	1	4	1 – 12	Quarternary Ammonium
Amberlite IRA-402	Cl^-	53 - 60	0.68	1.25	6	1 – 12	Quarternary Ammonium
Amberlite IRA-410	Cl^-	40 - 45	0.7	1.4	8	1 – 12	Quarternary Ammonium
Dowex 1-XB	Cl^-	43	0.7	1.33	8	1 – 14	Quarternary Ammonium
Dowex 2-XB	Cl^-	37	0.7	1.33	8	1 – 14	Quarternary Ammonium
Dowex 21K	Cl^-	57	0.7	1.25	N/A	1 – 14	Quarternary Ammonium
Duolite A113	Cl^-	48 - 55	0.73	1.3	N/A	1 – 14	Quarternary Ammonium
Duolite A161	Cl^-	53 - 57	0.7	1.1	N/A	1 – 14	Quarternary Ammonium
Amberlite IRA-93	Free Base	50 - 58	0.64	1.4	N/A	1 – 7	Polyamine
Amberlite IRA-45	OH^-	40 - 45	0.67	1.9	N/A	1 – 9	Polyamine
Amberlite IRA-67	OH^-	56 - 62	0.65 - 0.75	1.6	N/A	0 – 7	Polyamine
Duolite A303	Free Base	46 - 51	0.7	1.3	7 – 9	1 – 14	Polyamine
Duolite A378	Free Base	55 - 61	0.7	1.6	N/A	1 – 14	Polyamine

Bulk densities are generally not quoted by the manufacturers as this value depends on the packing fraction in a column which includes the voidage. For the Purolite sulphonic acid resin C100H used in column and chromatographic experiments, the bulk density based on column packing varied from 0.56 to 0.60 $g.cm^{-3}$.

This table demonstrates that the commercial resins give similar performance within the wet capacity values, densities, and moisture contents, depending on the active group and ion form supplied, despite differences in manufacturer. It also shows that although the moisture content can vary enormously, it is generally between 40 and 60 % and wet density lies between 0.64 and 0.85 $g.ml^{-1}$. This is largely dependent on the amount of cross-linking which has taken place within the resin and will impact on the physical as well as chemical performance of the resin as described above.

Another important consideration when selecting a resin is the pH range which can be accommodated by these resins. This is especially important when considering the mobile phase to be employed, as this may rule out the use of certain resins and zeolites or clinoptilolites as extremes of pH may lead to degradation, if not dissolution, of the exchange material.

The resins described above are all general anion or cation resins, more specific application resins such as chelating functional groups have been developed in particular by Eichrom Technologies Ltd. These are listed in Tables 1.6 and 1.7.

Table 1.6: Specific Eichrom resins, their matrix and target metals.

Solid matrix	Target actinides and FPs
TEVA resin an aliphatic quaternary amine	Tc, Np, Th
Sr resin impregnate containing 4,4'(5')-di-t-butylcyclohexano 18-crown-6 (crown ether)	Sr, Pb,
Diphonix resin Diphonix® resin is constructed of a polystyrene/divinylbenzene matrix in a spherical bead form. The resin is polyfunctional, containing diphosphonic and sulphonic acid groups bonded to the polymer matrix.	actinides
RE resin consists of 1 M octyl(phenyl)-N,N-diisobutylcarbamoylmethylphosphine oxide (abbreviated as CMPO) in tributyl phosphate (TBP) coated on an inert methacrylic polymeric support.	Np, Am, Cm
TRU resin impregnate containing octylphenyl-N,N-di-isobutylcarbamoylmethylphosphine oxide (abbreviated CMPO) dissolved in tri-n-butyl phosphate (TBP).	Pa, Np, Am, Cm

Table 1.7: k' of elements on three Eichrom resins. Taken from (53) and (54)

Resin	k' for Element in HNO_3										
	Pu	U	Np (IV)	Np (V)	Th	Am	Tc	Ce	Eu	Dy	Er
TEVA	80 - 30000	.9 - 10	.02 - 8000	0.6	9 - 300	.03 - 10	-	-	-	-	-
Diphonix	10000 - 100000	10000 - 1000000	90000 - 100000	-	30000 - 70000000	100 - 2000000	-	-	-	-	-
TRU Resin	700 - 600000	60 - 10000	9000 - 100000	8 – 9	100 - 6000	80 - 90	7 – 10	10 – 90	10 – 60	4 – 60	4 – 60
	Sr	K	Rb	Na	Cs						
Sr Resin	1 - 200	1 – 2	0.5 - 1	0.1 - 0.2	0.07 - 0.09						

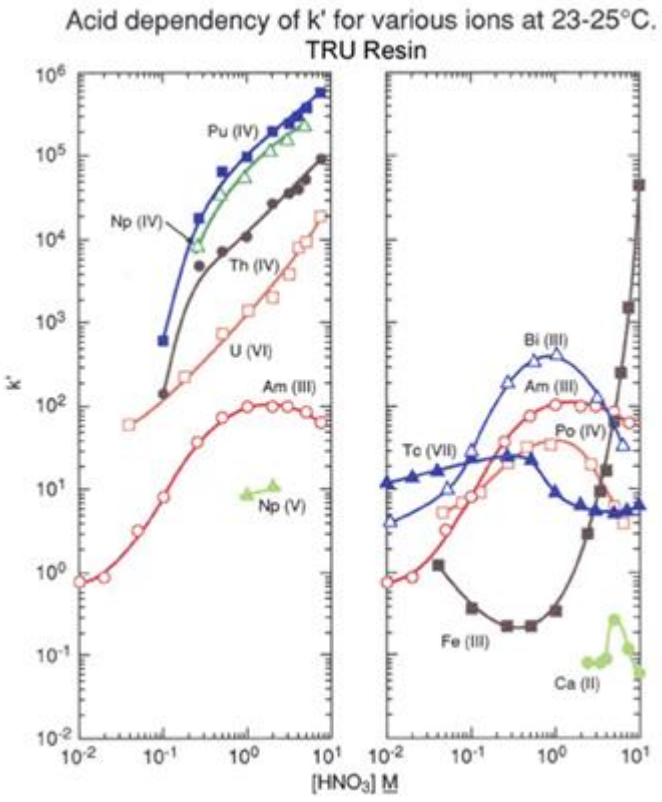

Figure 1.9 Acid Dependency of k' for various ions on TRU resin, taken from (55)

Table 1.7 shows the k' for the specific element ions on specific resins. This demonstrates a large variation in the k' values (free column bed volumes to the peak maxima) for a relatively

small change in the molarity of the mobile phase for each ion. This is further demonstrated by Figure 1.9. This graph, although showing just TRU resin, is typical for all of the resins described in Table 1.6. It should also be noted that the axis unit are presented logarithmically and not linearly.

$$k' = D * \frac{v_s}{v_m}$$

Equation 1.18: Free column volume to elution. Taken from (55).

where k' is the free column volumes to the peak maximum, D is the distribution ratio, v_s is the volume of the stationary phase and v_m the volume of the mobile phase.

This characteristic is common to all of the Eichrom resins exemplified in Table 1.7.

Purolite also produces a number of resins, a number with sulfonic acid functionality with varying amounts of cross-linkage and macro porous resins, as well as various different chelating functional groups. In collaboration with them, a number of possible candidate resins were sourced for experimentation and screening in the project. The proposed resins are listed in Table 1.8:

Table 1.8: Properties of resins provided for experimental work by Purolite.

Name	Functional Group	Polymer Structure	Ionic Form Shipped	Moisture Retention (% weight)
C100H	Sulfonic acid	Gel polystrene crosslinked with divinylbenzene	H+	51-55
C100x10MBH	Sulfonic acid	Gel polystrene 10 % crosslinked with divinylbenzene	H+	47-50
C100x16MBH	Sulfonic acid	Gel polystrene 16 % crosslinked with divinylbenzene	H+	35-40
C150H	Sulfonic acid	Macroporus polystyrene crosslinked with divinylbenzene	H+	54-59
C160H	Sulfonic acid	Macroporus polystyrene crosslinked with divinylbenzene	H+	43-48
S910	Amidoxime	Polyacrylic crosslinked with divinylbenzene	Free base	52-60
S920	Isothiouronium	Macroporus polystyrene crosslinked with divinylbenzene	H+	48-54
S930	Iminodiacetic	Macroporus crosslinked polymer	Na+	52-60
S940	Aminophosphonic	Marcroporus polystyrene crosslinked with divinylbenzene	Na+	55-65
S950	Aminophosphonic	Marcroporus polystyrene crosslinked with divinylbenzene	Na+	60-68

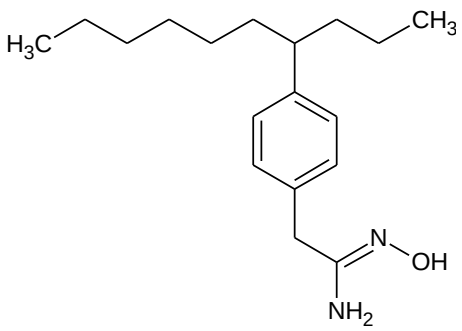

Figure 1.10: Active site of S910: an amidoxime resin.

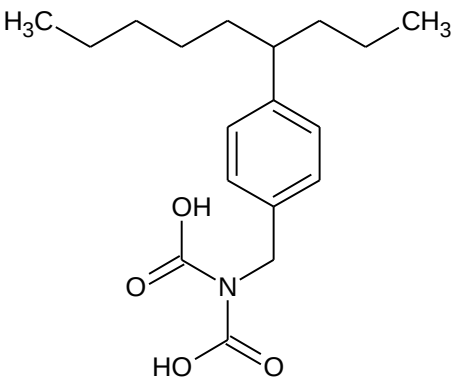

Figure 1.11: Active site of S930: a macroporous iminodiacetic resin

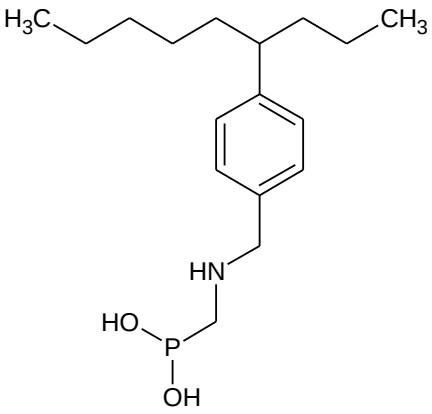

Figure 1.12: Active site of S940 and S950: both macroporous aminophosphonic resins

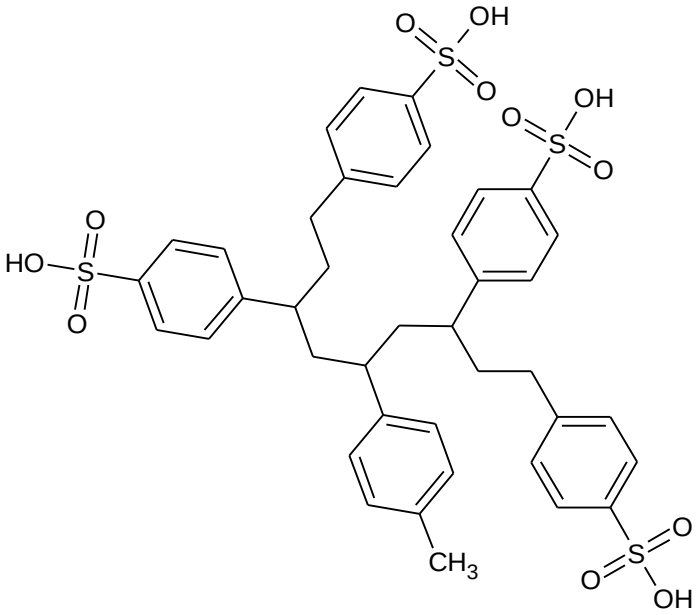

Figure 1.13 Structure of the sulfonic acid resins.

Amidoxime resin has a long association with the nuclear industry and continues to be a functional group of interest to researchers (56). High U (VI) selectivity has been described previously for amidoxime and phosphono groups in neutral media but low adsorptions from acidic media, due to their higher levels of free protons (57). The extraction of tetravalent and hexavelent actinide ions in nitric acid is usually performed by P=O or C=O bonds of TBP and monoamides in solvent extraction systems (57). However, as the project is using lower charged ions and would ideally prefer the uranium and plutonium to pass straight through the chromatographic column, these functional groups and bonds are best ignored for chelating resins with different functionality. This is demonstrated in the amidoxime, aminophosphonic and iminodiacetic acid resins provided by Purolite.

1.9 Exchange Process and Equilibria

The exchange processes are based on equilibria between ions in solution and like sign ions on the surface of the insoluble resin, or other natural ion exchangers such as zeolites or clays (58). For commercial cationic exchange resins, the most common active sites are strong acid-hydrogen type sulfonic acid groups ($-SO3^-H^+$) or weak acid carboxylic groups ($-COO^-H^+$). Anionic exchangers contain strongly basic tertiary amine groups ($-N(CH_3)^+_3\ ^+OH^-$) or the weakly basic primary amine groups ($-NH_3^+OH^-$) (58). In a cationic ion exchange this equilibrium is given by the equation:

$$xRSO_3^- \quad H^+ + M^{x+} \rightleftharpoons (RSO_3^-)_x M^{x+} + xH^+$$

Equation 1.19: Cationic exchange equilibrium

Therefore for a singly charged ion B, in a neutral solution, the reaction at the top of the column is:

$$RSO_3^- \quad H^+\ (s) + B^+(aq) \rightleftharpoons RSO_3^-\ \ B^+\ (s)\ + H^+(aq)$$

Equation 1.20: Chemical reaction for ion "B" at the top of an ion exchange column

Addition of dilute acid eluent to the top of the column moves the balance of the equation to the left, freeing the B ions into the mobile phase and moving them down the column. This can also be expressed as the equilibrium constant:

$$K_{ex} = \frac{\left[RSO_3^-\ \ B^+\right]_s [H^+]_{aq}}{\left[RSO_3^-\ \ H^+\right]_s [B^+]_{aq}}$$

Equation 1.21: An equilibrium constant for single ion on cationic resin

or rearranged as:

$$\frac{\left[RSO_3^- \quad B^+\right]_s}{[B^+]_{aq}} = K_{ex} \frac{\left[RSO_3^- \quad H^+\right]_s}{[H^+]_{aq}}$$

Equation 1.22: Rearranged Equilibrium Constant for a single ion on a cationic resin.

where K_{ex} is the equilibrium constant and $\left[RSO_3^-\ \ B^+\right]_s$ and $\left[RSO_3^- \quad H^+\right]_s$ are concentrations of B^+ and H^+ in the solid phase. During the elution, the hydrogen ions are present in high excess to the B ions in the eluent solution. This, coupled with a very large number of exchange sites, means consequently the right hand side of the equation remains at an almost constant equal to the distribution coefficient. Therefore;

$$\frac{\left[RSO_3^- \quad H^+\right]_s}{[B^+]_{aq}} = K = \frac{c_S}{c_M}$$

Equation 1.23: Distribution constant for ion "B" in a cationic resin

where K is the distribution coefficient, c_S the concentration in the stationary phase and c_M the concentration in the mobile phase.

The distribution ratio is difficult to calculate directly so the equation below is used experimentally:

$$D_W = \frac{A_o - A_s}{A_s} * \frac{V}{M}$$

Equation 1.24: Weight distribution ratio.

where D_W is the weight distribution ratio, $A_o - A_s$ is the activity sorbed onto a known weight of resin, A_s is the activity of a known volume of solution, V is the volume of liquid in ml and M is the mass of adsorbent in g.

The distribution ratio D is the volume of stationary phase per gram divided by D_W. The - volume of the stationary phase is calculated from the weight percent sorbed onto the inert support and divided by its density.

Although the concentration of cations under investigation was comparatively dilute, i.e. 5 mM, the ionic strength of the solution was on many occasions significantly higher due to the backing acid concentration, e.g. > 1 M. Hence the ionic strength of many of the solutions was above 1; ionic strength (μ) is a measure of the total concentration of ions in solution;

$$\mu = \frac{1}{2}(c_1 z_1^2 + c_2 z_2^2 + \ldots) = \frac{1}{2}\sum_i c_i z_i^2$$

Equation 1.25 Ionic strength from ion concentration in solution

where μ is the ionic strength, C_i is the concentration of the ith species and z_i is its charge.

When considering equilibria;

$$aA + bB \rightleftharpoons cC + dD$$

$$K = \frac{[C]^c[D]^d}{[A]^a[B]^b}$$

Equation 1.26 Distribution co-efficient when equilibria is considered.

Typically the ratio of concentrations is used, but is this is not constant under all conditions as concentration does not account for ionic strength differences; activities instead should be used that yields an equation for K that is truly constant.

Concentrations are related to activities by an activity coefficient (γ)

$$A_c = [C]\gamma_c$$

Equation 1.27 Activity relating to concentration of an ion

Where A_C is activity of C, [C] is concentration of C and γ_C is activity coefficient of C.

As the majority of the experiments carried out in this study were for a comparative exercise, ionic strength and activity coefficients have been set aside and the mM concentration of the cations has been considered. It is appreciated however that when comparing solutions of different nitric acid concentrations this is not strictly correct, but in all instances in this thesis the activity coefficient will be small as the ionic strength will be always > 1.

1.10 Considerations and Criteria in the selection of Stationary Phase for Nuclear Applications

In addition to the chromatographic and analytical considerations of separating a complex mixture of spent nuclear fuel, the physical properties also have to be considered. This includes the resistance of the resin to the radiation produced by the spent fuel as it moves through the column, the resilience to acidic environments - specifically nitric acid and the eventual final disposal route.

Table 1.9: Components of nuclear waste, their half-life and group name (16).

Component	Percentage of Irradiated Nuclear Fuel (%)	Half Life (Years)
Uranium	95.85	
Other Stable Isotopes	2.18	
Plutonium	1.02	
Lanthanides	1.01	
Cesium - 137	0.1	3.00E+01
Technetium - 99	0.08	2.00E+05
Zirconium - 93	0.07	1.53E+06
Strontium - 90	0.07	2.88E+01
Americium - 243	0.06	7.37E+03
Neptunium - 237	0.05	2.14E+06
Cesium - 135	0.03	2.30E+06
Iodine - 129	0.02	1.60E+07
Curium - 247	< 0.00	1.56E+07

Key	
	Bulk of Irradiated Fuel
	Actinides
	Long lived fission products
	Short lived fission products

With regard to the stationary phase resilience to radiation and pH, the main consideration would be in the manner of interaction of the eluent and ions in solution with the stationary phase. It has been known for some time that the extended exposure to radiation will cause a reduction in the capacity and damage to the resin (59).

Ionising radiation doses above 10 Gy (ten joules per kg of matter) significantly change the capacity, selectivity and exchange kinetics of many synthetic organic exchangers. Generally anion exchangers are more greatly affected than cation exchangers, but the chemistry (including composition, moisture content and extent of cross linkage) of the resin before radiation occurs is a major factor affecting the resin capabilities as well as the chemical environment the resin is contained in. It is suspected that there are two mechanisms at work in the disruption of resin function. Direct radiolytic effects can lead to scission of functional groups, free radical formation and further reactions of these species formed. It is also thought that interactions occur between ion exchangers and highly reactive radiolysis products of the surrounding medium (60).

Cationic, styrene-divinylbenzene sulfonic acid resins, due to their commercial importance, have been the most studied in relation to their radioactive chemical stability (60). The amount of damage sustained is linked to the degree of cross linkage derived from the amount of divinylbenzene in the resin, as demonstrated by Wedermeyer (61) and Cathers (62) as well as others. There are however a few exceptions to this (63).

It seems however that the actual damage caused is extremely specific to the resin in use and is limited to single resin types or those with very similar chemical compositions,

therefore making prediction of specific damage difficult to achieve even within the same "class" of resin.

Polycondensation type cation resins are generally more resistant to radiation than sulfonic acid resins but are significantly less resilient to chemical and thermal degradation, with reduction in capacity, swelling and production of gases just some of the issues (60).

Of the studies performed on quaternary ammonium groups, very few provided sufficient quantitative data, however the radiolytic damage was noticeable, with the evolution of free amines and gases as well as destruction and darkening of the resin matrix from radiation levels in the region of approximately 100 Gy (60).

The production of gaseous products is one of the issues investigated when the stability of resins was assessed in the presence of nitric acid.

In the studies described, two anion and one cation exchange resins were assessed for their stability with elevated levels of nitric acid and temperature (up to 5 M for the cation resin and up to 12 M for the anions up to 110℃). The resins were placed in an instrument which measured the temperature and pressure. With the nitric acid, the temperature was raised in order to recreate conditions potentially encountered within the working environment of the resins. Any gas created was vented and spectroscopically evaluated. The anion resins used were Reillex HPQ and Ionac A-641 (64). The cation resin was SuperLig 644 (65).

The results for the SuperLig 644 were that the resin completely dissolved in the 5 M HNO_3 at 90 °C with the conclusion drawn that exothermic and therefore hazardous, reactions had taken place especially at 5 M and at 55 ºC or higher. This conclusion was reached even though the solution/sludge of resin and nitric acid was not tested spectropically or otherwise and was not backed up by a 0.5 % rise in pressure, which was explained by a 16 ºC rise in air temperature within the pressurised container and was consistent throughout the blanks and HNO_3 experiments. Gas generation of CO_2 and NO_x was observed without nitrification of the resin (65).

Approximately half of the resin was dissolved in the deionised water at high temperature (95 °C) with most of this attributed to the dissolution of potassium bicarbonate within the resin, which was present from the manufacture of the resin. Interestingly the "blanks" made up of the resin and deionised water, when subjected to the same heating regime as the nitric acid and resin solution, caused the solution to change colour to red/brown. The remaining solid, however, did not show any degradation (65).

The anion resins were more thoroughly tested: in some of the tests the resin was preloaded with cerium (IV) while in another the resin was irradiated to ascertain if this would affect gaseous product formation or exothermal reaction rates. The experiment was designed so as the Reillex HPQ was compared and contrasted to the A-641 resin. The two resins performed comparably to one another (64).

The effect of cerium being preloaded onto the resin for the reactivity of both the non-irradiated and irradiated resin with the nitric acid was that no increase in reaction temperature or rate was observed. The energy that was released from the exothermic reaction was also not enough for it to become self-perpetuating. The gas products were identified as NO, CO_2 and NO_2. This was further investigated and found to be a reaction between the diethylbenzene and the high concentration of HNO_3 (64).

The paper discussing the anionic resin also concludes that there is the possibility of large volumes of gas being produced, especially if the resin was to approach temperatures of 70 to 80 °C. At the highest temperature and at the highest theoretical production the calculated amount of NO_2 was a total of 600 ± 200 l at a rate of 26 $l.min^{-1}$. The more likely reaction (which produces NO gas) was calculated to produce 26 ± 14 l at 2 $l.min^{-1}$. These are significant volumes for a column with a volume of 20 l. This could result in a failure of the system or worse an explosion (64).

1.11 Conclusion

The plutonium and uranium extraction method, PUREX, was developed during the Manhattan project of the 1940s. The main extracting solvent; TBP is well understood and accepted by industry; however it does have a number of associated issues. Amongst these is the production of large volumes of highly active aqueous liquors, TBP is also degraded by the radioactivity and nitric acid contact, the inherent lack of specificity in solvent extraction and resultant strict process condition parameters. The major drawback of the process however is that the majority components (uranium and plutonium) are extracted from the minority fission products and minor actinides (FPs and MAs). It is the intention of our research to reverse this inefficient separation method by extracting the FPs and MAs by a continuous chromatographic method leaving the U and Pu in the dissolver liquor.

The concept of replacing the PUREX process for reprocessing of irradiated uranium fuel is a significant challenge as several key conditions/considerations will require critical assessment and comparison with a technology that has been accepted and unchallenged for nearly sixty years. The more important challenges are addressed in this section. Separation processes, such as the PUREX process, have to satisfy not only a variety of interested parties such as

regulators and operators, but also meet some stringent specification conditions such as reliability, throughput, product quality and environmental impact

Chromatographic separations will also need to consider kinetics, particle size, porosity and density of the stationary phase, but in comparison with liquid-liquid extraction system such as PUREX, few others.

The broad aim of this thesis is to perform a proof of concept chromatographic separation of uranium from fission products at an elevated nitric acid concentration, i.e. > 1 M. Surrogates and isotopes will be employed in lieu of radioactive ions.

To achieve this, a range of commercially available resins and adsorbents will be tested to assess their suitability in regard to the separation factors of the ions over a range of nitric acid concentrations, kinetic uptake of ions at an elevated nitric acid concentration, uptake isotherm assessment at high nitric acid concentration, breakthrough studies and acid and oxidative resistivity in high concentration nitric acid concentrations before a chromatographic separation will be attempted and developed.

The initial assessment of adsorbents and subsequent inclusion or exclusion from the chromatographic development would be primarily based on the separation factors of the two most highly retained ions on the majority of the adsorbent media. The figures to which the adsorbents are working are a separation factor of 2 at the 3 M HNO_3 concentration level.

The adsorbents which achieve this would then be assessed on their kinetic and isotherm uptakes. This assessment of their ability to efficiently exchange the ions at the elevated nitric acid concentration and give an indication of the surface interaction occurring on the adsorbent media. These would be used in conjunction with the breakthrough and acid and oxidative resilience to eliminate all but one of the adsorbents for the chromatographic development.

The separation development will be kept as simple as possible with the only variables to be limited to eluent concentration, bed height and eluent flow rate. No mobile phase modifiers such as citric acid which may interfere with any subsequent, as yet, undetermined separation operations will be utilised. Baseline separation of the ions is desirable.

2. Experimental

2.1 Introduction

While this project aims to develop experimental techniques for the separation of uranium and plutonium from other fission products, there are significant experimental difficulties associated with the handling of isotopes of these ions. Consequently in this study Ce (III) and Ce (IV) have been used as a surrogate for uranium and plutonium. This is a widely accepted protocol with Ce being used as a surrogate in a variety of studies ranging from reprocessing, fuel fabrication and waste management (66). The liquid-liquid extraction of cerium ions from nitrate solution using tri butyl phosphate was well established before the conception of the PUREX process (67). The Ce (IV) ion forms relatively weak nitrato complexes in nitric acid solution (~1 M), with the Ce (IV) ion predominating but with $Ce(NO_3)^{3+}$ and $Ce(NO_3)_2^{2+}$ ions increasing in stronger nitric acid (68).

2.2 Materials

2.2.1 Standard Reagents

All materials used in this thesis have been bought from commercial suppliers and used without any further purification as described in Table 2.1:

Table 2.1 Reagents Used Within the Thesis

Compound	Formula	Supplier
Cerium (III) nitrate hexahydrate	$Ce(NO_3)_3 \cdot 6H_2O$	Sigma Aldrich
Cerium (IV) ammonium nitrate	$Ce(NH_3)_2(NO_3)_6$	Sigma Aldrich
Cesium nitrate	$CsNO_3$	Sigma Aldrich
Cobalt (II) nitrate hexahydrate	$Co(NO_3)_2 \cdot 6H_2O$	Sigma Aldrich
Copper (II) nitrate trihydrate	$Cu(NO_3)_2 \cdot 3H_2O$	Sigma Aldrich
Strontium nitrate	$Sr(NO_3)_2$	Sigma Aldrich
Zirconium (IV) oxynitrate hydrate	$ZrO(NO_3)_2 \cdot H_2O$	Sigma Aldrich

Sigma-Aldrich Company Ltd. Dorset, England

These cations were selected as:

- Their chemistries and behaviour are different
- They account for a significant amount of β/γ activity present in spent fuel dissolver liquor
- Zr is responsible for significant challenges in the PUREX process (69).

2.2.2 Commercial Ion Exchange Resins

Similarly all the resins and adsorbents used within the thesis were sourced commercially and are listed in Table 2.2:

Table 2.2 Commercial Resins and Adsorbents Used Within the Thesis

Name	Manufacturer	Functional Group	Form Shipped	Polymer Structure	Particle Size (μm)	Uniformity Coefficient
C100H	Purolite	Sulfonic Acid	H^+	Gel Polystyrene crosslinked with 8 % DVB	300 - 1200	1.3
C100X10MBH	Purolite	Sulfonic Acid	H^+	Gel Polystyrene crosslinked with 10 % DVB	425 - 1200	1.6
C100X16MBH	Purolite	Sulfonic Acid	H^+	Gel Polystyrene crosslinked with 16 % DVB	425 - 1200	1.6
C150	Purolite	Sulfonic Acid	Na^+	Macroporous Polystyrene crosslinked DVB	300 - 1200	1.7
C160	Purolite	Sulfonic Acid	Na^+	Macroporous Polystyrene crosslinked DVB	300 - 1200	1.7
D5529	Purolite	Unknown	Unknown	Unknown		
D5530	Purolite	Unknown	Unknown	Unknown		
G26	Dowex	Sulfonic Acid	H^+	Gel Polystyrene crosslinked with 8 % DVB	600 - 700	1.1
S910	Purolite	Amidoxime	Freebase	Polyacrylic crosslinked with DVB	300 - 1200	1.7
S930Plus	Purolite	Iminodiacetic	Na^+	Macroporous crosslinked polymer	425 - 1000	1.5
S940	Purolite	Aminophosphonic	Na^+	Macroporous crosslinked polymer	425 - 850	1.4
S950	Purolite	Aminophosphonic	Na^+	Macroporous Polystyrene crosslinked with 8 % DVB	300 - 1200	1.5

Particle sizes and uniformity coefficients are taken from the Purolite (70) and Dowex (71) commercial literature.

The uniformity coefficient is an indication as to the uniformity of size of the particles within a sample. It is a specialised measure of standard deviation and is calculated by dividing the value of the (theoretical) sieve size through which 60 % of the resin sample would be retained by that of the sieve size where 10 % of the resin sample would be retained (52).

Within liquid chromatography the particle size plays a significant role in the efficiency, speed and sensitivity of the chromatographic column. It therefore also plays a major role in the chromatographic conditions under which the column performs at its optimum for the separation of components within the mobile phase. Not least of these parameters is the back pressure required to keep a constant and optimised mobile phase flow rate through the packed bed of the column.

These parameters are linked to the Van Deemter equation (Equation 3.2) for column efficiency. It is generally accepted that a smaller particle diameter will provide a more uniform bed packing within the column and therefore a smaller "A" value within Van Deemter, increasing the efficiency of the column. However reducing the column void volume or free space means a greater resistance to its flow is encountered by the mobile phase. This higher resistance to the flow of the mobile phase means a higher pressure is required to force the mobile phase through the bed and maintain an equivalent flow rate to that of a bed with larger particles and a higher void volume.

Within this project it was decided to keep the pressure of the mobile phase to a minimum, relying on a gravity fed column with a reservoir of mobile phase above the bed, to keep a constant flow pressure within the column.

2.2.3 Instrumentation and Equipment

Table 2.3 details the instrumentation and equipment utilised throughout the thesis and includes salient information such as software.

Table 2.3 Instrumentation, Equipment and Software Used Within the Thesis

Instrument	Manufacturer	Model	Serial Number	Software
Deionised Water	ThermoFisher	Barnstead Nanopure	-	-
ICP-MS	Thermo	X-Series	2.5.11.321	PlasmaLab
Shaking water bath	Julabo	SW22	-	-
Fraction Collector	Bio Rad	2110	-	-
Peristaltic pump	Marlow	SCI Q 323	-	-
FT-IR	Jasco	FT-IR-410	1.50.00 Build 2	Spectral Manager
Mixer pump	Dionex	AGP-1	-	-
Balance	VWR	LA314i	-	-
Micropipettes	VWR	2 - 20 µl	42733365	-
Micropipettes	VWR	20 - 200 µl	42753479	-
Micropipettes	VWR	100 - 1000 µl	42765844	-

Fisher Scientific UK Ltd, Loughborough

Julabo, Peterborough.

Bio-Rad Laboratories, Hemel Hempstead, Herts.

Watson Marlow, Falmouth, Cornwall.
Dionex, Thermo Fischer, Hemel Hempstead, Herts.
VWR, Lutterworth, Leicestershire.

2.3 Experimental Protocols

2.3.1 Moisture Retention

Throughout this thesis, ion exchange capacities have been reported as $mg.g^{-1}$ of wet resin. However, in order that this could be reported with a reasonable degree of accuracy the resin or adsorbent was monitored to ensure no significant changes in moisture content occurred.

The moisture content was determined using the method described by Valenta *et al* (72). A known mass of the resin or adsorbent was weighed in a beaker. This was then placed in a fume cupboard in an air-conditioned laboratory for 48 hours and subsequently re-weighed. The beaker and resin or adsorbent was then placed in an oven at 105°C for 120 hours and re-weighed. The mass lost was calculated and converted to a percentage.

This was an experiment which ran throughout the project and was undertaken upon receipt of the resin and at the end of the cycle of experiments.

2.3.2 Ion Exchange Capacity as a Function of Acidity

As the acid molar strength of the feed solution would be a major determining and limiting factor on the separation of ions and efficiency of any chromatographic separations, batch studies on the effect of nitric acid strength on the uptake of the ions by all adsorbents were investigated first.

The range of HNO_3 under investigation was from 0 - 4 M. Experiments were carried out in 250 ml Durran bottles with 100 ml of the required concentration of nitric acid. A stock solution containing the ion of interest was added to the Durran bottle to bring the ion concentration within the bottle to 500 ppb, the bottle was then sealed and placed into the shaking water bath. The bottle was shaken for 30 minutes at 200 rpm and 25 ˚C to ensure heterogeneous mixing of the ion throughout the acid and in order that the temperature equilibrate. A sample was then taken for assay as described in Section 2.4.3.

A 1 g sample of the adsorbent or resin of interest was then added to the bottle, the bottle resealed and placed into the water bath for 16 hours. This was taken to be an approximation of equilibrium. After the 16 hours had elapsed the bottle was removed from the shaking water bath and a further sample taken for assay as described in Section 2.4.3.

The percentage uptake was calculated from Equation 2.1:

$$Percentage\ Uptake = \left(1 - \left(\frac{C_e}{C_0}\right)\right) * 100$$

Equation 2.1 Percentage Uptake of an ion

Where C_e is the concentration of the ion measured at equilibrium (mg.l^{-1}) and C_0 represents the initial concentration of the ion (mg.l^{-1}). This figure was then plotted against acid strength.

The distribution constant was calculated from Equation 2.2:

$$K_A = \frac{(C_A)_s}{(C_A)_M}$$

Equation 2.2 Distribution Constant for Ion A

where $(C_A)_s$ was the concentration of ion A on the solid and $(C_A)_M$ was the concentration of ion A within the mobile phase.

Selectivity co-efficient were calculated by Equation 2.3:

$$\alpha = \frac{K_B}{K_A}$$

Equation 2.3 Selectivity co-efficient

If the result was greater than one, the uptake of ion A was more favourable than Ion B, if less than one uptake of Ion B was more favourable.

2.3.3 Determination of the Rates of Ion Exchange

The determination of the rate of ion exchange was performed in a similar manner to that described in Section 2.3.2. With the main differences being that samples were taken for assay whilst the experiment continued, the experiment was also extended to run for 24 hours (1440 minutes) and the ion exchange rate was determined at three temperatures. As described in Section 3.2, there are four exchangers that fulfil the criteria required to warrant further study the C100H, C100X10MBH and S910 resins and the D5530 adsorbent.

To a Durran bottle, 100 ml of a liquor containing 3000 mg.l^{-1} Zr (IV) ion from $ZrO(NO_3)_2$ salt solution of 2 M HNO_3 was added. This was placed in the shaking water bath for 30 minutes at the temperature under investigation (25, 45 or 60 ˚C), shaking at 200 rpm to ensure equivalence between temperature for the initial and experimental samples. After 30 minutes a sample was taken for assay for initial concentration of the Zr (IV) ion as described in

Section 2.4.3. The zirconium (IV) ion was chosen as this was the only ion to display a significant exchange capacity on all of the resins under investigation at the HNO_3 concentration of the experiment.

A 0.5 g sample of the resin or adsorbent of interest was accurately weighed and added to the liquor. The bottle sealed and placed in the shaking water bath. Samples were taken for assay as described in Section 2.3.2 at 10, 20, 30, 45 and 60 minutes and at 2, 4, 8 and 24 hours after the initial addition of resin to the liquor.

The ion uptake capacity after 24 hours was taken as equilibrium. The ion mass uptake was calculated as the difference between the initial ion concentration of the liquor and the ion concentration of the sample divided by the mass of the resin or adsorbent. For the percentage uptake against time this 24 hour figure was set as 100 % uptake. The percentage uptake capacities were calculated as a percentage of the maximum uptake;

$$Percentage\ of\ Equilibrium\ Ion\ Uptake = \left(\frac{Ion\ Mass\ Uptake\ of\ Sample}{Initial\ Ion\ Mass\ of\ the\ Liquor}\right) * 100$$

Equation 2.4 Percentage of Equilibrium Ion Uptake

Due to these experiments having taken place after the Ion Exchange Capacity as a Function of Acidity studies, the moisture content of the exchangers has become a factor to take into consideration.

2.3.4 Determination of Ion Exchange as a Function of Zirconium Ion Concentration

The determination of Zr (IV) ion exchange as a function of ion concentration would allow the fitting of the data to a number of isotherm models. There are two main methods used within this thesis; a more graphic definition offered by Giles and Smith with a more numeric and traditional methodology proposed by both Freundlich (73) and Langmuir (74).

The four types of isotherm proposed by Giles and Smith in 1974 (75) describe a theoretical classification of adsorption isotherms for solutes in dilute solution, relating their characteristic shapes to parameters of the solvent and any second solute.

“C” isotherms are a linear graph with an origin at zero. The ratio between initial concentration and that on the adsorbent would remain constant. In practice it usually describes an isotherm that has not reached plateau.

In “L” isotherms, the ratio between the concentration on the stationary phase and of that in solution at equilibrium decreases as the initial liquid concentration increases, providing a

concave curve and suggesting a progressive saturation of the adsorbent. L isotherms can be further distinguished into adsorbents with a strict maximum sorption capacity and those which continue to increase minimally with increased initial solute concentration.

“H” isotherms could potentially be described as a sub group of L isotherms, as the curve profile was similar, however differentiation comes from the initial adsorption gradient: a very steep gradient, sometimes close to infinite, indicating an extremely strong affinity between solute and adsorbent.

“S” as the name suggests was sigmoidal and has a point of inflection, this indicates at least two opposite mechanisms. For metallic species the presence of a soluble ligand could provide such an isotherm.

The more common methods of modelling equilibrium data use the empirical Langmuir and Freundlich isotherms. The Langmuir isotherm (74) was devised to describe gas-solid adsorption, but has subsequently been substituted for use in liquid-solid adsorptions. It assumes a homogeneous solute adsorption from the liquid phase. The adsorption was finite, with no interference or interaction in adsorption behaviour between neighbouring sites, or in the preference displayed between sites for ion uptake.

The Freundlich isotherm (73) was an earlier attempt to describe nonlinear adsorption. The amount adsorbed was the sum of from all adsorption sites, the sites with the strongest affinity being filled preferentially until the bond energy has been exponentially reduced as the adsorption reaches saturation due to initial ion concentration.

The Langmuir isotherm given by:

$$q_e = \frac{QbC_e}{1 + bC_e}$$

Equation 2.5Langmuir isotherm

And the Freundlich isotherm by:

$$q_e = K_f C_e^{1/n}$$

Equation 2.6 Freundlich isotherm

where q_e was the mass of ion adsorbed on the adsorbent (mg.g^{-1}) Q was the maximum adsorption capacity, b was the constant related to the free energy of adsorption (L.mg^{-1}), C_e solution phase concentration at equilibrium (mg.l^{-1}) K_f is the constant indicative of the relative adsorption capacity (mg.g^{-1}) and $1/n$ is the constant indicative of the intensity of adsorption.

To determine how well the isotherm model fits the experimental curve, the sum of squares was calculated from:

$$SSE = \sum \left[\frac{(q_e - q_{theo})^2}{q_e^2} \right]$$

Equation 2.7 Sum of squares for equilibrium models from measured values

where q_{theo} is the theoretical mass of ion adsorbed on the adsorbent ($mg.g^{-1}$).

The smaller the sum of squares, the more closely the fit between the calculated values of the isotherm to that of the data collected.

The analytical method was developed from that described by Alyüz and Veli in 2009 (76).

The methodology for this experiment again follows that of the 2.3.2 Ion Exchange Capacity as a Function of Acidity in that 100 ml of 2 M HNO_3 liquor was used for all experiments. As the Zr (IV) ion concentration was the variable of interest the concentration of this ranged from 0 to 3 $g.l^{-1}$. The 100 ml of liquor with the concentration of Zr (IV) ion under investigation was added to a 250 ml Durran bottle, this was placed a shaking water bath at 25 °C shaking at 200 rpm for 30 minutes to equilibrate. A sample was taken for assay for initial concentration of the Zr (IV) ion as described in Section 2.4.3. The zirconium (IV) ion was chosen as this was the only ion to display a significant exchange capacity on all of the resins under investigation. A 0.5 g sample of the resin or adsorbent of interest was accurately weighed and added to the liquor. The bottle was sealed and placed in the shaking water bath for 16 hours. After 16 hours the liquor was resampled and assayed as described in Section 2.4.3. The difference between this assay and the initial concentration was calculated as the ion exchange capacity. In the case of the sulfonic acids (C100H and C100X10MBH), this figure was corrected by the same method as described in Section 2.3.3.

The ion exchange capacity was plotted against initial Zr (IV) concentration of the liquor. A line of best fit was also calculated and plotted on this graph. The equation for this line of best fit was used to calculate the experimental ion exchange figure in the sum of squares calculation. From this figure the Langmuir and Freundlich plots were calculated and optimised by utilising the “Solver” function of Microsoft Excel. This was achieved by minimising the difference between the experimental and theoretical ion capacities. The theoretical capacity was manipulated by the Solver function of Excel changing the variables within either the Langmuir or Freundlich equations.

2.3.5 Breakthrough and Elution in Columns

Breakthrough curves give a good indication of when a column has become saturated with a specific ion. Once this has occurred, the concentration of ion in the eluent leaving the column would be equal to that of the feed entering the column. The gradient of the curve also gives an indication of the specificity of ion adsorption, where a steeper curve indicates a more specific and robust adsorption at the particular column conditions.

Four feed stock solutions containing 0.5 and 3.0 $g.l^{-1}$ of both Zr (IV) and Ce (IV) ions were prepared in 1 and 3 M HNO_3. The density of this feed stock was calculated prior to each experiment. A sample of this solution was taken for assay for initial concentration (C_0) of the Zr (IV) Ce (IV) ions as described in Section 2.4.3.

The glass column had an internal diameter of 10 mm, and a length of 500 mm. At one end of the column a glass frit was fixed and below this there was a tap. At the other end of the column the diameter widened to an internal diameter of 20 mm with a length of 50 mm. The resin bed was prepared by slurrying 10 g of the resin or adsorbent of interest with an excess of deionised water in a beaker. This was then washed into the column at a 45 ° angle with the intention of maintaining a heterogeneous media particle size throughout the column length and reduce the chance of introducing air voids within the column bed. The base of the column was then placed in an ultrasonic bath for approximately a minute to further aid the settling of the particles. A glass wool plug (approximately 1.5 g) was then inserted approximately 10 mm above the bed height. As the resin or adsorbent had been prepared in deionised water, any swelling of the media would be at its height and consequently no interaction with the glass wool plug would occur. The purpose of the glass wool was to prevent agitation of the topmost portion of the resin or adsorbent bed when the feed stock was added to the top of the column. Before the experiment commenced, the excess water was drained to the top of the glass wool plug and subsequently the column was conditioned by running 10 bed volumes of HNO_3 at the same concentration as the feed stock to be used within the experiment through the column.

To begin the experiment, a 200 mm head pressure of the feed stock under investigation was allowed to build up above the glass wool plug within the column. This was regulated by a suction drain placed at 200 mm above the resin or adsorbent bed which fed back to the main feed stock reservoir. The column tap was opened to allow the feed liquor to flow through the column bed. The flow rate was regulated by tightening or relaxing a screw clip positioned on a flexible piece of tubing below the tap within the glass column, which was found to give more control over flow rate than the tap. The eluent was collected for 5.25 minutes (315 seconds) in 80 test tubes giving an experiment run time of 7 hours. The feed flow rate was

monitored and maintained between 5 and 6 bed volumes per hour throughout the experiment. Each of the 80 eluent samples was sampled for assay for concentration of the Zr (IV) Ce (IV) ions as described in Section 2.4.3. The ratio of eluent concentration and initial feed concentration was plot against the bed volume eluted.

Once the loading experiment had run for seven hours, the resin or adsorbent of interest was then subjected to an ion stripping study. This was performed in the same method as above with the omission of the pre-experiment column conditioning and that the feed liquor was 5 M HNO_3. The assay concentration of eluent was again plot against the bed volume eluted.

2.3.6 Chromatographic Separation

The challenge of performing chromatography with commercial ion exchange resins and adsorbents at the elevated HNO_3 levels required by the project was always going to be difficult with a simple isocratic eluent feed. It was therefore necessary to develop an elution profile which would provide a suitable separation through either a gradient elution, where the concentration of the eluent changes at a continuous rate or through a stepped elution, where the concentration of the eluent changes a number of times in distinct steps.

Within chromatographic method development, there are a number of variables which have to be taken into consideration. The vast majority of the experiments undertaken up to this point have been concerned with the identification and assessment of the properties of a stationary phase. With the chromatographic development process, the experiments become more dynamic with a larger number of variables to consider in order to achieve a suitable separation for the four ions used.

In order to give a proof of concept for the separation of these ions, variables such as the adsorbent bed were kept constant, the column diameter and mass of resin used were constant; the bed height varied with the swelling of the beads and therefore the acidity of the mobile phase.

To minimise any downstream interferences, the decision was made not to use any mobile phase modifiers, with the only variable being that of the concentration of the nitric acid eluent. The resin used was the C100H as this was determined to have performed most satisfactorily in the preceding experiments.

Therefore the goal for the chromatographic development was to give a method providing baseline separation for each of the ions, with only a change in the HNO_3 concentration as the variable.

The column bed was prepared as described in Section 2.3.5 with either 7.5 g for the initial experiment, rising to 15 g of the C100H resin. The maximum volume that the mixer/pump equipment could accurately deliver was limited to 4.5 $ml.min^{-1}$. In order to measure and monitor the volume eluted, each of the test tubes used for the experiment was weighed prior to the experiment starting and mass recorded. The density of each of the nitric acid concentrations to be used was calculated by measuring a known volume of the eluent straight from the mixer/pump prior to the experiment commencing.

Before the chromatograph was started, deionised water or 5 M HNO_3 was added to the applicable reservoirs of the mixer/pump. The mixer/pump was then programmed with the appropriate method as described in Table 2.4. To begin the experiment a 0.5 ml sample containing 5 $g.l^{-1}$ of Cs (I), Sr (II), Ce (IV) and Zr (IV) ions was introduced to the glass wool plug above the resin bed in order that no mixing with the mobile phase or resin bed occurred prior to the start of the experiment, mimicking the sample loop of a LC instrument. Once again a 50 mm reservoir of mobile phase was built up above the glass wool plug to maintain a pressure to drive the mobile phase through the resin bed. The exceptions to the equal concentration samples was for the final two experiments, where the ratios of the concentrations of the Cs (I), Sr (II) and Zr (IV) ions to the Ce (IV) ion was 1:50 and 1:300 for Experiments 15 and 16 respectively.

Once used in the experiment, the test tube and collected eluent were again weighed and the difference from the original mass calculated; this was then converted to a volume, using the density of the nitric acid calculated. A sample of this solution was taken for assay for concentration of Cs (I), Sr (II), Zr (IV) and Ce (IV) ions as described in Section 2.4.3 and this plotted against the volume eluted; this unit of measurement for the x-axis was chosen as a compromise between the traditions of both ion exchange and chromatography. The flow rate and any step or gradients applied to the mobile phase are displayed in Table 2.4. The chromatographic method was developed intuitively based on the accrued data and experience.

Once the experiment had been stopped, the column was flushed with 10 bed volumes of 7 M nitric acid. This was used to fully protonate the C100H and remove any of the ions which may have been retained by the resin after the experiment had finished. Once the ten bed volumes had been eluted, the column was flushed with HNO_3 at the starting concentration of the subsequent experiment for 10 bed volumes to re-hydrate the resin. An approximate 10 mm of a head reservoir was left above the resin bed over night to ensure that there was sufficient available to equilibrate the resin with required concentration of the nitric acid and ensure that the resin bed did not become dry.

Table 2.4 Experimental Parameters for Chromatographic Separations

Experiment Number	Figure Number	Flow Rate ($ml.min^{-1}$)	Initial HNO_3 Concentration (M)	Time (min)	Gradient ($M.hr^{-1}$)	2nd Concentration (M)	Time (min)	Gradient ($M.hr^{-1}$)	3rd Concentration (M)	Time (min)	Gradient ($M.hr^{-1}$)	4th Concentration (M)	Time (min)	Gradient ($M.hr^{-1}$)	5th Concentration (M)	Time (min)	Gradient ($M.hr^{-1}$)
1	3.39	1	3	240	Isocratic	-	-	-	-	-	-	-	-	-	-	-	-
2	3.40	3	3	240	Isocratic	-	-	-	-	-	-	-	-	-	-	-	-
3	3.41	3	2.5	240	Isocratic	-	-	-	-	-	-	-	-	-	-	-	-
4	3.42	2.5	1	180	1	4	60	Isocratic	-	-	-	-	-	-	-	-	-
5	3.43	2.5	0.5	60	Step to	1	80	Step to	3	40	1.3	4	60	Isocratic	-	-	-
6	3.44	2.5	0.5	60	Step to	1	80	Step to	3	40	Step to	4	60	Isocratic	-	-	-
7	3.45	2.5	1	60	Step to	2	60	Step to	3	60	Step to	4	60	Isocratic	-	-	-
8	3.46	4	1	90	Step to	2.1	60	Step to	2.8	30	Step to	4.5	30	Step to	5	30	Isocratic
9	3.47	3	1	90	Step to	2	60	Step to	3	90	Step to	5	60	Isocratic			
10	3.48	4	0.9	80	Step to	2	80	Step to	2.75	80	Isocratic	-	-	-	-	-	-
11	3.49	4	0.8	80	Step to	1.5	80	Step to	2.4	80	Isocratic	-	-	-	-	-	-
12	3.50	4	0.8	80	Step to	1.5	56	Isocratic	1.5	24	0.8	2.3	60	Isocratic	-	-	-
13	3.51	3	0.8	85	Step to	1.5	145	Step to	2.3	190	Step to	5	60	Isocratic	-	-	-
14	3.52	3	0.8	85	Step to	1.5	145	Step to	2.1	190	Step to	5	60	Isocratic	-	-	-
15	3.53	3	0.8	85	Step to	1.5	145	Step to	2.1	250	Isocratic	-	-	-	-	-	-
16	3.54	3	0.8	85	Step to	1.5	145	Step to	2.1	250	Isocratic	-	-	-	-	-	-

2.3.7 Acid Stability

An important consideration for the project was the stability of the resin to the oxidative effects of the nitric acid and radiation. The effects of radiation are not investigated within this thesis as non-radioactive isotopes have been used throughout. However, the effect of acidity on the adsorbents was relatively easy to study. To assess the stability of the adsorbents, they were subjected to an extended period exposed to acid which was substantially stronger than that of the proposed range within the project, in addition to a much longer exposure time.

The stability was assessed by a comparison of ion uptake capacity from treated and untreated adsorbents and resins: a significant difference between the treated and untreated ion capacities would indicate an instability within the resin or adsorbent.

For a more qualitative view, the adsorbents were dried and subjected to an infra-red spectrum: comparison of acid treated and untreated resins and adsorbents would theoretically be able to identify the bonds which have been affected by the acid (22).

The resin or adsorbent of interest was exposed to 250 ml of 7 M HNO_3 for a year. A 10 g sample of the resin or adsorbent was accurately weighed and added to a 250 ml Durran bottle. The 250 ml of 7 M HNO_3 was measured and added to the bottle and the bottle sealed. The bottle was then placed on a sample shaker and rotationally shaken at 200 rpm for an hour three times a week. The bottles were also inverted weekly.

After a year the liquid within the bottle was filtered over a Buckner flask and flushed with 2 l of deionised water. A sample of this wet resin was then tested for Zr (IV) ion capacity in the same manner as described in Section 2.3.4 with the exception that only a 3.0 $g.l^{-1}$ of Zr (IV) concentration was utilised. This ion exchange capacity was directly compared with that of a resin or adsorbent which had not been exposed to acid.

A sample of the acid treated resin or adsorbent was then analysed for moisture content as described in Section 2.3.1 and this result compared to an untreated sample. These dried resins and adsorbents were subsequently assayed by FT-IR as described in Section 2.4.4.

2.4 Experimental Techniques

2.4.1 Inductively Coupled Plasma – Mass Spectrometry

ICP-MS is a technique which can achieve very low detection limits for most elements coupled with high selectivity, accuracy and precision. A small volume of sample is aspirated through an argon plasma. This plasma has a high electron flux and temperature. The torch of the instrument is utilised as both atomiser and ioniser for the liquid sample. The liquid

solvent used is a weak acid solution (in the instrumentation used it is 1 % nitric acid). Due to the high sensitivity of the instrument, the concentration of the analyte is kept relatively low (77).

2.4.2 Infra-Red Spectroscopy

The infra-red region of the spectrum encompasses the wavelengths from 0.78 μm to 1 mm or wavenumbers (number of waves per unit of distance) between 12800 and 10 cm^{-1}. Analytically this is divided into three main regions: “near” between 780 nm and 2.5 μm, “middle” between 2.5 and 50 μm and “far” between 50 and 1000 μm with the majority of analytical spectroscopies using the 2.5 to 20 μm range and it was these wavelengths which were employed within this project (4000 to 500 cm^{-1}).

Infra-red (IR) adsorption or emissions arise from the changes brought about by the change in vibration or rotational energy of the bonds of molecules at different energy levels of the electromagnetic radiation it is exposed to. Due to the relatively low frequency of the IR radiation the energy is insufficient to cause the ionisation or electron transitions seen in ultra violet and even visible spectrometry; it is therefore limited to the small differences between the vibration and rotational energies within molecules and more specifically those where a net change in the dipole is present when it rotates or vibrates. The dipole within a molecule is determined by the distance and magnitude of charge difference between the charge centres. This would affect the electric field of the radiation causing adsorption within the molecule. Consequently any water molecules within the matrix of a sample would adsorb energy. As they constitute a larger proportion of the sample, composition would interfere and likely swamp the desired spectra response and is therefore required to be driven off before the sample spectra could be scanned. The introduction of a Fourier transform (FT) instrument to the IR increases the signal to noise ratio by an order of magnitude and therefore a similar increase in the detection limits of an instrument (78).

2.4.3 Analysis of Samples Using Inductively Coupled Plasma – Mass Spectrometry

For the ion concentration assays used in the majority of the experiments (Sections 2.3.2 to 2.3.7), the samples were diluted prior to their assay. In order to ensure a standard dilution throughout the assay, an internal standard ion (Ba (II)) was also introduced to the dilution solvent. To minimise any systematic error within the diluted sample, a relatively large (200 μl of a total 10 ml or 1/50th of the analysed sample) sample was taken from the experiment liquor. The internal standard of Ba was added in accordance with the method described in

Skoog (79). A constant amount added to each of the samples, blanks and calibration standards. The calibration is then a plot of the ratio of the analyte response to that of the internal standard as a function of the analyte concentration in the standards. The concentration of each of the analytes was then be calculated from this ratio.

The total volume of the sample tube which could be sampled by ICP-MS was 10 ml in volume. This consists of a 200 µl aliquot of the experimental liquor, 200 µl of 50 ppm internal standard of Ba (II) and the remainder to make up the volume of the sample up to 10 ml of 1 % analytical grade nitric acid. The 200 µl aliquots were measured using micropipettes calibrated using deionised water.

Prior to each sequence of assays a calibration was performed with each of the ions of interest. The concentration of which was based on the maximum possible concentration of the ion expected within the sample. The nominal value of this was to be 500 ppm. The concentrations within the calibration standards were set at 0, 150, 500, 850 and 1000 ppm (0, 30, 100, 140 and 200 % of the nominal value) following the calibration method described by Miller and Miller (80). The regression analysis of this calibration curve was required to achieve above an r^2 of 0.999 to be used in the thesis.

For each of the experimental conditions, (i.e. nitric acid concentration or temperature) two samples were taken for assay. The experimental conditions were also completed in duplicate and in some cases in triplicate depending on the standard deviation of the results. This regime gave a minimum of four data points for each of the experimental conditions to maximise accuracy.

A number of further blanks were also assayed within the sample sequence; these consisted of 200 µl of the internal standard and 200 µl of the acid utilised within the experiment, this was made up to 10 ml sample volume with the 1 % nitric acid. These were interspersed within the assay run after every five samples. These were used as the baseline concentration for the ions and used in the concentration calculation within the PlasmaLab software for each of the sample assays. It was also used as a confirmation test that the instrumentation was working to the calibration. In addition, between each of the assays, a 45 second wash of fresh 1 % nitric acid was applied, with a subsequent 30 second uptake of the sample before the assay measurement procedure began.

The mass spectrometer was set to scan between each of the ions with mass charge ratios (m/z) with a multiple ion monitoring of the most abundant isotope mass for each ion used within the experiment, a dwell time of 5 ms was used for each m/z ratio.

2.4.4 Analysis of Samples Using Infra-Red

Analysis by FT-IR of the resins and adsorbent was only performed in Section 2.3.7, the adsorbent to be assayed was crushed to a powder, in a mortar and pestle in order to increase the surface area, and dried for four days at 105 ˚C in an oven with manual mild agitation to ensure no clumping occurred between the particles. The instrument was then calibrated and blanked using a polystyrene standard. A sample of the powder was then placed on the sampler and clamped in place. This was then scanned and repeated for each sample with the acid treated and untreated variants of each adsorbent, then plot on the same spectra of absorbance against wavenumber for comparison.

3. Results and Discussion

3.1 Moisture Retention

Throughout this thesis ion exchange capacities have been reported as $mg.g^{-1}$ of wet resin (as received). However, in order that this could be reported with a reasonable degree of accuracy throughout the duration of the work it was essential that the resin was monitored periodically to ensure no significant changes have occurred. The moisture content was determined as previously described in Section 2.3.1. The moisture content was determined upon initial receipt of the resin or adsorbent (month 1) Table 3.1.

The resins were reanalysed for moisture content at month 22 for the resins and month 15 for the adsorbents; the results are contained in Table 3.2.

Table 3.1 Moisture Content of Adsorbents and Resins upon Receipt

Resin	Wet Resin Mass (g)	48 Hours Air Dried Mass (g)	120 hours Oven Dried Mass (g)	Percent Lost to Air Dry (%)	Percent Mass Lost Total (%)	Average Moisture Loss (%)	Standard Deviation
C100H	2.7809	1.7821	1.2808	35.92	53.94		
	2.6218	1.6895	1.2131	35.56	53.73	53.84	0.15
C100x10	2.5731	1.9226	1.5613	25.28	39.32		
MBH	2.6419	1.9739	1.6026	25.28	39.34	39.33	0.01
C100x16	2.6032	2.3074	1.6774	11.36	35.56		
MBH	2.6404	2.2817	1.7046	13.59	35.44	35.50	0.09
C150H	2.5548	1.4755	1.0966	42.25	57.08		
	2.5653	1.4616	1.1017	43.02	57.05	57.07	0.02
C160H	2.5591	1.7671	1.3383	30.95	47.70		
	2.5429	1.7458	1.3257	31.35	47.87	47.79	0.11
D5529	2.4891	1.4366	1.3539	42.28	45.61		
	2.5583	1.4652	1.3886	42.73	45.72	45.66	0.08
D5530	2.5245	1.7019	1.5944	32.58	36.84		
	2.4857	1.6732	1.5662	32.69	36.99	36.92	0.11
G26	2.4023	1.8526	1.3242	22.88	44.88		
	2.3975	1.8575	1.3222	22.52	44.85	44.86	0.02
S910	2.5761	1.4446	1.0704	43.92	58.45		
	2.4846	1.3995	1.0373	43.67	58.25	58.35	0.14
S930	2.5097	1.4828	1.2286	40.92	51.05		
	2.5111	1.4842	1.2382	40.89	50.69	50.87	0.25
S940	2.5622	1.4228	1.2655	44.47	50.61		
	2.4804	1.3706	1.2208	44.74	50.78	50.70	0.12
S950	2.5043	1.4068	1.27	43.82	49.29		
	2.4576	1.3737	1.2406	44.10	49.52	49.40	0.16

Table 3.2 Moisture Content of Adsorbents and Resins at Conclusion of Experiments

Resin	Wet Resin Mass (g)	48 Hours Air Dried Mass (g)	120 hours Oven Dried Mass (g)	Percent Lost to Air Dry (%)	Percent Mass Lost Total (%)	Average Moisture Loss (%)	Standard Deviation
C100H	0.5532	0.5100	0.3941	7.81	28.76		
	0.5452	0.5039	0.3920	7.58	28.10	28.43	0.47
C100x10	0.5053	0.4899	0.3929	3.05	22.24		
MBH	0.5257	0.5060	0.4068	3.75	22.62	22.43	0.26
C100x16	0.4858	0.4820	0.3633	0.78	25.22		
MBH	0.5040	0.5009	0.3765	0.62	25.30	25.26	0.06
C150H	0.5113	0.2830	0.2601	44.65	49.13		
	0.5269	0.2932	0.2713	44.35	48.51	48.82	0.44
C160H	0.5234	0.2646	0.2440	49.45	53.38		
	0.5053	0.2535	0.2341	49.83	53.67	53.53	0.20
D5529	0.4994	0.3184	0.2984	36.24	40.25		
	0.4936	0.3144	0.2946	36.30	40.32	40.28	0.05
D5530	0.4994	0.3547	0.3547	28.97	28.97		
	0.5111	0.3596	0.3386	29.64	33.75	31.36	3.38
G26	0.5832	0.4699	0.3809	19.43	34.69		
	0.4956	0.3979	0.3226	19.71	34.91	34.80	0.16
S910	0.5548	0.3052	0.2461	44.99	55.64		
	0.5014	0.2744	0.2232	45.27	55.48	55.56	0.11
S930	0.5215	0.3297	0.2640	36.78	49.38		
Plus	0.5175	0.3224	0.2558	37.70	50.57	49.97	0.84
S940	0.4772	0.2650	0.2438	44.47	48.91		
	0.5734	0.3218	0.2965	43.88	48.29	48.60	0.44
S950	0.5226	0.3630	0.3209	30.54	38.60		
	0.5005	0.3467	0.3067	30.73	38.72	38.66	0.09

The difference in moisture content of the resins and adsorbents was measured at the start and at completion of the experimental cycles is contained in Table 3.3.

Table 3.3 Percentage Change in Moisture Contents

Resin	Percentage Difference (%)
C100H	-25.4
C100X10MBH	-16.9
C100X16MBH	-10.3
C150H	-8.3
C160H	5.74
D5529	-5.4
D5530	-5.6
G26	-10.1
S910	-2.8
S930Plus	-0.9
S940	-2.1
S950	-10.8

The sulfonic acid resins C100H (25.4 %), C100X10MBH (16.9 %) and C100X16MBH (10.2 %) exhibited a significant loss of moisture content, this was inversely proportional to the extent of cross linking (71). This may be a consequence of the lower cross-linked resins having a greater initial water content and hence the potential for a greater loss of water throughout the period of investigation. While the extent of cross-linking is unknown (but

assumed to be greater than 16 % due to the macroporous structure) for the other sulfonic acid resins, namely C150H and C160H, they followed similar trend to that described above. The moisture loss of the G26 was not as expected. This resin has a similar structure and cross-linking to that of C100H but displayed a much lower difference in moisture contents. This may be a result of the initial moisture contents being lower in the G26 (44.9 % compared to the 53.8 % of the C100H), the less frequent use of the G26 within the project and the different containers in which the resins were supplied in and subsequently stored may have also been a factor.

Both the amidoxime (S910) and the iminodiacetic acid resins (S930Plus) lost less water throughout the duration of the experimental programme despite ~ 50% of their initial weight being due to absorbed water. Therefore it could be concluded that the water was more tightly bound to these resins than the sulfonic acid resins.

The S940 and S950 aminophosphonic acid resins displayed a significant difference between one another in moisture content. According to the literature from Purolite, the resins differ in their ability to discriminate between the atomic mass (70). The S940 is able to exchange a wider atomic weight range than the S950. The S950 range is focused on higher atomic weights. No information was given regarding the extent of crosslinking or DVB present within the structure and it was again difficult to speculate to a link between the amount of crosslinking and water retention within the resin. It may be ventured however, that the S950 has a more open structure than that of the S940 to accommodate the ions with the higher atomic weights. This more open structure may explain the difference between the moisture retentions of the two resins.

The inorganic adsorbents contained significant quantities of water (37- 47 %) however they did not significantly dehydrate over the course of the experimental programme.

As a consequence of this study the masses of resins used in Section 2.3.3 and 2.3.4 was corrected to ensure a consistent number of ion exchange sites were used in each experiment as described in Section 3.3.

3.2 Ion Exchange Capacity as a Function of Acidity

The performance of the resins and adsorbents was evaluated as a function of their selectivity co-efficient for Zr (IV) and Ce (IV) and as described in Section 2.3.2. A selectivity co-efficient of greater than 2.0 in a solution of 3 M HNO_3 was the threshold value, materials exhibiting a value greater than 2.0 were deemed worthy of further investigation.

The variation of ion exchange capacity as a function of nitric acid concentration is contained in Tables 3.4 to 3.15 and represented graphically in Figures 3.1 to 3.12.

3.2.1 Inorganic Absorbents

Materials D5529 and D5530 are both inorganic absorbents which have been independently trialled for the removal of radioactive ions from wastewater streams from the Fukushima site in Japan and supplied by Purolite.

Table 3.4 contains the data for adsorbent D5529 and shown graphically in Figure 3.1. This is a commercial material and the chemical composition was not disclosed. This material leeched significant quantities of zirconium and consequently the data for this ion has not been reported. The results for D5530 are contained in Table 3.5 and Figure 3.2. Notably this material did not appear to leach zirconium and consequently this data is recorded.

The data for these two media was collected from an original experiment and a single repeat, the results for each of the ions tested were compiled from four samples, this comprised two aliquots, being taken from both the original experiment and the repeat. Within the ICP-MS, the aliquots were subjected to three “passes”, where an assay was performed for each of the ions and the figure from these passes averaged, to give a single concentration for each of the four samples.

For the D5529 media, the average standard deviation for all of the ions across the whole of the HNO_3 concentrations was 1.42 % which gave an average 95 % confidence limit of +/- 2.77 %. Confidence limits were calculated with n-1 degrees of freedom.

For the D5530 media, the average standard deviation for all of the ions across the whole of the HNO_3 concentrations was 2.8 % which gave an average 95 % confidence limit of +/- 5.56 %.

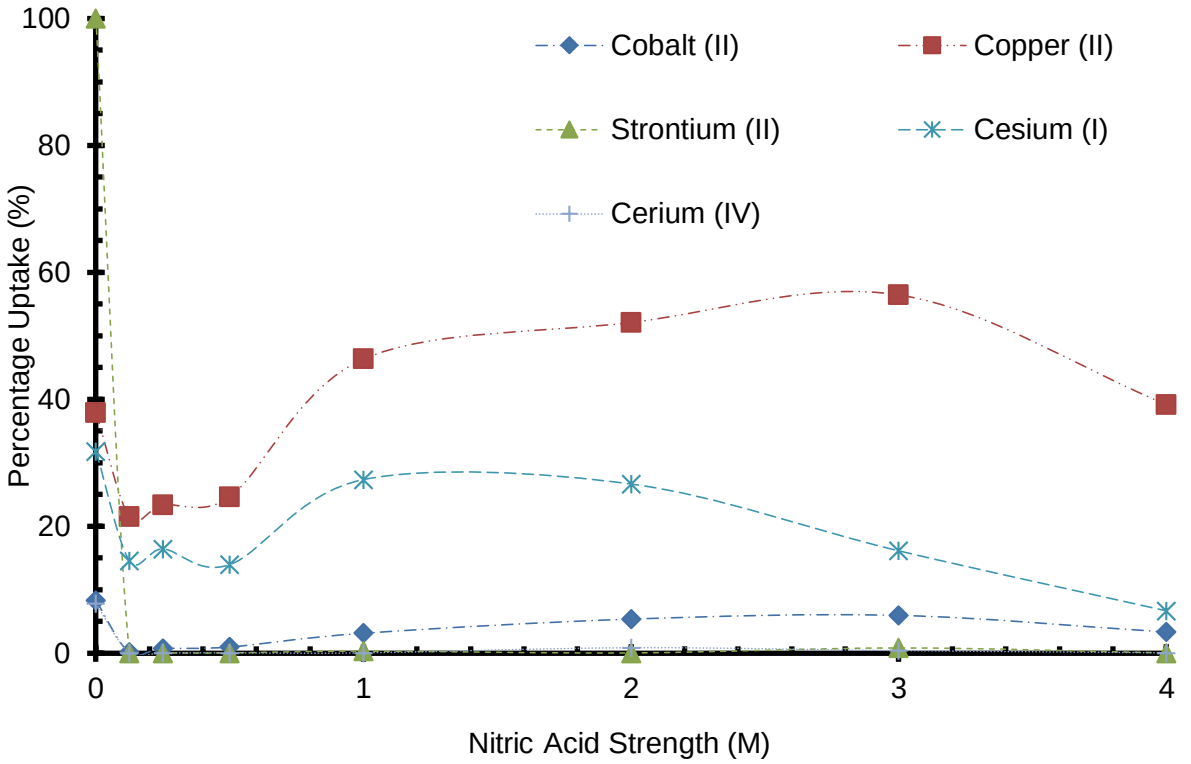

Figure 3.1 Ion Exchange Capacity as a Function of Acidity for D5529

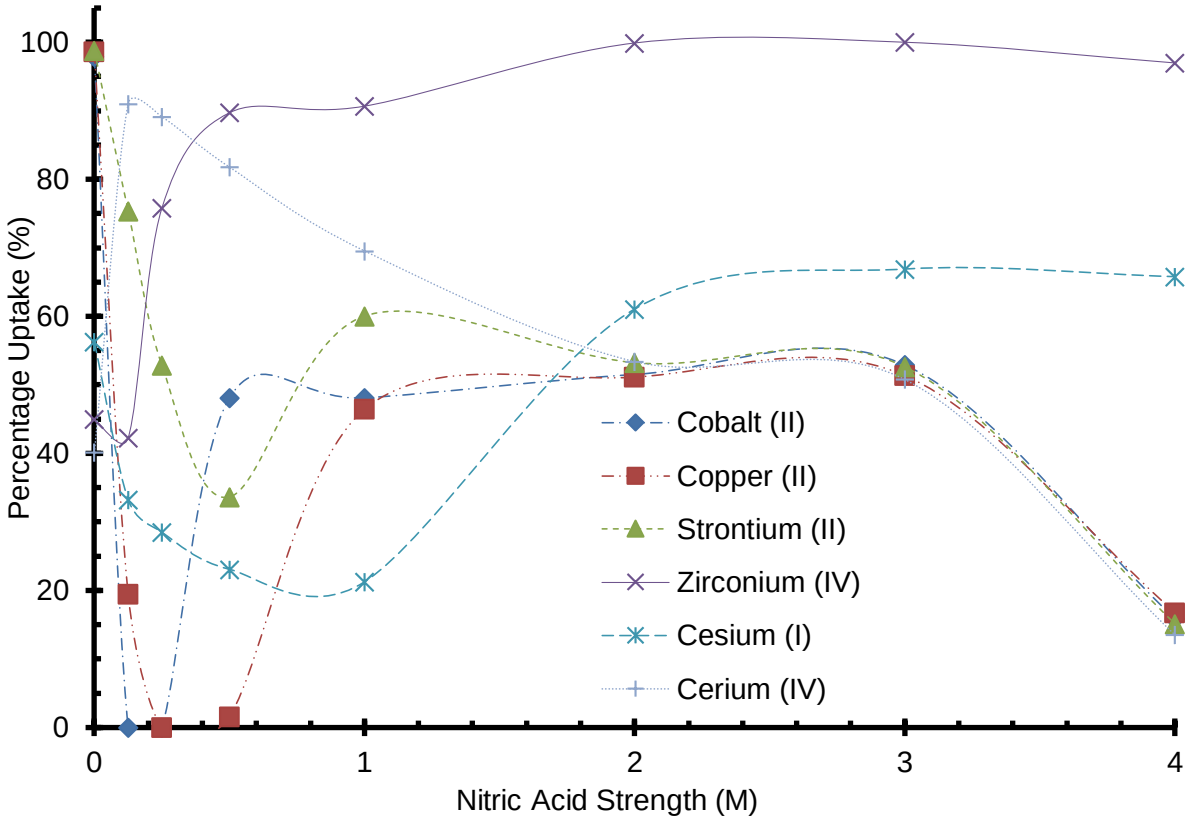

Figure 3.2 Ion Exchange Capacity as a Function of Acidity for D5530

Table 3.4 Ion Exchange Capacity as a Function of Acidity for D5529

Acid Strength (M)	Ion	Distribution Constant (K)	Selectivity Co-efficient (α) Co	Cu	Sr	Cs	Ce (IV)
0	Co (II)	0.09	-	0.15	0.00	0.19	1.07
	Cu (II)	0.61	6.77	-	0.00	1.31	7.24
	Sr (II)	∞	∞	∞	-	∞	∞
	Cs (I)	0.47	5.17	0.76	0.00	-	5.53
	Ce (IV)	0.08	0.93	0.14	0.00	0.18	-
0.125	Co (II)	0.00	-	0.00	∞	0.01	∞
	Cu (II)	0.27	303.68	-	∞	1.61	∞
	Sr (II)	0.00	0.00	0.00	-	0.00	∞
	Cs (I)	0.17	188.57	0.62	∞	-	∞
	Ce (IV)	0.00	0.00	0.00	∞	0.00	-
0.25	Co (II)	0.01	-	0.02	∞	0.04	∞
	Cu (II)	0.30	42.58	-	∞	1.56	∞
	Sr (II)	0.00	0.00	0.00	-	0.00	∞
	Cs (I)	0.20	27.37	0.64	∞	-	∞
	Ce (IV)	0.00	0.00	0.00	∞	0.00	-
0.5	Co (II)	0.01	-	0.03	∞	0.06	∞
	Cu (II)	0.33	33.59	-	∞	2.02	∞
	Sr (II)	0.00	0.00	0.00	-	0.00	∞
	Cs (I)	0.16	16.66	0.50	∞	-	∞
	Ce (IV)	0.00	0.00	0.00	∞	0.00	-
1	Co (II)	0.03	-	0.04	11.51	0.09	∞
	Cu (II)	0.86	26.74	-	307.68	2.30	∞
	Sr (II)	0.00	0.09	0.00	-	0.01	∞
	Cs (I)	0.38	11.63	0.43	133.80	-	∞
	Ce (IV)	0.00	0.00	0.00	0.00	0.00	-
2	Co (II)	0.06	-	0.05	∞	0.16	6.94
	Cu (II)	1.09	19.21	-	∞	3.00	133.25
	Sr (II)	0.00	0.00	0.00	-	0.00	0.00
	Cs (I)	0.36	6.40	0.33	∞	-	44.38
	Ce (IV)	0.01	0.14	0.01	∞	0.02	-
3	Co (II)	0.06	-	0.05	8.03	0.33	17.48
	Cu (II)	1.30	20.53	-	164.95	6.77	358.91
	Sr (II)	0.01	0.12	0.01	-	0.04	2.18
	Cs (I)	0.19	3.03	0.15	24.36	-	52.99
	Ce (IV)	0.00	0.06	0.00	0.46	0.02	-
4	Co (II)	0.03	-	0.05	∞	0.49	∞
	Cu (II)	0.64	18.74	-	∞	9.09	∞
	Sr (II)	0.00	0.00	0.00	-	0.00	∞
	Cs (I)	0.07	2.06	0.11	∞	-	∞
	Ce (IV)	0.00	0.00	0.00	∞	0.00	-

Table 3.5 Ion Exchange Capacity as a Function of Acidity for D5530

Acid Strength (M)	Ion	Distribution Constant (K)	Selectivity Co-efficient (α) Co	Cu	Sr	Zr	Cs	Ce (IV)
	Co (II)	46.39	-	0.66	0.57	56.77	36.01	69.16
	Cu (II)	70.43	1.52	-	0.87	86.18	54.67	104.99
	Sr (II)	80.97	1.75	1.15	-	99.08	62.85	120.69
0	Zr (IV)	0.82	0.02	0.01	0.01	-	0.63	1.22
	Cs (I)	1.29	0.03	0.02	0.02	1.58	-	1.92
	Ce (IV)	0.67	0.01	0.01	0.01	0.82	0.52	-
	Co (II)	0.00	-	0.00	0.00	0.00	0.00	0.00
	Cu (II)	0.24	∞	-	0.08	0.33	0.49	0.02
	Sr (II)	3.06	∞	12.65	-	4.18	6.15	0.30
0.125	Zr (IV)	0.73	∞	3.02	0.24	-	1.47	0.07
	Cs (I)	0.50	∞	2.06	0.16	0.68	-	0.05
	Ce (IV)	10.07	∞	41.67	3.29	13.78	20.24	-
	Co (II)	0.00	-	∞	0.00	0.00	0.00	0.00
	Cu (II)	0.00	∞	-	0.00	0.00	0.00	0.00
	Sr (II)	1.12	∞	∞	-	0.36	2.82	0.14
0.25	Zr (IV)	3.13	∞	∞	2.79	-	7.86	0.38
	Cs (I)	0.40	∞	∞	0.35	0.13	-	0.05
	Ce (IV)	8.16	∞	∞	7.28	2.61	20.51	-
	Co (II)	0.93	-	58.91	1.83	0.11	3.09	0.21
	Cu (II)	0.02	0.02	-	0.03	0.00	0.05	0.00
	Sr (II)	0.51	0.55	32.16	-	0.06	1.69	0.11
0.5	Zr (IV)	8.71	9.39	553.15	17.20	-	29.06	1.94
	Cs (I)	0.30	0.32	19.04	0.59	0.03	-	0.07
	Ce (IV)	4.48	4.83	284.71	8.85	0.51	14.96	-
	Co (II)	0.93	-	1.07	0.62	0.10	3.44	0.41
	Cu (II)	0.87	0.93	-	0.58	0.09	3.22	0.38
	Sr (II)	1.50	1.62	1.73	-	0.15	5.57	0.66
1	Zr (IV)	9.72	10.48	11.21	6.47	-	36.06	4.26
	Cs (I)	0.27	0.29	0.31	0.18	0.03	-	0.12
	Ce (IV)	2.28	2.46	2.63	1.52	0.23	8.47	-
	Co (II)	1.06	-	1.02	0.94	0.00	0.68	0.93
	Cu (II)	1.05	0.98	-	0.92	0.00	0.67	0.91
	Sr (II)	1.14	1.07	1.09	-	0.00	0.73	0.99
2	Zr (IV)	908.09	854.17	868.30	798.85	-	579.61	792.77
	Cs (I)	1.57	1.47	1.50	1.38	0.00	-	1.37
	Ce (IV)	1.15	1.08	1.10	1.01	0.00	0.73	-
	Co (II)	1.12	-	1.06	1.01	0.00	0.56	1.09
	Cu (II)	1.06	0.94	-	0.95	0.00	0.52	1.02
	Sr (II)	1.11	0.99	1.05	-	0.00	0.55	1.08
3	Zr (IV)	∞	∞	∞	∞	-	∞	∞
	Cs (I)	2.02	1.80	1.91	1.82	0.00	-	1.96
	Ce (IV)	1.03	0.92	0.98	0.93	0.00	0.51	-
	Co (II)	0.19	-	0.94	1.06	0.01	0.10	1.20
	Cu (II)	0.20	1.07	-	1.13	0.01	0.10	1.28
	Sr (II)	0.18	0.94	0.89	-	0.01	0.09	1.14
4	Zr (IV)	32.11	170.36	159.83	180.55	-	16.72	205.23
	Cs (I)	1.92	10.19	9.56	10.80	0.06	-	12.27
	Ce (IV)	0.16	0.83	0.78	0.88	0.00	0.08	-

In the broadest terms, the aim of the project was to separate the Ce (IV) ion (as a surrogate for U and Pu (IV)) from the Cs (I), Sr (II) and Zr (IV), the radioactive ions which cause the largest heat load to the storage of the irradiated fuel and which have the highest concentration within the irradiated fuel liquor (Table 1.1). Using a commercial ion exchange resin for a chromatographic separation should ensure that the quality assurance has been performed with respect to bead size and shape, capacity and therefore predictability. This was the most important characteristic of the adsorbents. This predictability of the adsorbents was also important when deciding on the conditions which would mean the adsorbent was subject to further experimentation or disregarded. The major factor and ultimately the one used for all of the adsorbents would be based on the separation factor between two of the major ions. The separation factor chosen was that between Ce (IV) from Zr (IV).

Unfortunately the structure or indeed the chemical composition of the adsorbents was unknown, which added complexity to the discussion of the results. The performance of the two adsorbents differed significantly in that for D5529 excessive amounts of Zr (IV) leeching was observed throughout the experiments. This adsorbent was therefore eliminated from any further experimental use within the project due to its instability at the elevated acid concentration and therefore not displaying a large enough separation factor between the Ce (IV) and Zr (IV) ions. Although not of use with the current restrictions imposed for a separation between Ce (IV) and Zr (IV) within this project, the uptake of Cs (I) over a wide range of HNO_3 concentrations may be of use. This was especially usefully when compared to the minimal uptake of Ce (IV). The Cs (I) uptake might be at the expense of the Zr (IV) ions within the adsorbent media, instead of the H^+ ions as was expected for the acidic exchangers. However as the composition of the media is unknown it was difficult to develop with any certainty this supposition.

As all of the experiments were performed on fresh adsorbents, it was impossible to know if the adsorbent could be re-generated with a concentrated Zr (IV) solution or once the ion exchange had occurred, the adsorbent would remain exhausted. Both of these situations could be exploited depending on the separation required. If the Cs (I) was to remain bound to the absorbent, with no regeneration possible with either an acidic or Zr (IV) rich solution and the other ions were unretained by the adsorbent, a separation had occurred. Due to the low concentration of the Cs ion within the irradiated fuel feed, a relatively large volume of this liquor could be processed for a small volume of this D5529 media. On the other hand if the media was able to be regenerated by either H^+ or Zr (IV) ions in solution, then it would be possible to perform a separation.

D5530 exhibited uptake of most of the ions over a wide range of acid concentrations (Figure 3.2). Although most ions displayed a dip in uptake as the concentration increases to the maximum tested at 4 M HNO_3, the Zr (IV) displayed a high uptake throughout the 0.5 to 4 M range, with a minimum at the 0.125 M concentration. With the exception of Ce (III) and (IV), the other ions displayed a similar uptake with minima at 0.5 M, a plateau between 1 and 3 M before a reduced uptake at 4 M.

A potential issue with this uptake graph was the consistently high uptake of the Zr above 0.25 M. Although it means that the likelihood of a satisfactory separation factor was observed, it was also indicative of a possible problem when it comes to releasing the ion from the media at a later stage, such as the media regeneration with strong nitric acid, which would have repercussions on media oxidation and the ability to perform a chromatographic separation.

As observed in the selectivity factors (Table 3.5), the Zr (IV) to Ce (IV) ratio was consistently and massively above the self-imposed value of 2, not just at the 3 M HNO_3 concentration. The media was therefore considered for use within the project and was subjected to further testing to assess its value.

3.2.2 Chelating Resins

The chelating resins studied were S910, S930Plus, S940 and S950 which were supplied by Purolite. The ion exchange capacity as a function of nitric acid strength for this series of resins are reported in Tables 3.6 to 3.9 and depicted graphically in Figures 3.3 to 3.6.

The data for these four resins was collected from an original experiment and two repeats, the results for each of the ions tested were compiled from six samples, this comprised two aliquots, being taken from both the original experiment and each of the repeats. Within the ICP-MS, the aliquots were subjected to three “passes”, where an assay was performed for each of the ions and the figure from these passes averaged, to give a single concentration for each of the six samples.

For the S910 resin, the average standard deviation for all of the ions across the whole of the HNO_3 concentrations was 4.09 %, which gave an average 95 % confidence limit of +/- 8.01 %. Confidence limits were calculated with n-1 degrees of freedom.

For the S930Plus, the average standard deviation for all of the ions across the whole of the HNO_3 concentrations was 2.64 %, which gave an average 95 % confidence limit of +/- 5.17 %.

For the S940, the average standard deviation for all of the ions across the whole of the HNO_3 concentrations was 1.34 %, which gave an average 95 % confidence limit of +/- 2.63 %.

For the S950 resin, the average standard deviation for all of the ions across the whole of the HNO_3 concentrations was 1.14 %, which gave an average 95 % confidence limit of +/- 2.23 %.

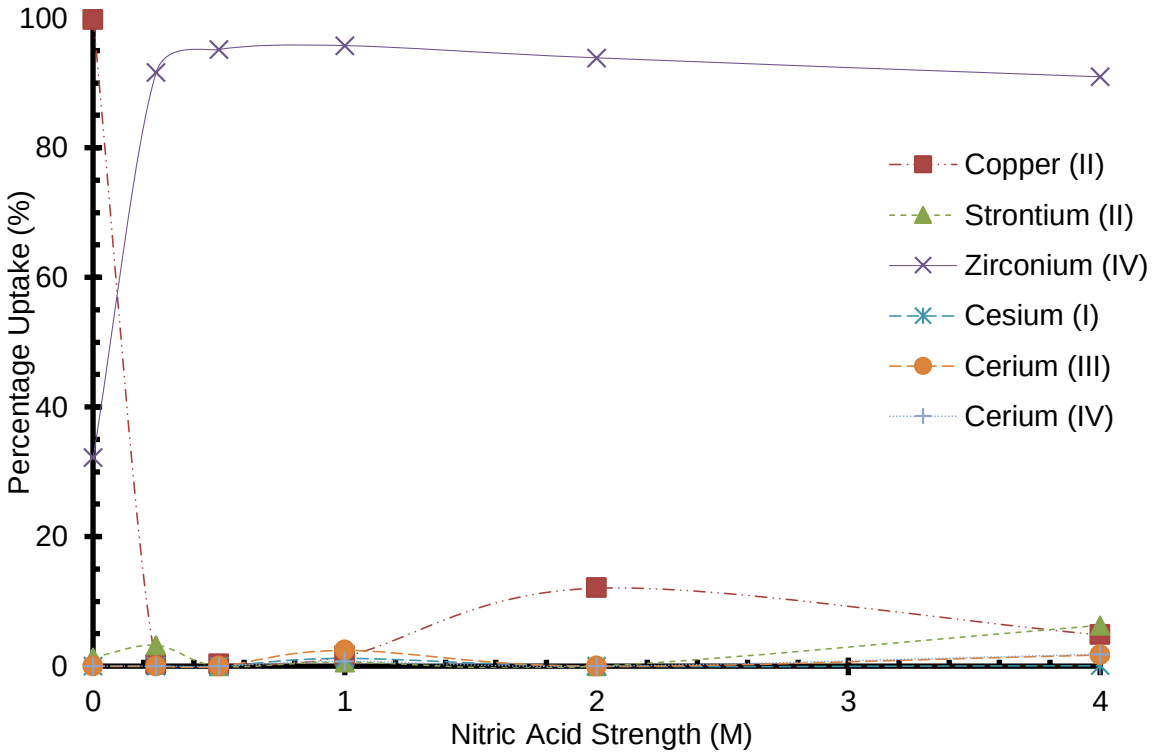

Figure 3.3 Ion Exchange Capacity as a Function of Acidity for S910

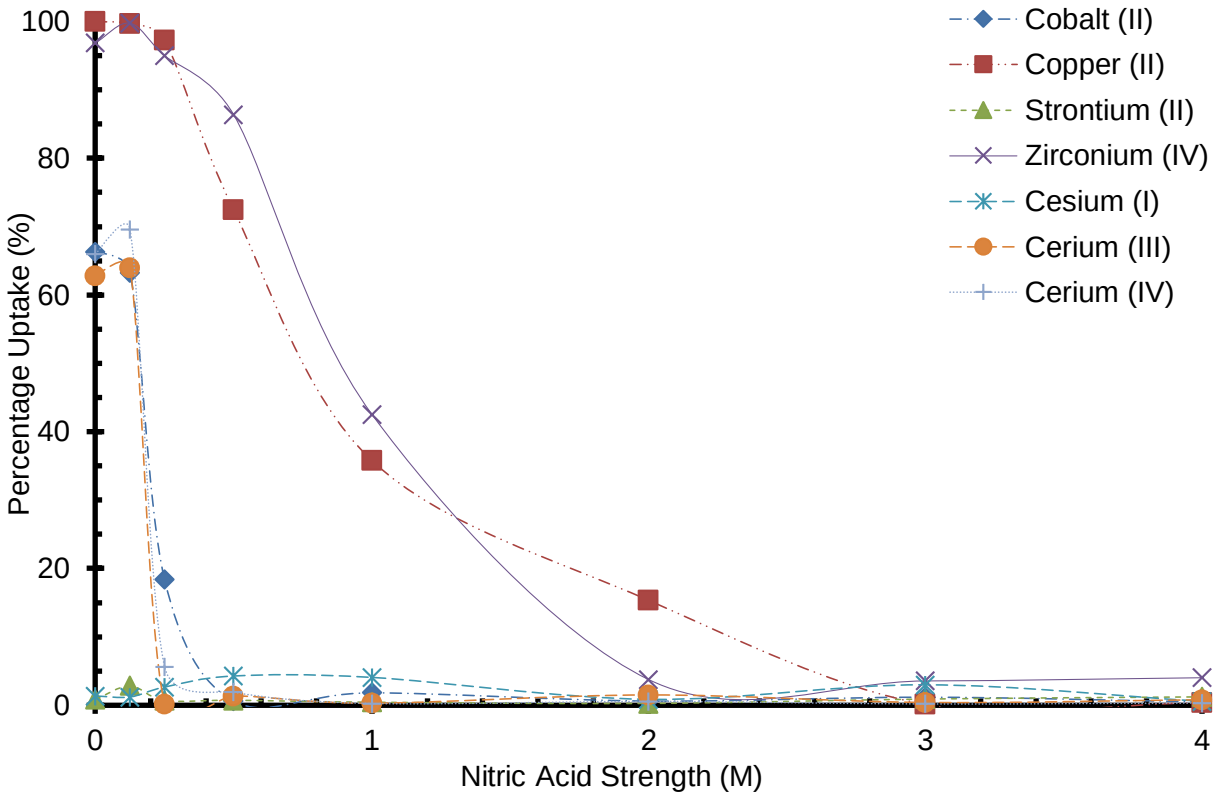

Figure 3.4 Ion Exchange Capacity as a Function of Acidity forS930Plus

Table 3.6 Ion Exchange Capacity as a Function of Acidity for S910

Acid Strength (M)	Ion	Distribution Constant (K)	Selectivity Co-efficient (α) Co (II)	Sr	Zr	Cs	Ce (III)	Ce (IV)
0	Co(II)	416	-	30148	876	∞	∞	∞
	Sr (II)	0.01	0.00	-	0.03	∞	∞	∞
	Zr (IV)	0.47	0.00	34.4	-	∞	∞	∞
	Cs (I)	0.00	0.00	0.00	0.00	-	∞	∞
	Ce (III)	0.00	0.00	0.00	0.00	∞	-	∞
	Ce (IV)	0.00	0.00	0.00	0.00	∞	∞	-
0.25	Co(II)	0.00	-	0.08	0.00	∞	∞	∞
	Sr (II)	0.03	13.3	-	0.00	∞	∞	∞
	Zr (IV)	10.9	4345.4	327.3	-	∞	∞	∞
	Cs (I)	0.00	0.00	0.00	0.00	-	∞	∞
	Ce (III)	0.00	0.00	0.00	0.00	∞	-	∞
	Ce (IV)	0.00	0.00	0.00	0.00	∞	∞	-
0.5	Co(II)	0.00	-	∞	0.00	∞	∞	∞
	Sr (II)	0.00	0.00	-	0.00	∞	∞	∞
	Zr (IV)	19.7	5465.50	∞	-	∞	∞	∞
	Cs (I)	0.00	0.00	∞	0.00	-	∞	∞
	Ce (III)	0.00	0.00	∞	0.00	∞	-	∞
	Ce (IV)	0.00	0.00	∞	0.00	∞	∞	-
1	Co(II)	0.02	-	2.55	0.00	1.30	0.64	2.06
	Sr (II)	0.01	0.39	-	0.00	0.51	0.25	0.81
	Zr (IV)	22.6	1401	3571	-	1818	890	2880
	Cs (I)	0.01	0.77	1.96	0.00	-	0.49	1.58
	Ce (III)	0.03	1.57	4.01	0.00	2.04	-	3.23
	Ce (IV)	0.01	0.49	1.24	0.00	0.63	0.31	-
2	Co(II)	0.14	-	∞	0.01	∞	∞	∞
	Sr (II)	0.00	0.00	-	0.00	∞	∞	∞
	Zr (IV)	15.3	111.65	∞	-	∞	∞	∞
	Cs (I)	0.00	0.00	∞	0.00	-	∞	∞
	Ce (III)	0.00	0.00	∞	0.00	∞	-	∞
	Ce (IV)	0.00	0.00	∞	0.00	∞	∞	-
4	Co(II)	0.05	-	0.76	0.01	72.9	2.83	2.71
	Sr (II)	0.07	1.31	-	0.01	95.8	3.73	3.56
	Zr (IV)	10.0	197	150	-	14347	558	533
	Cs (I)	0.00	0.01	0.01	0.00	-	0.04	0.04
	Ce (III)	0.02	0.35	0.27	0.00	25.7	-	0.96
	Ce (IV)	0.02	0.37	0.28	0.00	26.9	1.05	-

Table 3.7 Ion Exchange Capacity as a Function of Acidity for S930Plus

Acid Strength (M)	Ion	Distribution Constant (K)	Selectivity Co-efficient (α) Co	Cu	Sr	Zr	Cs	Ce (III)	Ce (IV)
	Co (II)	1.97	-	∞	232	0.06	147	1.17	1.02
	Cu (II)	∞	∞	-	∞	∞	∞	∞	∞
	Sr (II)	0.01	0.00	∞	-	0.00	0.63	0.01	0.00
0	Zr (IV)	30.6	15.6	∞	3618	-	2291	18.2	15.8
	Cs (I)	0.01	0.01	∞	1.58	0.00	-	0.01	0.01
	Ce (III)	1.69	0.86	∞	199	0.06	126	-	0.87
	Ce (IV)	1.94	0.98	∞	229	0.06	145	1.15	-
	Co (II)	1.72	-	0.01	58.7	0.00	144	0.97	0.75
	Cu (II)	302	175	-	10296	0.79	25294	170	132
	Sr (II)	0.03	0.02	0.00	-	0.00	2.46	0.02	0.01
0.125	Zr (IV)	384	223	1.27	13077	-	32126	216	168
	Cs (I)	0.01	0.01	0.00	0.41	0.00	-	0.01	0.01
	Ce (III)	1.78	1.03	0.01	60.6	0.00	149	-	0.78
	Ce (IV)	2.29	1.33	0.01	78.0	0.01	192	1.29	-
	Co (II)	0.23	-	0.01	31.97	0.01	8.31	188	3.77
	Cu (II)	35.6	158	-	5054	1.88	1314	29656	596
	Sr (II)	0.01	0.03	0.00	-	0.00	0.26	5.87	0.12
0.25	Zr (IV)	19.0	84.3	0.53	2695	-	701	15814	318
	Cs (I)	0.03	0.12	0.00	3.85	0.00	-	22.6	0.45
	Ce (III)	0.00	0.01	0.00	0.17	0.00	0.04	-	0.02
	Ce (IV)	0.06	0.27	0.00	8.48	0.00	2.20	49.7	-
	Co (II)	0.01	-	0.00	0.86	0.00	0.14	0.47	0.33
	Cu (II)	2.63	415	-	357	0.41	58.78	195	135
	Sr (II)	0.01	1.16	0.00	-	0.00	0.16	0.55	0.38
0.5	Zr (IV)	6.34	1000	2.41	862	-	142	471	326
	Cs (I)	0.04	7.05	0.02	6.08	0.01	-	3.32	2.30
	Ce (III)	0.01	2.13	0.01	1.83	0.00	0.30	-	0.69
	Ce (IV)	0.02	3.07	0.01	2.65	0.00	0.44	1.44	-
	Co (II)	0.02	-	0.03	4.22	0.03	0.44	6.89	7.15
	Cu (II)	0.56	29.9	-	126	0.75	13.1	206	214
	Sr (II)	0.00	0.24	0.01	-	0.01	0.10	1.63	1.70
1	Zr (IV)	0.74	39.7	1.33	168	-	17.4	273	284
	Cs (I)	0.04	2.28	0.08	9.60	0.06	-	15.7	16.3
	Ce (III)	0.00	0.15	0.00	0.61	0.00	0.06	-	1.04
	Ce (IV)	0.00	0.14	0.00	0.59	0.00	0.06	0.96	-
	Co (II)	0.01	-	0.03	2.43	0.16	0.76	0.42	1.13
	Cu (II)	0.18	28.6	-	69.6	4.64	21.7	12.1	32.2
	Sr (II)	0.00	0.41	0.01	-	0.07	0.31	0.17	0.46
2	Zr (IV)	0.04	6.16	0.22	15.0	-	4.67	2.60	6.94
	Cs (I)	0.01	1.32	0.05	3.21	0.21	-	0.56	1.49
	Ce (III)	0.02	2.37	0.08	5.76	0.38	1.79	-	2.67
	Ce (IV)	0.01	0.89	0.03	2.16	0.14	0.67	0.37	-
	Co (II)	0.01	-	10.0	1.31	0.33	0.39	3.16	6.33
	Cu (II)	0.00	0.10	-	0.13	0.03	0.04	0.31	0.63
	Sr (II)	0.01	0.76	7.64	-	0.25	0.30	2.41	4.82
3	Zr (IV)	0.04	3.06	30.6	4.01	-	1.20	9.65	19.3
	Cs (I)	0.03	2.55	25.6	3.34	0.83	-	8.05	16.1
	Ce (III)	0.00	0.32	3.17	0.42	0.10	0.12	-	2.00
	Ce (IV)	0.00	0.16	1.58	0.21	0.05	0.06	0.50	-
	Co (II)	0.01	-	1.31	0.41	0.12	0.94	0.65	1.55
	Cu (II)	0.00	0.76	-	0.31	0.09	0.72	0.50	1.18
	Sr (II)	0.01	2.43	3.18	-	0.30	2.29	1.58	3.76
4	Zr (IV)	0.04	8.17	10.7	3.36	-	7.71	5.33	12.7
	Cs (I)	0.01	1.06	1.39	0.44	0.13	-	0.69	1.64
	Ce (III)	0.01	1.53	2.01	0.63	0.19	1.45	-	2.37
	Ce (IV)	0.00	0.65	0.85	0.27	0.08	0.61	0.42	-

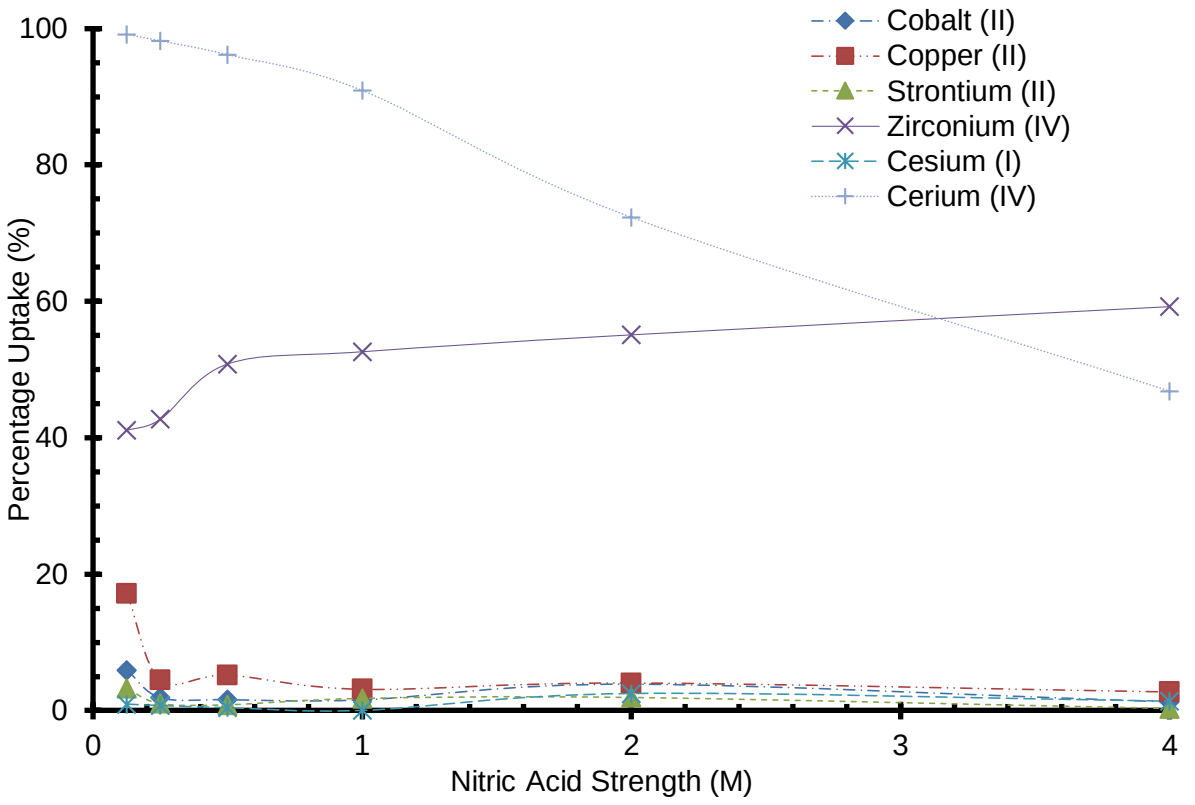

Figure 3.5 Ion Exchange Capacity as a Function of Acidity for S940

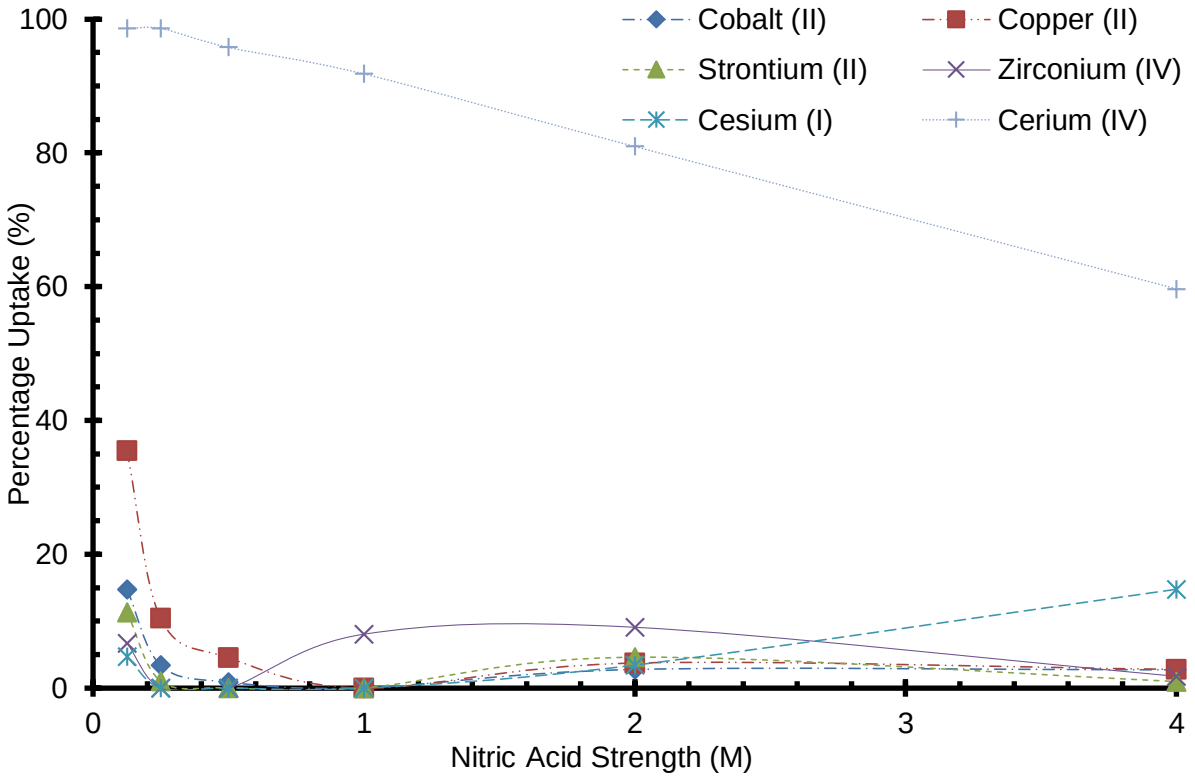

Figure 3.6 Ion Exchange Capacity as a Function of Acidity for S950

Table 3.8 Ion Exchange Capacity as a Function of Acidity for S940

Acid Strength (M)	Ion	Distribution Constant (K)	Selectivity Co-efficient (α) Co	Cu	Sr	Zr	Cs	Ce (IV)
	Co (II)	0.06	-	0.30	1.89	0.09	6.79	0.00
	Cu (II)	0.21	3.29	-	6.21	0.30	22.3	0.00
	Sr (II)	0.03	0.53	0.16	-	0.05	3.59	0.00
0.125	Zr (IV)	0.70	11.1	3.36	20.9	-	75.1	0.01
	Cs (I)	0.01	0.15	0.04	0.28	0.01	-	0.00
	Ce (IV)	113	1787	543	3375	162	12130	-
	Co (II)	0.02	-	0.41	1.88	0.03	2.71	0.00
	Cu (II)	0.05	2.44	-	4.58	0.06	6.60	0.00
	Sr (II)	0.01	0.53	0.22	-	0.01	1.44	0.00
0.25	Zr (IV)	0.75	38.5	15.8	72.3	-	104	0.01
	Cs (I)	0.01	0.37	0.15	0.69	0.01	-	0.00
	Ce (IV)	53.05	2739	1123	5148	71	7419	-
	Co (II)	0.02	-	0.30	1.91	0.02	4.07	0.00
	Cu (II)	0.05	3.35	-	6.40	0.05	13.66	0.00
	Sr (II)	0.01	0.52	0.16	-	0.01	2.13	0.00
0.5	Zr (IV)	1.03	63.1	18.8	121	-	257	0.04
	Cs (I)	0.00	0.25	0.07	0.47	0.00	-	0.00
	Ce (IV)	24.8	1514	452	2890	24	6169	-
	Co (II)	0.02	-	0.50	0.88	0.01	∞	0.00
	Cu (II)	0.03	2.01	-	1.77	0.03	∞	0.00
	Sr (II)	0.02	1.14	0.56	-	0.02	∞	0.00
1	Zr (IV)	1.11	69.2	34.4	60.9	-	∞	0.11
	Cs (I)	0.00	0.00	0.00	0.00	0.00	-	0.00
	Ce (IV)	9.96	621	308	547	8.98	∞	-
	Co (II)	0.04	-	0.95	2.05	0.03	1.58	0.02
	Cu (II)	0.04	1.05	-	2.14	0.03	1.66	0.02
	Sr (II)	0.02	0.49	0.47	-	0.02	0.77	0.01
2	Zr (IV)	1.23	30.5	29.1	62.3	-	48.2	0.47
	Cs (I)	0.03	0.63	0.60	1.29	0.02	-	0.01
	Ce (IV)	2.61	64.8	61.8	133	2.13	103	-
	Co (II)	0.01	-	0.46	4.27	0.01	0.94	0.01
	Cu (II)	0.03	2.19	-	9.36	0.02	2.06	0.03
	Sr (II)	0.00	0.23	0.11	-	0.00	0.22	0.00
4	Zr (IV)	1.45	113	51.5	483	-	106	1.65
	Cs (I)	0.01	1.06	0.49	4.55	0.01	-	0.02
	Ce (IV)	0.88	68.5	31.3	293	0.61	64.4	-

Table 3.9 Ion Exchange Capacity as a Function of Acidity for S950

Acid Strength (M)	Ion	Distribution Constant (K)	Selectivity Co-efficient (α) Co	Cu	Sr	Zr	Cs	Ce (IV)
	Co (II)	0.17	-	0.31	1.35	2.42	3.53	0.00
	Cu (II)	0.55	3.18	-	4.31	7.68	11.2	0.01
	Sr (II)	0.13	0.74	0.23	-	1.78	2.61	0.00
0.125	Zr (IV)	0.07	0.41	0.13	0.56	-	1.46	0.00
	Cs (I)	0.05	0.28	0.09	0.38	0.68	-	0.00
	Ce (IV)	71.5	413	130	560	998	1459	-
	Co (II)	0.03	-	0.30	3.45	∞	∞	0.00
	Cu (II)	0.12	3.32	-	11.5	∞	∞	0.00
	Sr (II)	0.01	0.29	0.09	-	∞	∞	0.00
0.25	Zr (IV)	0.00	0.00	0.00	0.00	-	∞	0.00
	Cs (I)	0.00	0.00	0.00	0.00	∞	-	0.00
	Ce (IV)	72.0	2064	622	7127	∞	∞	-
	Co (II)	0.01	-	0.18	∞	∞	∞	0.00
	Cu (II)	0.05	5.53	-	∞	∞	∞	0.00
	Sr (II)	0.00	0.00	0.00	-	∞	∞	0.00
0.5	Zr (IV)	0.00	0.00	0.00	∞	-	∞	0.00
	Cs (I)	0.00	0.00	0.00	∞	∞	-	0.00
	Ce (IV)	22.8	2661	481	∞	∞	∞	-
	Co (II)	0.00	-	∞	∞	0.00	∞	0.00
	Cu (II)	0.00	∞	-	∞	0.00	∞	0.00
	Sr (II)	0.00	∞	∞	-	0.00	∞	0.00
1	Zr (IV)	0.09	∞	∞	∞	-	∞	0.01
	Cs (I)	0.00	∞	∞	∞	0.00	-	0.00
	Ce (IV)	11.2	∞	∞	∞	128.39	∞	-
	Co (II)	0.03	-	0.73	0.59	0.28	0.80	0.01
	Cu (II)	0.04	1.37	-	0.81	0.39	1.10	0.01
	Sr (II)	0.05	1.70	1.24	-	0.48	1.36	0.01
2	Zr (IV)	0.10	3.53	2.57	2.08	-	2.82	0.02
	Cs (I)	0.04	1.25	0.91	0.74	0.36	-	0.01
	Ce (IV)	4.25	150	109	88.6	42.6	120	-
	Co (II)	0.03	-	0.96	2.88	1.56	0.16	0.02
	Cu (II)	0.03	1.04	-	2.99	1.62	0.17	0.02
	Sr (II)	0.01	0.35	0.33	-	0.54	0.06	0.01
4	Zr (IV)	0.02	0.64	0.62	1.85	-	0.10	0.01
	Cs (I)	0.17	6.26	6.03	18.0	9.77	-	0.12
	Ce (IV)	1.48	53.5	51.5	154	83.4	8.54	-

The ability of amidoxime resins to remove cations from acid solutions has been reported on several previous occasions (82 - 85).

Vernon (84) studied various transition metals such as Ni, Co, Cu, Pb V, Fe and U, Hg and Au in near neutral to acid solutions (pH values 6.0 to 1.0) and reported that V and Au had the highest capacities of ≈ 0.8 $mM.g^{-1}$ and ≈ 2.5 $mM.g^{-1}$ respectively (capacities extrapolated to zero pH value). The resin also had a high uptake for copper but at pH value of 6 (3.2

mM.g^{-1}). In 1 M nitric acid this resin demonstrated capacities for Fe(III), Ti, Mo, V, Bi and Zr of 0.1, 0.9, 0.8, 1.3, 0.4 and 1.2 mM.g^{-1} respectively whilst the capacity for the actinide was zero. This amidoxime resin was also capable of removing 98 % of the Zr (IV) and 67 % of the Mo from a 1 M nitric acid solution containing 5 % w/v uranyl nitrate solution containing 100 ppm of Zr and Mo (84). It was therefore considered a good candidate for the use within this separation.

The S910 is an amidoxime resin and behaves consistently with the data reported above, as it has been previously reported to display a high capacity for copper ions (40 g.l^{-1} equivalent to ≈ 0.5 mM.g^{-1}) (70). In the current study S910 gave a separation factor between the Zr and Ce ions above the prescribed level of 2; indeed only the Zr (IV) was adsorbed in any significant quantity above 0.5 M HNO_3 (Figure 3.3). These values would potentially give a very good separation and therefore the resin was subjected to further testing to assess its potential. The lack of a reduction of the Zr ion uptake across the acid range tested, could be a negative characteristic for a stationary phase, as for chromatography to occur, there has to be operating conditions under which the adsorption of the ion to the stationary phase could be reversed. If the ion was retained too strongly by the stationary phase it would not be eluted. Whilst this resin afforded the required separation of the Zr (IV) and Ce (IV) ions it was far from ideal for a stationary phase capable of separating four or more ions.

The S910 amidoxime resin uptake might be expected to perform in a similar manner to that of weak acid due to its structure, however the high uptake of the Zr across the nitric acid concentration disputes this theory. This might suggest that bonds are being formed between the Zr complexes and the resin. This may have positive connotations for the project in that if the ion is sequestered onto the media and cannot be removed it would mean that the resin could be directly disposed of once the capacity for the ion is reached. The ability of the ion to be removed from the resin would be displayed in the breakthrough studies undertaken later.

For S910, the uptake was experienced by only Zr (IV) and Ce (IV) in any considerable percentage above 0.25 M HNO_3. This becomes an issue within the project as not only was the separation factor in the favour of the Ce (IV) ion, as these are the most highly retained, but this would require a significantly higher volume of resin to create the separation required due to the orders of magnitude difference (Table 1.1) in the concentration of U and Pu compared to that of the FPs. It was therefore not considered for any further experimentation within this project.

Iminodiacetic acids are moderate to weak proton donors, with pKa values varying from 2.98 to 9.89 (85). The ability of iminodiacetic resins to remove cations from aqueous solutions has

been reported on several previous occasions (83) (84) but much less frequently for slightly acidic solutions (pH 5-7) (88). The use of cation uptake from a stronger sulfuric acid at pH 1 to 3 was reported in Mendes and Martins 2004 (85). In this article a number of iminodiacetic resins are tested against one another, in order to assess their ability to uptake Co and Ni from a simulated "pressure acid leach liquor" also containing Zn, Fe, Cu, Mg and Mn ions. The S930Plus is an example of an iminodiacetic acid resin. It displayed uptake of all the ions tested at low nitric acid concentrations (those below 1 M). However, the uptake of all tested ions reduced as the acidity of the liquor increased to the point where at 3 M HNO_3 there was little uptake of any of the ions. There was little uptake of the Cs (I) or Sr (II) ions across the acid range tested, with only the Zr (IV) and Cu (II) ions displaying any significant uptake above 0.5 M. Exchange capacity between 60 and 70 % was observed for the Ce (III) and (IV) and Co ions in the range 0 to 0.125 M HNO_3 this reduced to 18 % for Co, 6 % for the Ce (IV) and 1 % for the Ce (III) at 0.5 M HNO3. The inability of this resin to adsorb any of the ions tested above 3 M was deemed to be a significantly detrimental and consequently it was decided that the resin did not warrant further experiments.

An interesting feature of the S930Plus was the difference in the adsorption of the Co and Cu ions. Both ions had a charge of 2^+ with ionic radii of 74.5 and 73 pm respectively and on this basis it is somewhat difficult to explain the ion exchange preference for Cu over Co (86). A difference in the charge density was evident in the other ions which share the same charge (Ce and Zr (IV)). Although these ions share the same charge, the Ce ion is significantly larger than the Zr (IV) it being 103 pm for the Ce compared to 73 pm for the Zr (IV). Consequently, this may go some way to explaining the differences in exchange capacity between Ce and Zr ions, however, the difference between the capacities observed for the Co and Cu it must be concluded that charge density may not be the sole factor (87) (88).

Again there was little uptake of the Cs, Sr, Co or Cu ions above 0.25 M HNO_3 across the acidic range tested, with only the Zr and both Ce ions displaying any significant uptake above 0.25 M. Uptake was observed for the Co, Cu and Sr ions from 0 to 0.125 M HNO_3 before falling to close to 0 % uptake at 0.25 M HNO_3. Cs displays virtually no uptake across the acid range tested, with the exception of the 3 M data point that displays an approximate 20 % uptake before returning to close to 0 % uptake.

The S940 and S950 resins, aminophosphonic acids are medium to weak donors, with the pKa values varying from 2.8 to 8.23 (89). The ability of aminophosphonic acids resins to remove cations from acid solutions has been reported by Deepatana and Valix 2006, utilising the Purolite S950 resin (90). In this they describe the uptake of nickel and cobalt ions from a variety of organic acids. Uptakes of between 16 - 18 and 5.4 – 9 $mg.g^{-1}$ were

observed for nickel and cobalt respectively in 0.01 to 0.1 M of citric, malic and lactic acids. The resin was subsequently used to assess the adsorption isotherms in much the same method as presented later within the thesis.

On the S940 resin the exchange of all ions reduces as the acidity of the liquor decreases, with the exception of Zr (IV) which gradually increases with acidity, again there was little uptake of the Cs (I), Sr (II), Co (II) or Cu (II) ions above 0.25 M HNO_3, with only the Zr (IV) and both Ce (III) and (IV) ions displaying any significant uptake above 0.25 M. Uptake was observed for the Co, Cu and Sr ions from 0 to 0.125 M HNO_3, before falling to close to no exchange at 0.25 M HNO_3. Cs (I) displayed virtually no exchange capacity across the acid range tested.

For the S950 resin, the uptake was experienced by only the Ce (IV) ions in any considerable percentage above 0.25 M HNO_3. This again becomes an issue within the project, as not only was the separation factor in the favour of the Ce ions, as these are the most highly retained, this would also require the higher volume of resin to create the separation required due to the orders of magnitude difference in the concentration of U and Pu compared to that of the FPs. It was therefore not considered for any further experimentation within this project.

A relatively straight line was observed for exchange capacity of Ce (IV) for both aminophosphonic resins tested; a slight difference was that the S940 displayed a lower capacity for the Ce (IV) than by the S950. This might be due to competition for the exchange sites as at the higher HNO_3 concentrations, Zr (IV) also displays an exchange capacity in addition to the Ce (IV).

As the selection criteria for both the S940 and S950 were not met, these resins were rejected from further use within the project.

3.2.3 Sulfonic Acid Resins

The sulfonic acid resins studied were C100H, C100X10MBH, and C100X16MBH. This series of resins was supplied by Purolite and differed in the extent of cross linking which was 8 % 10 % and 16% respectively. The Dowex G26 was also evaluated; however this resin is very similar to C100H in terms of both acid site and crosslinking density. The ion exchange capacity as a function of nitric acid concentration for C100H, C100X10MBH, C100X16MBH and G26 are reported in Tables 3.10 to 3.13 and graphically in Figures 3.7 to 3.10.

C150 and C160 are also sulfonic acid resins; however, they differ from the resins described above in that they possess a macroporous structure. The data for these resins is contained in Tables 3.14 and 3.15 and Figures 3.11 and 3.12.

The data for the Purolite resins (all except the G26) was collected from an original experiment and one repeat, the results for each of the ions tested were compiled from four samples, and this comprised two aliquots, being taken from both the original experiment and the repeat. Within the ICP-MS, the aliquots were subjected to three "passes", where an assay was performed for each of the ions and the figure from these passes averaged, to give a single concentration for each of the four samples.

For the C100H resin, the average standard deviation for all of the ions across the whole of the HNO_3 concentrations was 2.65 %, which gave an average 95 % confidence limit of +/- 5.19 %. Confidence limits were calculated with n-1 degrees of freedom.

For the C100X10MBH resin, the average standard deviation for all of the ions across the whole of the HNO_3 concentrations was 1.86 %, which gave an average 95 % confidence limit of +/- 3.65 %.

For the C100X16MBH, the average standard deviation for all of the ions across the whole of the HNO_3 concentrations was 1.05 %, which gave an average 95 % confidence limit of +/- 2.05 %.

For the C150 resin, the average standard deviation for all of the ions across the whole of the HNO_3 concentrations was 1.24 %, which gave an average 95 % confidence limit of +/- 2.43 %.

For the C160 resin, the average standard deviation for all of the ions across the whole of the HNO_3 concentrations was 1.85 %, which gave an average 95 % confidence limit of +/- 3.63 %.

For the G26 resin, the average standard deviation for all of the ions across the whole of the HNO_3 concentrations was 2.72 %, which gave an average 95 % confidence limit of +/- 5.33 %. This data comes from an experiment and two repeats.

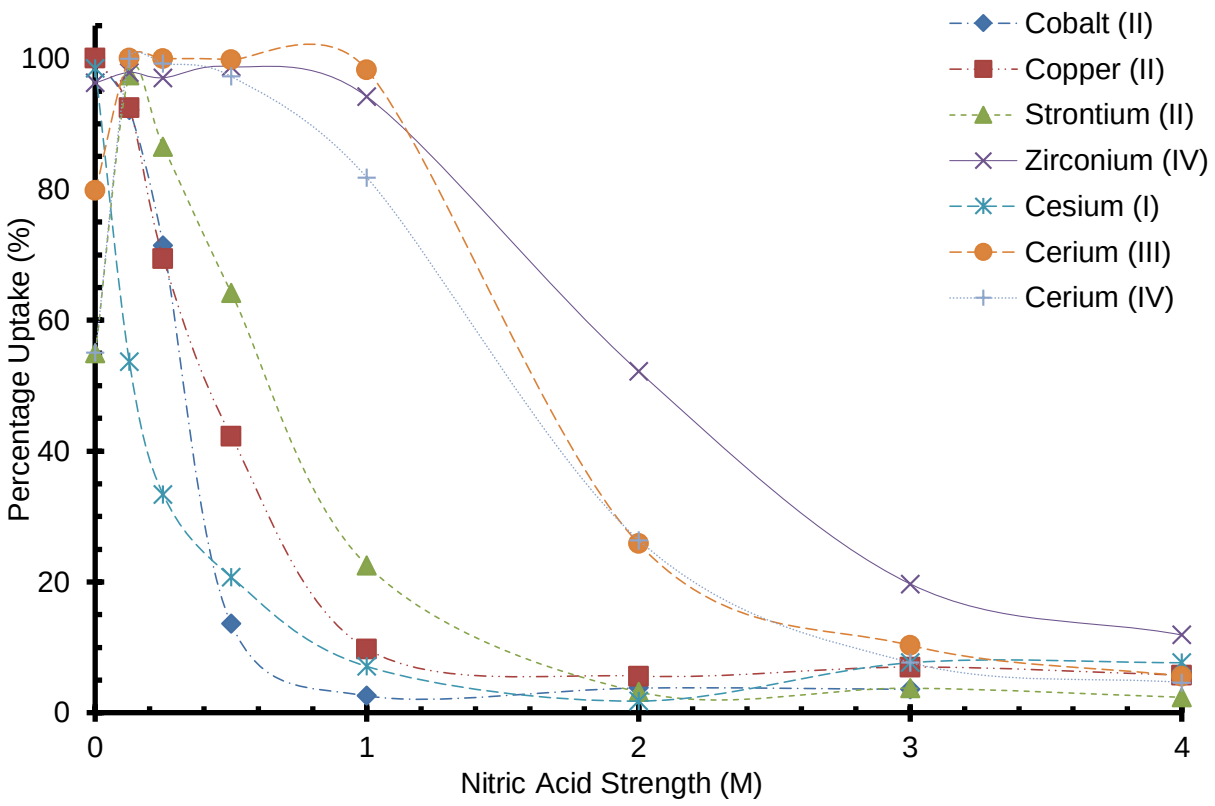

Figure 3.7 Ion Exchange Capacity as a Function of Acidity for C100H

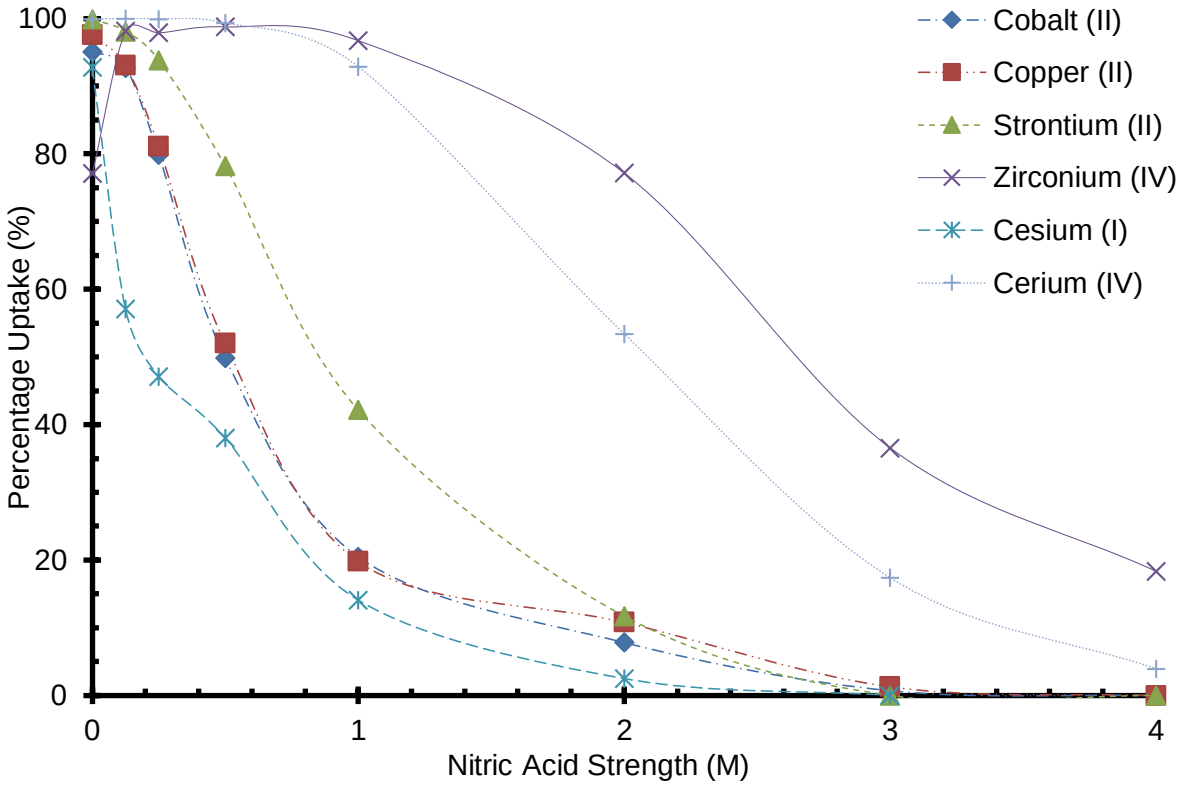

Figure 3.8 Ion Exchange Capacity as a Function of Acidity for C100X10MBH

Table 3.10 Ion Exchange Capacity as a Function of Acidity for C100H

Acid Strength (M)	Ion	Distribution Constant (K)	Selectivity Co-efficient (α) Co	Cu	Sr	Zr	Cs	Ce (III)	Ce (IV)
	Co (II)	∞	-	∞	∞	∞	∞	∞	∞
	Cu (II)	∞	∞	-	∞	∞	∞	∞	∞
	Sr (II)	1.22	∞	∞	-	0.05	0.02	∞	1.00
0	Zr (IV)	25.7	∞	∞	21.0	-	0.40	∞	21.0
	Cs (I)	63.9	∞	∞	52.3	2.49	-	∞	52.2
	Ce (III)	∞	∞	∞	∞	∞	∞	-	∞
	Ce (IV)	1.22	∞	∞	1.00	0.05	0.02	∞	-
	Co (II)	11.7	-	0.96	0.31	0.26	10.1	0.00	0.00
	Cu (II)	12.2	1.04	-	0.33	0.27	10.6	0.00	0.00
	Sr (II)	37.3	3.18	3.05	-	0.81	32.2	0.01	0.01
0.125	Zr (IV)	45.9	3.91	3.75	1.23	-	39.7	0.01	0.01
	Cs (I)	1.16	0.10	0.09	0.03	0.03	-	0.00	0.00
	Ce (III)	4999	426	408	134	109	4319	-	1.00
	Ce (IV)	4999	426	408	134	109	4319	1.00	-
	Co (II)	2.50	-	1.10	0.39	0.08	4.99	0.00	0.02
	Cu (II)	2.27	0.91	-	0.35	0.07	4.54	0.00	0.02
	Sr (II)	6.41	2.57	2.82	-	0.19	12.8	0.01	0.05
0.25	Zr (IV)	32.9	13.2	14.5	5.13	-	65.8	0.06	0.26
	Cs (I)	0.50	0.20	0.22	0.08	0.02	-	0.00	0.00
	Ce (III)	555	222	244	86.5	16.9	1109	-	4.42
	Ce (IV)	126	50.3	55.3	19.60	3.82	251	0.23	-
	Co (II)	0.75	-	1.02	0.42	0.01	2.85	0.01	0.02
	Cu (II)	0.73	0.98	-	0.41	0.01	2.79	0.01	0.02
	Sr (II)	1.79	2.40	2.45	-	0.02	6.84	0.03	0.05
0.5	Zr (IV)	79.0	106	108	44.1	-	302	1.42	2.23
	Cs (I)	0.26	0.35	0.36	0.15	0.00	-	0.00	0.01
	Ce (III)	55.8	74.8	76.3	31.2	0.71	213	-	1.57
	Ce (IV)	35.5	47.5	48.5	19.8	0.45	135	0.64	-
	Co (II)	0.16	-	1.46	0.54	0.01	2.07	0.04	0.04
	Cu (II)	0.11	0.68	-	0.37	0.01	1.42	0.03	0.02
	Sr (II)	0.29	1.84	2.69	-	0.02	3.80	0.07	0.06
1	Zr (IV)	16.1	102	149	55.5	-	211	4.08	3.60
	Cs (I)	0.08	0.48	0.71	0.26	0.00	-	0.02	0.02
	Ce (III)	3.95	25.0	36.5	13.6	0.24	51.7	-	0.88
	Ce (IV)	4.48	28.4	41.5	15.4	0.28	58.7	1.14	-
	Co (II)	0.03	-	0.46	0.83	0.02	1.48	0.08	0.08
	Cu (II)	0.06	2.19	-	1.81	0.05	3.23	0.17	0.17
	Sr (II)	0.03	1.21	0.55	-	0.03	1.79	0.09	0.09
2	Zr (IV)	1.09	40.2	18.4	33.3	-	59.4	3.14	3.05
	Cs (I)	0.02	0.68	0.31	0.56	0.02	-	0.05	0.05
	Ce (III)	0.35	12.8	5.86	10.6	0.32	18.9	-	0.97
	Ce (IV)	0.36	13.2	6.03	10.9	0.33	19.5	1.03	-
	Co (II)	0.04	-	0.53	1.02	0.16	0.48	0.35	0.48
	Cu (II)	0.08	1.89	-	1.93	0.31	0.90	0.66	0.90
	Sr (II)	0.04	0.98	0.52	-	0.16	0.47	0.34	0.47
3	Zr (IV)	0.25	6.17	3.27	6.30	-	2.96	2.14	2.96
	Cs (I)	0.08	2.09	1.11	2.13	0.34	-	0.72	1.00
	Ce (III)	0.11	2.88	1.53	2.94	0.47	1.38	-	1.38
	Ce (IV)	0.08	2.09	1.11	2.13	0.34	1.00	0.72	-
	Co (II)	0.04	-	0.62	1.56	0.28	0.45	0.64	0.78
	Cu (II)	0.06	1.62	-	2.52	0.45	0.73	1.03	1.26
	Sr (II)	0.02	0.64	0.40	-	0.18	0.29	0.41	0.50
4	Zr (IV)	0.14	3.58	2.21	5.59	-	1.63	2.28	2.79
	Cs (I)	0.08	2.20	1.36	3.44	0.62	-	1.40	1.72
	Ce (III)	0.06	1.57	0.97	2.45	0.44	0.71	-	1.23
	Ce (IV)	0.05	1.28	0.79	2.00	0.36	0.58	0.82	-

Table 3.11 Ion Exchange Capacity as a Function of Acidity for C100X10MBH

Acid Strength (M)	Ion	Distribution Constant (K)	Selectivity Co-efficient (α) Co	Cu	Sr	Zr	Cs	Ce (IV)
	Co (II)	19.3	-	0.48	0.02	5.74	1.50	0.02
	Cu (II)	40.5	2.10	-	0.04	12.03	3.15	0.03
	Sr (II)	999	51.7	24.7	-	297	77.7	0.80
0	Zr (IV)	3.37	0.17	0.08	0.00	-	0.26	0.00
	Cs (I)	12.9	0.66	0.32	0.01	3.82	-	0.01
	Ce (IV)	1249	64.6	30.8	1.25	371	97.2	-
	Co (II)	12.8	-	0.95	0.25	0.24	9.61	0.00
	Cu (II)	13.5	1.06	-	0.26	0.26	10.1	0.00
	Sr (II)	51.9	4.06	3.84	-	0.99	39.0	0.01
0.125	Zr (IV)	52.5	4.10	3.88	1.01	-	39.4	0.01
	Cs (I)	1.33	0.10	0.10	0.03	0.03	-	0.00
	Ce (IV)	4999	391	370	96.3	95.3	3754	-
	Co (II)	3.97	-	0.92	0.26	0.09	4.45	0.00
	Cu (II)	4.30	1.08	-	0.28	0.09	4.82	0.00
	Sr (II)	15.2	3.84	3.55	-	0.33	17.1	0.01
0.25	Zr (IV)	46.2	11.6	10.7	3.03	-	51.8	0.04
	Cs (I)	0.89	0.22	0.21	0.06	0.02	-	0.00
	Ce (IV)	1249	315	291	82.0	27.1	1402	-
	Co (II)	0.99	-	0.92	0.28	0.01	1.62	0.01
	Cu (II)	1.08	1.09	-	0.30	0.01	1.77	0.01
	Sr (II)	3.59	3.61	3.31	-	0.05	5.85	0.02
0.5	Zr (IV)	79.6	80.1	73.4	22.2	-	130	0.55
	Cs (I)	0.61	0.62	0.57	0.17	0.01	-	0.00
	Ce (IV)	144	145	133	40.1	1.81	234	-
	Co (II)	0.26	-	1.04	0.35	0.01	1.57	0.02
	Cu (II)	0.25	0.96	-	0.34	0.01	1.51	0.02
	Sr (II)	0.73	2.83	2.95	-	0.02	4.46	0.06
1	Zr (IV)	29.5	114	119	40.4	-	180	2.26
	Cs (I)	0.16	0.63	0.66	0.22	0.01	-	0.01
	Ce (IV)	13.0	50.5	52.7	17.9	0.44	79.5	-
	Co (II)	0.09	-	0.70	0.64	0.03	1.39	0.07
	Cu (II)	0.12	1.43	-	0.91	0.04	1.98	0.11
	Sr (II)	0.13	1.56	1.09	-	0.04	2.16	0.12
2	Zr (IV)	3.38	39.7	27.8	25.4	-	55.1	2.95
	Cs (I)	0.06	0.72	0.51	0.46	0.02	-	0.05
	Ce (IV)	1.15	13.5	9.44	8.64	0.34	18.7	-
	Co (II)	0.01	-	0.55	∞	0.01	0.29	0.03
	Cu (II)	0.01	1.81	-	∞	0.02	0.52	0.06
	Sr (II)	0.00	0.00	0.00	-	0.00	0.00	0.00
3	Zr (IV)	0.58	78.4	43.4	∞	-	22.8	2.74
	Cs (I)	0.03	3.44	1.91	∞	0.04	-	0.12
	Ce (IV)	0.21	28.6	15.9	∞	0.37	8.31	-
	Co (II)	0.00	-	∞	∞	0.00	∞	0.00
	Cu (II)	0.00	∞	-	∞	0.00	∞	0.00
	Sr (II)	0.00	∞	∞	-	0.00	∞	0.00
4	Zr (IV)	0.22	∞	∞	∞	-	∞	5.48
	Cs (I)	0.00	∞	∞	∞	0.00	-	0.00
	Ce (IV)	0.04	∞	∞	∞	0.18	∞	-

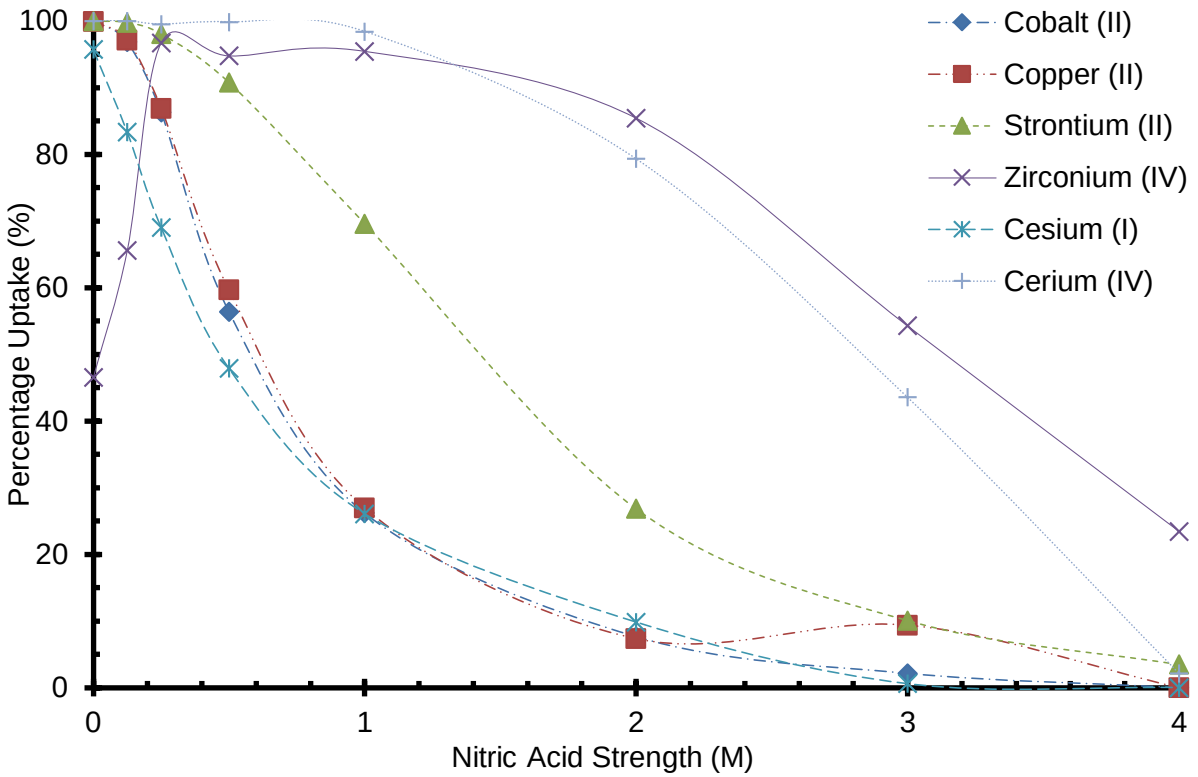

Figure 3.9 Ion Exchange Capacity as a Function of Acidity for C100X16MBH

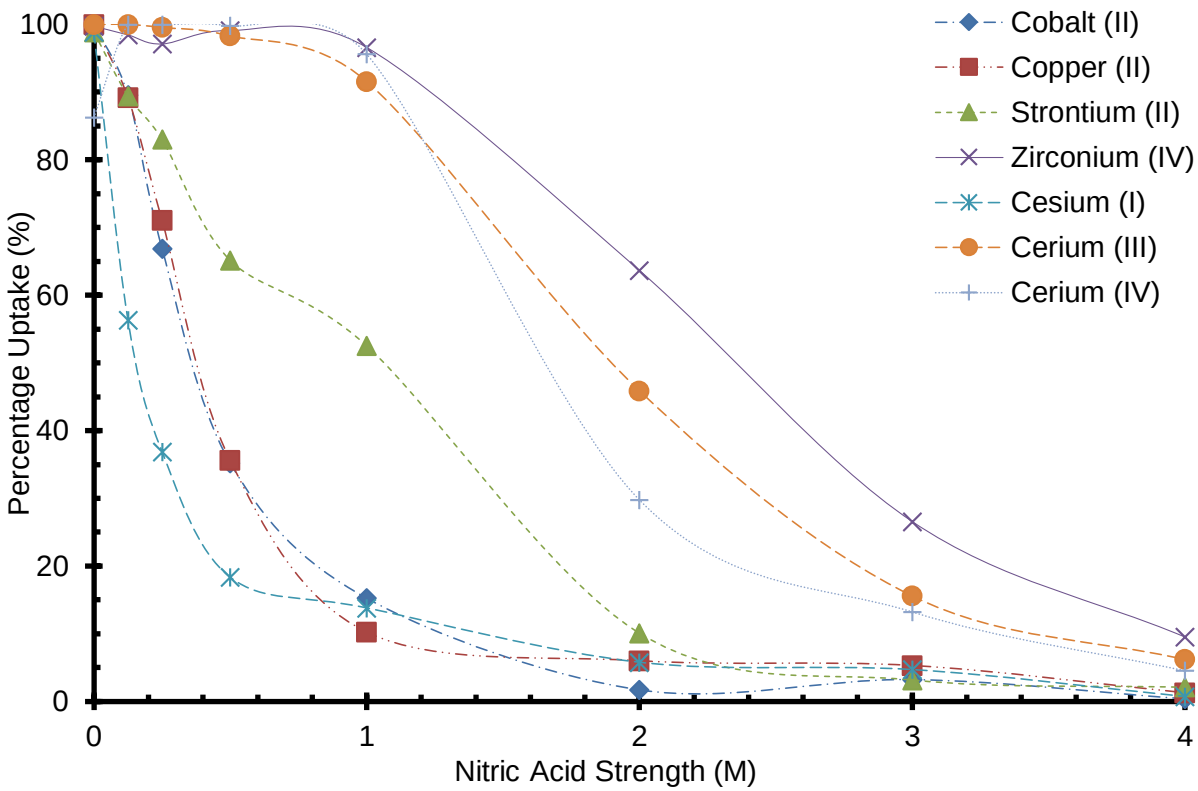

Figure 3.10 Ion Exchange Capacity as a Function of Acidity for G26

Table 3.12 Ion Exchange Capacity as a Function of Acidity for C100X16MBH

Acid Strength (M)	Ion	Distribution Constant (K)	Selectivity Co-efficient (α) Co	Cu	Sr	Zr	Cs	Ce (IV)
0	Co (II)	∞	-	∞	∞	∞	∞	∞
	Cu (II)	908	∞	-	0.64	1044	40.7	∞
	Sr (II)	1428	∞	1.57	-	1640	64.0	∞
	Zr (IV)	0.87	∞	0.00	0.00	-	0.04	∞
	Cs (I)	22.3	∞	0.02	0.02	25.6	-	∞
	Ce (IV)	∞	∞	∞	∞	∞	∞	-
0.125	Co (II)	30.5	-	0.91	0.08	16.0	6.12	∞
	Cu (II)	33.6	1.10	-	0.09	17.7	6.73	∞
	Sr (II)	384	12.6	11.4	-	202	76.8	∞
	Zr (IV)	1.90	0.06	0.06	0.00	-	0.38	∞
	Cs (I)	5.00	0.16	0.15	0.01	2.62	-	∞
	Ce (IV)	∞	∞	∞	∞	∞	∞	-
0.25	Co (II)	6.28	-	0.95	0.13	0.21	2.82	0.03
	Cu (II)	6.62	1.05	-	0.13	0.23	2.97	0.03
	Sr (II)	49.5	7.89	7.48	-	1.68	22.2	0.25
	Zr (IV)	29.4	4.68	4.44	0.59	-	13.2	0.15
	Cs (I)	2.23	0.36	0.34	0.05	0.08	-	0.01
	Ce (IV)	199	31.7	30.1	4.02	6.77	89.2	-
0.5	Co (II)	1.29	-	0.87	0.13	0.07	1.41	0.00
	Cu (II)	1.48	1.14	-	0.15	0.08	1.61	0.00
	Sr (II)	9.80	7.58	6.63	-	0.54	10.7	0.02
	Zr (IV)	18.0	14.0	12.2	1.84	-	19.6	0.03
	Cs (I)	0.92	0.71	0.62	0.09	0.05	-	0.00
	Ce (IV)	587	455	398	59.9	32.5	639	-
1	Co (II)	0.35	-	0.96	0.15	0.02	1.01	0.01
	Cu (II)	0.37	1.04	-	0.16	0.02	1.04	0.01
	Sr (II)	2.29	6.46	6.21	-	0.11	6.49	0.04
	Zr (IV)	20.9	58.9	56.7	9.13	-	59.2	0.34
	Cs (I)	0.35	0.99	0.96	0.15	0.02	-	0.01
	Ce (IV)	61.5	174	167	26.9	2.95	174	-
2	Co (II)	0.08	-	1.04	0.23	0.01	0.76	0.02
	Cu (II)	0.08	0.96	-	0.22	0.01	0.73	0.02
	Sr (II)	0.37	4.44	4.63	-	0.06	3.37	0.10
	Zr (IV)	5.85	70.8	73.9	16.0	-	53.8	1.53
	Cs (I)	0.11	1.32	1.37	0.30	0.02	-	0.03
	Ce (IV)	3.83	46.3	48.4	10.4	0.65	35.2	-
3	Co (II)	0.02	-	0.21	0.19	0.02	3.75	0.03
	Cu (II)	0.10	4.73	-	0.92	0.09	17.7	0.13
	Sr (II)	0.11	5.13	1.09	-	0.09	19.2	0.15
	Zr (IV)	1.19	54.2	11.5	10.6	-	203	1.54
	Cs (I)	0.01	0.27	0.06	0.05	0.00	-	0.01
	Ce (IV)	0.77	35.3	7.46	6.87	0.65	132	-
4	Co (II)	0.00	-	∞	0.00	0.00	∞	0.00
	Cu (II)	0.00	∞	-	0.00	0.00	∞	0.00
	Sr (II)	0.04	∞	∞	-	0.12	∞	1.64
	Zr (IV)	0.31	∞	∞	8.49	-	∞	13.9
	Cs (I)	0.00	∞	∞	0.00	0.00	∞	0.00
	Ce (IV)	0.02	∞	∞	0.61	0.07	∞	-

Table 3.13 Ion Exchange Capacity as a Function of Acidity for G26

Acid Strength (M)	Ion	Distribution Constant (K)	Selectivity Co-efficient (α) Co	Cu	Sr	Zr	Cs	Ce (III)	Ce (IV)
	Co (II)	∞	-	∞	∞	∞	∞	∞	∞
	Cu (II)	1666	∞	-	18.70	4.34	19.04	∞	265
	Sr (II)	89.09	∞	0.05	-	0.23	1.02	∞	14.2
0	Zr (IV)	384	∞	0.23	4.31	-	4.38	∞	61.1
	Cs (I)	87.50	∞	0.05	0.98	0.23	-	∞	13.9
	Ce (III)	∞	∞	∞	∞	∞	∞	-	∞
	Ce (IV)	6.28	∞	0.00	0.07	0.02	0.07	∞	-
	Co (II)	8.55	-	1.04	1.01	0.13	6.63	∞	∞
	Cu (II)	8.25	0.96	-	0.98	0.13	6.40	∞	∞
	Sr (II)	8.43	0.99	1.02	-	0.13	6.53	∞	∞
0.125	Zr (IV)	63.52	7.43	7.70	7.54	-	49.3	∞	∞
	Cs (I)	1.29	0.15	0.16	0.15	0.02	-	∞	∞
	Ce (III)	∞	∞	∞	∞	∞	∞	∞	∞
	Ce (IV)	∞	∞	∞	∞	∞	∞	∞	-
	Co (II)	2.02	-	0.82	0.41	0.06	3.46	0.01	0.00
	Cu (II)	2.46	1.22	-	0.50	0.07	4.21	0.01	0.00
	Sr (II)	4.88	2.42	1.99	-	0.14	8.36	0.02	0.00
0.25	Zr (IV)	33.7	16.7	13.7	6.91	-	57.7	0.16	0.01
	Cs (I)	0.58	0.29	0.24	0.12	0.02	-	0.00	0.00
	Ce (III)	216	107	88.1	44.3	6.42	371	-	0.04
	Ce (IV)	4999	2474	2035	1024	148	8559	23.1	-
	Co (II)	0.54	-	0.98	0.29	0.00	2.42	0.01	0.00
	Cu (II)	0.55	1.02	-	0.30	0.00	2.46	0.01	0.00
	Sr (II)	1.87	3.44	3.38	-	0.02	8.32	0.03	0.00
0.5	Zr (IV)	111	205	202	59.65	-	496	1.95	0.22
	Cs (I)	0.22	0.41	0.41	0.12	0.00	-	0.00	0.00
	Ce (III)	57.1	105	104	30.6	0.51	255	-	0.11
	Ce (IV)	499	919	904	267	4.48	2225	8.73	-
	Co (II)	0.18	-	1.58	0.16	0.01	1.12	0.02	0.01
	Cu (II)	0.11	0.63	-	0.10	0.00	0.71	0.01	0.01
	Sr (II)	1.11	6.16	9.7	-	0.04	6.92	0.10	0.05
1	Zr (IV)	28.4	158	249	25.69	-	178	2.62	1.30
	Cs (I)	0.16	0.89	1.40	0.14	0.01	-	0.01	0.01
	Ce (III)	10.9	60.5	95.3	9.8	0.38	67.9	-	0.50
	Ce (IV)	21.9	122	192	19.78	0.77	137	2.01	-
	Co (II)	0.02	-	0.27	0.15	0.01	0.28	0.02	0.04
	Cu (II)	0.06	3.71	-	0.57	0.04	1.04	0.08	0.15
	Sr (II)	0.11	6.51	1.76	-	0.06	1.83	0.13	0.26
2	Zr (IV)	1.75	102	27.5	15.7	-	28.7	2.07	4.13
	Cs (I)	0.06	3.56	0.96	0.55	0.03	-	0.07	0.14
	Ce (III)	0.85	49.3	13.3	7.58	0.48	13.9	-	2.00
	Ce (IV)	0.42	24.7	6.66	3.79	0.24	6.94	0.50	-
	Co (II)	0.03	-	0.59	1.02	0.09	0.68	0.18	0.22
	Cu (II)	0.06	1.68	-	1.71	0.15	1.14	0.30	0.37
	Sr (II)	0.03	0.98	0.58	-	0.09	0.66	0.18	0.21
3	Zr (IV)	0.36	10.9	6.49	11.1	-	7.37	1.96	2.37
	Cs (I)	0.05	1.48	0.88	1.51	0.14	-	0.27	0.32
	Ce (III)	0.18	5.56	3.31	5.67	0.51	3.76	-	1.21
	Ce (IV)	0.15	4.60	2.74	4.69	0.42	3.11	0.83	-
	Co (II)	0.00	-	0.29	0.17	0.03	0.51	0.05	0.08
	Cu (II)	0.01	3.50	-	0.60	0.12	1.80	0.19	0.27
	Sr (II)	0.02	5.85	1.67	-	0.20	3.00	0.32	0.44
4	Zr (IV)	0.11	29.1	8.30	4.97	-	14.9	1.60	2.21
	Cs (I)	0.01	1.95	0.56	0.33	0.07	-	0.11	0.15
	Ce (III)	0.07	18.2	5.19	3.11	0.63	9.33	-	1.38
	Ce (IV)	0.05	13.2	3.76	2.25	0.45	6.75	0.72	-

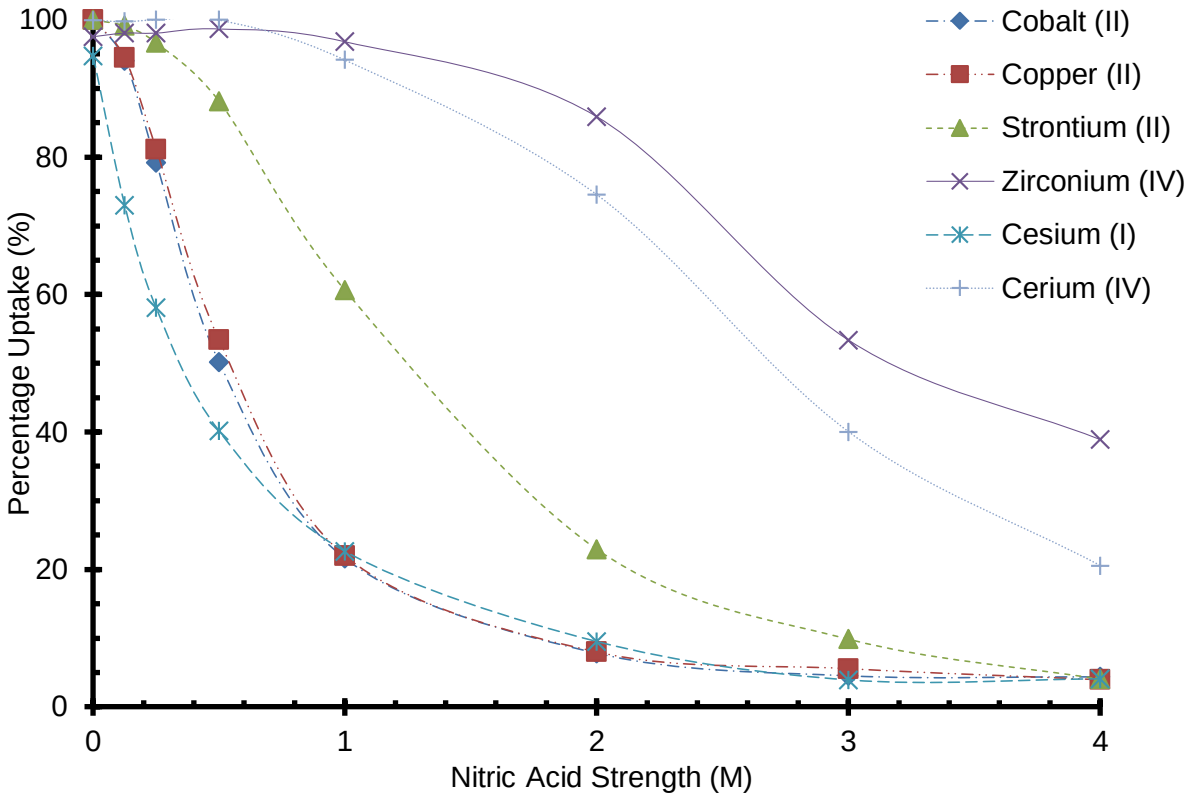

Figure 3.11 Ion Exchange Capacity as a Function of Acidity for C150

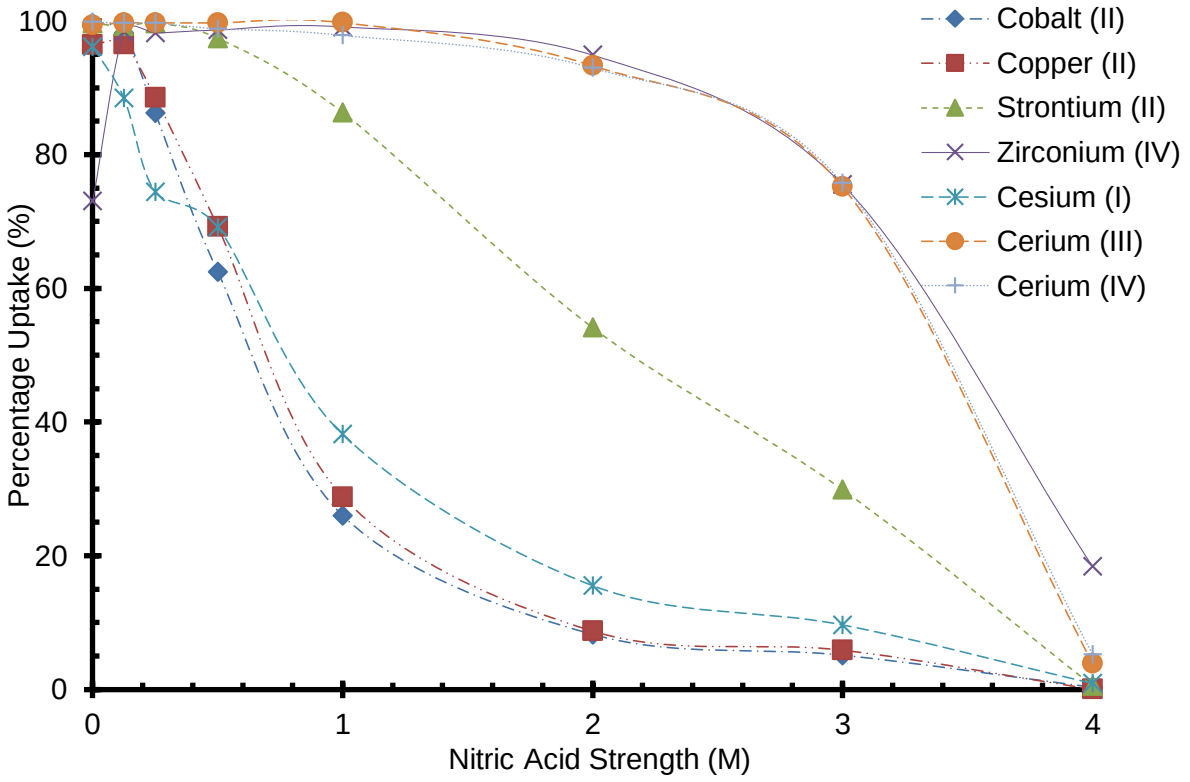

Figure 3.12 Ion Exchange Capacity as a Function of Acidity for C160

Table 3.14 Ion Exchange Capacity as a Function of Acidity for C150

Acid Strength (M)	Ion	Distribution Constant (K)	Selectivity Co-efficient (α) Co	Cu	Sr	Zr	Cs	Ce (IV)
	Co (II)	2499	-	∞	∞	63.29	139.3	1.25
	Cu (II)	∞	∞	-	∞	∞	∞	∞
	Sr (II)	∞	∞	∞	-	∞	∞	∞
0	Zr (IV)	39.5	0.02	∞	∞	-	2.20	0.02
	Cs (I)	17.9	0.01	∞	∞	0.45	-	0.01
	Ce (IV)	1999	0.80	∞	∞	50.6	111	-
	Co (II)	15.8	-	0.93	0.14	0.31	5.85	0.04
	Cu (II)	17.1	1.08	-	0.15	0.34	6.30	0.04
	Sr (II)	113	7.11	6.61	-	2.24	41.6	0.29
0.125	Zr (IV)	50.3	3.18	2.95	0.45	-	18.6	0.13
	Cs (I)	2.71	0.17	0.16	0.02	0.05	-	0.01
	Ce (IV)	384	24.2	22.5	3.41	7.63	142	-
	Co (II)	3.81	-	0.88	0.13	0.08	2.75	∞
	Cu (II)	4.31	1.13	-	0.15	0.09	3.12	∞
	Sr (II)	28.9	7.61	6.71	-	0.58	20.9	∞
0.25	Zr (IV)	50.3	13.2	11.7	1.74	-	36.3	∞
	Cs (I)	1.38	0.36	0.32	0.05	0.03	-	∞
	Ce (IV)	∞	∞	∞	∞	∞	∞	-
	Co (II)	1.01	-	0.88	0.14	0.01	1.50	0.00
	Cu (II)	1.15	1.14	-	0.15	0.02	1.71	0.00
	Sr (II)	7.44	7.39	6.49	-	0.10	11.10	0.00
0.5	Zr (IV)	73.1	72.6	63.8	9.82	-	109.0	0.01
	Cs (I)	0.67	0.67	0.58	0.09	0.01	-	0.00
	Ce (IV)	4999	4969	4362	672	68.4	7458	-
	Co (II)	0.28	-	0.98	0.18	0.01	0.94	0.02
	Cu (II)	0.28	1.0	-	0.18	0.01	0.96	0.02
	Sr (II)	1.54	5.6	5.47	-	0.05	5.27	0.10
1	Zr (IV)	30.15	110	107	19.6	-	103	1.87
	Cs (I)	0.29	1.1	1.04	0.19	0.01	-	0.02
	Ce (IV)	16.09	58.4	57.2	10.4	0.53	55.02	-
	Co (II)	0.08	-	0.98	0.28	0.01	0.81	0.03
	Cu (II)	0.09	1.03	-	0.29	0.01	0.83	0.03
	Sr (II)	0.30	3.52	3.43	-	0.05	2.84	0.10
2	Zr (IV)	6.09	71.9	70.16	20.4	-	58.1	2.08
	Cs (I)	0.10	1.24	1.21	0.35	0.02	-	0.04
	Ce (IV)	2.93	34.6	33.7	9.83	0.48	27.94	-
	Co (II)	0.05	-	0.81	0.43	0.04	1.17	0.07
	Cu (II)	0.06	1.24	-	0.54	0.05	1.45	0.09
	Sr (II)	0.11	2.31	1.86	-	0.10	2.70	0.16
3	Zr (IV)	1.15	24.1	19.4	10.4	-	28.2	1.72
	Cs (I)	0.04	0.855	0.69	0.37	0.04	-	0.06
	Ce (IV)	0.67	14.1	11.3	6.09	0.58	16.4	-
	Co (II)	0.05	-	1.11	1.08	0.07	1.08	0.18
	Cu (II)	0.04	0.898	-	0.97	0.06	0.97	0.16
	Sr (II)	0.04	0.924	1.03	-	0.07	1.00	0.16
4	Zr (IV)	0.64	13.9	15.5	15.0	-	15.0	2.46
	Cs (I)	0.04	0.924	1.03	1.00	0.07	-	0.16
	Ce (IV)	0.26	5.643	6.29	6.11	0.41	6.11	-

Table 3.15 Ion Exchange Capacity as a Function of Acidity for C160

Acid Strength (M)	Ion	Distribution Constant (K)	Selectivity Co-efficient (α)						
			Co	Cu	Sr	Zr	Cs	Ce (III)	Ce (IV)
0	Co (II)	249	-	9.11	0.85	92.0	9.94	0.62	0.32
	Cu (II)	27.3	0.11	-	0.09	10.1	1.09	0.07	0.04
	Sr (II)	293	1.18	10.7	-	108	11.7	0.73	0.38
	Zr (IV)	2.71	0.01	0.10	0.01	-	0.11	0.01	0.00
	Cs (I)	25.0	0.10	0.92	0.09	9.25	-	0.06	0.03
	Ce (III)	399	1.60	14.6	1.36	147	15.9	-	0.52
	Ce (IV)	768	3.09	28.1	2.62	284	30.7	1.93	-
0.125	Co (II)	54.9	-	2.00	0.44	0.93	7.17	0.14	0.16
	Cu (II)	27.5	0.50	-	0.22	0.46	3.59	0.07	0.08
	Sr (II)	126	2.29	4.57	-	2.12	16.4	0.33	0.37
	Zr (IV)	59.2	1.08	2.15	0.47	-	7.74	0.15	0.17
	Cs (I)	7.65	0.14	0.28	0.06	0.13	-	0.02	0.02
	Ce (III)	384	6.99	14.0	3.05	6.48	50.1	-	1.12
	Ce (IV)	344	6.27	12.5	2.74	5.80	44.9	0.90	-
0.25	Co (II)	6.26	-	0.81	0.02	0.11	2.15	0.02	0.02
	Cu (II)	7.72	1.23	-	0.03	0.14	2.65	0.02	0.02
	Sr (II)	255	40.8	33.1	-	4.66	87.7	0.67	0.74
	Zr (IV)	54.9	8.76	7.11	0.21	-	18.8	0.14	0.16
	Cs (I)	2.91	0.46	0.38	0.01	0.05	-	0.01	0.01
	Ce (III)	384	61.3	49.7	1.50	6.99	132	-	1.12
	Ce (IV)	344	54.9	44.5	1.35	6.27	118	0.90	-
0.5	Co (II)	1.67	-	0.74	0.04	0.02	0.74	0.00	0.02
	Cu (II)	2.25	1.35	-	0.06	0.03	1.00	0.01	0.03
	Sr (II)	38	22.6	16.7	-	0.51	16.7	0.09	0.43
	Zr (IV)	73	43.9	32.5	1.94	-	32.5	0.18	0.84
	Cs (I)	2.25	1.35	1.00	0.06	0.03	-	0.01	0.03
	Ce (III)	416	250	185	11.1	5.69	185	-	4.75
	Ce (IV)	87	52.5	38.9	2.33	1.20	39.0	0.21	-
1	Co (II)	0.35	-	0.87	0.06	0.00	0.57	0.00	0.01
	Cu (II)	0.40	1.15	-	0.06	0.00	0.66	0.00	0.01
	Sr (II)	6.30	17.9	15.6	-	0.06	10.2	0.04	0.14
	Zr (IV)	111	317	275	17.66	-	180	0.64	2.41
	Cs (I)	0.62	1.76	1.52	0.10	0.01	-	0.00	0.01
	Ce (III)	174	496	431	27.7	1.57	283	-	3.78
	Ce (IV)	46.2	131	114	7.32	0.41	74.8	0.26	-
2	Co (II)	0.09	-	0.94	0.08	0.00	0.49	0.01	0.01
	Cu (II)	0.10	1.07	-	0.08	0.01	0.52	0.01	0.01
	Sr (II)	1.18	13.2	12.3	-	0.06	6.41	0.08	0.09
	Zr (IV)	18.6	207	194	15.7	-	101	1.33	1.40
	Cs (I)	0.18	2.05	1.93	0.16	0.01	-	0.01	0.01
	Ce (III)	14.0	156	146	11.9	0.75	76.0	-	1.06
	Ce (IV)	13.2	148	138	11.2	0.71	71.9	0.95	-
3	Co (II)	0.05	-	0.87	0.13	0.02	0.50	0.02	0.02
	Cu (II)	0.06	1.16	-	0.15	0.02	0.58	0.02	0.02
	Sr (II)	0.43	7.90	6.83	-	0.14	3.98	0.14	0.14
	Zr (IV)	3.08	57.1	49.4	7.24	-	28.8	1.02	0.99
	Cs (I)	0.11	1.98	1.72	0.25	0.03	-	0.04	0.03
	Ce (III)	3.03	56.2	48.7	7.12	0.98	28.3	-	0.97
	Ce (IV)	3.12	57.9	50.1	7.33	1.01	29.2	1.03	-
4	Co (II)	0.00	-	16.55	0.58	0.01	0.36	0.08	0.06
	Cu (II)	0.00	0.06	-	0.03	0.00	0.02	0.00	0.00
	Sr (II)	0.01	1.73	28.7	-	0.03	0.62	0.14	0.10
	Zr (IV)	0.23	68.0	1126	39.3	-	24.5	5.53	4.05
	Cs (I)	0.01	2.77	45.91	1.60	0.04	-	0.23	0.17
	Ce (III)	0.04	12.3	203	7.10	0.18	4.43	-	0.73
	Ce (IV)	0.06	16.8	278	9.70	0.25	6.06	1.37	-

The C100H was first of the sulfonic acid resins reported. It was expected that the pattern of ion uptake would be similar for all of the resins with similar active sites and once the uptake mechanism is described, any observed differences within the uptakes would be due to the composition of the resins themselves.

The Purolite "C100" group of resins along with the Dowex G26 are all examples of sulfonic acid resins. These were the first commercially available type of cation ion exchange resin. While the nature of the acid site was the same for all these resins, there are structural differences resulting from variations in the amount of divinylbenzene (DVB) used in the crosslinking of the structure. The Purolite C150 and C160 have a macroporous component to them, it was anticipated that this might perform some form of separation based on size exclusion of the ions as is observed from a channel within a zeolite.

With all of the sulfonic acid resin graphs (Figures 3.7 to 3.12), the ion exchange capacity of the ions displayed a reduction as the acidity of the liquor was increased. The uptake values were also dependent on the charge density of the ion where a higher capacity was displayed for the more highly charged ions. The other important factor from these experiments was that as the molarity of the acid increases, all of the ions uptakes were reduced. This means that the resin should be able to be stripped of an absorbed ion and then subsequently regenerated if a strong and large enough volume of acid is applied to a column of the resin.

At the one molar nitric acid concentration, the dissociation of sulfonic acid is impaired, and as the nitric acid concentration increases, the dissociation of SO_3H will be further reduced in order to maintain the equilibrium:

$$SO_3H \rightleftharpoons SO_3^- + H^+ \quad pK_a \text{ of } \sim -2.8 \quad (91)$$

However, Ce (IV) and Zr (IV) ions are capable of overcoming this lack of dissociation by replacing the hydrogen ion attached to the functional group. As the measured maximum uptake for these ions is of the order 50 µg/g, this would entail only 10^{-3} % dissociation of the sulfonic acid group for a 1:1 SO_3-Zr complex. The uptake of ions is higher for the more charged species, so zirconium (IV) is more retained than cerium (IV) > cerium (III) > strontium (II) > copper and cobalt (II) > caesium (I); this sequence is consistent with previously measured selectivities for sulfonic acid resins. Cerium and zirconium ions are capable of forming nitrato- complexes in nitric acid which might assist in the uptake of these ions by the sulfonic acid functional group. This **may** be due to the interesting chemistry displayed by zirconium speciation at low acid concentrations (ZrO^{2+}, Zr^{4+} and $[Zr_4(OH)_8(H_2O)_{16}]^{8+}$). The deviation in charges, hydrated radii and compound diameters displayed at these low nitric acid concentrations would have a dramatic effect on the adsorption on to the

resin. The pore size of the resin, density of active sites on its surface and capacity would all be limiting factors affecting uptake. A large molecules such as the $[Zr_4(OH)_8(H_2O)_{16}]^{8+}$ ion would be less able to penetrate the internal structures and active sites within a resin than that of smaller molecule or ion such as ZrO^{2+} or Zr^{4+}. It would also take more active sites on the resin to adsorb an 8+ charged molecule than that of a 4+ ion or 2+ molecule. This would effectively reduce the capacity of the resin for Zr, however as the concentration of the Zr in the liquor is close to that of the capacity of the resin, this effect should be observed if it does occur to cause a reduction in the uptake of the ions (92) (93).

As explained above, the actual pattern of uptake of the ions was likely to be very similar between all of the strongly acidic cationic resins. As the active sites are all sulfonic acid, any observed differences should be due to the differences in the structure of the actual resin.

The most noticeable difference between the 8 and 10 % DVB content resins was that although the uptake pattern was of a similar morphology, at comparable acid strengths the uptake of ions was significantly larger (almost double) on the more highly cross-linked resin. For example on the C100H at the 1 M HNO_3 acid concentration, the uptake for Cs, Cu and Sr was approximately 7, 10 and 22 % as opposed to 14, 20 and 42 on the C100X10 MBH and this was mirrored at the 2 M HNO_3 concentration where the uptake for Ce (III), Ce (IV) and Zr was 10, 26 and 52 % compared to 53, 55 and 77 % on the more highly cross-linked resin. This continued over the range of ions and acid molarity.

Another notable difference between the C100H and C100X10MBH (Figures 3.7 and 3.8) was the unevenness of the curves, most noticeable on the cesium curve where a “bulge” is observed at the 0.5 M HNO_3 concentration: whereas on the C100H resin the reduction in exchange capacity was a smooth downward curve toward the baseline, on the C100X10MBH graph there seemed to be a more linear reduction in capacity, especially manifest in both the Ce ions, but also in the Zr (IV) ion. Indeed the uptake in Zr (IV) was less than the approximate 100 % for the deionised water. This could be associated with the complexion of the Zr ion as described above.

With a view to the manufacture of the resins, with the increase in the DVB and therefore crosslinking of the polystyrene, this would reduce the available sites for attaching the active site in this case: sulfuric acid. It therefore follows that as the DVB percentage is increased, the capacity of the resin would be reduced. If the reduction in exchange capacity of Zr (IV) at the low HNO_3 concentrations or the deionised water is observed in the C100X16 MBH resin, this would go a way to corroborate that the capacity was being reduced and possibly that the Zr ion was behaving in the method described above.

The C100X16 MBH followed the general morphology of that displayed in the other sulfonic acid resins, in that as the acidity of the liquor was increased, the uptake across the ions tested was decreased, based on their charge, with one notable exception. Again the uptake was reduced for the Zr (IV) ion as the HNO_3 concentration approaches 0, unlike the C100X10MBH. However, this was also displayed in the 0.125 M concentration. Also notable was that as the cross-linking of the resin was doubled, the uptake was effectively halved from 96.25 to 46.5 % with the difference between the 8 and 10 % cross-linked resins of the C100H and the C100X10MBH falling to 77.1 % at the deionised water level. This 25 % increase in cross-linking was of a similar magnitude to the 19.15 % reduction in the uptakes observed. However, this link may be an anomaly chanced upon by the three amounts of cross-linking observed in this specific experiment rather than a real and linear relationship effect, caused by the increased cross-linking affecting the uptake capacity of the resins.

A similar result was observed for the other ions tested, as the cross-linking is increased within the resin structure and the uptake of each ion was also increased at comparable HNO_3 concentrations.

The Dowex G26 resin followed the general trends to those displayed by the other sulfonic acid resins, in that as the acidity of the liquor was increased, the uptake across the ions tested was decreased, based on their charge.

With the similar structural cross-linking and active sites, the G26 and C100H were expected to give similar uptake graphs. This was broadly the case for the majority of the ions tested, with the exception of the Sr (II) and of the Ce (III). As the separation factor was slightly less than that of the C100H and given that the structures were essentially identical, this resin was not investigated further.

The C150 and C160 also followed the same general trend displayed by the C100 series resins in that as the acidity of the liquor was increased, the uptake across the ions tested decreased based on their charge density. Again as the cross-linking increased within the resin structure, the uptake of each ion increased. The uptake on the C150 and C160 was significantly higher at comparable HNO_3 concentrations compared to the C100H and C100X10MBH resins. The C160 resin had the greatest amount of DVB of all those tested. At the exchange capacity at 3 M HNO_3 the uptake of Zr, Ce (III) and (IV) was still approximately 75 %. Also noticeable was that the Cs (I), Co (II) and Cu (II) all behaved in a very similar manner above 1 M HNO_3 as do the Ce (IV) and Zr (IV) ions; more so than the previously described Purolite resins.

3.3 Determination of the Rate of Ion Exchange

In this section resins which demonstrated a selectivity co-efficient of 2.0 or greater as described in section 3.2 have been studied.

The rate of ion exchange was studied as a function of temperature over a 24 hour period using a 500 $mg.l^{-1}$ concentration of Zr (IV) of a $ZrO(NO_3)_2$ salt solution. The uptake curves are expressed in both a percentage of the maximum uptake and as a mass ($mg.g^{-1}$) and displayed in Figures 3.12 to 3.19.

The data for these two media was collected from an original experiment and a single repeat. The results for each of the ions tested were compiled from four samples, this comprised two aliquots being taken from both the original experiment and the repeat. Within the ICP-MS, the aliquots were subjected to three “passes” where an assay was performed for each of the ions and the figure from these passes averaged, to give a single concentration for each of the four samples.

As described in Section 3.1 there was a significant reduction in the moisture content of the C100H and the C100X10MBH resins of 25.4 and 16.9 % respectively. In order that the reporting of the ion capacity uptake was consistent throughout all results, the mass exchange capacities reported in Sections 3.4 and 3.5 were required to be modified so that of the non-dried equivalent of resin. Therefore, the exchanged mass of the ion was standardised by dividing the measured mass exchanged in the experiment by 1.254 and 1.169 for the C100H and C100X10MBH respectively.

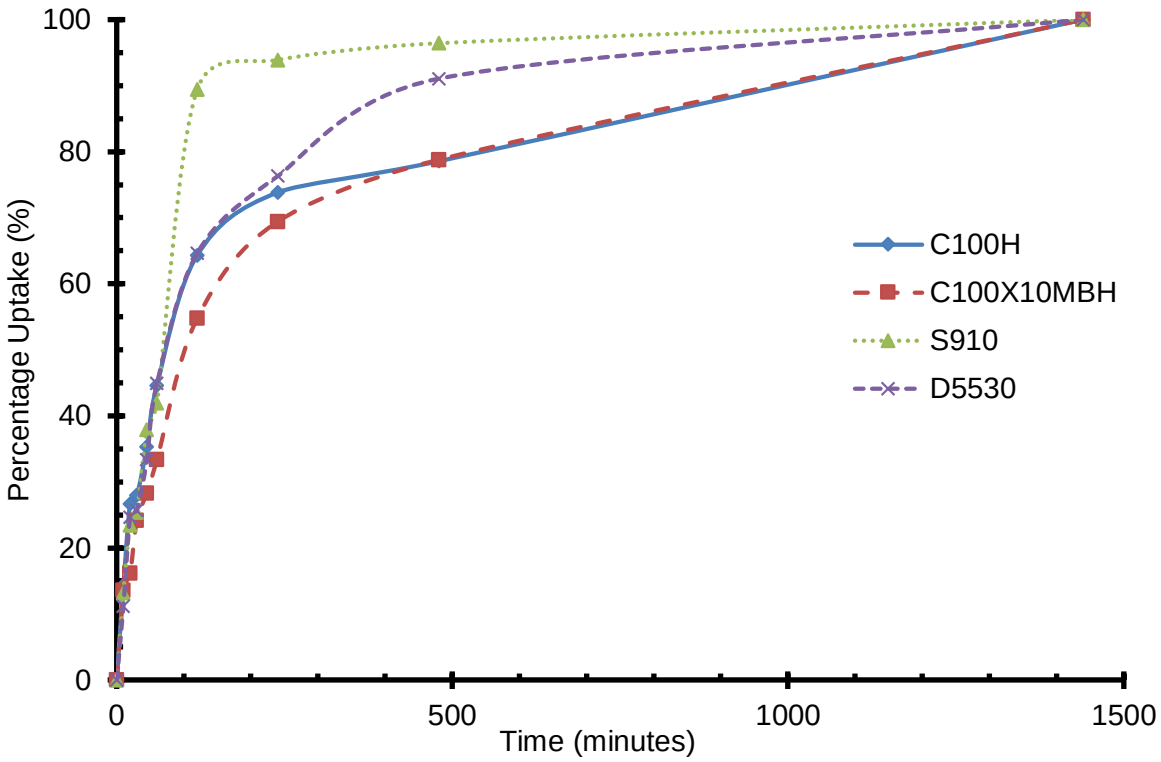

Figure 3.13 Percentage Ion Exchange Rate as a Function of Temperature at 25 ˚C

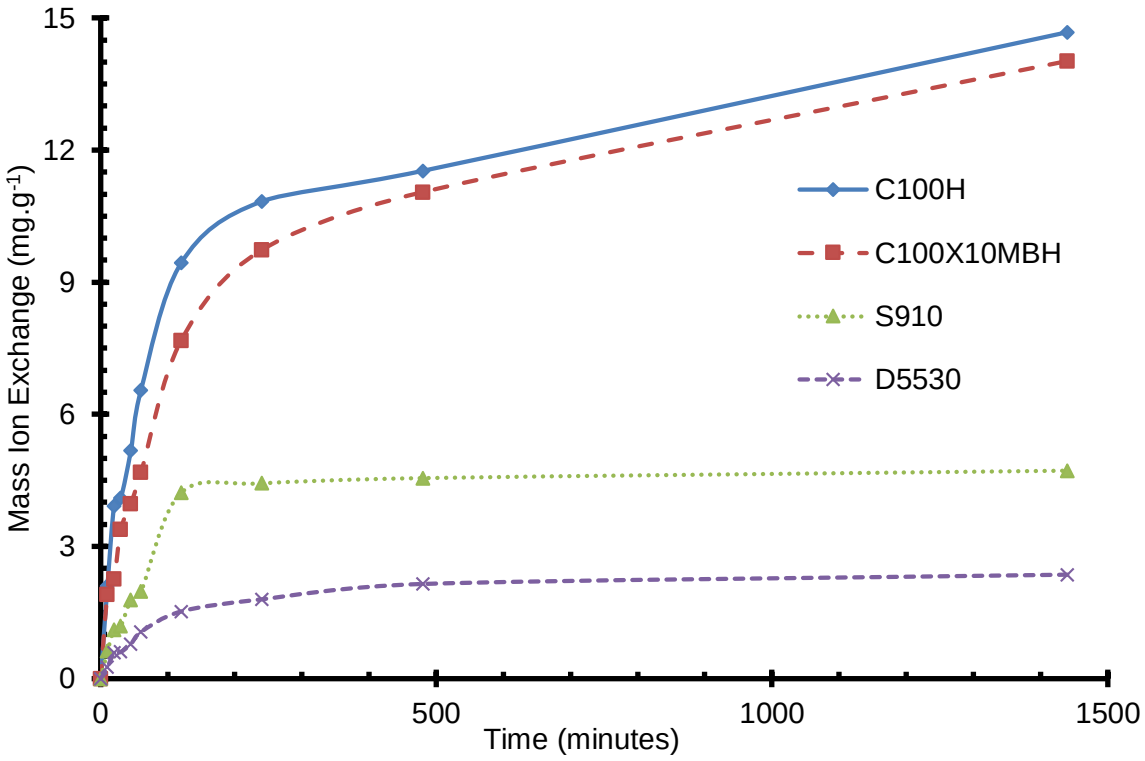

Figure 3.14 Mass Ion Exchange Rate as a Function of Temperature at 25 ˚C

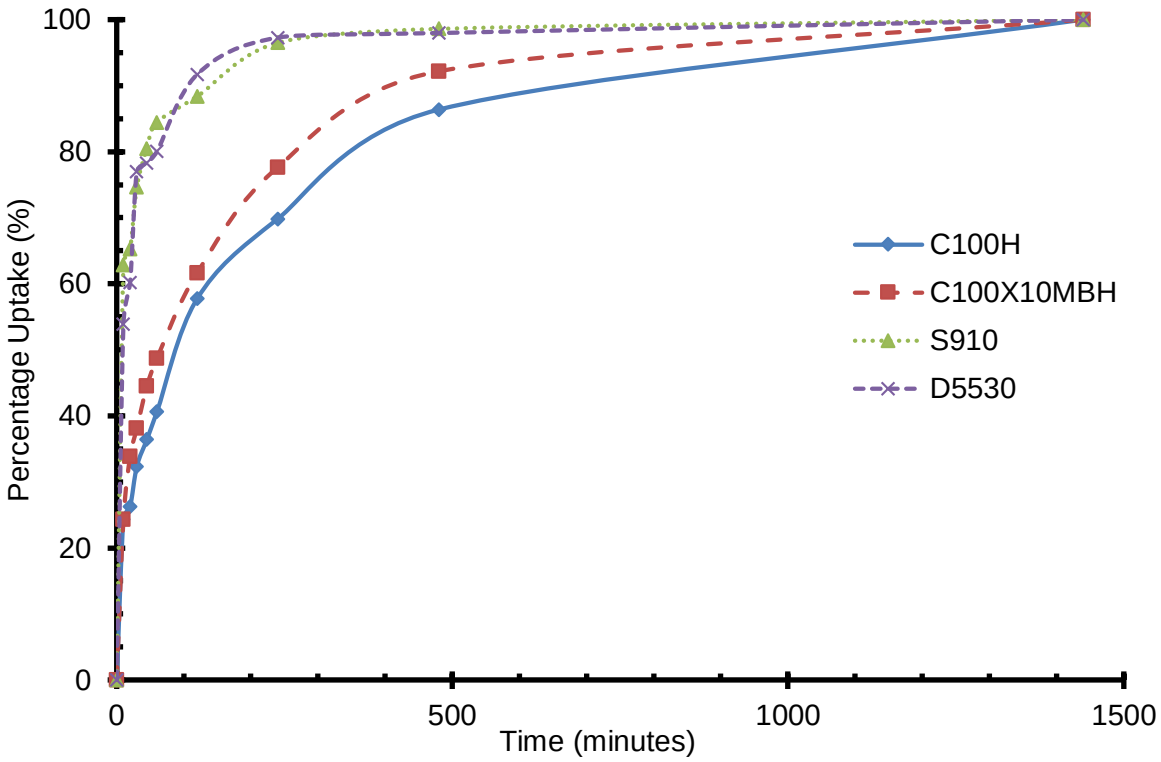

Figure 3.15 Percentage Ion Exchange Rate as a Function of Temperature at 45 ˚C

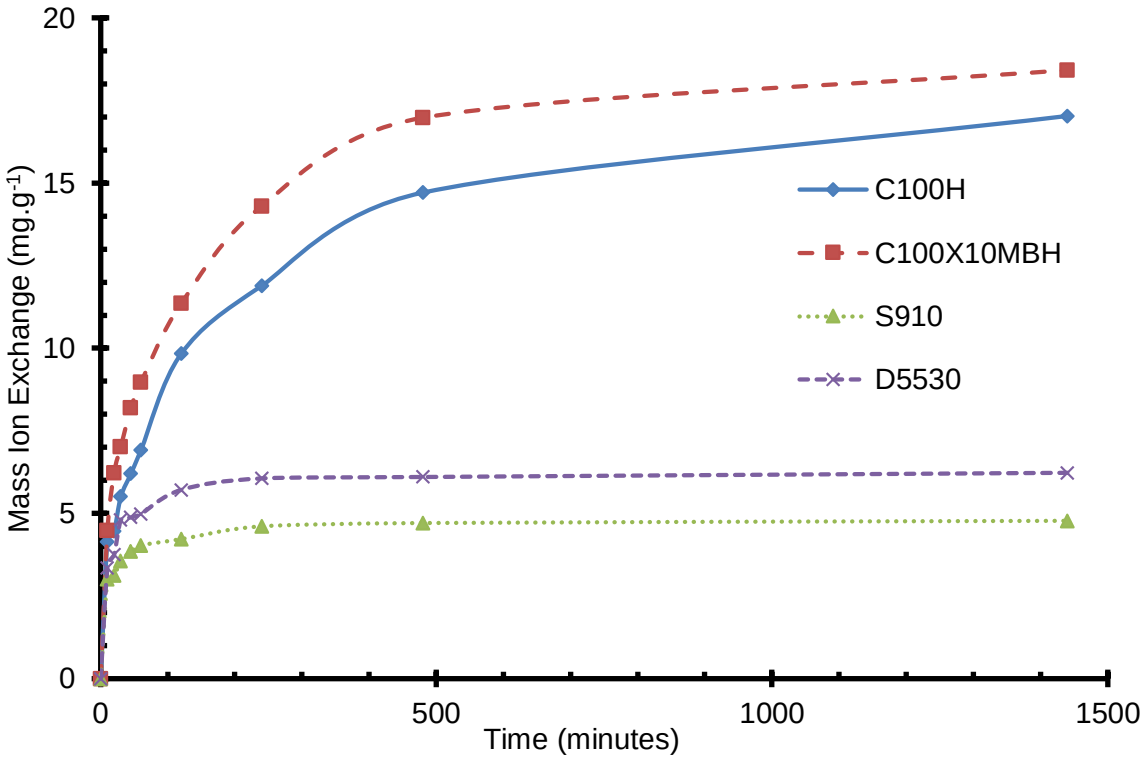

Figure 3.16 Mass Ion Exchange Rate as a Function of Temperature at 45 ˚C

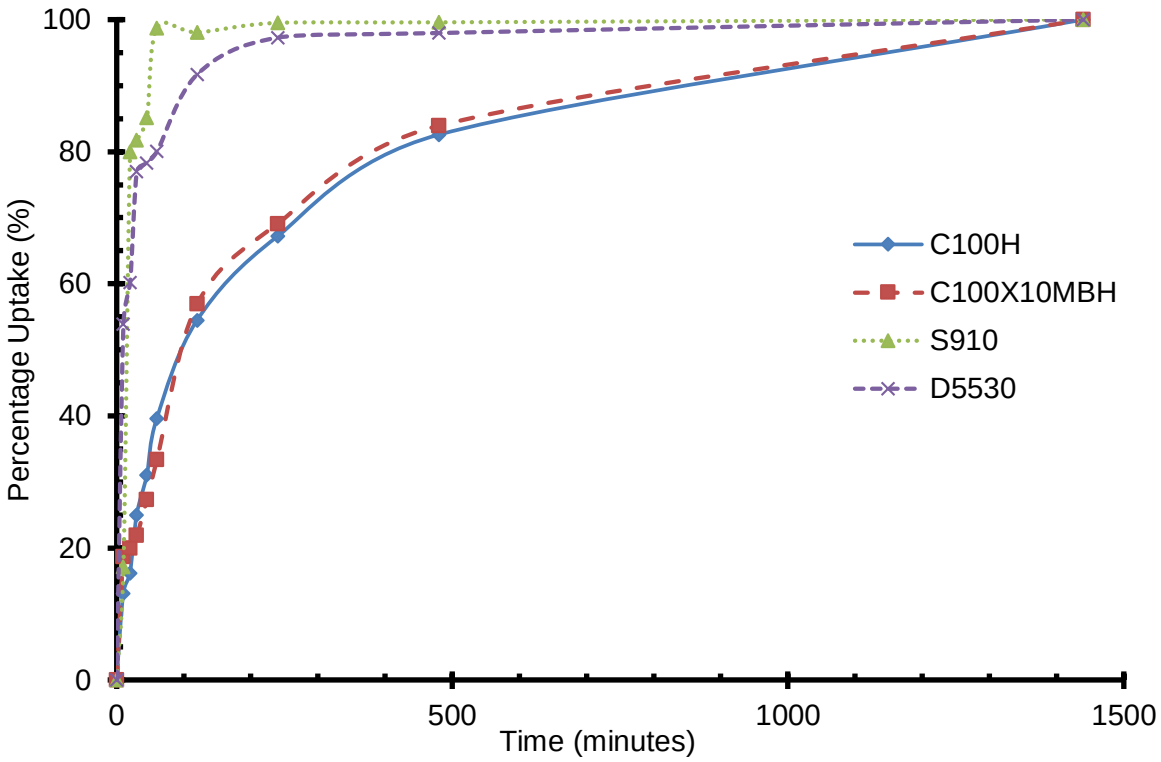

Figure 3.17 Percentage Ion Exchange Rate as a Function of Temperature at 60 ˚C

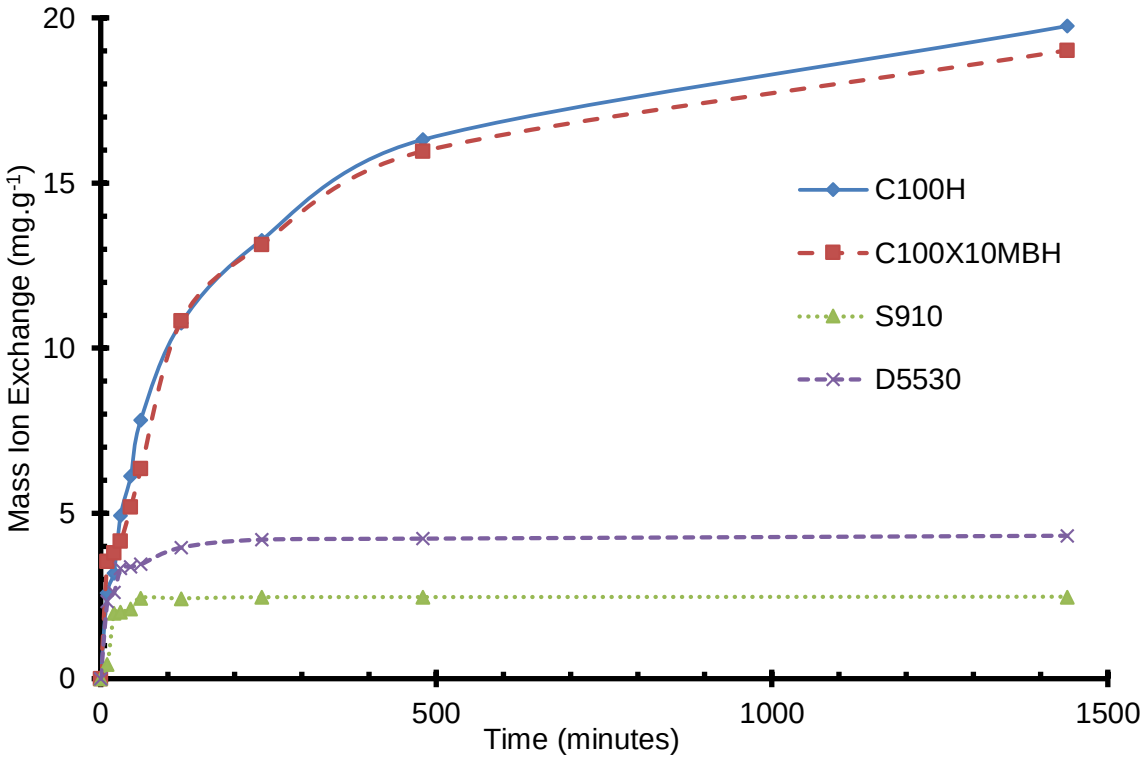

Figure 3.18 Mass Ion Exchange Rate as a Function of Temperature at 60 ˚C

The only experimental variable made to experiments described in this Section was the temperature of the liquor. Zr (IV) was the only ion utilised, as it was the only ion to display

any significant uptake on each of the resins and adsorbent under assessment. The resins and adsorbent used throughout this section were C100H, C100X10MBH, S910 and D5530.

It was expected that as the temperature was increased the rate of ion exchange would also increase. This increased rate was proposed on the basis that there is an activation barrier associated with the ion exchange process and the increased temperature assist ions to overcome this barrier. It has also been hypothesised that increased temperature may also cause electrostatic reactions to become weaker and subsequently a reduction in the solvent sphere within HNO_3 liquor resulting in a reduction in the effective ion radius, causing an increase in the diffusion coefficients through both the film coating and resin matrix. This would in turn produce a higher ion exchange velocity between the solution and the resin (94). This has previously been described in many articles and therefore expected for both the sulfonic acid and amidoxime resins tested. (22) (94 - 96)

The process of ion exchange in resins occurs initially as a diffusion through the thin fluid film on the resin surface and subsequently through the resin matrix itself (94). It was expected that as the cross linking of resin matrix was increased, so too would the time taken for equilibrium between the ion in solution and ion exchange capacity to occur.

Figures 3.13, 3.15 and 3.17 show the percentage ion exchange as a function of time, which can be used to assess the difference in the rate of ion exchange between each of the resins and adsorbents. As this data is expressed as a percentage of the total ion exchange capacity it is independent of the total ion mass exchanged. Whereas Figures 3.14, 3.16 and 3.18 display the difference in ion mass exchanged against time.

Table 3.16 Maximum Zr (IV) Ion Exchange Capacity at Various Temperatures

	Zr (IV) Ion Exchange Capacity ($mg.g^{-1}$)					
Temperature (°C)	25		45		60	
Resin		+/-		+/-		+/-
C100H	14.6	0.0	17.0	0.4	19.8	0.9
C100X10MBH	14.0	1.3	18.4	1.7	19.0	0.0
S910	4.7	1.7	4.6	0.6	2.4	0.7
D5530	2.4	1.2	6.1	0.5	4.2	0.2

From the data in Table 3.16 it can be seen that for both C100H and C100X10MBH sulfonic acid resins, the Zr (IV) exchange capacity increases with the temperature. Comparison of the data in the corresponding Figures 3.13 – 3.18 show that the rate of ion exchanges also increased in the range 25 - 45°C, however, there is no noticeable increase in rate between 45 and 60°C, this may be a result of the system operating under conditions of diffusion control.

The C100H resin displayed the largest ion exchange capacity in the 25 and 60 °C experiments. The more highly cross-linked C100X10MBH was expected to display a lower exchange capacity for the ion than the C100H. The difference in performance of the two resins was marginal and within the statistical uncertainty of the experiments there is no significant difference.

Of significance was the observed increase in ion exchange capacity as a function of temperature for the sulfonic acid resins. This observation is in line with that of Alvarez (94) who observed a similar phenomenon when studying the uptake of cadmium onto Dowex 50 (a similarly structured sulfonic resin).

The S910 amidoxime displayed a different relationship to the sulfonic acid resins. For the amidoxime resin there was little difference observed between the ion exchange capacities at 25 and 45 °C, with a significant reduction of ion exchange capacity at the 60 °C level.

The S910 was consistently the swiftest of the resins and adsorbent to achieve the 100 % ion exchange capacity over the 24 hour period. However, as the total ion exchange capacity is significantly smaller, the actual rate of ions exchanged is subsequently less.

The D5530 performed in a more unpredictable manner, producing a maximum exchange capacity at 45 °C with the lowest at 25 °C. The rate of ion exchange on the inorganic D5530 adsorbent was consistently between those observed for the amidoxime and sulfonic acid resins. The rate of exchange closely more resembled that of the S910.

Although of interest, the rates of ion exchange are not as important to the development of the chromatographic separation as the separation coefficients within Section 4.2. However, they did provide a suggestion of the maximum possible flow rate of the eluent within a chromatographic separation. The rate of ion exchange observed for each of the resins and adsorbents tested should be sufficiently rapid for use within the project. A one gram sample of resin was shown to be able to adsorb an amount within a 10 minutes period which was far in excess of the amount expected within a chromatographic column operating under predicted regimes of ion concentration and feed rate.

3.4 Determination of Ion Exchange as a Function of Zirconium Ion Concentration

This study again focused on those resins which have been shown to display desirable selectivity. The variation in exchange capacity as a function of concentration has been investigated over a Zr (IV) ion concentration rate between 200 and 3000 $mg.l^{-1}$, The uptake data has been fitted to a polynomial (to achieve a line of best fit) and also to equations for Langmuir and Freundlich isotherms; Figures 3.19 to 3.22. The maximum adsorption and Langmuir constant as determined from fitting the data to the Langmuir equation; the constant indicative of relative adsorption capacity and the Freundlich constant from fitting the data to a Freundlich isotherm are all contained in Table 3.17.

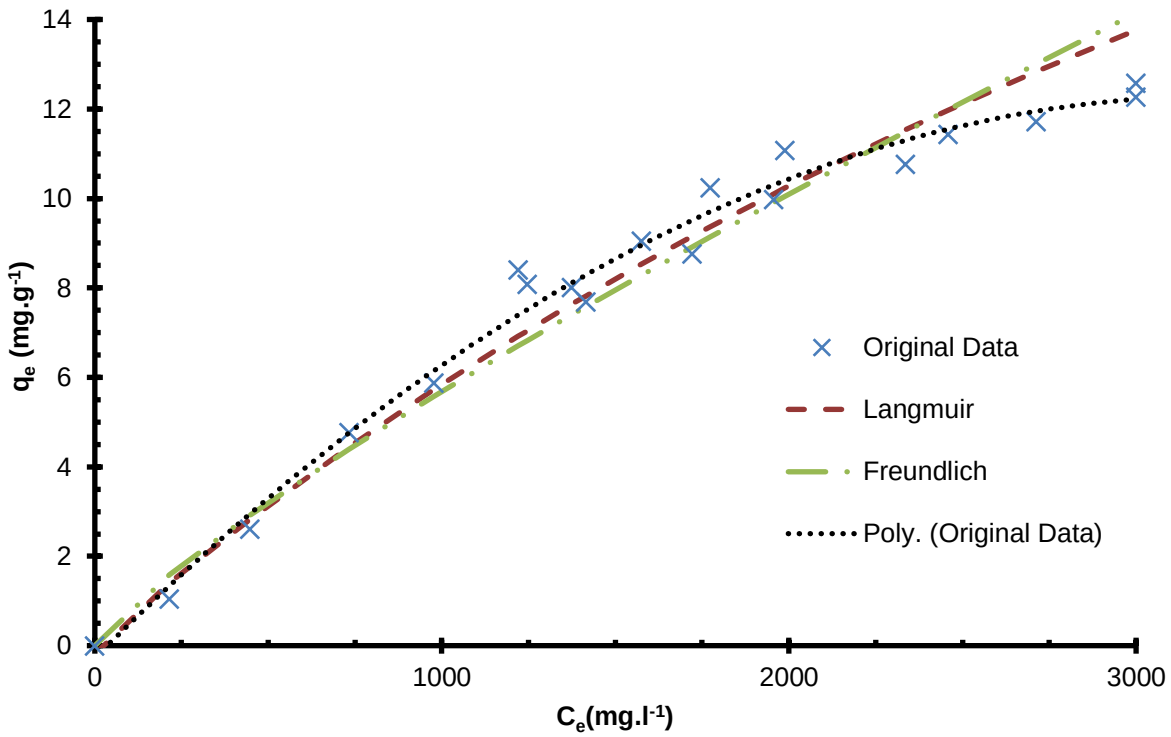

Figure 3.19 Ion Exchange Capacity as a Function of Zr ion Concentration for C100H

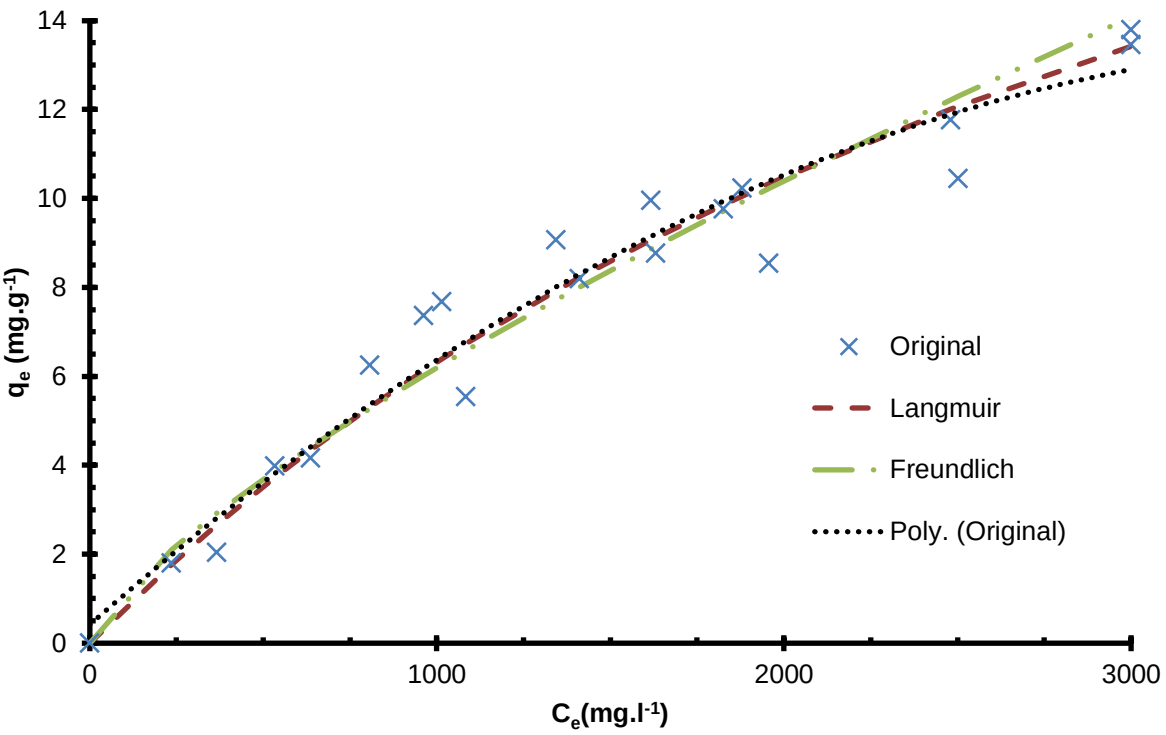

Figure 3.20 Ion Exchange Capacity as a Function of Zr ion Concentration for C100HX10MBH

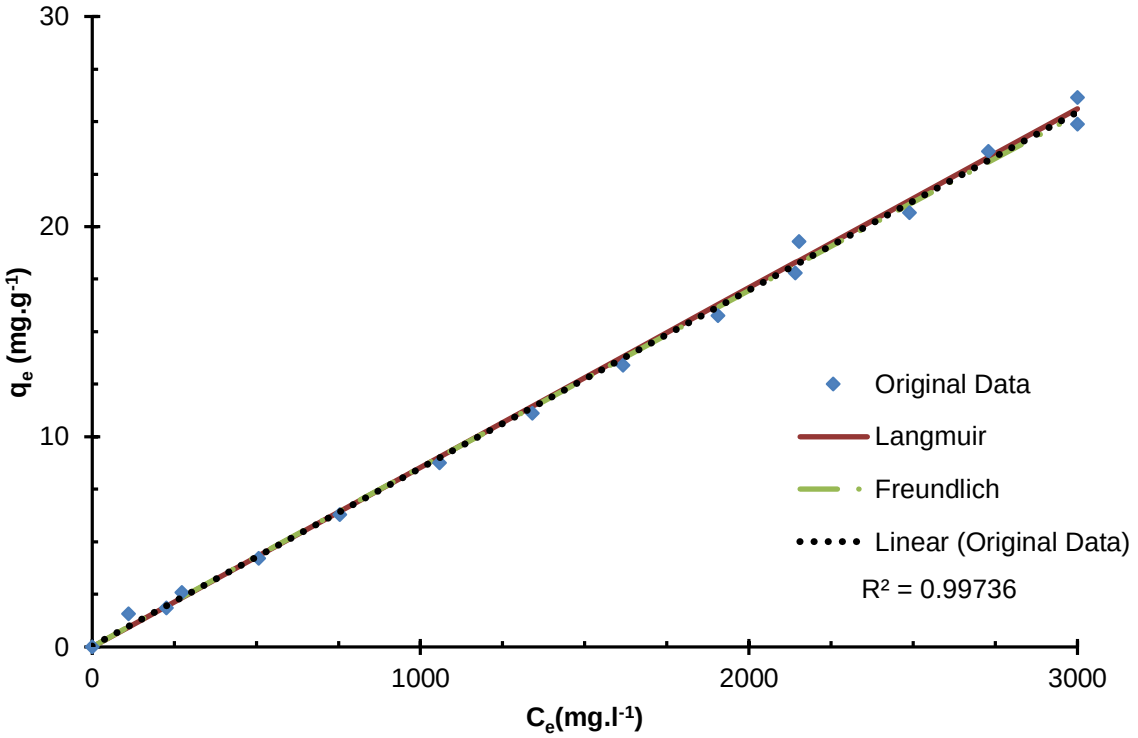

Figure 3.21 Ion Exchange Capacity as a Function of Zr ion Concentration for S910

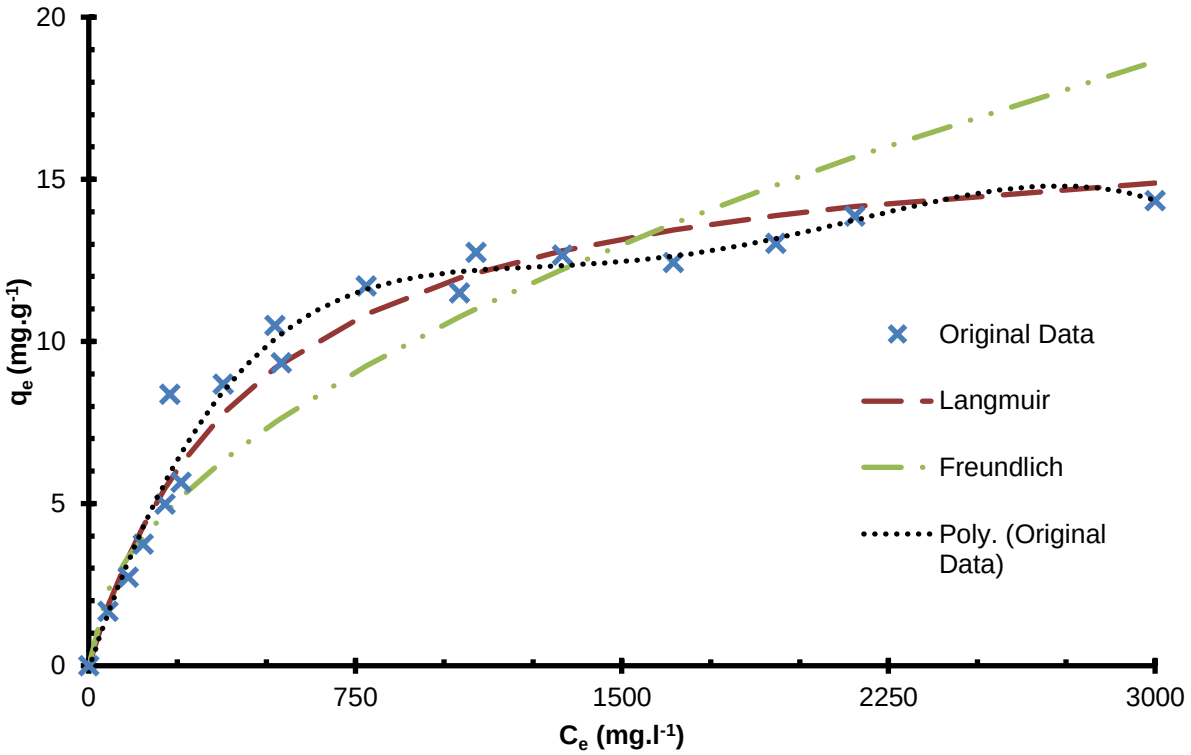

Figure 3.22 Ion Exchange Capacity as a Function of Zr ion Concentration for D5530

Table 3.17 Figures Calculated from Fitting Data to Langmuir and Freundlich Isotherms

Langmuir			
Resin	Q Maximum adsorption capacity (mg.g^{-1})	b Constant related to free energy of adsorption (L mg^{-1})	Sum of Squares
C100H	42.52	1.60E-04	7.30E-02
C100X10MBH	30.58	2.62E-04	2.00E-02
D5530	17.11	2.25E-03	6.20E-02
Freundlich			
	K_f Constant indicative of adsorption capacity (mg.g^{-1})	n Constant indicative of intensity of adsorption	Sum of Squares
C100H	1.87E-02	8.29E-01	1.58E-01
C100X10MBH	3.58E-02	7.47E-01	2.90E-02
D5530	2.97E-01	5.17E-01	6.87E-01

The adsorption isotherms have been produced with the aim of furthering the understanding of the behaviour of the resin or adsorbent under differing ion concentrations. This is important as it could potentially assist in understanding the operation of the stationary phase under the differing operational regimes encountered during chromatographic separation (96). The difference between Langmuir and Freundlich isotherms is due to either mono or multilayer adsorption. From the structure and literature, it was expected that both sulfonic acid resins would display the Langmuir adsorption type. For the S910 amidoxime it was possible that due to the chelate structure and uptake mechanism it may display the Freundlich isotherm. As the structure of the D5530 media was unknown, the isotherm was more difficult to hypothesise upon. However, the calculation of the best fit isotherm from experimental data was used to assess the nature of the uptake by the media and therefore the adsorption surface. A polynomial regression has also been employed in order to maintain the integrity of the data and aid in the visualisation of the Giles isotherm types.

The two sulfonic acid resins displayed similar ion exchange isotherms as shown in Figures 3.19 and 3.20 with the C100X10MBH resin displaying a higher ion exchange capacity than the C100H. Utilising the Giles method of identification, the isotherms most closely resemble an “L” shaped morphology implying a Freundlich behaviour, however, the sum of squares calculation in Table 3.17 shows that for both sulfonic acid resins produce a more reliable fit to a Langmuir type isotherm. The difference in the sum of squares for the C100H when making a comparison between the Langmuir to Freundlich isotherms doubled from 0.073 to 0.158, whilst the C100X10MBH resin displayed a better fit to both isotherm types as depicted by the value being closer to 0, there was a much smaller difference between the sum of squares (0.020 as opposed to 0.029), however, there was still a slightly better fit to Langmuir compared to Freundlich.

The S910 amidoxime resin, gave a “C” shaped isotherm (Figure 3.21) with a linear relationship between ion exchange capacity and initial concentration of the liquor. This linear relationship cannot continue indefinitely as at some point the maximum ion exchange capacity will be achieved, however, during these experiments the resin had not reached full ion capacity for zirconium. Had the initial Zr (IV) concentration been increased further then the exchange capacity would have become exhausted and the mass of ion exchanged begin to level out.

The Langmuir and Freundlich modelling analysis of the linear adsorption isotherm did not provide much insight. The difference between the sum of squares was minimal. Although the sum of squares calculation displays a preference for the Langmuir isotherm, the linear morphology of the curve means that this was unresolved.

The D5530 adsorbent most closely conforms to an “H” type isotherm (Figure 3.22), implying Langmuir type behaviour. A comparison between the sulfonic acid resins and the D5530 adsorbent demonstrates the obvious difference between the isotherms. Differentiation comes from the initial adsorption gradient being very steep, indicating a strong affinity between Zr (IV) and adsorbent. There was also a better defined maximum capacity, albeit that the ion exchange capacity was observed to be still increasing slightly as the Zr (IV) ion concentration was increased. Maximum Zr (IV) ion exchange capacity experimentally observed on the sulfonic acid resins and the D5530 adsorbent was approximately 14.1 $mg.g^{-1}$ of resin for zirconium. From the regression analysis the D5530 adsorbent was better represented by the Langmuir isotherm model than Freundlich, as the sum of squares observed was approximately an order of magnitude smaller. The D5530 also displayed the most complete isotherm. This media had the lowest uptake capacity of all resins and adsorbents tested.

The data calculated from these models was not without issue. Even discounting the S910 resin, the figures calculated in Table 3.17 required for the Langmuir model give the maximum capacity (Q value) to be double that measured experimentally, while the free energy constant (b value) was much smaller than observed in a comparable study by Mendes and Martin (85). This was mirrored in the Freundlich isotherm where the adsorption capacity figure (K_f value) and intensity of adsorption (n value) are both smaller than would be expected from a similar type of resin. However, this may be a facet of utilising the solver function within Microsoft Excel, which gave the smallest sum of squares and therefore best theoretical fit for the raw data and equations provided, despite this being practically impossible. The high theoretical Zr (IV) capacities are likely to be due to resins or adsorbents not having reached an ion exchange plateau at maximum uptake within the experimental range of Zr (IV) in the liquor and subsequent calculation of the isotherms. This was displayed by the D5530 adsorbent which came closest to reaching the maximum ion exchange capacity plateau. The subsequently calculated theoretical maximum uptake was closest to the experimentally measured figure. For both the C100H and C100X10MBH resins the largest divergence between the experimental data and the Langmuir and Freundlich models are observed at the most concentrated Zr (IV) liquor concentrations.

3.5 Breakthrough and Elution in Columns

The data in this section complements the capacity measurements previously described in Section 2.3.2. However this data provides information concerning the resin performance in a dynamic setting.

The analysis of the breakthrough studies provides further information as to the worth of the adsorbent for use in continuous chromatography instrumentation. Using a binary ion solution indicates whether the separation was effective in a dynamic system, as opposed to the quasi-equilibrium of the batch experiments. It was a simplification of the proposed eventual process, but one which would give an improved understanding of the exchange chemistry occurring.

The breakthrough curves were produced using Zr (IV) and Ce (IV) as described in Section 2.3.5. The curves produced using 1 M HNO_3 solutions are shown in Figures 3.23, 3.25, 3.27 and 3.29, while the curves produced using 3 M HNO_3 solutions are shown in Figures 3.31, 3.33, 3.35 and 3.37.

Also included is the subsequent stripping of the column with 5 M HNO_3 once the ion had been loaded onto the media. This would primarily display if the ion could be removed from the adsorbent once it has been adsorbed and therefore if a chromatographic separation could be performed. If the ion could be removed, a peak would be observed. If the ion remains bound to the adsorbent, or if there was no uptake from the feed, the ICP-MS assay would not display any ion within the eluent. These are displayed in the even figures between Figure 3.24 and 3.38.

This data provides information concerning the capacity of the resin and also its preference in a competitive situation as can be seen when one ion was displaced, resulting in a C/C_0 value greater than 1.

Breakthrough curves can also give information as to the chromatographic performance of a column. Using a simple equation, the number of theoretical plates for a column could be calculated for the column (97) (98). This would be of use within the chromatographic development.

$$N = \frac{V_R(V_R - \sigma_V)}{\sigma_V^2}$$

Equation 3.1 Theoretical Plates from Breakthrough Curve

Where N is the number of theoretical plates in column, V_R is the volume eluted for C/C_0 to equal 0.5 and σ_V is the standard deviation of the breakthrough curve (calculated from the Gaussian model). This data is displayed in Table 3.18.

Due to the high number of fractions collected for each of these experiments, time constraints and the volume of virgin resin required, these experiments were run singly. The results displayed represent an average of two aliquots taken from the same fraction. If the relative standard deviation was greater than 5 % a further sample of the fraction was assayed until the relative standard deviation was found to be at an acceptable level. Again as described in Section 3.2, within the ICP-MS, the aliquots were subjected to three “passes” where an assay was performed for each of the ions and the figure from this averaged, to give a single concentration for the fraction sample.

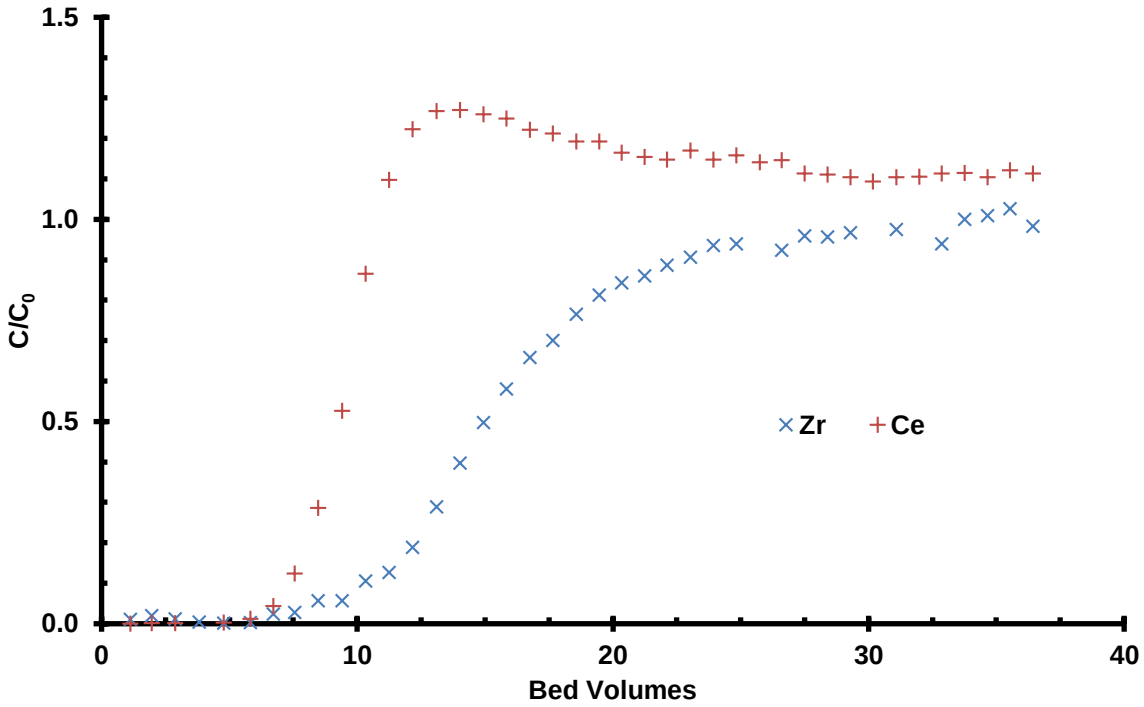

Figure 3.23 Breakthrough Curve for C100H Resin in 1 M HNO_3

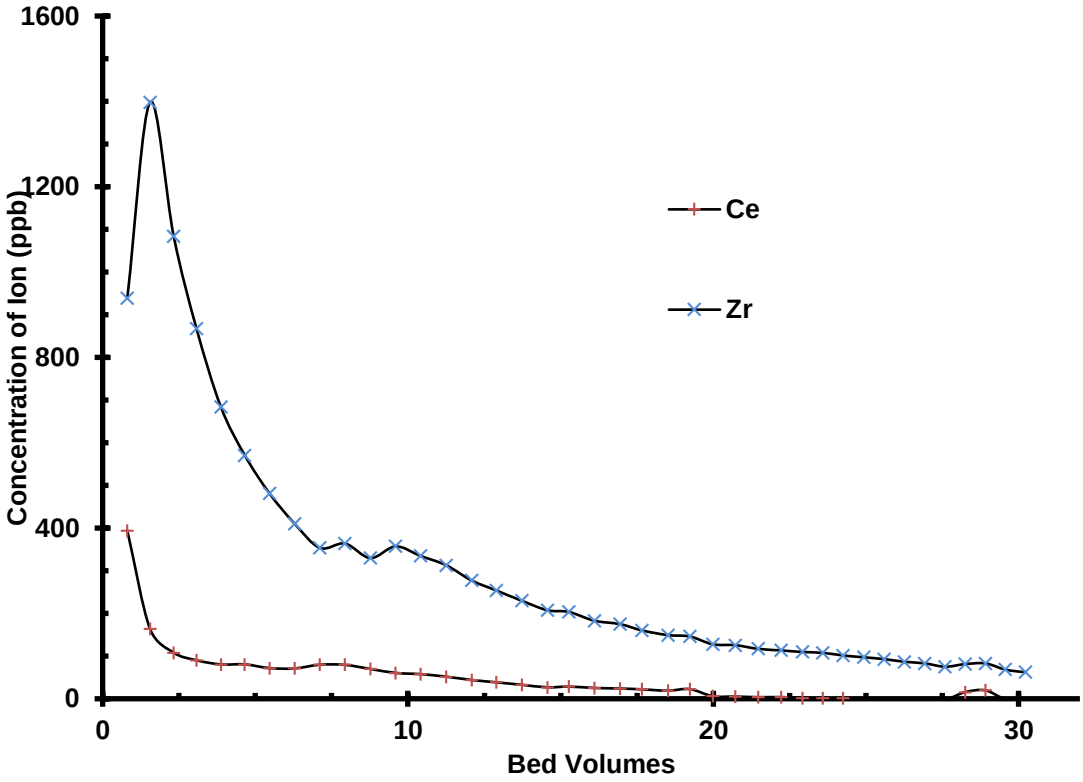

Figure 3.24 Stripping Profile for C100H Resin in 5 M HNO_3

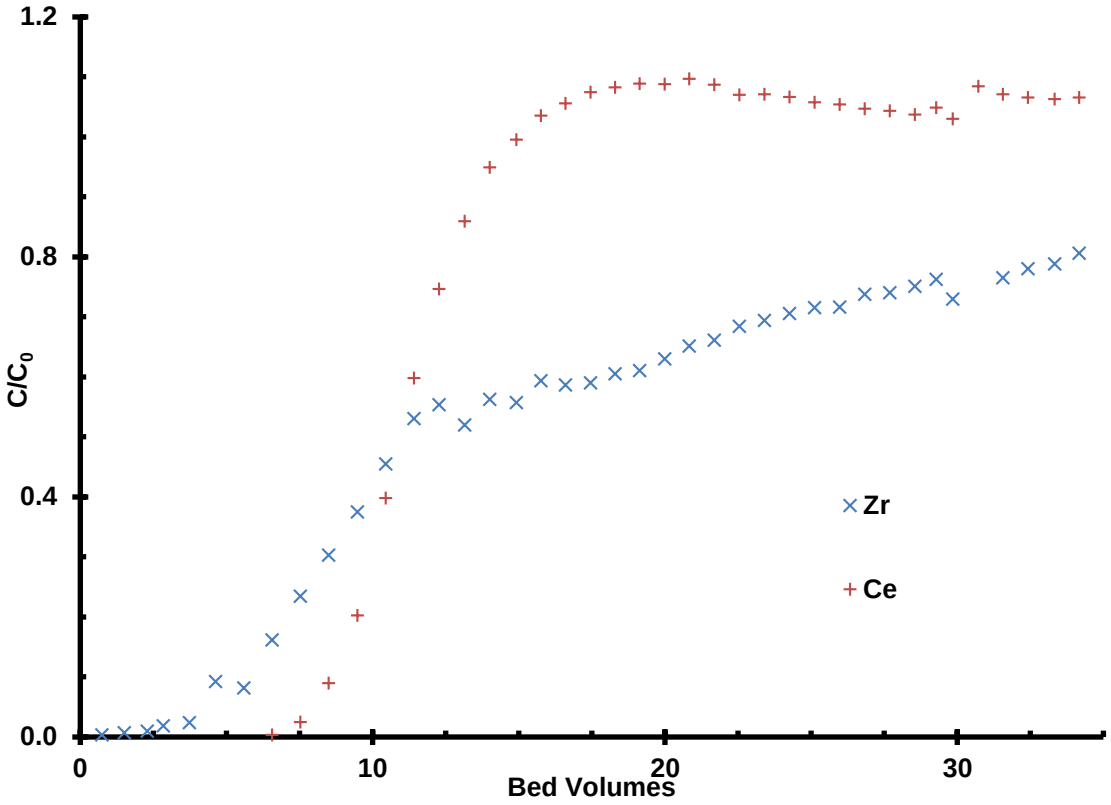

Figure 3.25 Breakthrough Curve for C100X10MBH Resin in 1 M HNO_3

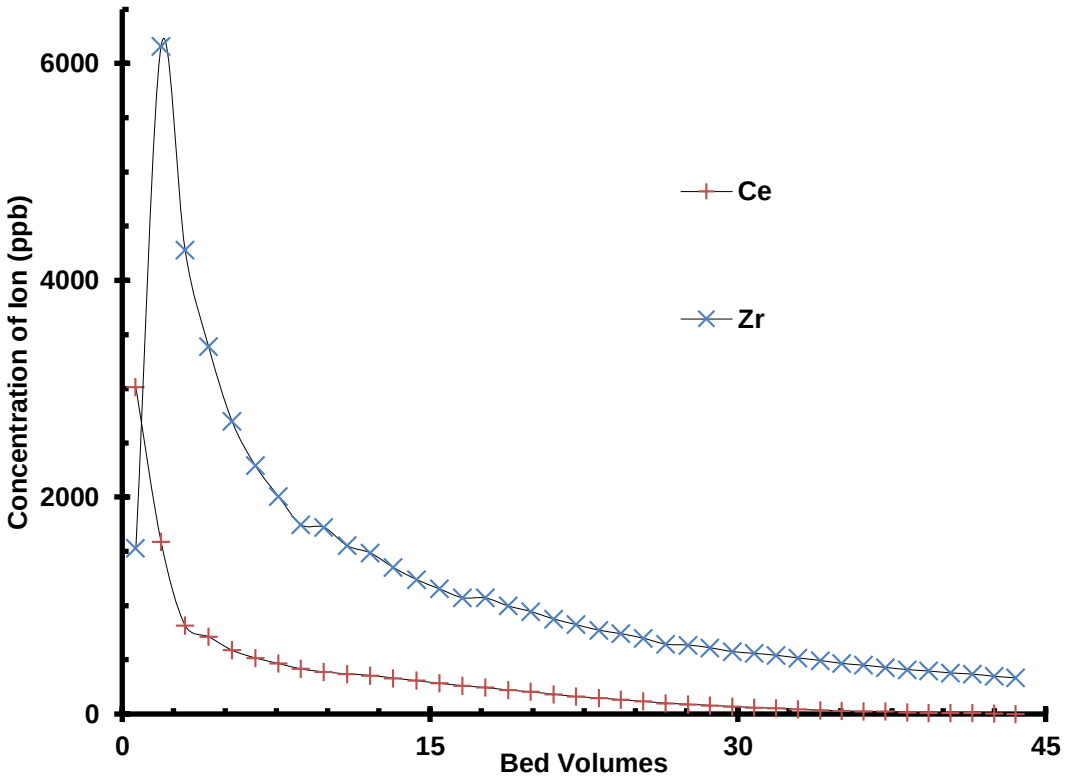

Figure 3.26 Stripping Profile for C100X10MBH Resin in 5 M HNO_3

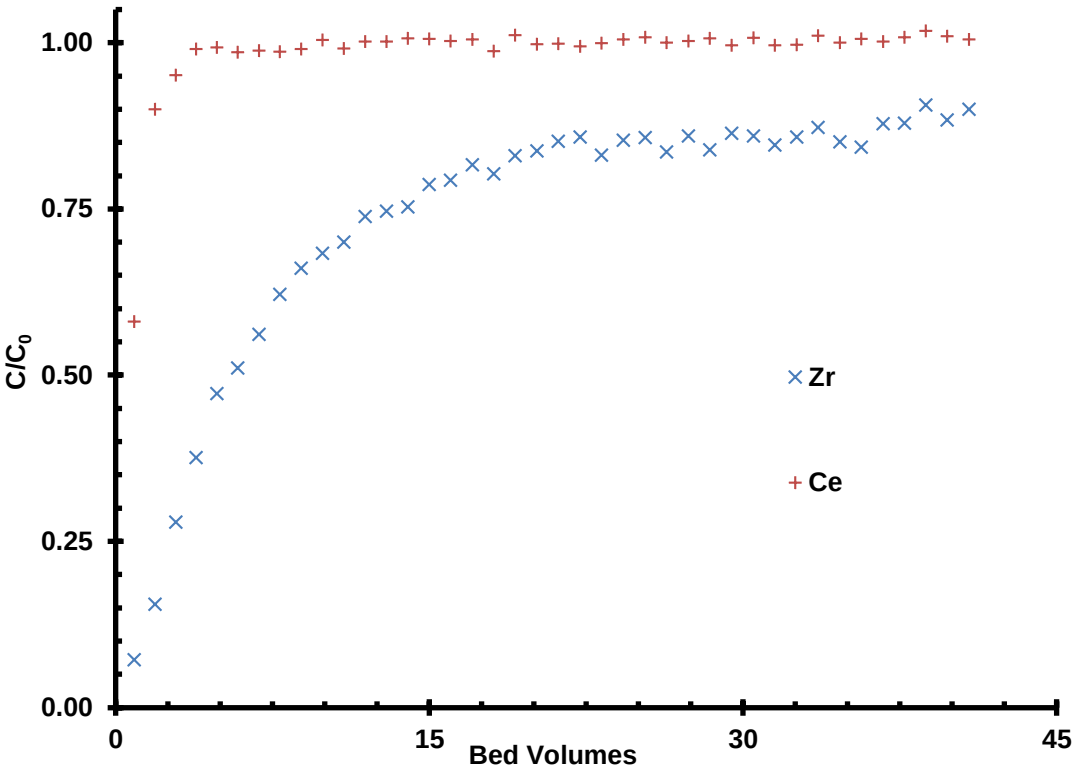

Figure 3.27 Breakthrough Curve for S910 Resin in 1 M HNO_3

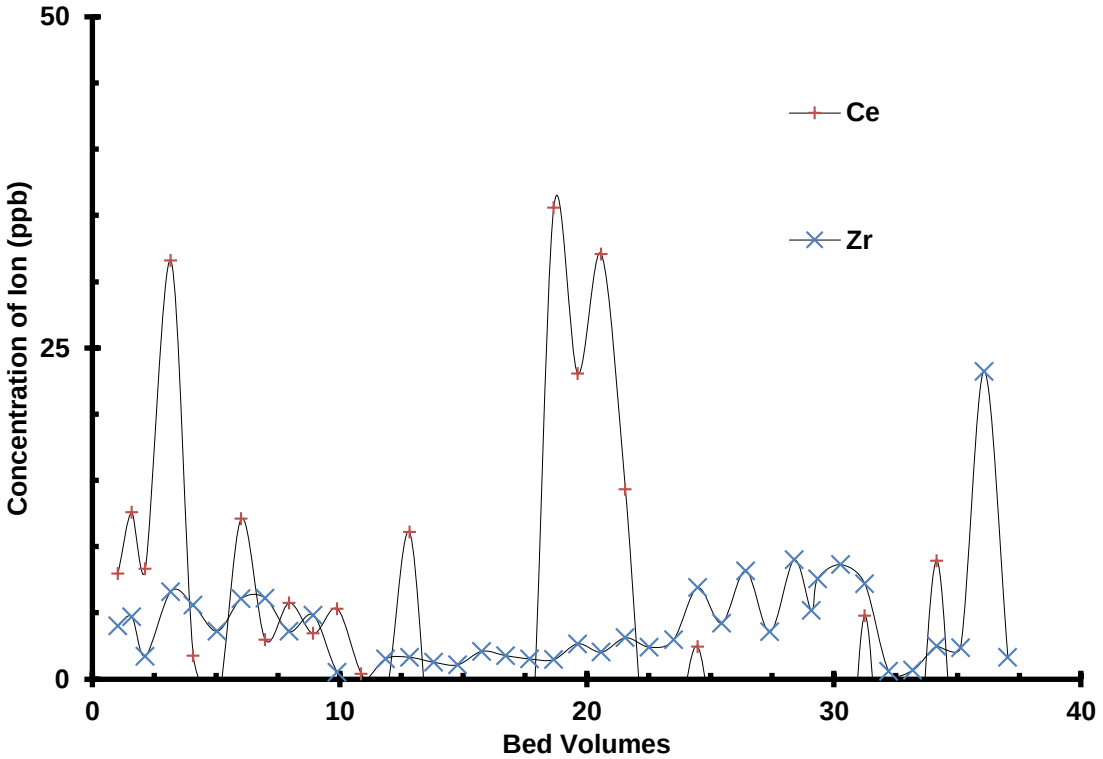

Figure 3.28 Stripping Profile for S910 Resin in 5 M HNO_3

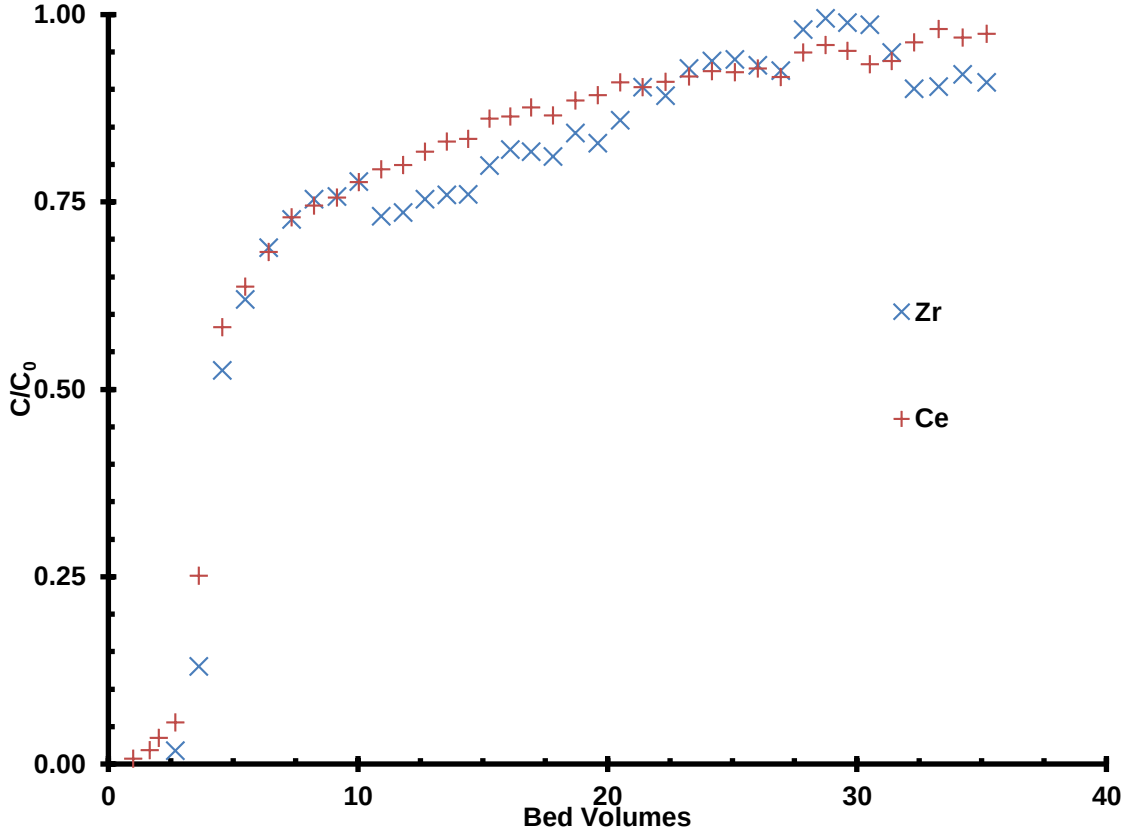

Figure 3.29 Breakthrough Curve for D5530 Resin in 1 M HNO_3

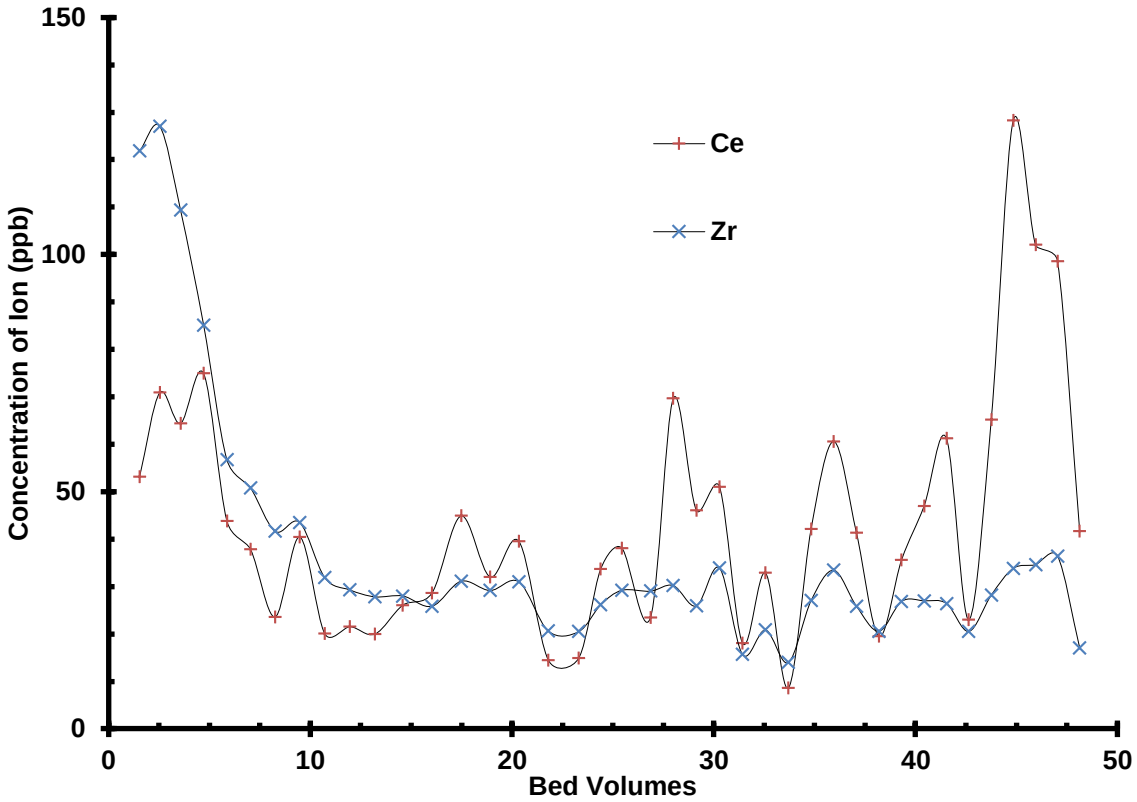

Figure 3.30 Stripping Profile for D5530 Resin in 5 M HNO_3

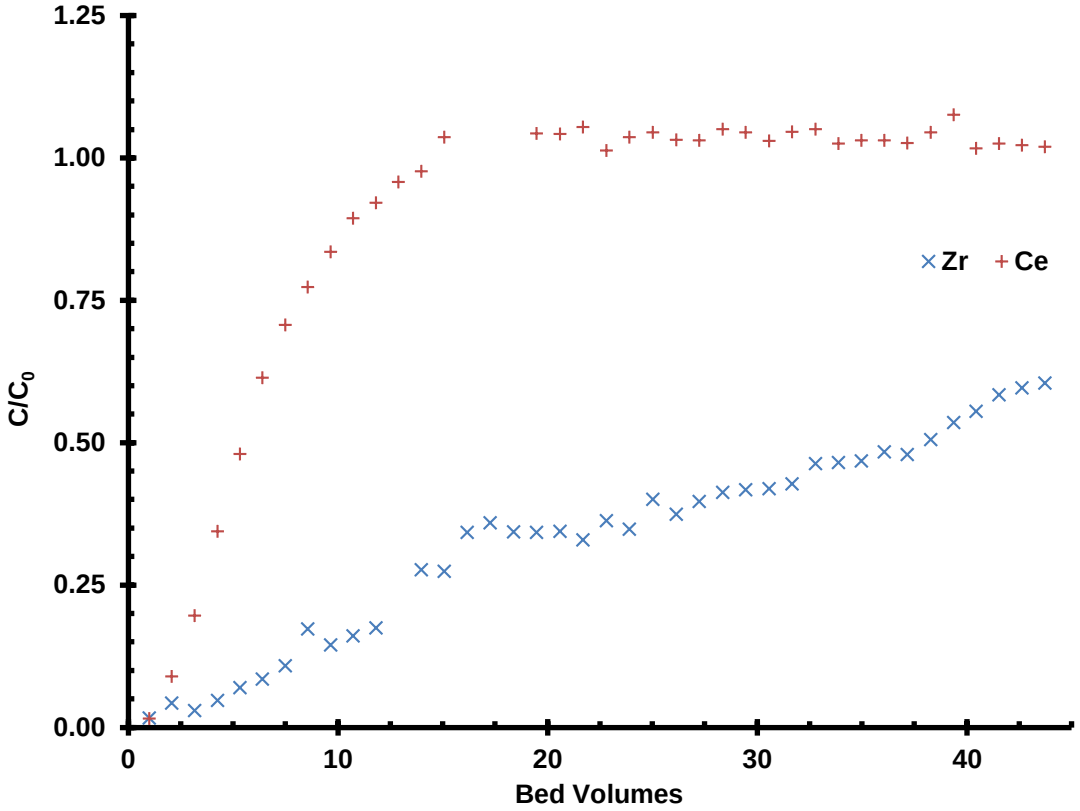

Figure 3.31 Breakthrough Curve for C100H Resin in 3 M HNO_3

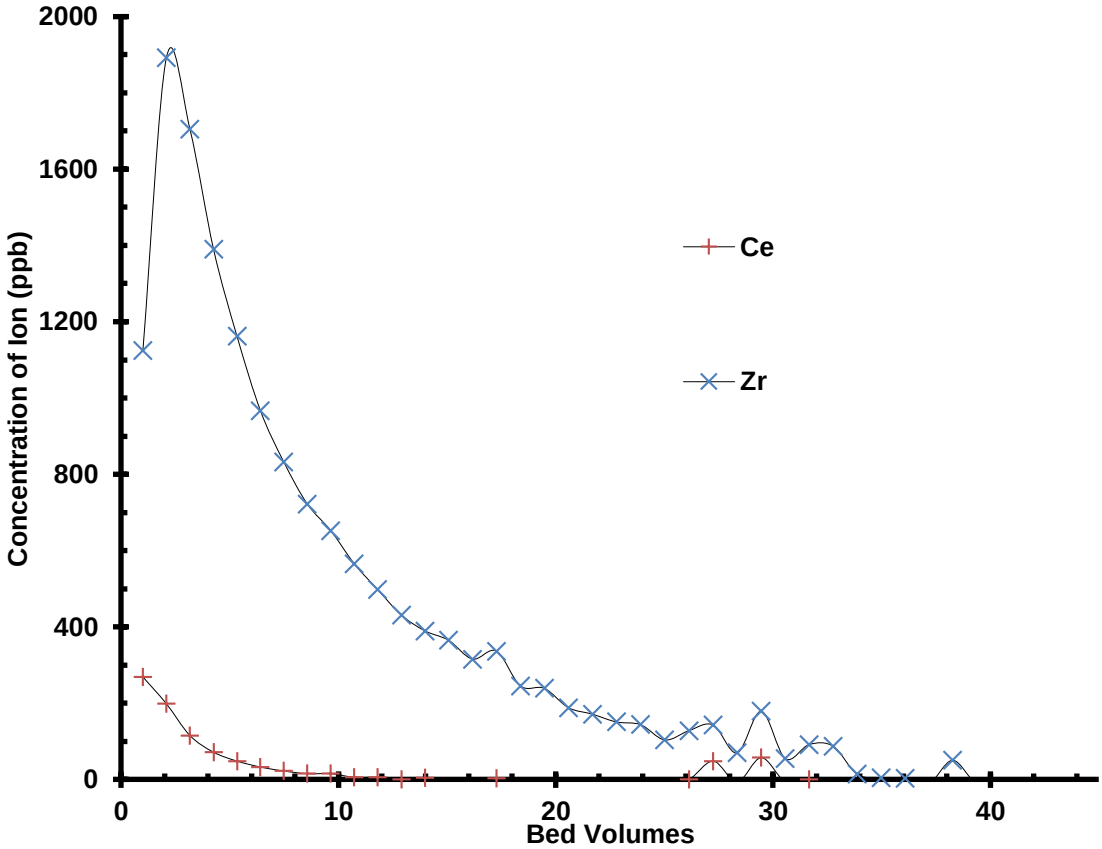

Figure 3.32 Stripping Profile for C100H Resin in 5 M HNO_3

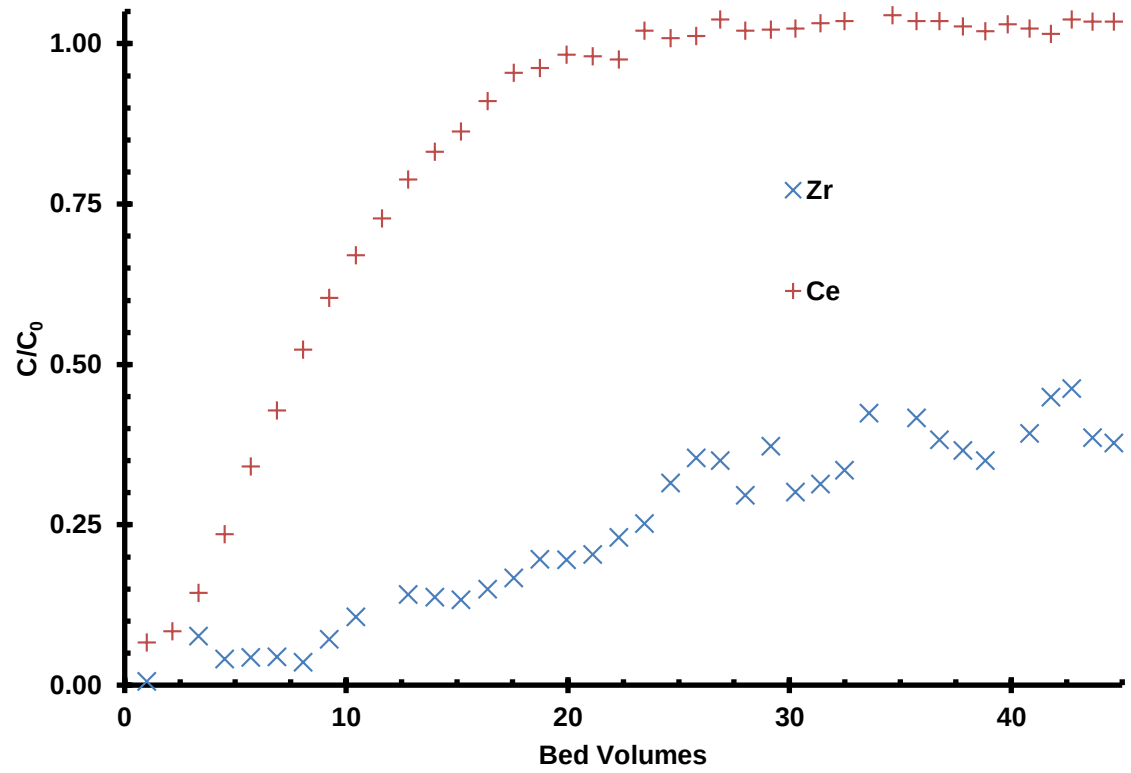

Figure 3.33 Breakthrough Curve for C100X10MBH Resin in 3 M HNO_3

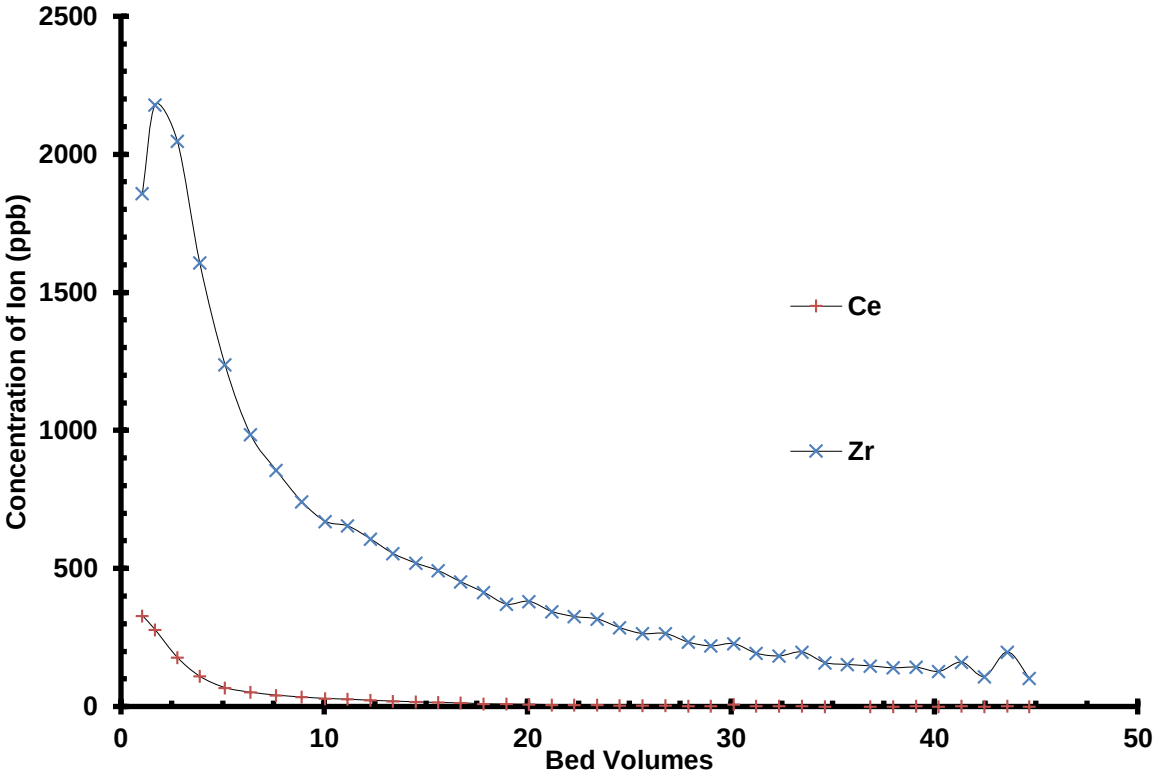

Figure 3.34 Stripping Profile for C100X10MBH Resin in 5 M HNO_3

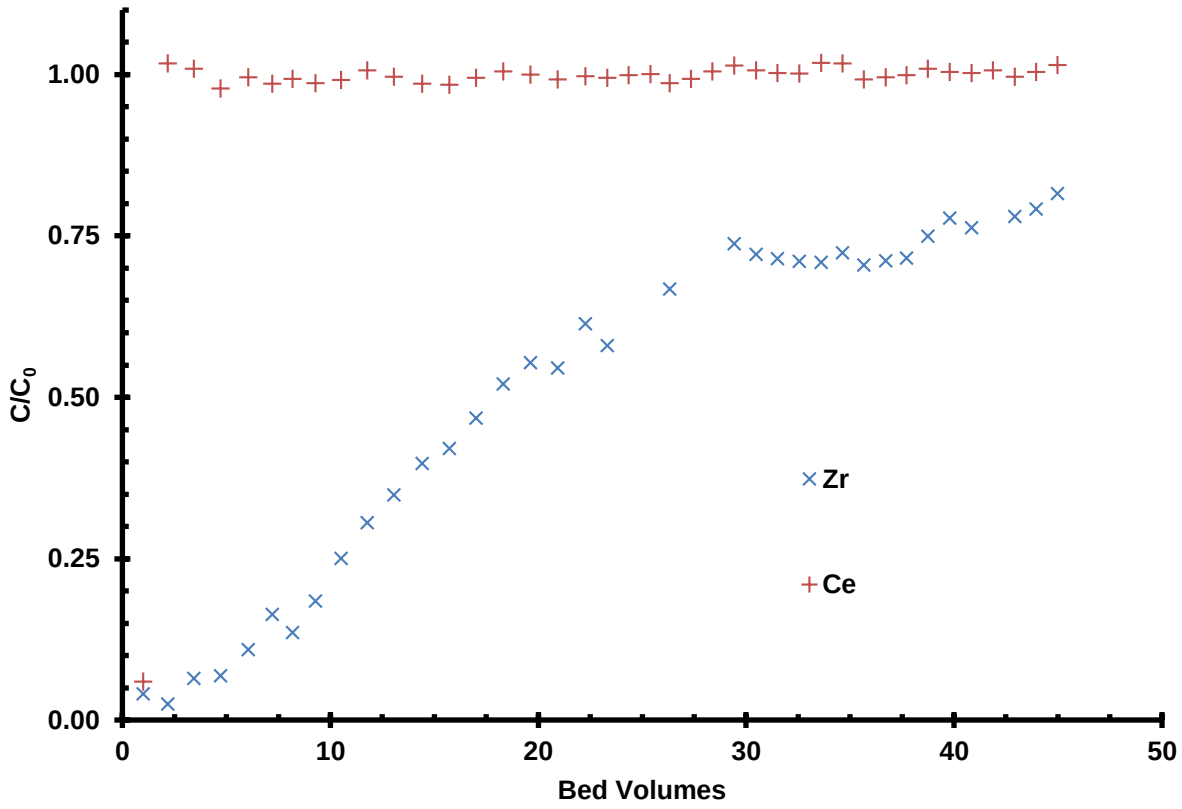

Figure 3.35 Breakthrough Curve for S910 Resin in 3 M HNO_3

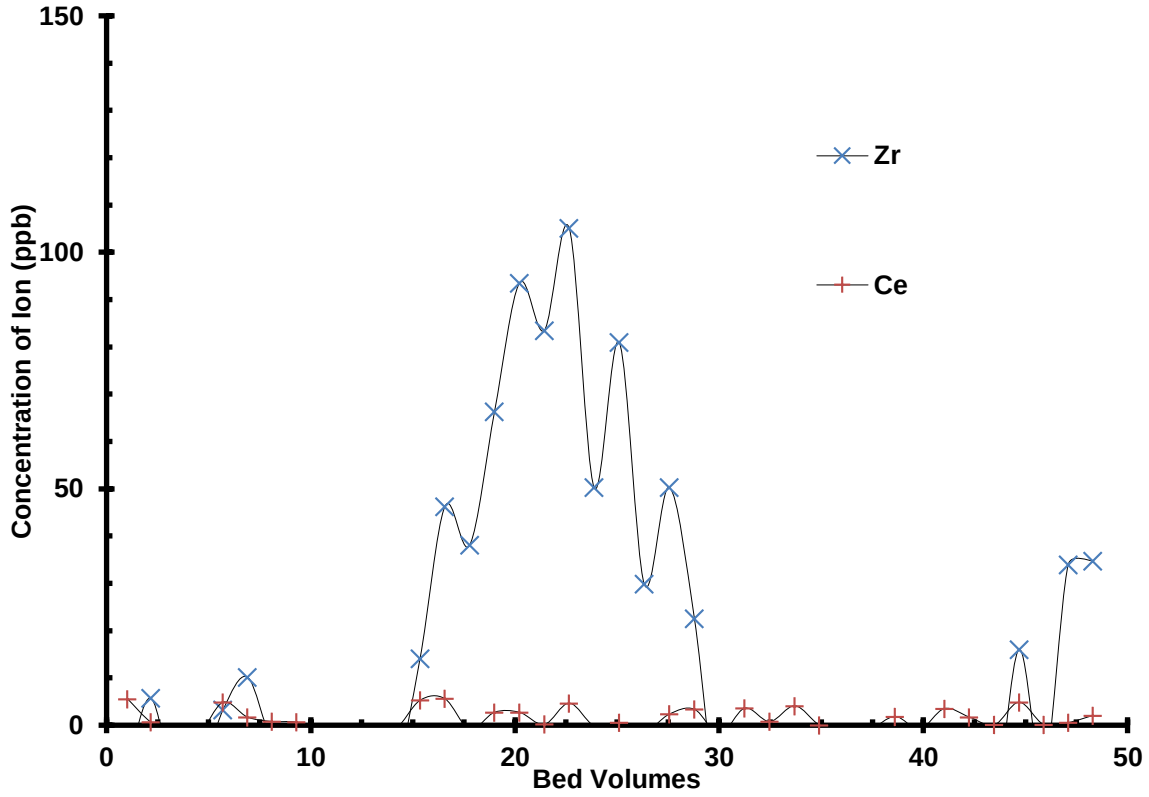

Figure 3.36 Stripping Profile for S910 Resin in 5 M HNO_3

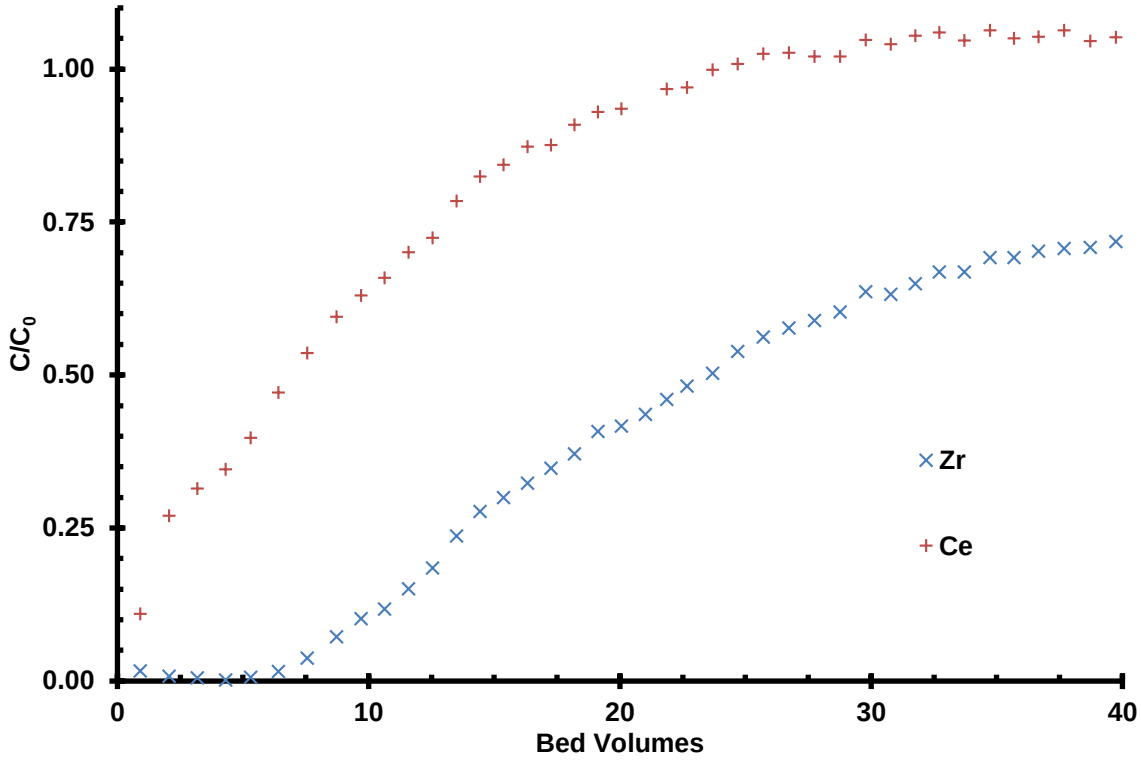

Figure 3.37 Breakthrough Curve for D5530 Resin in 3 M HNO_3

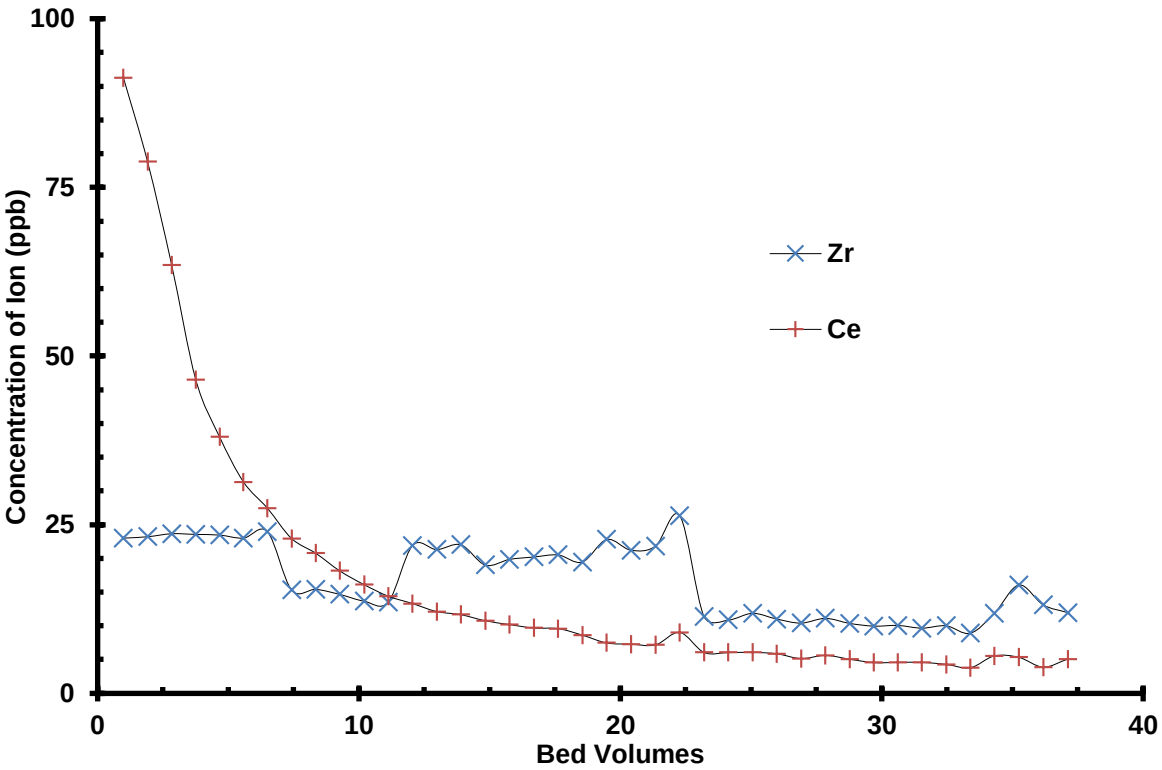

Figure 3.38 Stripping Profile for D5530 Resin in 5 M HNO_3

Table 3.18 Column Characteristics Calculated from Elution Profiles

Resin	Acid Concetration (M)	C/C_0	Volume of Elution for Zr Ion (ml)	Volume of Elution for Ce Ion (ml)	Theoretical Plates for Column For Zr Ion	Plates Per Metre
C100H	1	0.159	175.40	117.78	0.44	2.0
		0.5	232.89	146.59		
C100H	3	0.159	155.85	45.99	9.16	41.6
		0.5	556.02	77.49		
C100X10MBH	1	0.159	97.61	140.81	1.28	5.8
		0.5	169.61	169.61		
C100X10MBH	3	0.159	249.59	47.23	3.45	15.7
		0.5	-	114.48	Calculated from Ce	
S910	1	0.159	24.20	11.91	7.18	32.7
		0.5	78.08	11.91		
S910	3	0.159	97.20	-	3.93	17.9
		0.5	247.44	-		
D5530	1	0.159	34.98	34.98	0.33	1.5
		0.5	44.09	44.09		
D5530	3	0.159	156.69	12.33	2.13	9.7
		0.5	320.03	86.59		

These experiments give the best indication of how the stationary phases perform under chromatographic conditions. The analysis of the breakthrough studies provided further information as to the worth of the adsorbent for use in continuous chromatography instrumentation. A binary ion solution of the two most highly retained ions indicated the effectiveness of a separation in a dynamic system, as opposed to the near equilibrium of the batch experiments. The experiments display a simplification of the proposed chromatographic process but one which would give an improved understanding of the exchange chemistry occurring. The breakthrough curves also gave an indication of the capacity for each of these ions. The curve also provided an indication of the ion preference of the adsorption sites, with the ion that broke through first displaying a lower affinity for the resin. An ion (ion A) concentration of greater than 1 in the eluent stream indicated that ion A that had previously been adsorbed onto the resin or adsorbent and was then being displaced by an ion (ion B) with a greater affinity for the resin or adsorbent.

Stripping profiles of the adsorbed ions on the column using 5 M HNO_3 are also displayed. This primarily displayed whether the ion could be removed from the resin or adsorbent once it has been adsorbed and therefore if a chromatographic separation could be performed. If the ion could be removed in the 5 M HNO_3, a significant concentration would be observed within the eluent. However, if the ion remained bound to the resin or adsorbent, or if there was no uptake from the feed, no significant ion concentration would be observed within the eluent.

Breakthrough curves also gave information as to the chromatographic performance of a column, using Equation 3.1. The number of theoretical plates for a column was calculated

for the column (97) (98). This would be of use within the chromatographic development discussed in Section 3.6.

For the C100H resin in 1 M HNO_3 depicted in Figure 3.23 there was a relatively large number of bed volumes eluted before either the Zr (IV) or Ce (IV) displayed a breakthrough. The cumulative Gaussian morphology of these breakthrough curves indicates that at the column conditions utilised within the experiment, the rate of ion exchange was sufficient for a chromatographic separation to occur. If ion exchange was not occurring to the full extent, the curve would display a straight line as opposed to the Gaussian shape observed.

Results from the C100H resin show that Ce (IV) was less retained than the Zr (IV). This confirmed the data from Table 3.10 in Section 3.2.3. The initial breakthrough of Ce (IV) was observed at 7.56 B.V. with 50% breakthrough of the initial concentration at 9.4 B.V. and 100% at 10.33 B.V. in comparison with the Zr (IV) values which occurred at 10.33, 14.93 and 33.77 B.V. respectively.

A Ce (IV) C/C_0 concentration greater than 1 implies that the column had become fully saturated with both ions and also that the Zr (IV) was starting to preferably exchange for the Ce (IV). A maximum C/C_0 ratio of 1.27 for the eluted Ce (IV) was recorded at 13.10 B.V., the C/C_0 then reduced towards the initial feed concentration as the rate of exchange of zirconium slowed. The Zr (IV) ion concentration in the eluent until the column was saturated and the final concentration of both ions in the eluent approximate to that in the feed.

The number of theoretical plates determined for this column was 2.0 plates per metre when determined from the 1 M HNO_3. This increased to 41.6 plates when 3 M when HNO_3 was used. The data from the experiments with 3 M HNO_3 clearly shows that the adsorption of the Ce (IV) is greatly reduced with $C/C_0 = 0.5$ being achieved at 5.33 B.V. therefore the number of sites available to adsorb Zr is greatly increased and consequently the Zr (IV) break through curve does not reach a value of C/C_0 during this experiment. This may be a result of the flow being such that there was insufficient time for equilibrium to be established and this manifested itself in a non-Gaussian peak shape resembling the phenomenon referred to as fronting in traditional chromatographic separation. There is clear evidence from the data in Figure 3.14 that the rate of ion exchange is relatively slow in comparison to the time spent on the column. Using 3M HNO_3 the Ce (IV) ion concentration did achieve a C/C_0 value greater than 1, it did not reach 1.27 observed in the 1 M HNO_3 eluent. This is as expected given that the equilibrium concentration of adsorbed ions is far less with 3M HNO_3 that with 1 M HNO_3.

The ion stripping of C100H at 5 M HNO_3 displays a good correlation between the elution profiles in both the 1 M and 3 M HNO_3 eluent experiments. This was positive for the project in that the ion adsorption was reversible and therefore the resin could be used for a chromatographic separation.

The C100x10MBH resin in the 1 M HNO_3 eluent, displayed in Figure 3.25, does not behave as expected from the previous studies. The initial breakthrough for Ce was at 8.52 B.V. with 50% breakthrough of the initial concentration at 11.0 B.V. and 100% at 14.94 B.V. as opposed to the Zr where initial break through occurred at 4.65 B.V., 50% at 11.0 B.V. and reached 81% by the end of the experiment at 34.18 B.V. It was expected that the Zr (IV) would be second to breakthrough, as observed in both C100H experiments, however zirconium was the first ion to breakthrough in the 1M experiment at approximately four B.V. before cerium. This again may be an indication that the mobile phase flow-rate was quicker than that of the rate of exchange for zirconium uptake. This would make sense due to the rate of ion exchange being reduced due to the higher percentage of crosslinking (10% compared to 8%) of the C100x10MBH resin compared to that of the C100H observed in Section 3.3 at 25 °C. This slower uptake was also demonstrated as the zirconium did not reach a C/C_0 of 1 by the end of the experiment. The deviation from the Gaussian shape affected the calculated number of theoretical plates.

The C100X10MBH in the 3 M HNO_3 eluent breakthrough curve was more in keeping with that expected, with the Ce (IV) displaying the initial breakthrough. The difference for both sulfonic acid resins in the C/C_0 at the conclusion of the experiment, was the major difference between the nitric acid concentrations. The rate of ion exchange was slower for the more concentrated nitric acid eluent feed.

The ion stripping of the C100X10MBH resin at 5 M HNO_3 displays a good agreement between the morphology of the peaks in both eluent strengths tested. This was encouraging as it displayed that the ion exchange was reversible and therefore the resin could be used for a chromatographic separation. However, due to the deviation of the breakthrough curves from the Gaussian form expected due to the reduced rate of ion exchange, the C100X10MBH was eliminated from the development of a chromatographic separation.

The S910 resin behaved as expected from the results observed in Section 3.2.2. In the 1 M HNO_3 eluent the initial breakthrough for cerium was immediate and the C/C_0 ratio reached 1 by ~ 4 B.V.. The equivalent Zr (IV) figures occurred at 1.88, 50 % being achieved at 5.84 B.V. and reached 90 % by the end of the experiment at 40.81 B.V.. This result again displayed that there was little affinity between the cerium and resin with the ion passing through unhindered. This confirmed by the fact that whilst zirconium was adsorbed onto the

resin, the C/C_0 ratio for Ce (IV) remained at approximately 1. The initial breakthrough of zirconium was observed at a relatively low eluent volume, this could be a result of the rate of adsorption being low, as indicated in Figure 3.14.

The major difference between the eluent HNO_3 concentrations for the S910 resin was the rate of ion exchange observed being slower for more concentrated nitric acid eluent feed. As observed in the higher eluent strengths of the sulfonic acid resins, the Zr ion displayed a straight line as opposed to the normal distribution observed in the lower nitric acid concentration eluents. Again this is indicative of an imbalance between the rate of ion exchange and the flow rate of the eluent.

The number of theoretical plates calculated for the column was relatively high. This was likely to be due to the low capacity but high affinity of the resin for the Zr ion, indicated by the relatively low volume of eluent required for the eluent concentration to be half that of the feed. Although not directly comparable, the high selectivity coefficient for the Zr observed by S910 might also be a contributing factor for the plate number.

The ion stripping of the S910 resin at 5 M HNO_3 displayed good agreement between both of the experiments at the different eluent HNO_3 concentrations. However the concentration of ions within the eluent is extremely low. The ion exchange does not appear to be reversible and therefore the resin could not be used for a chromatographic separation as the resins appeared to retain the Zr (IV) ion; the only one adsorbed.

Therefore the S910 was deemed not to be suitable for the chromatographic development, despite giving the largest selectivity coefficient in Section 3.2.2, the adsorption of Zr (IV) was too strong and since none of the other ions were retained at the nitric acid concentration levels required, it was discarded from consideration and development for chromatography.

The D5530 adsorbent did not display the types of elution curve expected according to the results of Section 3.2.1. At the 1 M HNO_3 eluent concentration, the concentration ratio of both the Zr and Ce ions in the eluent was very similar throughout the experiment, suggesting a similar affinity for the stationary phase, which was not observed in Section 3.2.1. This may be a factor of the use of a more dynamic system where the ions are not at equilibrium and may have exhibited a different ion exchange characteristic in the more dynamic flow through a column. However, it was again difficult to resolve this deviation from the expected results, owing to the uncertainty about the composition and structure of the adsorbent. The 1 M HNO_3 column also displays a relatively high number of theoretical plates. However as this appears when the separation factor of the two principal ions would appear to be very small, the ability to utilise this might prove limited.

The results from 3 M HNO_3 nitric acid eluent breakthrough are more akin to the results expected from the results of Section 3.2.1. A broadly Gaussian morphology was observed for both the Ce and Zr ions.

The ion stripping at 5 M HNO_3 of the D5530 did not display a good correlation between the graphs in both eluent concentration experiments. The stripping observed in the 1 M HNO_3 eluent depicts an extremely busy baseline and does not display any definable morphology. The stripping observed in the 3 M HNO_3 was more akin to the ion stripping profiles expected and observed in the C100H and C100X10MBH resins, but only for the stripping of the Ce (IV) ion. It would appear that the Zr (IV) ion remains adsorbed onto the media. Although the concentration of the eluent was never 0 ppm, there was no appreciable morphology with the concentration that was eluted. This lack of elution in the eluent suggests that the ion adsorption was not reversible and therefore the resin could not be used for a practical chromatographic separation.

The conclusion of the breakthrough and elution column work was that C100H was considered as the best candidate resin or adsorbent on which to perform a chromatographic separation of the ions. This resin gave the best performance in terms of the number of theoretical plates and in the shape of the breakthrough curve. It also displayed the expected affinity for the Zr (IV) over the Ce (IV) at both of the mobile phase concentrations tested and the ability for the Zr and Ce ions to be subsequently eluted in high nitric acid concentrations.

3.6 Chromatographic Separation

The chromatographic separation using C100H resin was performed as described in Section 2.3.6. The experimental variables which were optimised during the study were nitric acid concentration (mobile phase) and mobile phase flow rate. The method was developed intuitively, based on the accruing data set and experience.

The experiments performed, including the experimental parameters are included in Table 2.4 and resulting chromatographs are shown as indicated in Figures 3.39 to 3.55

Due to the high number of fractions collected for each of these experiment, time constraints and the volume of virgin resin required, these experiments were run singly. The results displayed represent an average of two aliquots taken from the same fraction. If the relative standard deviation was greater than 5 % a further sample of the fraction was assayed until the relative standard deviation was found to be at an acceptable level. Again as described in Section 3.2, within the ICP-MS, the aliquots were subjected to three "passes" where an assay was performed for each of the ions and the figure from this averaged to give a single concentration for the fraction sample.

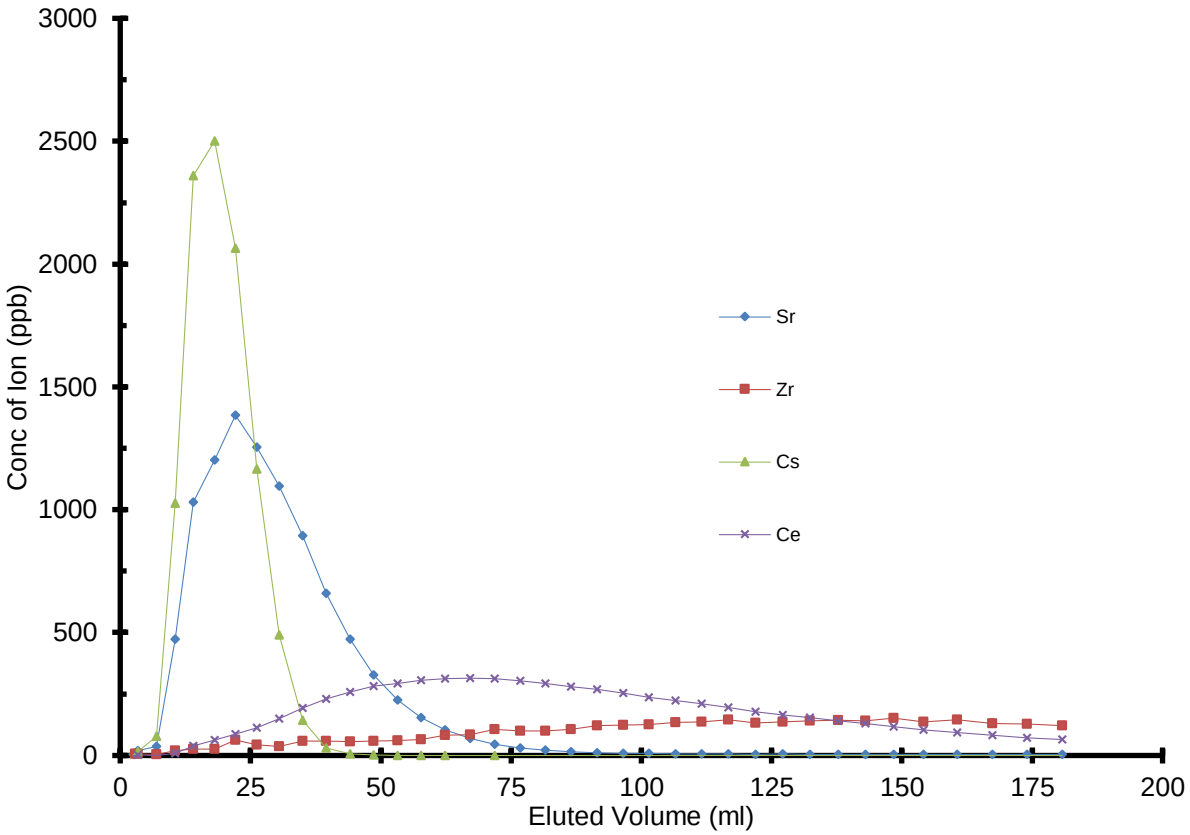

Figure 3.39 Experiment 1: 3 M HNO_3 Isocratic Elution at 1 $ml.min^{-1}$

3.6.1 Experiment 1: 3 M HNO_3 Isocratic Elution at 1 ml.min^{-1}

The 3 M HNO_3 mobile phase strength was chosen for this first experiment as it this was the bench mark acid concentration at which the selectivity coefficients were calculated in Section 3.2. The mobile phase flow rate was relatively modest at 1 ml.min^{-1}. The column was composed of 7.512 g of C100H resin with a bed height of 162 mm. The aim of this initial chromatogram was to assess the broad characteristics of the column.

The results of Section 3.2 would suggest that only the Zr ion would be retained by the stationary phase at any significant level with a small affinity also displayed for the Ce. This profile was shown to be evident, with a similar retention time observed for the Sr and Cs ions. The cerium peak observed was broad with the peak being eluted after that of the Sr and Cs ions. However, due to peak broadening both Ce and Zr are co-eluted throughout the majority of the chromatogram, meaning that these conditions were not sufficient to perform a separation.

Although a good starting point for the chromatographic experiments, there are a number of issues which are required to be addressed. The peak width was extremely high, probably being exacerbated by tailing; this was especially associated with the Ce peak. To create a better Gaussian peak shape on the chromatogram and increase the separation power of the column (increase the number of theoretical plates), there are two options open when the mobile phase composition was restricted.

Looking at the Van Deemter equation:

$$H = A + \frac{B}{u} + C \cdot u$$

Equation 3.2 Van Deemter equation. (21)

where H was the height equivalent to theoretical plate; A was the eddy diffusion of the ion through the column depending largely on the particle size and the homogeneousness of the bed packing and would remain constant for a column bed; B was the longitudinal diffusion which was a factor of the time spent within a column; C was the mass transfer between the solid and mobile phases and u was linear velocity of the mobile phase through the column.

To achieve a better power of separation, the H value should be minimised. As observed in Figure 3.40 (utilising arbitrary units) there is quite a wide margin of error with the minimum HETP when changing the linear velocity, especially when C was small:

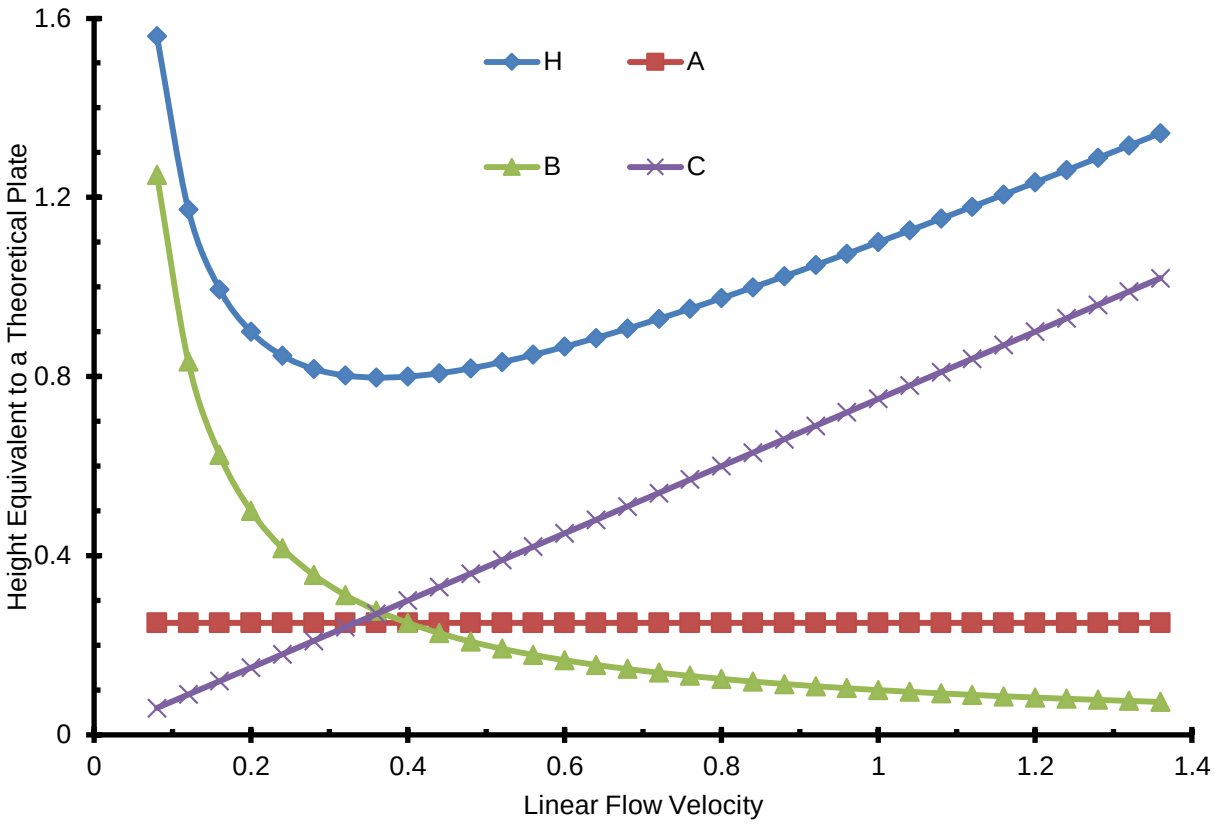

Figure 3.40 Van Deemter curve showing relationship between HETP and linear flow velocity. Arbitrary units.

For the column used in this thesis, A would remain constant so long as the column length was not increased or the bed packing disturbed, B is reduced as the flow rate is increased, the C value has a linear relationship with u, so as the flow rate is increased so too would the C value and therefore the height equivalent to a theoretical plate.

Once the HETP has been minimised then if the length of the column was increased the number of plates would increase. Therefore for the next experiment, both the length of the column bed and the flow rate were increased in order to minimise the HETP and maximised the efficiency of the column.

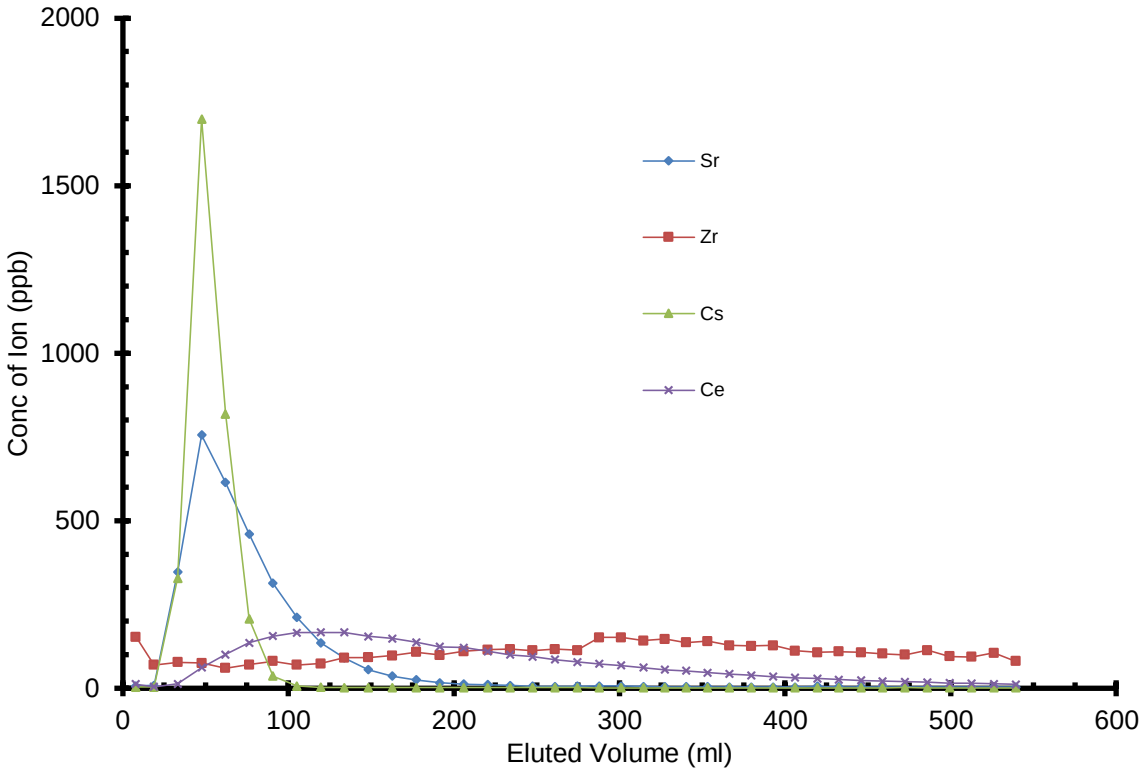

Figure 3.41 Experiment 2: 3 M HNO_3 Isocratic Elution at 3 ml.min^{-1}

3.6.2 Experiment 2: 3 M HNO_3 Isocratic Elution at 3 ml.min^{-1}

The mass of the resin in the column was increased to 15.030 g, which gave a bed height of 335 mm and also the flow rate of the mobile phase increased to 3.0 ml min^{-1}. The changes in the chromatographic conditions gave a very similar shaped graph to that observed in Figure 3.39. The observed separation of peak maxima between Cs and Sr has actually decreased, with both peak maxima eluting at the same elution volume. The peak maxima for Experiment 1 for Cs and Sr were observed at approximately 18 and 22 ml while in this experiment with double the bed height, both peak maxima were observed at approximately 48 ml. The exception to the similarity between the two chromatograms was the presence of Zr ion throughout the entire graph. Up to the 120 ml elution point this was fairly consistent at approximately 70 ppb, after which it becomes a gradual increase, as the chromatogram continues in the same manner as that of the first chromatogram.

Comparing the HETP, using a slightly altered version of:

$$N = 16\left(\frac{t_R}{w_b}\right)^2$$

Equation 3.3 Number of theoretical plates from a chromatogram (21).

where N are the number of theoretical plates, t_R was the retention time (s) and $w_b$was the width of the peak at base (s). However as the x-axis was being measured in volume, this would be substituted into the equation within this discussion.

The columns displayed theoretical plate numbers of 4.89 and 7.04 respectively; an increase of 2.15 theoretical plates (approximately 44 %) with doubling of bed height. The increase is most noticeable when the sharpness of the peaks was compared. In Figure 3.39 the Cs peak was seven data points in width, compared to the 5 in Figure 3.41.

Owing to the long-time period used to collect each of the eluted fractions, the resolution of the chromatograms was also relatively low with the consequence that the calculation of theoretical plates was relatively inexact. However, the calculation displayed a significant increase in plate number and therefore the separation power of the column and as a result all further experiments were performed using a column length of 335 mm. However due to changing two variables in one experiment the separation observed in Figure 3.39 was not observed in 3.41. The experiment was therefore repeated at a lower mobile phase concentration in order that a resolution could be measured and an estimate of the required column length calculated.

For baseline separation to be achieved an R_s of 1.5 is required, given the data attained from experiments 1 and 2 the length of column required to provide a separation (R_s = 1.5) can be calculated from the equation:

$$R_s = \frac{\sqrt{N}}{4}\left(\frac{\alpha - 1}{\alpha}\right)\left(\frac{k_B}{1 + k_B}\right)$$

Equation 3.4 Resolution of two components from separation factor and retention factor.

When rearranged for plate number becomes;

$$N = \left(\frac{4R_S}{\left(\frac{\alpha - 1}{\alpha}\right)\left(\frac{1 + k_B}{k_B}\right)}\right)^2$$

Equation 3.5 Required number of theoretical plates from resolution, separation factor and retention factor.

However, as there was no separation at this concentration for the Cs and Sr ions, it was decided to reduce the mobile phase concentration in order to calculate a required number of theoretical plates and therefore the length of column required to perform a resolution of 1.5.

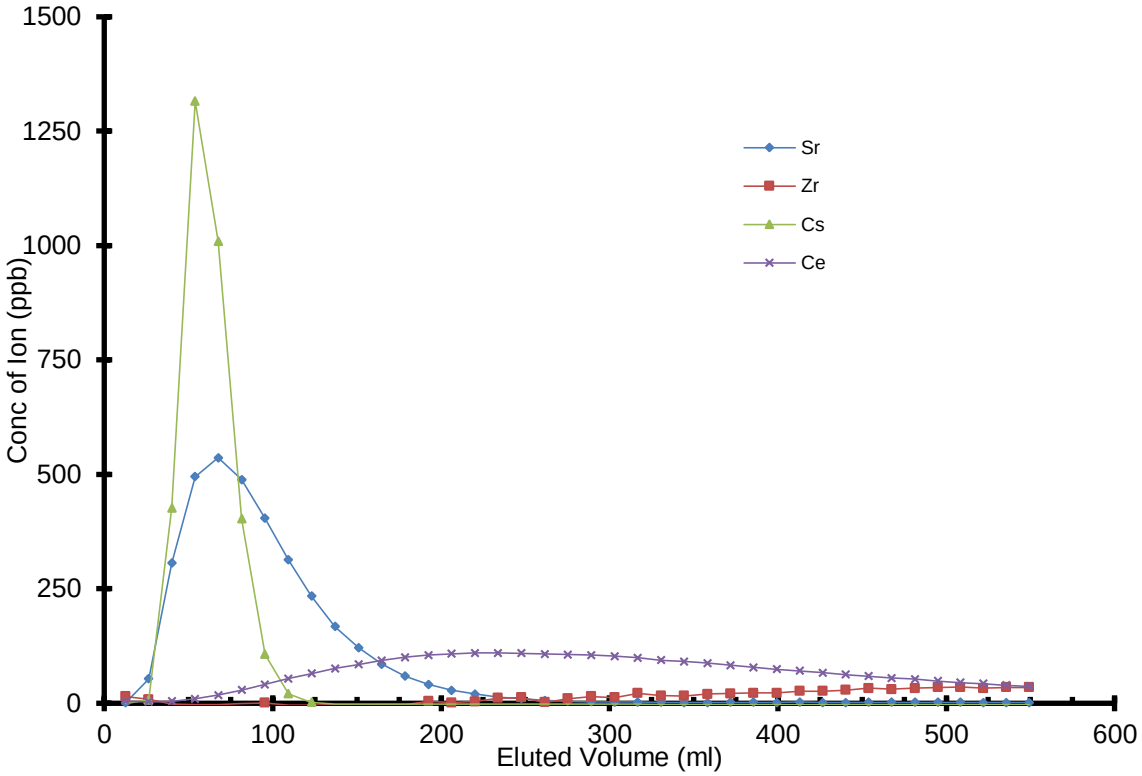

Figure 3.42 Experiment 3: 2.5 M HNO_3 Isocratic Elution at 3 ml.min^{-1}

3.6.3 Experiment 3: 2.5 M HNO_3 Isocratic Elution at 3 ml.min^{-1}

The chromatogram displayed in Figure 3.42 was the final experiment to use an isocratic mobile phase profile with a single concentration. A reduced mobile phase concentration of 2.5 M HNO_3 was chosen to test whether a simple separation could be achieved with timely elution of the ions. However the similarity to the Cs and Sr peaks in Figures 3.39 and 3.41 are striking and virtually indistinguishable in shape and timings. The near Gaussian shape of the Cs peak observed in the first three experiments may indicate that at the 2.5 M HNO_3 mobile phase concentration, the Cs was un-retained by the C100H column. This was then taken to be the time taken for an unretained species to pass through the column (t_M) and consequently is the volume of liquid required for an unretained mobile phase component to travel from the top to bottom of a column. This dead volume is also indicative of the volume of the inter-bead space within a column and was calculated to be 24.42 ml.

The results from Section 3.2 would suggest that the affinity displayed by the Cs and Sr ions should be similar in the 2.5 M HNO_3 mobile phase. There is an observed difference in the peaks for these ions. The peak maximum is observed at 54 ml for the Cs and at 68 ml for the Sr ion. The Sr peak also displayed significant tailing, not observed in the near normal distribution displayed by the Cs peak.

The Ce was more highly retained in this 2.5 M mobile phase concentration than that of the 3 M HNO_3. The most highly retained Zr ion was also not observed at a significant concentration until approximately 250 ml had been eluted. This chromatogram displays that at this mobile phase strength, all four ions begin to be eluted to greater or lesser extents. It was therefore obvious that an isocratic elution would not provide a sufficient separation of ions.

Given that the dead volume of the column was now calculated from the Cs peak on these three isocratic chromatograms, the number of theoretical plates required for a resolution of 1.5 between the Cs and Sr ions was calculated to be 144. The number of theoretical plates achieved on this column was calculated as 6.74 in the 335 mm column or 20.11 plates.m^{-1}. Therefore the required length of the column bed would be over seven metres long (7.16 m) to perform an isocratic separation in 2.5 M HNO_3. Although the mobile phase strength for an isocratic separation could be optimised it is unlikely that it would sufficiently reduce the required column length to a practical level.

A mobile phase profile with differing concentrations of HNO_3 will affect the retention factors for each of the ions and retention times. The use of a gradient elution in conjunction with the dead volume calculated for the column should give an indication of at which mobile phase concentration each of the ions would begin to elute. In the next experiment the mixer/pump was employed for the first time to provide this gradient profile.

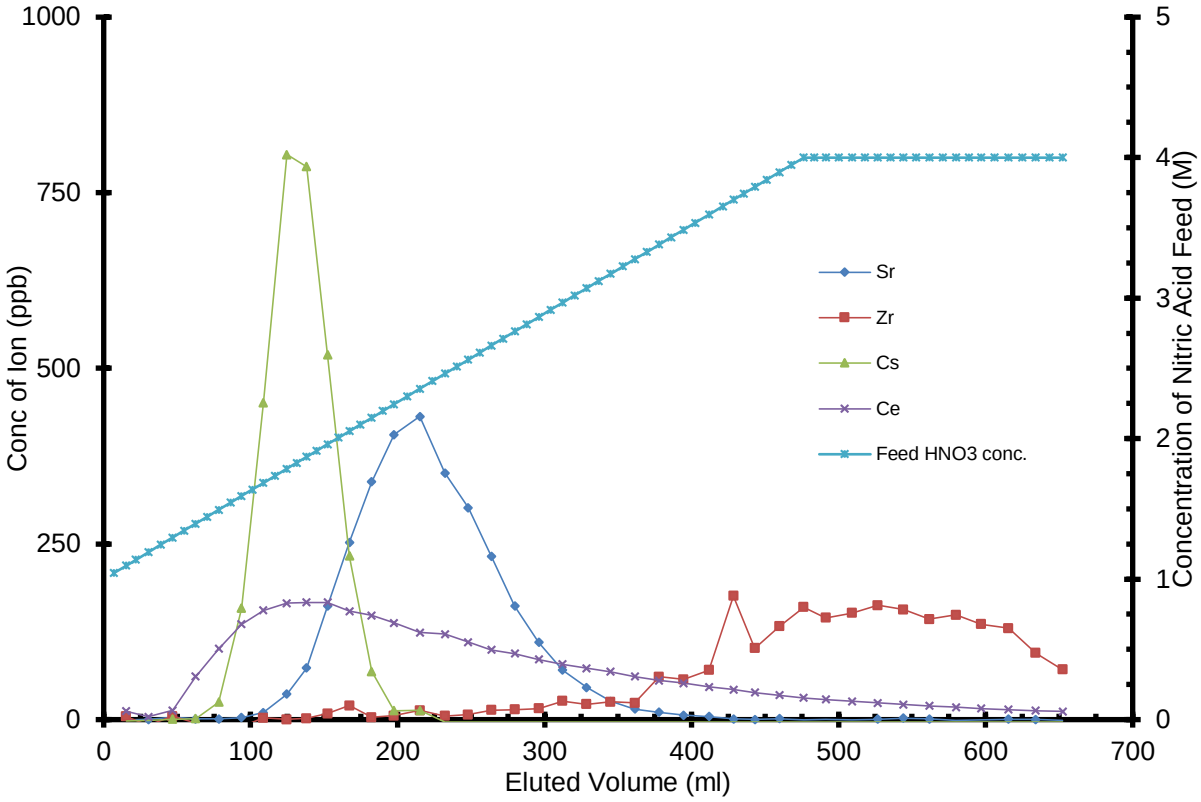

Figure 3.43 Experiment 4: 1 to 4 M HNO_3 Gradient Elution at 2.5 ml.min^{-1}

3.6.4 Experiment 4: 1 to 4 M HNO_3 Gradient Elution at 2.5 ml.min^{-1}

The chromatogram was encouraging as a foundation for the separation occurring between the four ions. The changing concentration of the eluent feed, when used in conjunction with the dead volume calculated from the previous experiment, gave an indication of the retention conditions for each of the ions within the column.

With the gradient starting at 1 M HNO_3, the first ion elution peak was not until approximately 63 ml has been eluted. This was at least twice as long as the previous chromatograms with similar elution flow rates and therefore suggests that a degree of retention was occurring for all the ions. This notion that retention was occurring for all ions was most clearly represented by the increase in width of the Cs ion peak and also by the difference in elution volumes between the peak maxima for the Cs and Sr ions.

The better chromatographic separation performance was also displayed in the shape of the Zr peak. Although the peak was not resolved to the baseline by the end of the experiment and was also extremely broad, it did display a definite peak maximum after which the peak returns to the baseline, albeit gradually. With the exception of the anomalous response at 428 ml, the Zr peak displayed an acceptable peak shape, but with room for improvement.

There was however a number of disappointing factors within the chromatogram. The most notable being that the Ce ion was the first to be detected. The shape of peak was also not as anticipated with extended tailing observed. It would be expected that Ce, after elution at close to the start of the chromatogram or 1 M HNO_3, would be retained by the resin less and would therefore be eluted relatively quickly. This does not happen and the peak tails throughout the chromatogram. The expected elution order for the ions was expected to follow the charge density of the ions: Cs (I), Sr (II), Ce (IV) and then Zr (IV), as was demonstrated in the results of Section 3.2. However the chromatogram does not bear this out and was an erroneous result when compared to the previous results from capacity against acidity and even the breakthrough studies. It was also expected that at 4 M HNO_3 there would be negligible capacity and any remaining ions would be swiftly eluted.

In terms of the project however, this result could potentially be very beneficial. As Ce is being used as a surrogate for uranium, and on this chromatogram the Ce ion was un-retained at the relatively low HNO_3 concentrations, this would mean that the bulk component of irradiated nuclear fuel would not take up the capacity of the resin in the column and therefore the throughput of any system would be significantly increased. The next experiment was used to assess the validity of this experiment; determining whether Ce was retained by this resin at this and lower HNO_3 concentrations.

The next experiment includes both a step and gradient profile, in order to gauge the behaviour of Ce at low HNO_3 concentrations. The eluent profile would be stepped from 0.5 to 1 to 3 with a gradient up to 4 M HNO_3. The concentration of the mobile phase steps were estimated from the point at which the ions were eluted on Figure 3.44 with the previously calculated dead volume taken into account.

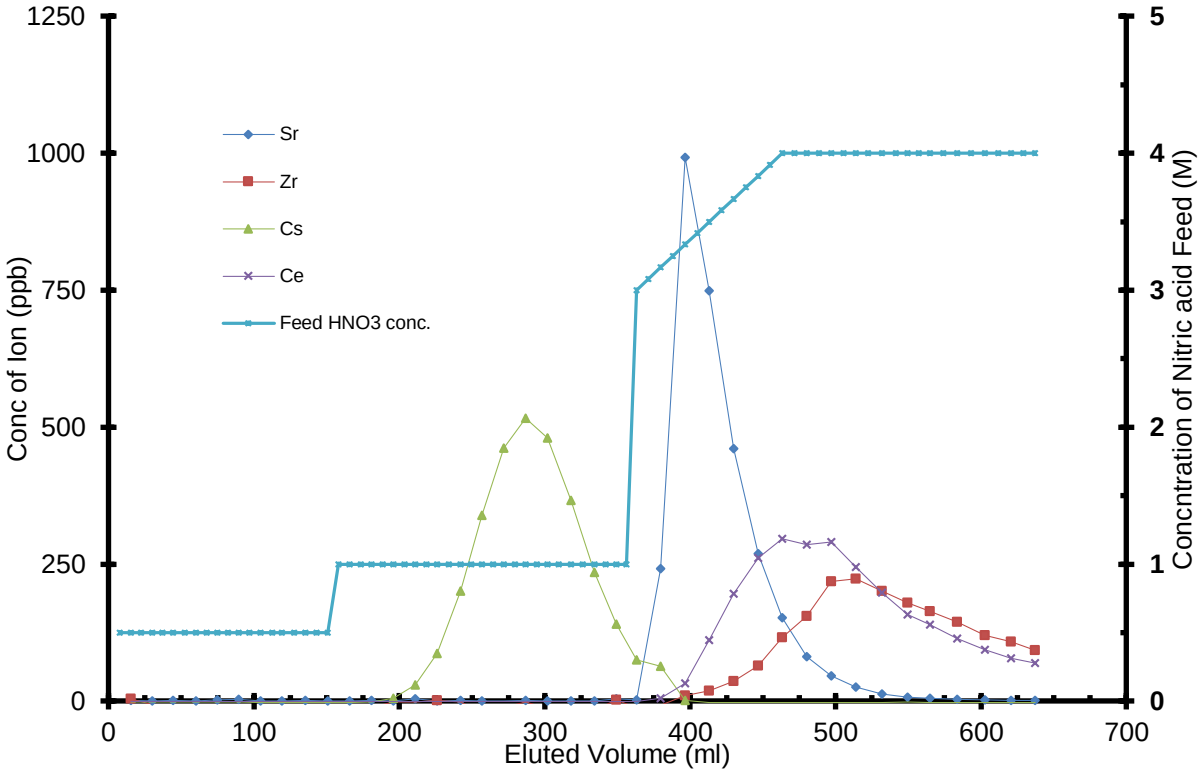

Figure 3.44 Experiment 5: 0.5, 1, 3 and 4 M HNO_3 Stepped and Gradient Elution at 2.5 ml.min^{-1}

3.6.5 Experiment 5: 0.5, 1, 3 and 4 M HNO_3 Stepped and Gradient Elution at 2.5 ml.min^{-1}

The experiment again displays an improvement in the separation between the Cs and Sr ions. Cs was eluted with a close to Gaussian shaped peak, almost within the 1 M HNO_3 mobile phase step. The Cs peak was close to achieving baseline separation from the Sr peak. This was not achieved as the step change to 3 M HNO_3 occurred before the Cs peak was fully resolved and completely eluted. The calculated resolution from Equation 3.4 gave a resolution of 0.44.

The step change from 1 to 3 M HNO_3 was intended to elute the Sr swiftly. However, as observed, this also induced elution of the Ce (IV) which was further compounded by the gradient step increasing the eluent concentration from 3 to 4 M HNO_3. This can be visualised as the difference between the elution volume for the initial breakthrough of the Sr and Ce ion peaks being ~ 7 ml (only a single collected fraction). This large and sudden change in the mobile phase concentration accompanied by the gradient caused the affinity of the ion for the stationary phase to fall dramatically. This reduction in affinity meant that all of the ions remaining on the column began to be eluted within the gradient section. However, there is significant tailing of all the more strongly retained ions. Unfortunately, when using a simple chromatographic system where the only variable within the system was

the concentration of the mobile phase, without any phase modifiers: The chromatography was simple but could be limited in the precision and elegance.

As the proposed process was a bulk, as opposed to an analytical separation, the peak area was not under any mathematical requirement to be measured via integration. The peak tailing was therefore not such a critical factor other than the adding to the elution volume required to elute the ion which would therefore increase the dilution factor.

The issue from the previous experiment of the Ce ion eluting out of charge order was not evident from this experiment, even at the much lower starting point than that of the previous experiment. The expected elution order was maintained and therefore the elution in the previous experiment could be viewed as an erroneous result.

As the elution behaviour of the Ce in this and the previous experiment was under close investigation and after reviewing the slope of the gradient in this experiment, the next elution profile would be restricted to a step elution. Although this would make it more difficult to estimate at what concentration the ion becomes un-retained by the resin, it would give a definitive response as to the concentrations of eluent at which the ions are retained.

Therefore the experiment would be run as before but without the gradient between 3 and 4 M HNO_3.

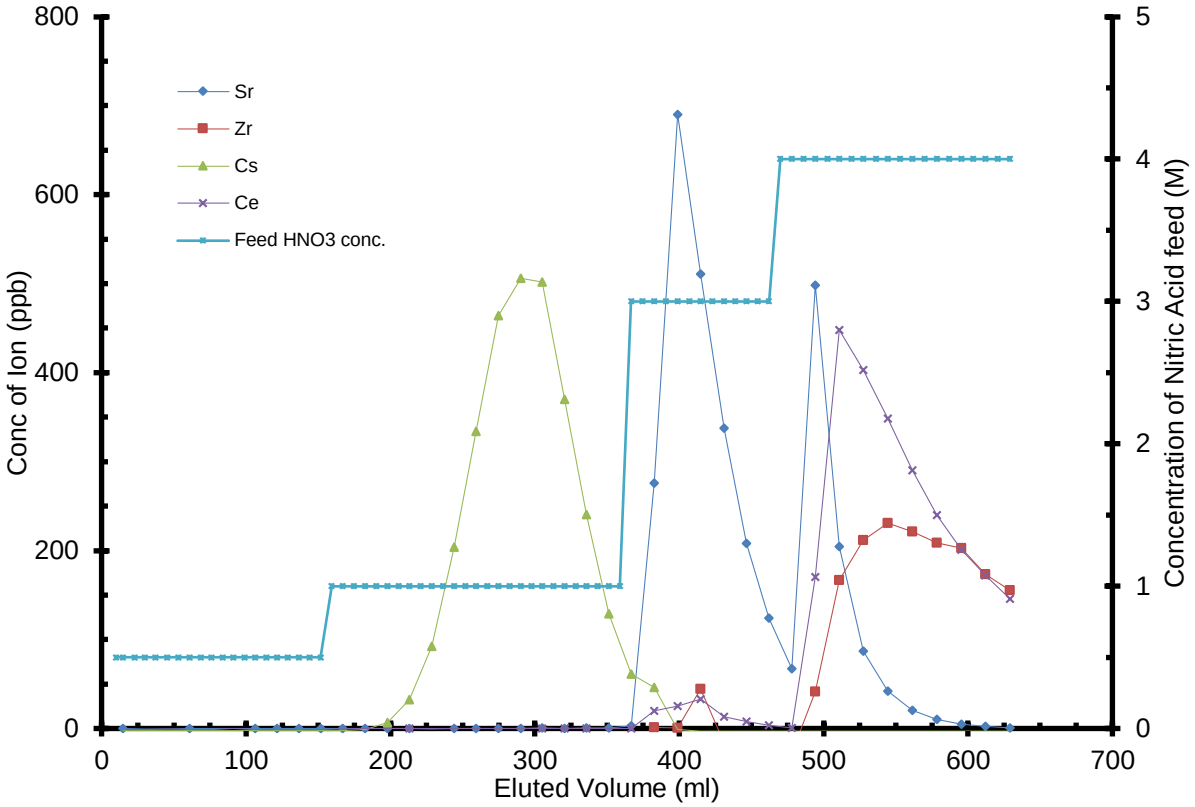

Figure 3.45 Experiment 6; 0.5, 1, 3 and 4 M HNO_3 Stepped Elution at 2.5 $ml.min^{-1}$

3.6.6 Experiment 6: 0.5, 1, 3 and 4 M HNO_3 Stepped Elution at 2.5 $ml.min^{-1}$

As the mobile phase profile was similar to that of the previous experiment, it was therefore pleasing to note that up until the divergence between the mobile phase profiles there was a good measure of agreement between the two chromatograms, the Cs ion peak shapes are similar. The two maxima are comparable at 516 and 506 ppm and were observed at approximately 516 ml eluent and are both close to being resolved to the baseline before the elution step to 3 M HNO_3 occurs. This was agreeable in that it demonstrates reproducibility between experiments for this ion. The return to the baseline should be able to be resolved with a longer time (higher volume eluted) at the 1 M HNO_3 concentration.

The step from 1 to 3 M HNO_3 also gives a very sharp peak for the Sr ion. This shape was similar to that displayed in the previous experiment until the step to 4 M HNO_3 where a second, smaller but just as sharp, peak was observed. This is likely to be due to the lack of affinity of the Sr ion for the stationary phase in the strong concentration stationary phase causing this to be eluted in a large concentration.

The mobile phase step from 1 to 3 M could also be interpreted to have occurred before the entirety of the Cs ion had been eluted displayed by the “shoulder” observed as the peak

returned to the baseline. This step could, as observed in the previous experiment, be seen as too large due to the presence of a small amount of Ce within the eluent before the step to 4 M HNO_3. Therefore to achieve a separation of the Cs and Sr from the Ce and Zr the mobile phase profile concentration would again have to be lowered so as the Cs and Sr could be eluted whilst the Ce and Zr are retained.

To be noted was that all three of the ions remaining within the column were detected in the eluent in the 4 M step. Again there was a different elution volume maximum for each of the ions suggesting some possibility of a chromatographic separation at this concentration; however, it would require a column with a much larger number of plates.

A calculation of the number of plates for this column (from the Cs peak) gave a number of approximately 40, given the difference in peak maxima; if this plate number was significantly increased, a separation at this eluent concentration would be possible. However, with the equipment available within this project, this would require a significant and unfeasible increase in column length and therefore, this solution was not practical.

This finding is in accordance with the work of Begovich and Sisson (3) who utilised a length of annulus height of 600 mm to separate Hf from Zr on a CAC instrument. This is in comparison to the approximate 300 mm available within this project. The Begovich and Sissons separation was performed with a mobile phase subjected to a pressure of 275 kPa and a 15 litre per hour mobile phase flow rate. This is in comparison to the gravity fed arrangement utilised at UCLan. Even with these chromatographic advantages, on the CAC, the peak broadening was large, as the Zr was eluted in a band equivalent to 2 hours (20 to 100 º after the inlet, with the annulus rotating at 39 º per hour) with the Hf eluted between 1.25 hours (between 170 to 220 º) after injection.

The required length of column to perform an isocratic separation with the same diameter and packing utilised at UCLan can be calculated from the equation:

$$R = \frac{\sqrt{N}}{4}\left(\frac{\alpha - 1}{\alpha}\right)\left(\frac{1 + k'}{k'}\right)$$

Equation 3.6 Resolution of two components from number of theoretical plates, separation factor and free column volumes to component peak maximum

which when considering the separation factor and retention factors garnered from the results of Section 3.2 gives a required plate number of approximately 80. This was double the number calculated for this column in this experiment. For a chromatographic separation to occur on this column, assuming the same conditions, this would require the bed height to be

increased by a factor of 7 and 5 assuming that the HETP remains in the same ratio as bed height was increased. This would require a bed height of 640 mm.

Within this project the simplicity required of the separation system was simultaneously the greatest strength, when looking to implement within nuclear reprocessing- (and weakness as a chromatographic separation). The limiting factors of an inability to increase the pressure of the eluent through the resin bed; the use of commercial ion exchange resins and the single component mobile phase would inevitably restrict the chromatographic ability of the column and a true chromatographic separation of the ions probably would not be achievable over the small bed height currently available. However the simplicity and reproducibility was the chief consideration when trying to unseat an incumbent technology with approximately 60 years of tried and tested service. It might therefore be more accurate to look towards the separation as more of a merger between ion exchange and chromatography rather than purely chromatographic as the plate numbers required to achieve a chromatographic separation are higher than was possible with the equipment currently available to the project.

The peak width is also of importance, as this would have an effect on the volume of eluent in which the ion would be eluted and therefore the factor by which the ion was diluted. Obviously the smaller the volume and dilution factor, the less work would have to be undertaken post separation. As a major portion of this would be the evaporation of the eluent to a required volume and consequently quite energy intensive, it would decrease the overall efficiency of the proposed process. Although this was an important consideration and one which would have to be addressed, it was secondary in concern to that of creating an actual separation of the ions. The subsequent experiment would try to achieve a full separation of all four of the ions, and would consist of a fairly simple equal timed 1, 2, 3 and 4 M HNO_3 sections. The extra 2 M step should give an opportunity for the Sr to be eluted before the Ce and Zr.

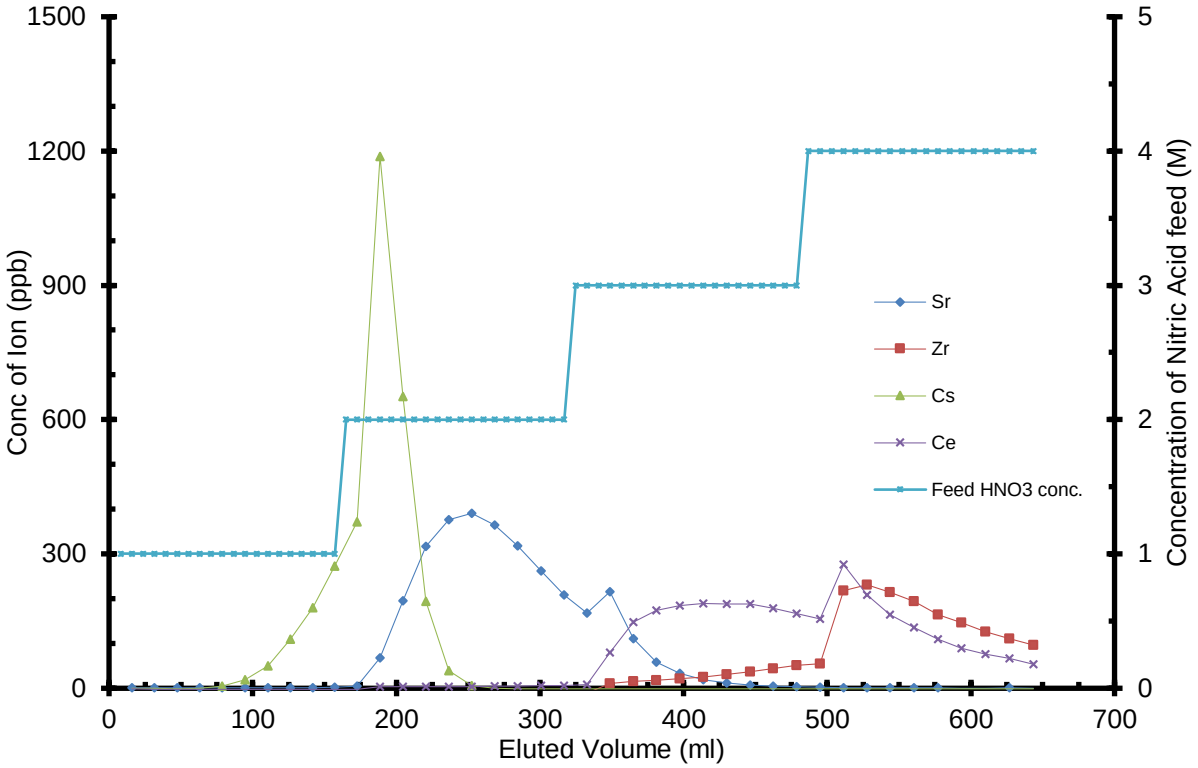

Figure 3.46 Experiment 7: 1, 2, 3 and 4 M HNO_3 Stepped Elution at 2.5 $ml.min^{-1}$

3.6.7 Experiment 7: 1, 2, 3 and 4 M HNO_3 Stepped Elution at 2.5 $ml.min^{-1}$

The chromatogram in this experiment was an improvement on the previous experiments, although it was not perfect due to the simultaneous elution of two ions or three ions being observed for portions of the chromatogram. Encouragingly, the eluent concentrations would appear to be approximately correct for the Cs and Sr as there was no “bleeding” (where the ion which was due to be eluted at the next eluent concentration begins to be eluted with a gradually increasing concentration) as opposed to the Ce and Zr ions at the 3 M elution. The Zr ion begins to bleed into the Ce elution from a very early point. It was however difficult to definitively say whether or not bleeding between the Sr and Cs peaks was occurring, as the peaks are co-eluted due to the change in eluent strength before the Cs peak was resolved to the baseline. To minimise the chances of the bleeding occurring the concentration of the eluent would have to be adjusted to be as low as possible. Unfortunately, this would mean that a larger volume would be required to elute the ion from the column, which introduces the problem of a much diluted ion concentration post column. Therefore the strongest concentration possible was required without the bleeding effect occurring. This balance in the elution concentration would be the focus of the remaining chromatograph experiments.

The chromatogram displayed split peaks for the Sr and Ce ions, with a large increase also displayed by the Cs eluent concentration after the step change from 1 to 2 M HNO_3. These all occurred approximately 24 ml (23.61, 24.02 and 24.39 ml for Cs, Sr and Ce respectively) after the eluent switched to the higher strength, indicating that this was the dead volume of the column. This was consistent with the previous experiment where the dead volume measured was 24.42 ml.

The length of the tails for the peaks and bleeding of ions into the less concentrated mobile phase profiles, demonstrates that the column would not be able to achieve a separation with this elution profile. The volume eluted at each concentration of eluent would have to be significantly increased in order that the ion was fully eluted before the eluent concentration was increased and the bleeding observed by the Zr into the 3 M HNO_3 step would require a reduction of the eluent concentration from that used in this step.

The mixer/pump could achieve an accurate flow rate of 4 $ml.min^{-1}$, and this should provide a large enough volume of eluent to achieve an ion separation. This would also require a shorter collection time per test tube for a similar volume to be collected and would therefore increase the resolution, as 150 fractions would be collected as opposed to the 80 fraction collected in the previous experiments.

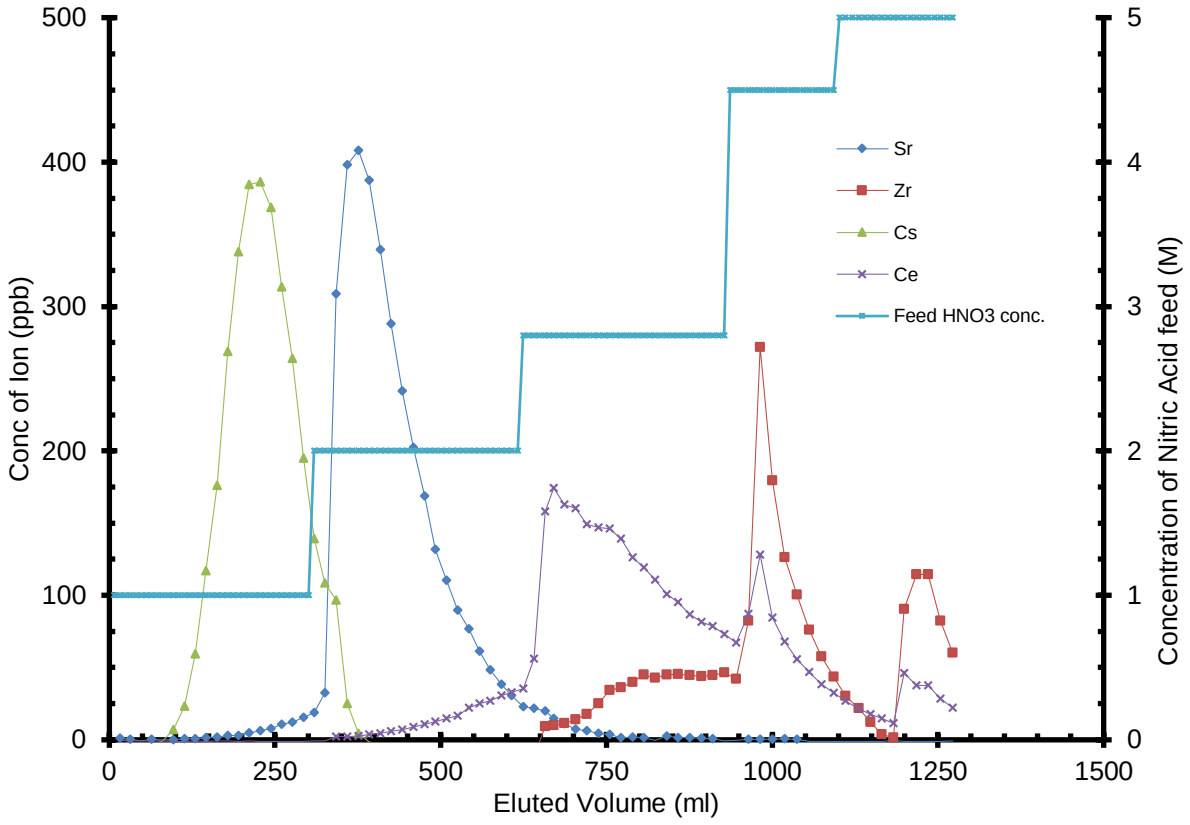

Figure 3.47 Experiment 8: 1, 2.1, 2.8, 4.5 and 5 M HNO_3 Stepped Elution at 4 $ml.min^{-1}$

3.6.8 Experiment 8: 1, 2.1, 2.8, 4.5 and 5 M HNO_3 Stepped Elution at 4 $ml.min^{-1}$

The increase from 2.5 to 4 $ml.min^{-1}$ flow rate had an adverse effect on the bleeding of the Sr into the Cs ion peak and the calculated resolution between the Sr and Cs peaks was 0.360, less than recorded in Experiment 5. The decision behind the increase in flow rate was to increase the volume eluted at each step of the separation. Although the peak shapes of the Cs and Sr are sharper than that observed in Figure 3.46, bleeding was observed for the Ce and Zr ions into the previously eluted ion peaks. It also displays a previously unobserved phenomenon of the Sr bleeding into the Cs peak.

The chromatogram was very disappointing due to the amount of bleeding between Ce and Zr at the 2.8 M HNO_3 step. The bleeding was more evident than in the previous experiment which, in conjunction with the other ions performing in a similar manner; however this might be explained by the increase in the eluent flow rate. There was also a point in the chromatogram where three ions were eluted simultaneously for a short period (657 to 738 ml ≈ 6 % of the total run) during the 2.8 M HNO_3 step.

The issue of the bleeding aside, the shape of the peaks in the case of both the Sr and Cs ions was quite positive, as the peak shape was an approximation of a Gaussian distribution with a small amount of tailing evident.

As the only significant change from the previous experiment was the mobile phase flow rate it was this which was believed to be the major cause in the increase of the co-elution. For the next experiment the mobile flow rate would therefore be reduced with the intention that this would reduce the bleeding observed between the ions

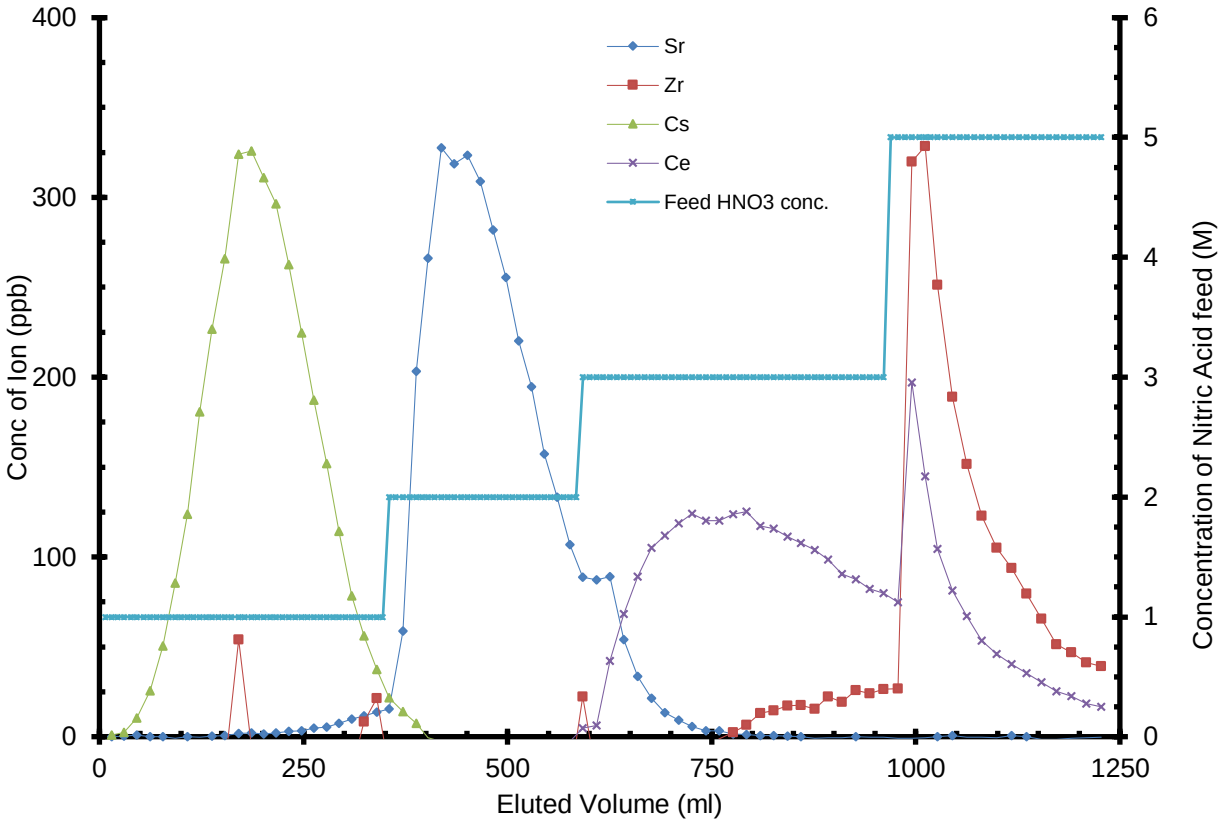

Figure 3.48 Experiment 9: 1, 2, 3 and 5 M HNO_3 Stepped Elution at 3 ml.min^{-1}

3.6.9 Experiment 9: 1, 2, 3 and 5 M HNO_3 Stepped Elution at 3 ml.min^{-1}

The chromatogram displayed a much better separation than the previous two, but not flawless. Although there was a small amount of co-elution observed between the Cs and Sr ions and a somewhat larger degree between the Ce and Zr ions, this was much reduced from that in Experiment 8. The Cs was not fully eluted by the end of the 1 M elution step. There was also no co-elution of the Ce and Sr ions within the 2 M HNO_3 step, indicating that the Ce was suitably retained at these column conditions. As the final concentration step was being eluted, the shape of the peak followed that of the previous experiments where there was a very high initial detector response observed from the ions remaining on the column, with a tailing peak thereafter for both. This indicates that the balance between the retention of the ions by the stationary and mobile phases was again not struck.

If the sole purpose of the separation was the highly active FPs (Cs and Sr) from the Ce and Zr ions, it could be argued that it was broadly achieved within this chromatogram. Although there was co-elution of the Sr with the Cs from approximately 148 ml, it was only the Cs and Sr ions which were detected from the start of the chromatogram until 608 ml had been eluted, where the Ce was first detected. Although there are Zr "peaks" these are single

fraction responses and as they do not form actual peak and can be regarded as erroneous. This could in effect, with more volume eluted at the 2 M HNO_3 level (or indeed a single 2 M HNO_3 step incorporating the volume eluted at the 1 M step), form the basis of a simple separation of the FPs from the U, Pu and Zr. However, to gain a greater understanding of the chromatography and the ion exchange, I will attempt to fully separate all the four ions on the single column in a single experiment.

As co-elution was occurring with the Cs and Sr at 1 M HNO_3 it was necessary to reduce this, in addition it would also require a higher elution volume due to the reduction in the affinity of the ion for the mobile phase due to the reduction in concentration. This requirement was also true of the Sr ion; the tail on the Sr peak requires that the elution volume would have to be increased substantially in order that all of the ion was eluted before the mobile phase step to elute the Ce was initiated. To combat the co-elution of the Zr with the Ce, the concentration at this step of the chromatogram should also be reduced; again this would necessitate a higher elution volume. Therefore, in order that the required time was available for the separation to occur, a slight short cut was employed where the Zr would be left on the column once the chromatographic assay has finished. The Zr could then be eluted later with a high concentration HNO_3, or even during the regeneration step post experiment. The next experiment would therefore have a lower HNO_3 concentration but larger elution volumes for the Cs elution step; the same HNO_3 concentration but a larger elution volume for the Sr elution step and a reduced concentration and higher volume for the Ce elution.

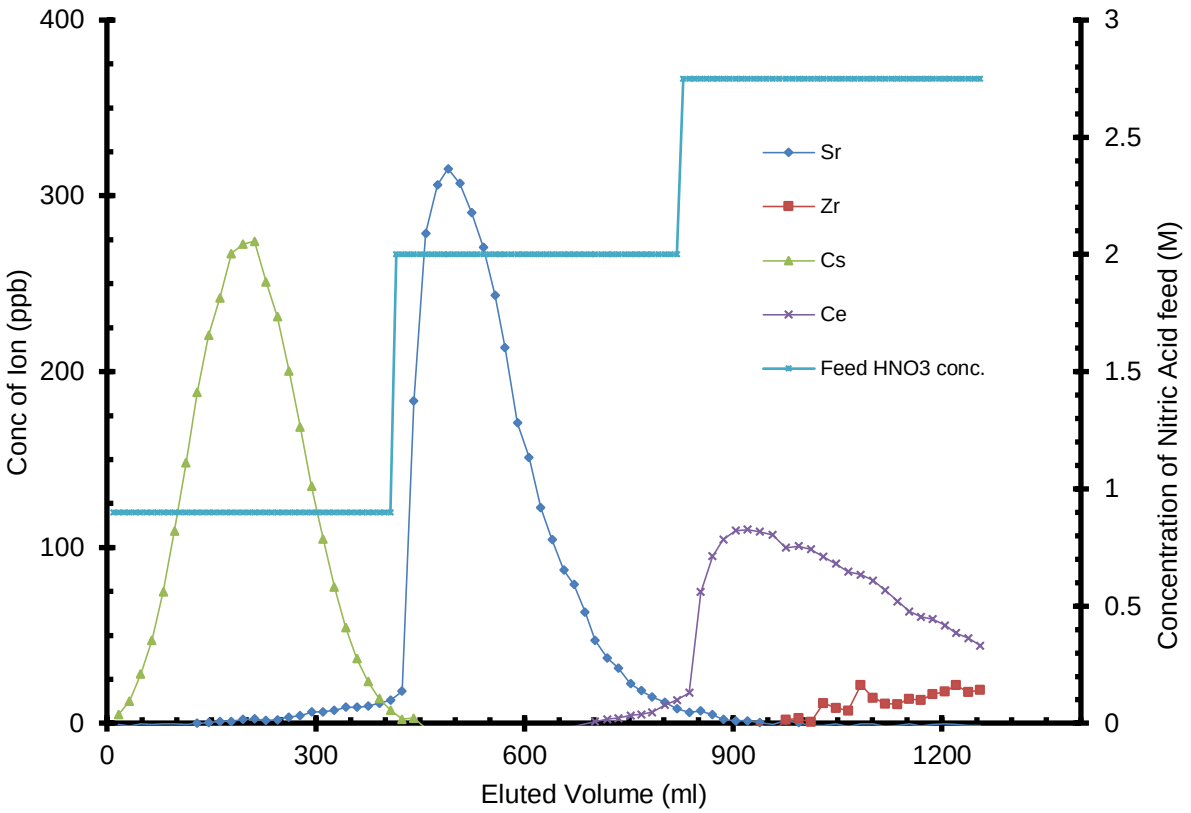

Figure 3.49 Experiment 10; 0.9, 2 and 2.75 M HNO_3 Stepped Elution at 4 $ml.min^{-1}$

3.6.10 Experiment 10: 0.9, 2 and 2.75 M HNO_3 Stepped Elution at 4 $ml.min^{-1}$

The complete separation of the three ions was not achieved; very small amount of bleeding co-elution of Cs and Sr was observed, as was Ce with Sr and Zr with Ce. This means that the concentration of the eluent was still too strong for a balanced affinity between the mobile and stationary phase and still biased toward the mobile phase. This was most obvious in the step change from 0.9 to 2 M HNO_3, where the Sr peak displayed there was tailing observed. This was echoed by the shape of the Ce peak, albeit at a lower concentration.

There is also the added negative that despite the reduction in the eluent concentration, co-elution was still occurring between the Cs and Sr ions. This would mean that in order to counter this, the eluent concentration would have to be reduced further, and since the peaks are not resolved back to the baseline within the steps, this elution volume at each of the steps would again be required to increase.

The shape of the Cs peak was good in that it approximately exhibits a Gaussian shape despite the co-elution of the Sr from the 145 ml point. To reduce the likelihood of the co-elution occurring in the next experiment the concentration of the initial step was reduced from 0.9 M HNO_3 to 0.8 M. The concentration of the second step was reduced dramatically

from 2 to 1.5 M HNO_3 in order that the Ce was not co-eluted with the Sr and hopefully to give an approximate Gaussian shaped peak. The concentration was also reduced in the third step, where the elution concentration was changed from 2.75 to 2.4 M HNO_3.

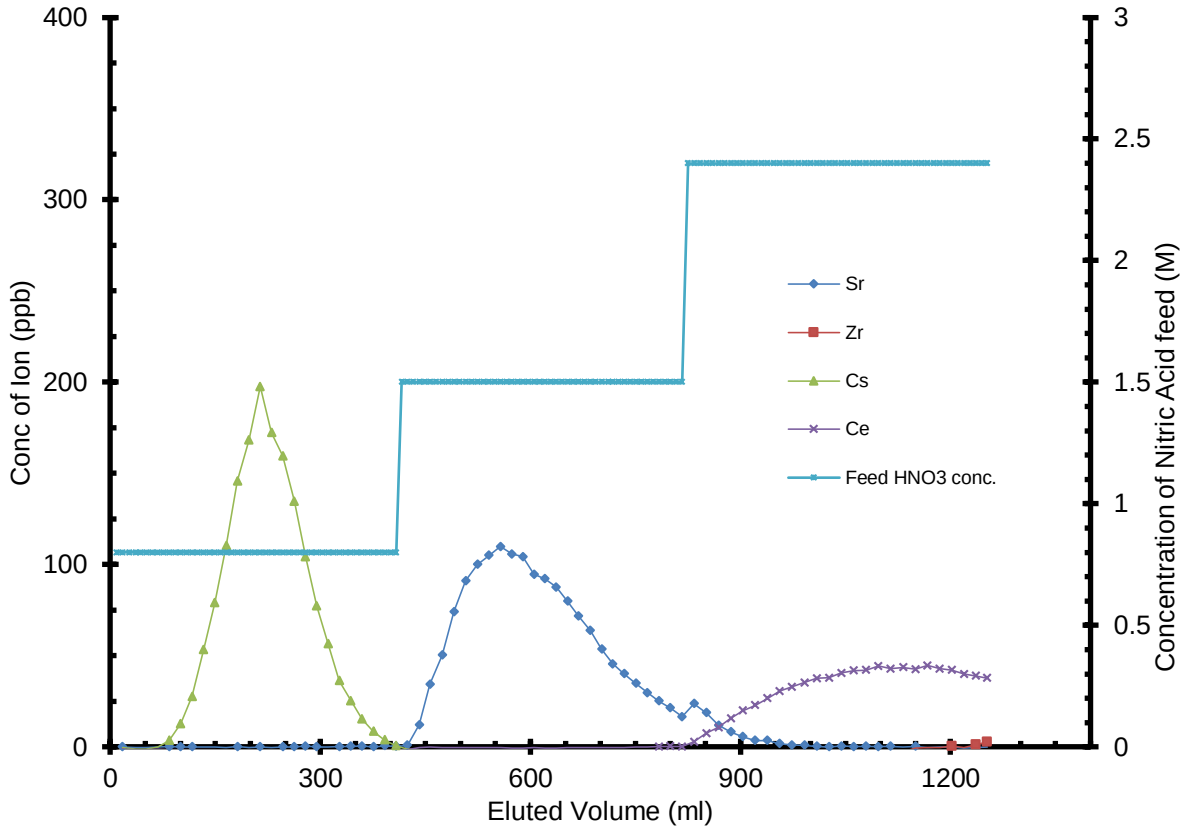

Figure 3.50 Experiment 11: 0.8, 1.5 and 2.4 M HNO_3 Stepped Elution at 4 ml.min^{-1}

3.6.11 Experiment 11: 0.8, 1.5 and 2.4 M HNO_3 Stepped Elution at 4 ml.min^{-1}

This chromatogram was the most positive yet. There was minimal co-elution of the ions, with none observed between the Cs and Sr ions and only minimally between the Sr and Ce as the eluent concentration strength increased. This was again more due to the length of the tail associated with the Sr peak rather than that of the Ce ion being eluted in the 1.5 M HNO_3 concentration step.

The theoretical plate number for this column from the Cs peak was 18.9. This was more akin to that of the previous experiment and the values calculated in Section 3.5. This suggests that the column is working well and in agreement with the figures previously calculated. There was however a slight appearance of the Zr ion towards the end of the chromatogram and this would have to be addressed if it persists in the next experiment.

Therefore the only changes which need to be addressed in order that the three ions are eluted totally separately, was to separate the Sr and Ce ions and observe the appearance of the Zr ion towards the end of the experiment.

In order to separate the Sr and Ce ions, the experiment would again include a gradient section in addition to the steps in the eluent concentration. This should cause a gradual increase in the mobile phase affinity for the Sr ion, causing it to be eluted more readily and in a more timely manner than in the previous experiment and therefore give a separation between the ions. The increase in the eluent strength would also increase the affinity of the Ce to the mobile phase; the gradient elution would therefore stop short of the concentration used in this experiment utilised to elute the Ce ion.

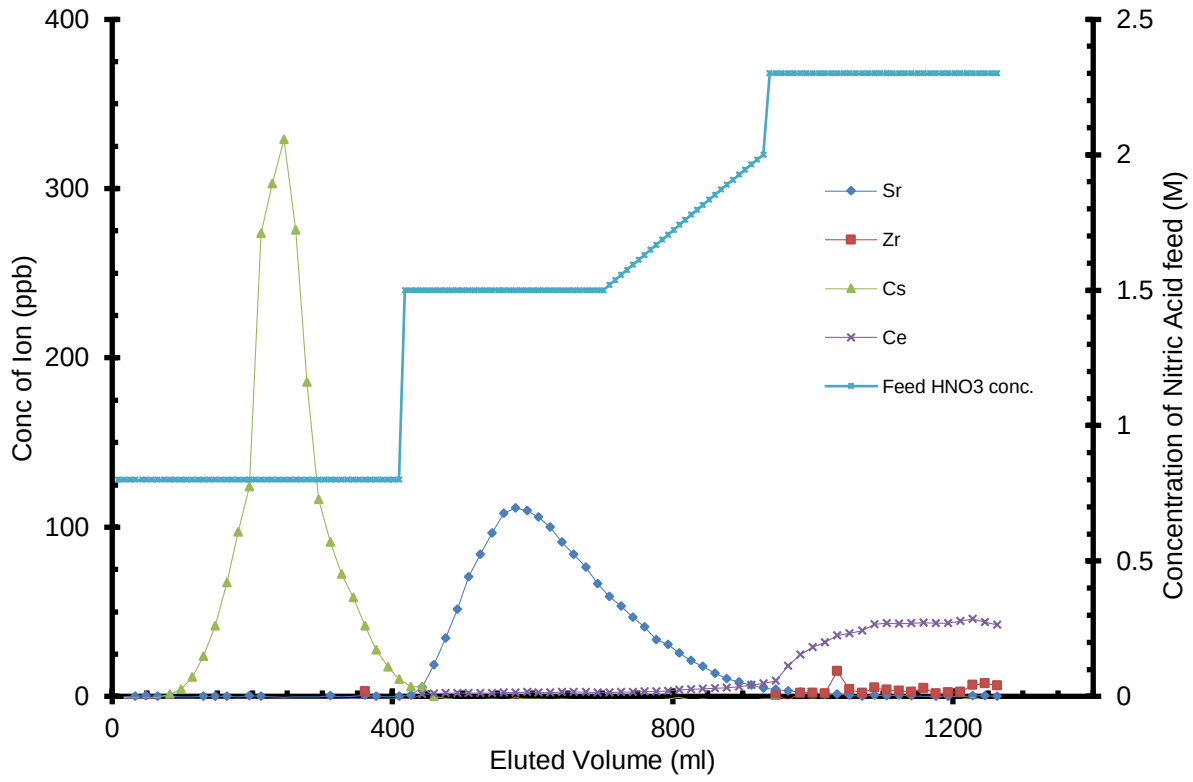

Figure 3.51 Experiment 12: 0.8, 1.5 and 2.3 M HNO_3 Stepped and Gradient Elution at 4 $ml.min^{-1}$

3.6.12 Experiment 12: 0.8, 1.5 and 2.3 M HNO_3 Stepped and Gradient Elution at 4 $ml.min^{-1}$

One of the intentions with this experiment was to define the eluent HNO_3 concentration levels for the elution of Sr and Ce ions, however, this chromatogram exhibits a small amount of co-elution of both Ce within the Sr peak as well as Zr within the Ce peak. This was incredibly frustrating, as it was hoped that this chromatogram would merely be a confirmation of the concentrations used in the previous experiment were sufficient to provide a good separation, but it seems to require further development of the step for separations.

The graduated part of the mobile phase profile seems to have had minimal effect on the elution of Sr or indeed the small volume of the Ce ion co-eluting. The co-elution of the Ce ion in the Sr peak increases at a steady rate from the step up to 1.5 M HNO_3 indicating that this was a chromatographic elution where the ion affinity between stationary and mobile phases at this flow rate are still not quite balanced. However due to the small increase observed in the increase in concentration these are not too far from being balanced. This was also true of the Zr co-eluting within the Ce peak. There was again a gradual increase in the response for Ce as the chromatogram continued, again suggesting that the solvent strength was too high, resulting in the elution of the Ce ion.

The peak shape of the Cs was, broadly speaking, a normal distribution with slight tailing evident. This tailing increases significantly for the Sr ion and the normal peak shape was absent in the Ce response. Despite the flow rate being the swiftest that the mixer/pump could supply, the Ce peak was not resolved back to the baseline and was in fact closer to half way through the peak. As the elution profile would have to be altered either by the reduction of the flow rate or the elution strength, to reduce the co-elution of the ions, this would require a significant increase in the volume and therefore time required for the later elution steps.

With this in mind the next experiment increased to over 8 hours. The mobile phase flow rate was reduced to 3 $ml.min^{-1}$. The reduction in the flow rate has, in previous experiments, reduced the likelihood of co-elution of finely balanced separations and should reduce the possibility of this occurring in this separation. As the flow rate has been reduced and co-elution was not observed in the previous separation at these eluent strengths, the concentration of the mobile phase would remain at the same concentration as performed in Experiment 12. As there is a longer run time it was hoped that the addition of a 5 M eluent section at the end of the chromatogram would be able to elute the Zr, giving a separation of all four ions on the same chromatogram.

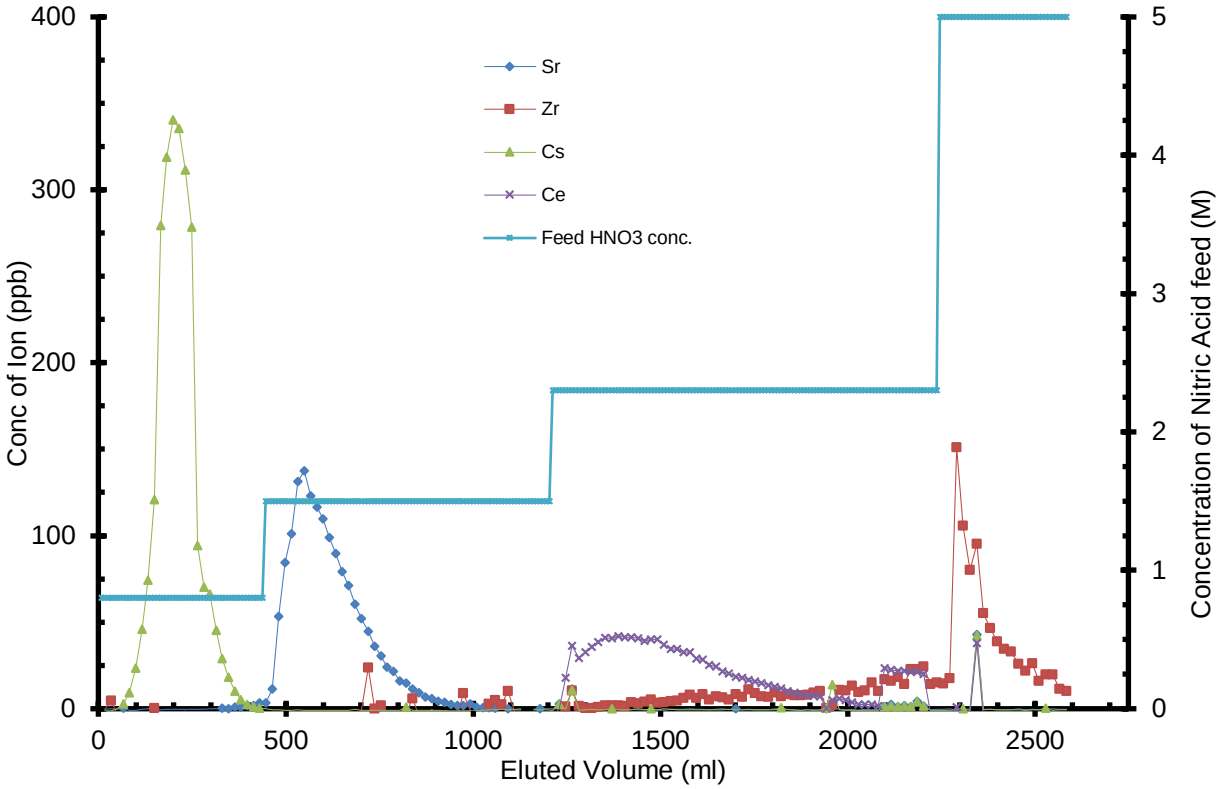

Figure 3.52 Experiment 13: 0.8, 1.5, 2.3 and 5 M HNO_3 Stepped Elution at 3 ml.min^{-1}

3.6.13 Experiment 13: 0.8, 1.5, 2.3 and 5 M HNO_3 Stepped Elution at 3 ml.min^{-1}

The reduction in the flow rate has had the desired effect on the Cs and Sr ions and after 1000 ml the FPs are separated from the Ce and Zr. The Cs exhibits a largely Gaussian shape, as it has throughout the previous experiments; the Sr exhibits a tailing peak but was fully eluted by the end of the 2nd mobile phase concentration step. Although there was separation of the Ce and Zr ions, there was however some bleeding of the Zr ion into the Ce peak; the Zr exhibits a similar peak shape to that of the previous experiment, which steadily increases throughout the 2.4 M step.

A further issue with this chromatogram was the single responses of the Zr ion throughout the Cs and Sr elution steps. This ion should not be eluted at this concentration and these single response “peaks” are considered to be ambiguous and could even be a consequence of some cross contamination.

The large detector response peak shape in the Ce peak was also mirrored in the Zr peak as the eluent strength switches to the 5 M HNO_3 step. This mirroring of the peak shape was further evidence that the mobile phase step change for the Ce ion was too large and could therefore be lowered again.

Therefore the third step was reduced from 2.3 M to 2.1 M in the hope that this would provide the required difference in retention to separate the Ce from the Zr.

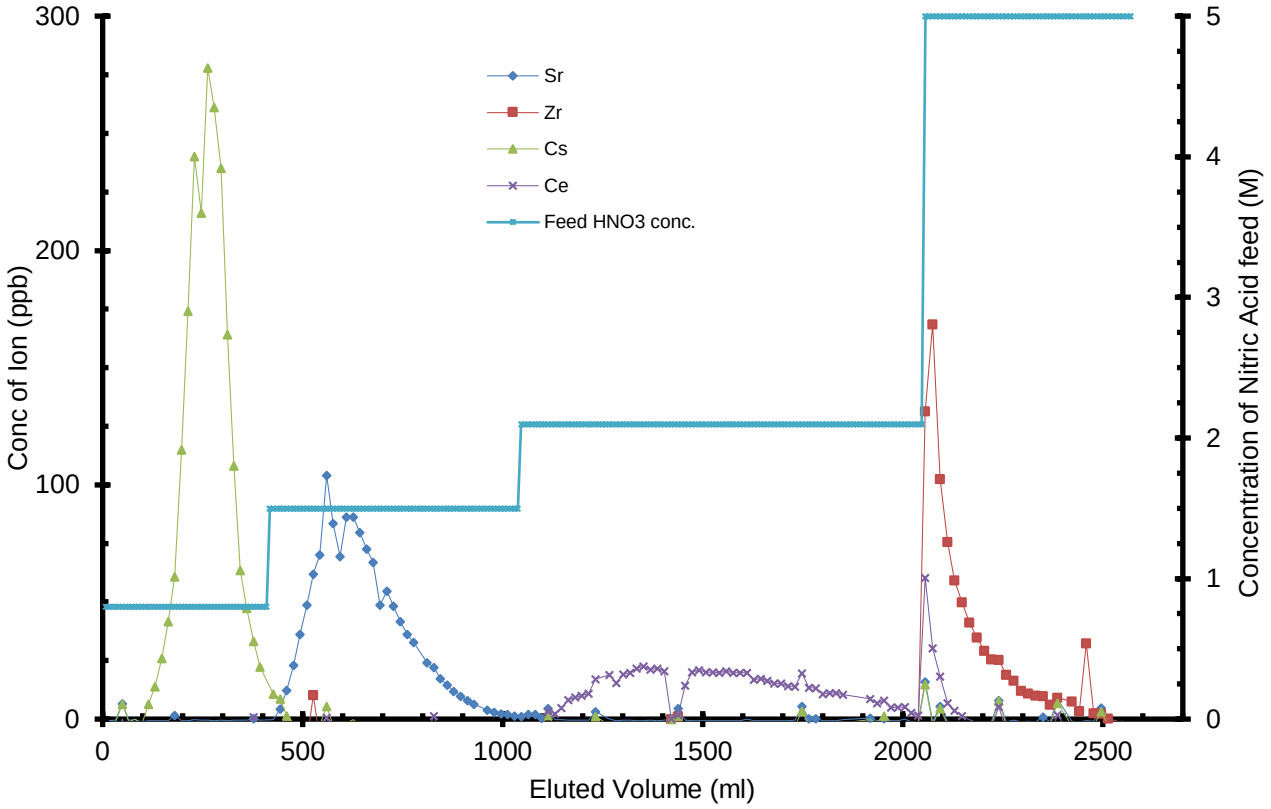

Figure 3.53 Experiment 14: 0.8, 1.5, 2.1 and 5 M HNO_3 Stepped Elution at 3 $ml.min^{-1}$

3.6.14 Experiment 14: 0.8, 1.5, 2.1 and 5 M HNO_3 Stepped Elution at 3 $ml.min^{-1}$

The chromatogram from this experiment has all the attributes required of the separation of the four ions. There was negligible to no co-elution of the ions within the specified volumes at each mobile phase concentration step, although the timing and volumes of these steps may not be sufficient as there was a remainder of the Ce ion still on the column when the mobile phase step changes occurred. There are however some single ion peaks of all four ions throughout the chromatogram. These are generally Cs and Sr ions within the end of the Ce and Zr peaks, which again might imply cross contamination through the reuse of the test tubes.

A possible explanation for the slightly untimely elution of the ions was due to the split peaks observed in each of the first three peaks eluted. The split peak observed over three peaks

was most likely to be due to the initial introduction of the sample to the top of the column. This initial introduction is liable to extend the band width of the peak and therefore caused the ions peaks to be wider than those of previous experiments and caused the co-elution seen at the ends of the Cs and Ce peaks into the Sr and Zr elution steps. Also the initial "breakthrough" of the Cs peak was considerably later than that of the previous experiment, this too could be indicative of the issue of the poor or slow sample introduction to the stationary phase bed with the consequence that the timings and therefore the volumes eluted before each of the elution step changes would not be sufficient in order to elute all of the ion before the step concentration changes and the next (more highly retained) ion was eluted.

The next experiment focused on separating the Cs, Sr and Ce ions in much the same manner as Experiment 10 within the chromatogram elution volume, whilst leaving the Zr on the column to be removed via the cleaning and regeneration of the resin. In order to achieve this, the 2.1 M elution step would be extended by removing the 5 M HNO_3 step, in order to allow all of the Ce to be eluted. The experiment would also be run with an altered concentration of ions. The Ce would be maintained at the 5 $g.l^{-1}$ but the concentration of the Cs, Sr and Zr would be reduced by a factor of 50 to 0.1 $g.l^{-1}$. This was designed to represent the concentrations more closely associated with that of the expected concentrations expected from Table 1.1: with the final experiment running at a dilution factor of 300 from Ce as compared to Cs, Sr and Zr.

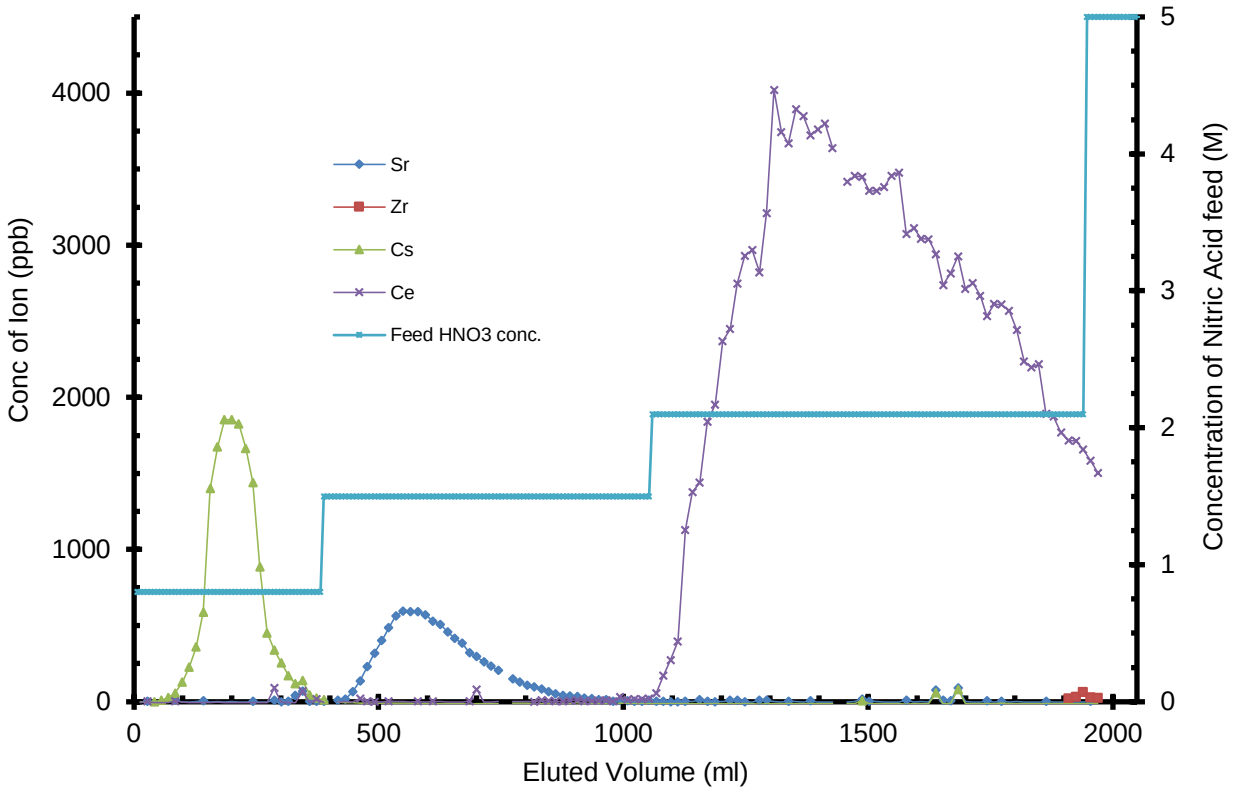

Figure 3.54 Experiment 15: 0.8, 1.5 and 2.1 M HNO_3 Stepped Elution at 3 ml.min^{-1}

3.6.15 Experiment 15: 0.8, 1.5 and 2.1 M HNO_3 Stepped Elution at 3 ml.min^{-1}

The chromatogram from this experiment was the first major divergence from the ICP-MS sampling procedure. In this and the following experiment instead of the 0.1 ml aliquot of the eluent from the base of the column, 1 ml was taken for the assay with the internal standard and dilution volume suitably altered to keep the volume at 10 ml. Although it was somewhat unnecessary for this experiment, it was most definitely useful in the visualisation for the final 300:1 dilution experiment.

To be noted here was that the volume eluted was only approximately 2000 ml. (268 sample tubes, 7 hours 9 minutes) This was lower than that of the subsequent and previous experiments, due to an issue with the mixer/pump not delivering the mobile phase. The experiment was ceased after the pump malfunction but the data up to that point was included in the thesis due to the near completion of the chromatogram and as up to the malfunction the data was still valid.

The Cs and Sr ions are well separated from one another and exhibit a large gap between these FPs and the Ce peak. The Cs peak again exhibits a broadly Gaussian morphology

with the tailing shape of Sr peak reaching the origin before the next step of the elution profile begins.

It has to be acknowledged that there was a certain, albeit small, amount of co-elution of the Ce in the Sr peak, similar to that displayed in the chromatogram in Figure 3.52. At the height of the observed co-elution this cross contamination represents approximate 0.005 % of the Ce peak maximum (19.63 and 4021 ppm). The volume eluted whilst the co-elution was occurring was 234.48 ml, with a concentration of 9.4 ppb. This represents approximately 0.9 % of the mass of the Ce added to the top of the column. However as the mass of the Cs and Sr are to be reduced to 1/300 the concentration of that of the Cerium, it was likely that in the next experiment, the peak and therefore the associated tailing exhibited by the Sr and would be fully eluted at a lower volume than observed in this chromatogram.

The slight co-elution of the Zr with the Ce was also a slight concern, although the single blips of unexpected ions occurring throughout the chromatogram could be explained by poor cleansing between the reuse of test tubes. The grouping of Zr towards the end of the chromatogram is more difficult to explain as erroneous, however, it was likely to be due to the failure of the mixer/pump occurring as it does towards the end of the chromatogram. As the mixer/pump stopped working correctly the acidic concentration of the mobile phase entering the top of the column is likely to have changed.

When the mixer/pump failed the pump stopped pumping the water into the mobile feed which caused air to be introduced into the mixer pump meaning that the 5 M HNO3 was the only mobile phase being introduced onto the top of the column. This might have been a gradual problem with a reducing amount of the water being drawn into the mixing chamber for a time until only 5 M acid was being pumped onto the top of the column. The mixer/pump problem was resolved for the following experiment, which was performed with the same mobile phase profile. With the exception that the concentration of the Ce was 300x larger than the Cs, Sr and Zr ions.

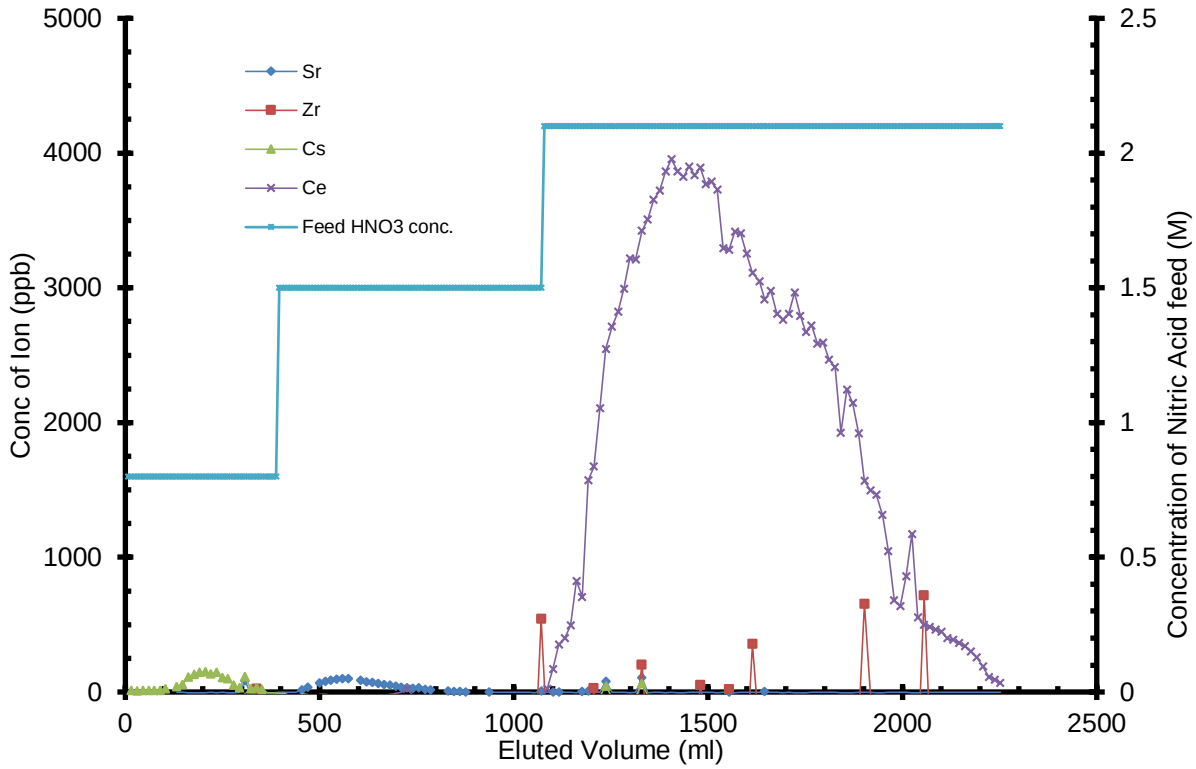

Figure 3.55 Experiment 16; 0.8, 1.5 and 2.1 M HNO_3 Stepped Elution at 3 $ml.min^{-1}$

3.6.16 Experiment 16: 0.8, 1.5 and 2.1 M HNO_3 Stepped Elution at 3 $ml.min^{-1}$

The chromatogram displayed a separation of all four ions, with the Cs, Sr and Ce being eluted and the Zr remaining on the column resin. Although there are single responses for Zr throughout the chromatogram, these are only single fractions and do not fit with an expected shape of an eluting peak and were consider to be erroneous.

Although the Ce peak does not quite return to the baseline, it was almost complete. As this experiment finishes at the 2250 ml point, if it was left to continue the Ce peak would most likely have resolved by 2400 ml. The Zr could then be washed off in a relatively small volume of much stronger acid.

3.6.17 Conclusion of Chromatographic Separation

The C100H gave a separation of the Cs, Sr, Ce and Zr ions in a chromatographic separation utilising an ion exchange mechanism. Although performed in a column, the transfer of this method of separation to that of a CAC would not be as challenging as the development of the separation itself. Indeed a similar separation of two metal ions has previously been achieved by Begovich (3) on a similar resin and a large scale separation able to separate the Cs and Sr from uranium, plutonium and other minor actinides would be beneficial to irradiated fuel reprocessing.

The resin also exhibited a potential use as an isocratic chromatographic separator. However the instrumentation and equipment currently available to the project were insufficient to achieve the necessary length of column and therefore theoretical plates for this.

The issue with these techniques would be the dilution factors of the ions; in the final chromatogram (Figure 3.55) the Ce ion was applied to the column in a 0.5 ml sample. The volume required to elute the entire ion was more than a litre, consequently the dilution factor was over 2000. Although the separation has not been optimised for the reduction of the dilution factor, this was literally and figuratively a massive factor to consider. The Ce ion was the largest dilution factor to consider but even the Cs, which has the lowest factor, has a dilution factor of over 600.

3.7 Acid Stability

The effect of prolonged exposure (1 year) of the resins and adsorbent to 7 M HNO_3 and their ability to adsorb Zr (IV) is contained in Table 3.19. The data indicates that the sulfonic acid resins and amidoxime resins displayed an increase in exchange capacity. The inorganic D5530 displayed a decrease in exchange capacity.

The water content of the as received and acid treated resins and adsorbent, is contained in Table 3.20. Comparison of this shows that the acid treated C100H, C100X10MB and S910 all had significantly more residual water content than the untreated resins. The water content of the acid treated and untreated D5530 are largely the same.

The infra-red spectra of the virgin and untreated materials are shown in Figures 3.56 to 3.59 the main adsorption bands have been tabulated and assigned in Table 3.21

Table 3.19 Zr (IV) Exchange Capacity of Acid Treated and Untreated Resins and Adsorbent

Resin	Repeat	Dry Mass (%)	Wet Resin Capacity ($mg.g^{-1}$)	Average Wet Resin Capacity ($mg.g^{-1}$)	Dry Capacity ($mg.g^{-1}$)
C100H virgin	1		15.729		
(as received)	2	63.23	16.298	16.01	25.33
C100H	1		11.905		
Acid Treated	2	41.97	11.771	11.84	28.21
C100X10MBH virgin	1		14.468		
(as received)	2	68.90	14.182	14.33	20.79
C100X10MBH Acid	1		12.163		
Treated	2	42.82	11.915	12.04	28.12
S910 virgin	1		2.954		
(as received)	2	57.44	3.067	3.01	5.24
S910	1		12.318		
Acid Treated	2	27.04	12.693	12.51	46.25
D5530 virgin	1		4.418		
(as received)	2	62.51	4.343	4.38	7.01
D5530	1		2.124		
Acid Treated	2	60.58	1.575	1.85	3.05

Table 3.20 Water Content of Acid Treated and Untreated Resins and Adsorbent

Resin	Wet Resin Mass (g)	48 Hours Air Dried Mass (g)	120 Hours Oven Dried Mass (g)	Percentage Mass Loss to Air Dry (%)	Percentage Mass Loss Total (%)	Average Moisture Loss (%)
C100H virgin	1.0154	0.8563	0.6424	15.67	36.73	
(as received)	1.0047	0.8472	0.6350	15.68	36.80	36.77
C100H Acid	0.9912	0.5348	0.4128	46.05	58.35	
Treated	1.0645	0.5838	0.4502	45.16	57.71	58.03
C100X10MBH	1.0232	0.8477	0.7047	17.15	31.13	
virgin (as received)	1.0199	0.8446	0.7030	17.19	31.07	31.10
C100X10MBH Acid	1.0017	0.5556	0.4300	44.53	57.07	
Treated	0.9796	0.5410	0.4184	44.77	57.29	57.18
S910 virgin (as	1.0022	0.7186	0.5758	28.30	42.55	
received)	1.0624	0.7602	0.6100	28.45	42.58	42.56
S910	0.9876	0.2951	0.2650	70.12	73.17	
Acid Treated	1.0441	0.3170	0.2845	69.64	72.75	72.96
D5530 virgin	1.0316	0.6918	0.6445	32.94	37.52	
(as received)	1.0009	0.6698	0.6261	33.08	37.45	37.49
D5530 Acid	1.0269	0.6500	0.6225	36.70	39.38	
Treated	1.0638	0.6732	0.6440	36.72	39.46	39.42

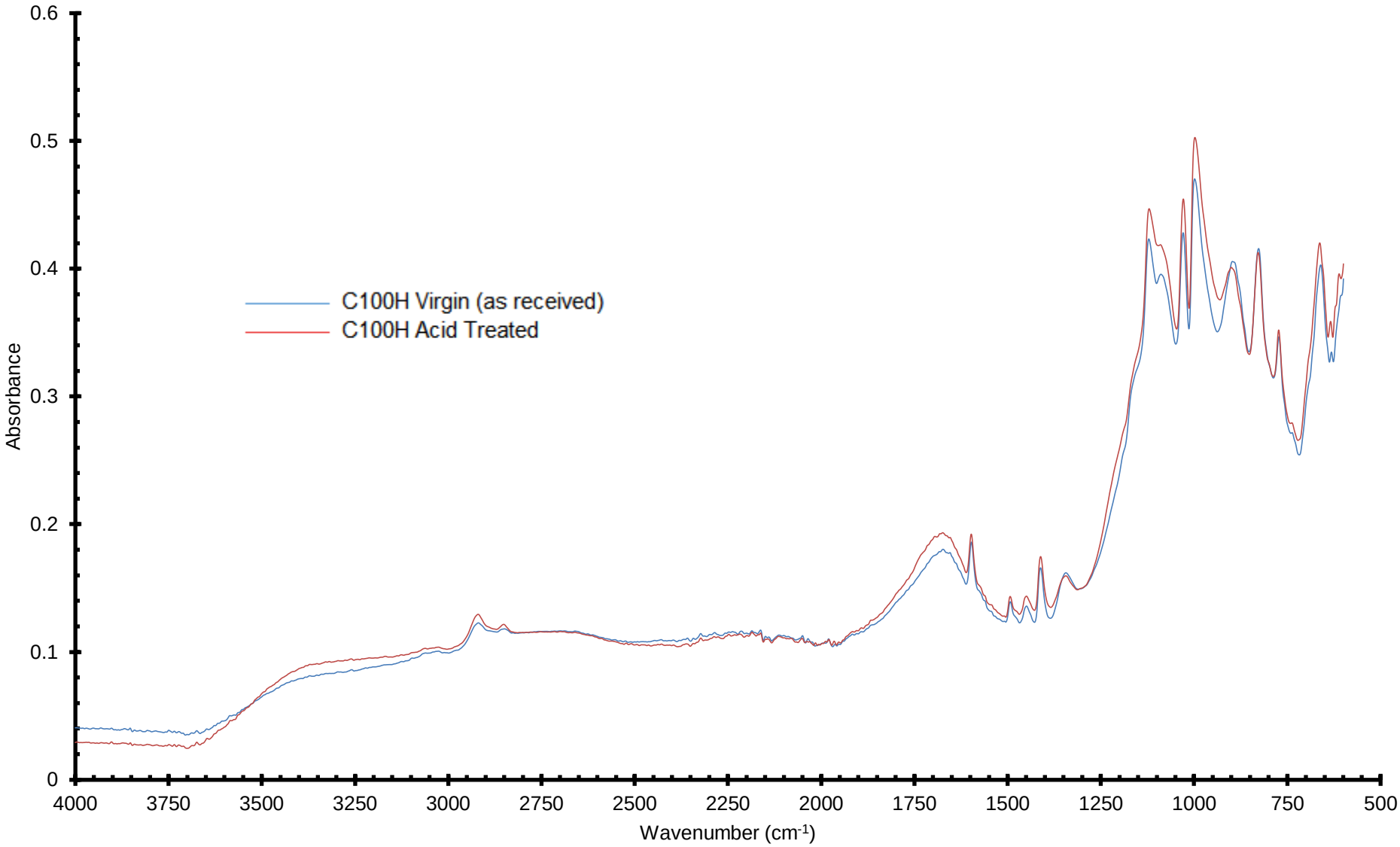

Figure 3.56 Infra-Red Spectra of Acid Treated and Virgin C100H Resins

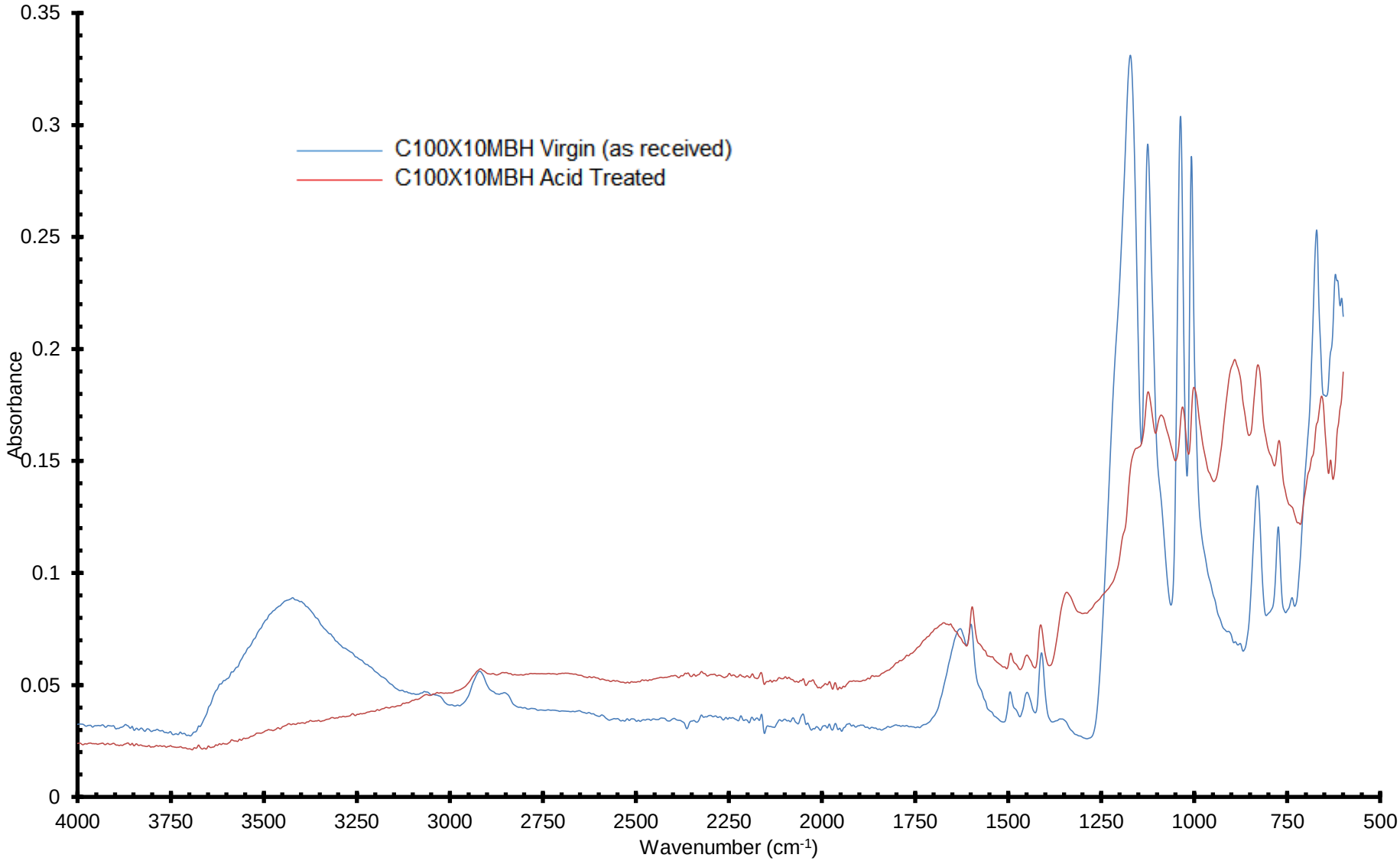

Figure 3.57 Infra-Red Spectra of Acid Treated and Virgin C100X10MBH Resins

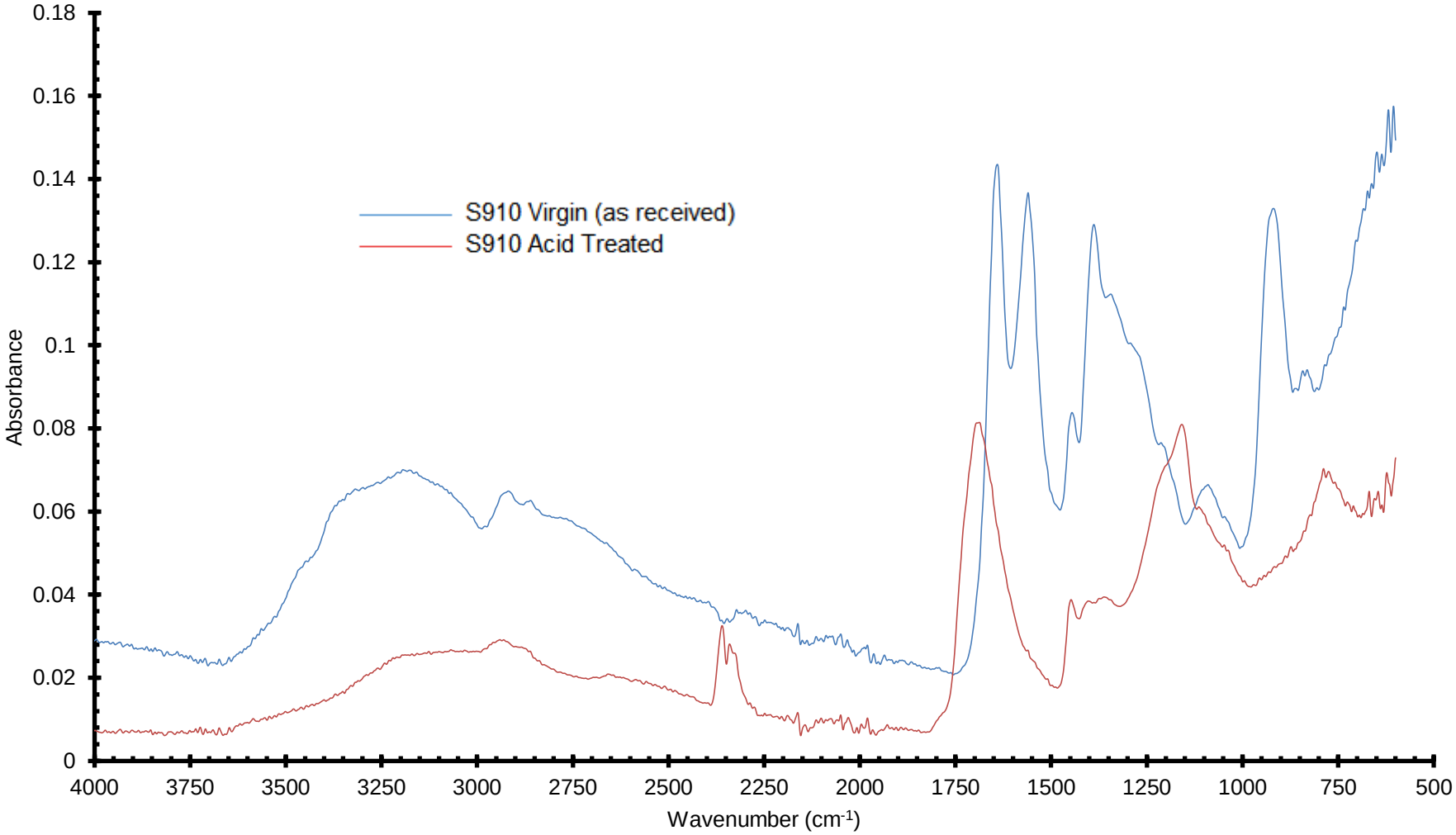

Figure 3.58 Infra-Red Spectra of Acid Treated and Virgin S910 Resins

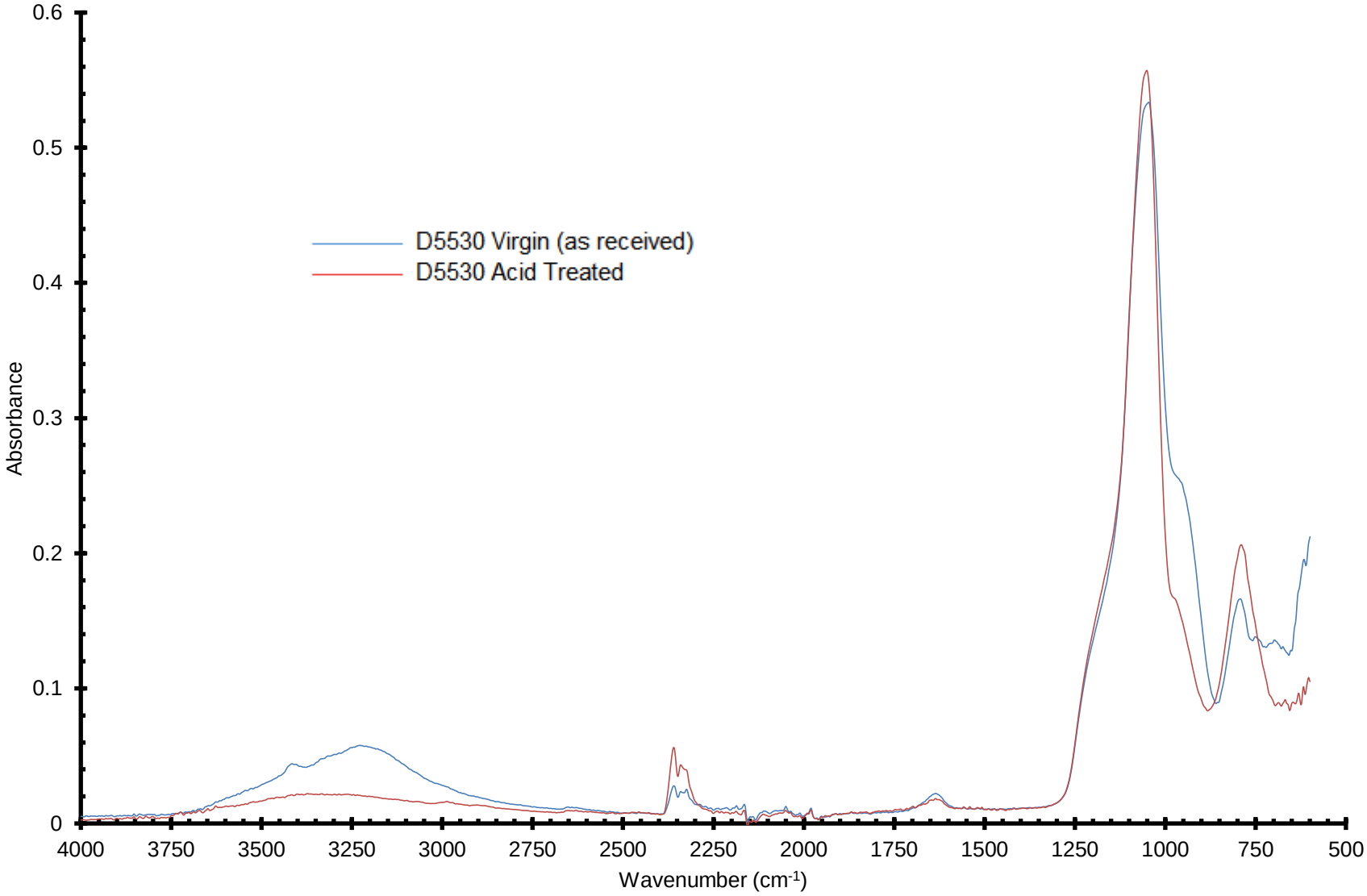

Figure 3.59 Infra-Red Spectra of Acid Treated and Virgin D5530 Adsorbent

Table 3.21 Main Adsorption Bands of Acid Treated and Untreated Resins and Adsorbent.

C100H Untreated	
Wavenumber (cm^{-1})	Assignment
1680	C=O stretch
1600	C=C stretch (aromatic)
1150	S=O stretch sulphonic
1100	acid doublet
1050	S=O stretch sulphonic
1020	acid doublet
C100H Acid Treated	
Wavenumber (cm^{-1})	Assignment
As above	

C100X10MBH Untreated	
Wavenumber (cm^{-1})	Assignment
3450 (broad)	O-H stretch
	C-H stretch (aromatic)
1640	C=C stretch (aromatic)
1600	C=C stretch
1170	S=O stretch sulphonic acid
1120	doublet
1070	S=O stretch sulphonic acid
1025	doublet
C100X10MBH Acid Treated	
Wavenumber (cm^{-1})	Assignment
1700	C=O
1600	C=C (aromatic)

S910 Untreated	
Wavenumber (cm^{-1})	Assignment
3200 (very broad)	N-H stretch O-H stretch C-H stretch (aromatic)
2900	C-H stretch (aliphatic)
1660	C=N oxime
1580	C=C (aromatic)
1390	C-N
950	C=C bend
840	C-H bend 1,4-disubstituted

S910 Acid Treated	
Wavenumber (cm^{-1})	Assignment
3150 (very broad)	O-H stretch
1700	C=O
770	C-H monosubstituted

D5530 Untreated	
Wavenumber (cm^{-1})	Assignment
3200	O-H stretch
1050	Si-O-Si stretch
S910 Acid Treated	
Wavenumber (cm^{-1})	Assignment
1050	Si-O-Si

The untreated sulfonic acid resins show infra-red spectra which are consistent with that expected from a sulfonic acid resin. However, the S=O stretch for the more highly cross-linked C100X10MBH are much more clearly defined than the C100H; although the reason for this is not understood. Acid treatment of these resins however has markedly different results. While both materials show a significant increase in their ion exchange capacity for Zr (IV) and an increase in water retention which could be explained by increased swelling of the structure, providing greater access for the Zr (IV) ion. The infra-red spectra post acid treatment are markedly different; the C100H post treatment is identical to the untreated material. However the C100X10MBH displays a markedly different infra-red spectra post acid treatment to that displayed before; the S=O stretches of the sulfonic acid groups are much more poorly defined, there is a broadening of the peak which is now centred at 1700

cm^{-1} indicating the possible formation of an C=O group. There is also the loss of the O-H stretch at 3450 cm^{-1}. The infra-red spectra of the acid treated C100X10MBH resembles more the infra-red spectra of the C100H, which could be indicative that the acid treatment reduces the amount of cross-linking in the structure of the resin.

The amidoxime resin post acid treatment shows the greatest increase in ion exchange capacity for the Zr (IV) 5.2 to 46.2 $mg.g^{-1}$. The infra-red spectra of the acid treated materials is significantly different from that of the untreated material. In the spectrum of the acid treatment the features consistent with the amidoxime have largely been lost and have been replaced with a C=O stretch at 1700 cm^{-1} and given the shape of the broad band at 3150 cm^{-1} and O-H stretch is present. Therefore, it can be hypothesised that the amidoxime group has been oxidatively cleaved resulting in the formation of a carboxylic acid group. In acid solution the resulting carboxylic acid has a significantly greater ion exchange capacity than the amidoxime; this is perhaps understandable as in acid solution the amidoxime would be protonated which will lessen its ability to chelate the Zr (IV) ion.

The D5530 appears to be a silica based material exhibiting a Si-O-Si stretch at 1050 cm^{-1}. There is relatively little difference between the acid treated and untreated material in terms of the infrared spectra, the only difference being the loss of the O-H stretch at 3200 cm^{-1} presumably due to the dehydration of the surface resulting in the loss of surface O-H group; this may account for the reduction in the ability of the acid treated material to adsorb Zr (IV).

4. Conclusion

The current separation of the components of irradiated nuclear fuels relies on a well-established and understood but we believe a somewhat flawed solvent extraction technique, PUREX. The major flaws of PUREX lie in the point that it is the bulk components of the irradiated fuels which are removed from the contaminants and the degradation of the extractants used for the process. It is believed that a separation which removed the much smaller concentrations of FPs and MAs from the bulk components of U and Pu would be much more efficient in both solvent used and the floor space required.

A number of commercially available resins and adsorbents with differing uptake mechanisms and structures were assessed in their capability as a stationary phase of a continuous chromatographic separation of the dissolved ionic components of an irradiated nuclear fuel in strong nitric acid concentration.

To achieve this, the absorbents and resins were tested with surrogate and isotope ions to those found within an irradiated fuel feed. The thesis reports the separation coefficients between these ions, as well as the ion exchange capacity as a function of both time and of Zr (IV) concentration. The resins and adsorbents were then subjected to evaluation within more dynamic breakthrough studies and for the best performing resin the development of a chromatographic separation. The resins and adsorbents were also subjected to an extended exposure to a high concentration of nitric acid to assess the resistance to oxidative and acidic attack.

Of the four cations of interest, the greatest selectivity co-efficient at 3 M HNO_3 were found for Cs on the D5529 with a selectivity co-efficient of 24.36 against Sr, however the uptake for Cs was < 20 %. The Sr ion was not the most highly retained on any of the media tested and was rarely retained at the 3 M HNO_3 concentration. It did however display a significantly different distribution constant to the other ions on the sulfonic acid resins and most notably on the C100X16MBH resin at both the 1 and 2 M HNO_3 concentrations. Although less well retained than the Zr and Ce (IV) ions, it was significantly more highly retained than the Cs. The Zr (IV) ion was most highly retained ion on the D5530, S910 and all of the sulfonic acid resins, with the largest selectivity co-efficient and distribution constant observed on the S910. However as it was retained too intensely by this media, the C100H and C100X10MBH resins were found to be more useable for the proposed chromatographic separation. The Ce (IV) ion was most highly retained by the S940 and S950 aminophosphonic resins with the largest selectivity co-efficient observed on the S950 of

42.6, this was largely due to the low adsorption observed in the other ions tested. However, the distribution constant of 4.25 observed for the Ce (IV) ion was impressive.

It was generally observed that as the acid concentration of the liquor increased the adsorbance of the ions decreased. This is especially true of the sulfonic acid resins with low ion exchange capability observed above the 3 M HNO_3 level. The inorganic unknown structured media, D5529 and D5530 did not display this reduction ion exchange capacity with relatively stable exchange capacities observed above 1 M HNO_3. The chelating resins displayed the general loss in exchange capacity as the acid concentration of the liquor increased with the S930Plus exhibiting a very similar uptake capacity to that observed in the sulfonic acid resins, however the iminodiacetic (S910) and the phosphonic resins (S940 and S950) displayed a very specific capacity for either Ce (IV) or Zr (IV) which decreased more gradually than observed in the sulfonic acid resins as the liquor concentration increased.

With this column chromatographic separation it is hoped that this could be seen as a proof of concept for the eventual development of a continuous chromatographic separation of irradiated nuclear fuels, be that either continuous annular chromatograph or a simulated moving bed.

From the results discussed within this thesis, there remains the option for the further development of both continuous annular and simulated bed chromatography for consideration as a relevant technique for the separation of the components of irradiated nuclear fuels.

The sulfonic acid resins are capable, in a nitric acid mobile phase, of separating the ions due to their valance and charge density. A chromatographic separation was described of Cs, Sr, Ce and Zr based mainly on the charge density of the ion. The Cs and Sr ions of most interest were satisfactorily separated from one another, as well as the Ce used as a surrogate for the bulk U and Pu. This could be utilised as a separation between FPs and the bulk components of irradiated nuclear fuel.

When evaluating the initial aims of the project, there are somewhat mixed results:

Although not explicitly demonstrated, a chromatographic method which could be applied to the reprocessing of irradiated nuclear fuels has been demonstrated. A similar separation, with a comparable stationary phase has been employed for separating Zr from Hf previously (29) and there is no reason to expect that with the correct apparatus an equivalent separation could be achieved with the method described in this thesis. Further work would require either the development of a robust model for the separation on either the CAC or

SMB instrumentation or the application of the separation described to a continuous chromatographic instrument. Models have been proposed for both CAC and SMB instrumentation and could be applied to the described separation.

Although no direct comparisons have been made between the environmental impact of PUREX and a CC instrument, it is expected that the use of a single solvent (nitric acid) for an eluent would reduce the solvent and energy use of a separation process, not least as the minor contaminants will be extracted from the bulk and not the other way round. Additionally the reduced use of tributyl phosphate (an organophosphate) should also reduce environmental impact. Organophosphates inhibit the function of acetylcholinesterase and have found uses as both insecticides and nerve agents (99) (100). The assessment of the environmental impact will remain difficult until a separation has been performed and optimised on a continuous chromatographic instrument.

The separation of the FPs from the MAs and bulk Ce demonstrated within the thesis could reduce the volume which is required to be sent to a geological disposal facility by the recategorisation of nuclear waste. As the most radioactive isotopes within irradiated nuclear fuels are generally associated with the Sr and Cs fission products, the ability to separate this small volume of the irradiated fuel from the bulk component would aid in both the ability to recategorise and reduce the environment impact of the irradiated fuel. The use of a continuous chromatographic system will also inherently increase the flexibility in operating parameters, so long as the ion concentration is kept below a maximum concentration, the instrument would be able to achieve the required separations.

4.1 Further Work

The work as demonstrated, in particular, that the separation is possible using a chromatographic technique, but there are still some significant challenges to address. Consequently further work is required to address these major challenges, the areas worthy of further investigation are:

- The stationary phase; the materials evaluated were commercial available ion exchange resins and two inorganic adsorbents and were not designed for the application in the area under investigation in this thesis, i.e. nuclear reprocessing. Their selectivity and affinity were compromised by the acid concentrations used in this study. Solid materials that have specific affinity for Cs and/or Sr should be prepared and evaluated, notwithstanding their stability to acid, ease of preparation and other properties addressed in this thesis. Several such materials have been prepared and applied in nuclear waste management but none has

been investigated for the removal of fission products from liquors containing significant quantities of uranium and/or plutonium.

- The selectivity of the commercially available resins evaluated within this thesis were not marketed for either Cs and/or Sr selectivity. Although some demonstrated good affinity for one of these fission products it is unlikely that they could achieve the separation required. Nonetheless these materials are worthy of further evaluation particularly when coupled with continuous chromatography, whether annular or simulating moving bed.
- The elution of the ions, which was not optimised within the thesis, indicate that the elution of radionuclides from commercial resins could be a significant challenge. Optimisation of loading, washing and elution, if necessary, under continuous operation will require significant attention to ensure dilution of feed liquor is minimised.
- The rate of uptake of the appropriate cations by the stationary phase will be important to the dimensions of the chromatographic columns, flow rate and other chromatographic conditions. Uptake rates are normally connected with the resin water regain value and hence stationary phases should be developed that retain water throughout the synthesis process.
- Within the thesis experiments it was decided not to use radio-tracers for a variety of reasons, not least the number of experiments underway at any one time would have imposed a major challenge for the small radio-lab at UCLan. Incorporating radio-tracers could have provided a wealth of addition information such as the diffusion of radionuclides within the resin matrices.
- A demonstration of continuous chromatography with the ions and proposed separation observed in Figure 3.55. It was not possible to demonstrate continuous chromatography due to the lack of appropriate equipment. Appropriate equipment should be acquired to underpin the column studies undertaken in this project. These continuous studies should concentrate on the degree of separation i.e. purity of uranium and/or plutonium, recovery of fission products and dilution factors. To meet these four criteria the effect of rotation period, extract flow rate, feed flow rate, column (section) length, mass transfer units, of a SMB apparatus will require to be evaluated for specific stationary phases.
- Other analytical techniques such as TGA and NMR were not employed due to time and work load constraints. It is appreciated that these techniques would

have provide other additional information that would have shed light on how the simulated radionuclides diffuse into the stationary phase matrix.

- For continuous chromatographic separations, modelling of the dynamic system would be of great value. This modelling could pursue two avenues; the first process would be focused on modelling an SMB instrument and would be used to determine the size and number of columns grounded on the more traditional chromatography modelling equations and the data from the results of experiments more akin to those described in Section 2.3.5. This modelling would also concentrate on modelling fluid flow such as continuous-flow models and diffusion within particles possibly based on the “Monte Carlo” models already employed by the nuclear industry.

  The second part of the modelling would focus on the use of a CAC instrument. This would follow the Brozio and Bart model described in Equation 1.10. The various complicating factors (such as multiple components and axial dispersion) could be introduced once a working model of Equation 1.10 was configured, until the fully modelled separation according to Equation 1.13 was operational and this could then be used to hone the separation by sharpening the elution peaks, reducing the dilution factor and therefore reducing solvent use.

5. References

1. **Marks, A.,** 2014, *Physics of Uranium and Nuclear Energy*, Available at: http://www.world-nuclear.org/info/Nuclear-Fuel-Cycle/Introduction/Physics-of-Nuclear-Energy/, Accessed March 2015.

2. **National Nuclear Laboratory,** 2014**,** *Minor Actinide Transmutation, Position Paper.* Available at: http://www.nnl.co.uk/media/1053/minor_actinide_transmutation_-_position_paper_-_final_for_web1.pdf, Accessed September 2015.

3. **Begovich J. M. and Sisson W. G.,** 1982, *A Rotating Annular Chromatograph for Continuous Metal Separation and Recovery,* Resource and Conservation, Vol. 9. pp 2119-2129.

4. **National Decommissioning Authority,** 2011, *The 2010 UK Radioactive Waste Inventory.* Available at: http://www.nda.gov.uk/wp-content/uploads/sites/2/2014/02/14D037_NDASTSTY140007_-_UKRWI_2011_Summary_of_Data_for_International_Reporting.pdf, Accessed December 2011.

5. **Bond G. and Eccles H.,** 2013, *Continuous Chromatographic Separation of Fission Products and Minor Actinides from Irradiated Nuclear Fuel.* UK Patent Application No 1317553.4.

6. **World Nuclear Authority,** 2012, *The Nuclear Fuel Cycle.* Availbable at: http://www.world-nuclear.org/info/Nuclear-Fuel-Cycle/Introduction/Nuclear-Fuel-Cycle-Overview/. Accessed September 2014.

7. **Draganic I. G., Draganic Z. D. and Adloff J.P.,** 1993 *Radiation and Reactivity on Earth and Beyond.* Boca Raton, CRC Press, pp. 252-254.

8. **World Nuclear Association,** 2015, *Nuclear Basics.* Availabale at: http://world-nuclear.org/Nuclear-Basics/, Acessed August 2015.

9. **Nuclear Energy Institute,** 2006, *Nuclear Waste Disposal for the Future: The Potential of Reprocessing and Recycling.* Available at: http://www.nei.org/corporatesite/media/filefolder/whitepaper_reprocessingandrecycling_0306.pdf**.**, Accessed August 2014.

10. **Bunn M., Fetter S., Holdren J. P. and van der Zwaan R.,** 2003, *The Economics of Reprocessing vs. Direct Disposal of Spent Nuclear Fuel.* Cambridge, Massachusetts : John F. Kennedy School of Government, Available at: http://belfercenter.ksg.harvard.edu/files/repro-report.pdf, Accessed September 2014

11. **Nuclear Decommissioning Authority,** 2012, *An Overview of NDA Higher Activity Waste.* Available at https://www.nda.gov.uk/wp-content/uploads/2012/02/An-overview-of-NDA-higher-activity-waste-February-2012.pdf, Accessed Septemeber 2013.

12. **World Nuclear Accociation,** 2013, *Mixed Oxide Fuels (MOX).* Available at: http://www.world-nuclear.org/info/Nuclear-Fuel-Cycle/Fuel-Recycling/Mixed-Oxide-Fuel-MOX/, Accessed September 2014.

13. **Belgoprocess,** Unknown Publication Date, *Eurochemic,* Available at: http://www.eurochemic.be/eng/index-eng.html, Accessed July 2014.

14. **MacKerron, G.,** 2012, *Evaluation of Nuclear Decommissioning and Waste Management. SPRU University of Sussex for the Department of Energy and Climate Change*. Available at : http://sro.sussex.ac.uk/40037/1/Evaluation_of_nuclear_decommissioning_and_waste_management.pdf, Accessed July 2013.

15. **International Atomic Energy Agency,** 2008, *Spent Fuel Reprocessing Options.* Available at http://www-pub.iaea.org/MTCD/publications/PDF/te_1587_web.pdf, Accessed July 2013.

16. **Koyama S., Suzuki T., and Ozawa M.,** 2010, *From waste to resource, nuclear rare metals as a dream of modern alchemists.* Energy Conservation and Management, Vol. 51. pp 1799-1805.

17. **Stepanov S. I., Boyarintsev A. V., Vazhenkov M. V., Myasoedov B. F., Nazarov E. O., Safiulina A. M., Tananaev I. G., So H. V., Chekmarev A. M. and Yu A.,** 2011*, CARBEX Process, A New Technology of Reprocessing of Spent Nuclear Fuel.* Russian Journal of General Chemistry, Vol. 81, Issue 9, pp 1946-1959.

18. **IAEA Nuclear Energy Series,** 2011, *Impact of High Burnup Uranium Oxide and Mixed Uranium–Plutonium Oxide Water Reactor Fuel on Spent Fuel Management.* Available at: http://www-pub.iaea.org/MTCD/Publications/PDF/Pub1490_web.pdf, Accessed January 2014.

19. **Silverio L. B., and de Queiroz Lamas W.,** 2011, *An analysis of development and research on spent nuclear fuel reprocessing.* Energy Policy. Vol. 39, Issue 1, pp 281-289.

20. **Skoog D. A., Holler F. J. and Crouch S. R.,** 2007, *An Introduction to Chromatographic Separations.* In Principals of Instrument Analysis. 6th Edition, Belmont, Thomson, Brooks, Cole, pp.762-787.

21. **Dong, M. W.,** 2006. *Modern HPLC for Practicing Scientists.* 1st Edition, Hoboken, Wiley, pp. 15-24.

22. **Dizge N., Keskinler B. and Barlas H.,** 2009, *Sorption of Ni (II) ions from aqueous solution by Lewatit cation-exchange resin.* Journal of Hazardous Materials, Vol. 167. Issue 1-3, pp 915-926.

23. **Hilbrig F. and Freitag R.,** 2003, *Continuous Annular Chromatography.* Journal of Chromatography B, Vol. 790, Issue 1-2, pp 1-15.

24. **Juza M., Mazzotti M. and Morbidelli M.,** 2000, *Simulated Moving-Bed Chromatography and its Application to Chirotechnology.* Trends in Biotechnology, Vol. 18, Issue 3, pp 108-118.

25. **Brozio J., and Bart H-J.,** 2004, *A Rigorous Model for Annular Chromatography.* Chemical Engineering Technology, Vol. 27, Issue 9, pp 962-970.

26. **Upson P. C.,** 1983, *Highly active liquid waste management at Sellafield.* Progress in Nucelar Energy, Vol. 13, Issue 1, pp 31-47.

27. **Martin A. J. P.,** *Disscussions of the Faraday Society,* 1949, Royal Society of Chemistry, Vol. 7, p 332.

28. **DeCarli J. P., Carta G. and Byers C. H.,** 1989, *Advanced Techniques for Energy Efficient Industrial-Scale Continuous Chromatography.* Available at: http://web.ornl.gov/info/reports/1989/3445603477100.pdf, Accessed July 2011.

29. **Begovich J. M. and Sisson W. G.,** 1983, *Continuous Ion Exchange Separation of Zirconium and Hafnium using Annular Chromatography.* Hydrometallurgy, Vol. 10, Issue 1, pp 11-20.

30. **Scott C.D., Spence R.D. and Sisson W.G.,** 1976, *Pressurized, Annular Chromatography for Continuous Separations,* Journal of Chromatography, Vol. 126, pp 381-400.

31. **Byers C., Bloomingburg G. F., Bauer J. S. and Carta G.,** 1991, *Continuous Separation of Proteins by Annular Chromatography,* Industrial and Engineer Chemical Research, Vol. 30, Issue 5, pp 1061-1067.

32. **Carta, A. J. and Howard G.,** 1988, *Separation of Sugars by Continuous Annular Chromatography,* Industrial and Engineer Chemistry, Vol. 27, Issue 10, pp 1873-1882.

33. **Dinelli D., Polezzo S. and Taramasso M.,** 1962, *Rotating Unit for Preparative Scale Gas Chromatography.* Journal of Chromatography A, Vol. 7, pp 477-484.

34. **Fox J.B., Calhoun R.C. and Eglinton W.J.,** 1969, *Continuous Chromatography Apparatus: 1 Construction.* Journal of Chromatography, Vol. 43. pp 48-54.

35. **Svensson H., Agrell C.E., Dehlen S.O. and Hagdahl L.,** 1955, *An apparatus for for continuous chromatographic separation.* Science Tools, Vol. 2, pp 17-21.

36. **Nicholas R.A. and Fox J.B.,** 1969, *Continuous Chromatography Apparatus; III Application*, Journal of Chromatography, Vol. 43, pp 61-65.

37. **Canon R. M., Begovich J. M. and Sisson W. G.,** 1980, *Pressurized Continuous Chromatography.* Separation Science Technology, Vol. 15, Issue 3, pp 655-688.

38. **Canon R. M. and Sisson W. G.,** 1978, *Operation of an Improved, Continuous Annular Chromatograph.* s.l. : Journal of Liquid Chromatography & Related Technologies, Vol. 1, Issue 4, pp 427-441.

39. **Cussler, E. L.,** 2003. Chapter 12 Differential Distillations, Chapter in *Diffusion, Mass Transfer in Fluid Systems.* 2nd Edition, Cambridge, Cambridge University Press, pp 353-374.

40. **Thompson, H. S.,** 1850, *On the Absorbent Power of Soil.* Journal of the Royal Agricultural Society of England, Vol. 11, pp 68-74.

41. **Way, J. T.,** 1850, *On the Power of Soils to Adsorb Manure.* Journal of the Royal Agricultural Society of England, Vol. 11, pp 313-379.

42. **Adams B. A. and Holmes E. J.,** 1935, *Journal of the Society of Chemical Industry (London).* Vol. 54, pp 1-6.

43. **Kressman T. R. E. and Kitchener J. A.,** 1949, *Cation Exchange with a Synthetic Phenolsulphonate Resin,* Journal of the Chemical Society, pp 1190-1201.

44. **D'Alelio G. F.,** 1942, *Production of Synthetic Polymeric Compositions comprising sulphonated polymerisates of Polyvinylaryl Compounds and Treatment of Liquid Media Therein.* US Patent 2,366,077.

45. **Bauman W. C. and McKellar R. (Dow Chemical Company),** 1948, *Anion Exchange Resins.* US Patent 2,614,099.

46. **Bodamer G. W. (Rohn and Haas Co),** 1952, *Strongly Basic Anion-Exchange Resins.* US Patent 2,597,440.

47. **Erlenmeyer H. and Dahn H.,** 1939, *Beitrag zur chromatographischen Methode in der anorganischen Chemie.* Helvetica Chimica Acta, Vol. 22, pp 1369-1371.

48. **Skogseid, A.,** 1952, *Preparations of Polymeric Organic Cation Resin Exchangers Containing Imino Groups.* US Patent 2,592,350.

49. **Heller A., Marcus Y. and I. Eliezer.,** 1963, *Poly-(1-hydroxy-4-vinlpyridinium) anion exchangers.* Journal of the Chemical Society, pp 1579-1582.

50. **Kennedy J., Lane E. S. and Robinson B. K.,** 1958, *Synthesis of Metal Complexing Polymers. I. Phosphoylated Polymers.* Journal of Applied Chemistry, Vol. 8, Issue 7, pp 459-464.

51. **Fritz J. S. and Gjerde D. T.,** 2000, *Ion Chromatography,* 3rd Edition, Weinheim, Wiley, pp. 1-26 and 279-349.

52. **Mitsubishi Kasei Corporation,** 1991, *DIAION Manual of Ion Exchange Resins and Synthetic Adsorbent.* 1st Edition, Tokyo, Mitsubishi Kasei Corporation Specialty Polymers Division, pp 1-251.

53. **Horwitz E. P., Dietz M. L., Chiarizia R., Diamond H., Maxwell III S. L. and Nelson M. R.,** 1995, *Separation and Preconcentration of Actinides by Extraction Chrmatography Using a Supported Liquid Anion Exchanger: Application to the Characterization of High Level Nuclear Waste Solutions.* Analytica Chimica Acta, Vol. 310, pp 63-78.

54. **Chiarizia R., Horwitz E. P., Alexandratos S. D. and M. J. Gula.,** 1997, *Diphonix Resin: A Review of its Properties and Applications.* Separation Science and Technology, Vol. 32, Issue 1-4, pp 1-35.

55. **Horwitz E. P., Chiarizia R., Dietz M. L., Diamond H. and D. M. Nelson.,** 1993, *Separation and Pre-concentration of Actinides from Acidic Media by Extraction Chromatography.* Analytica Chimica Acta, Vol. 281, pg 361-372.

56. **T. Hirotsu, S. Katoh , K. Sugasaka , N. Takai , M. Seno and T. Itagaki.,** 1987, *Adsorption of Uranium on Cross-Linked Amidoxime Polymer from Seawater.* Industrial & Engineering Chemistry Research, Vol. 26, Issue 10, pp 1970–1977.

57. **Nogami M., Ishihara T., Suzuki K. and Ikeda Y.,** 2007, *Synthesis and adsorption behavior of monoamide resinswith porous silica support for selective recovery of uranium*

(VI) from nitric acid media. Journal of Radioanalytical and Nuclear Chemistry, Vol. 273, Issue 1, pp 37-41.

58. **Skoog D. A., Holler F. J. and Crouch S. R.,** 2007, Liquid Chromatography. In *Principals of Instrumental Analysis.* 6th Edition, Belmont, Thomson, Brooks, Cole pp 816-851.

59. **Gangwer T. E., Goldstein M. and Pillay K. K. S.,** 1977, *Radiation Effects on the Ion Exchange Materials.* Brookhaven, Oakridge Nation Laboratory, Available at http://www.osti.gov/scitech/servlets/purl/6548668/, Accessed February 2013.

60. **Marsh S. and Pillay K. K. S.,** 1993, *Effects of Ionising Radiation on Modern Ion Exchange Materials.* Los Alamos, Los Alamos National Laboratory, Available at: http://www.iaea.org/inis/collection/nclcollectionstore/_public/25/024/25024729.pdf, Accessed February 2013

61. **Wedemeyer R. E.,** 1953, *The stability of ion exchange resins to x-rays, Ph. D. Thesis.* Vanderbilt University, Nashville, Ph.D Thesis, pp 1-25.

62. **Cathers G. I.,** 1956, *Radiation damage to radiochemical processing reagents.*, Progress in Nuclear Energy Series III Process Chemistry. New York, Pergammon Press, pp 1-15.

63. **Tulupov, P., Butaev. A. M., Greben, V. P. and Kasperovich, A. I.,** 1973, *Effect of content of divinylbenzene in KU-2 cation-exchange resins on its resistance to irradiation in water.* Russian Journal of Physical Chemistry, Vol. 47, Issue 4, pp 975-979.

64. **Crooks III W. J., Kyser III E. A. and Walter S. R.,** 2000. *Qualification of Reillex HPQ Anion Exchange Resin for Use in SRS Processes.* Westinghouse Savannah River Company, Avaliable at http://sti.srs.gov/fulltext/tr9900317/tr9900317.pdf, Accessed February 2013.

65. **Saito H. H., Crooks III W. J., McCabe D. J. and Nash C. A.,** 2001. *SuperLig 644 Ion Exchange Resin Stability in Nitric Acid at Elevated Temperatures.* Westinghouse Savannah River Company, Available at: http://sti.srs.gov/fulltext/tr2000411/tr2000411.pdf, Accessed April 2013.

66. **Lopez C., Deschanels X., Bart J. M., Jollivet P. and Denauwer C.,** 1996, *Structural study of plutonium surrogates in nuclear glasses.* Ceramic Transactions, Vol. 72, pp 399-408.

67. **Warf J.C.,** 1949, *Extraction of Cerium (iv) nitrate by Butyl Phosphate.* Journal of the American Chemical Society, Vol. 71, Issue 9, pp 3257-3258.

68. **Bayulken S. and Sarac A.S.,** 1996, *Distribution of Ce (iv) species in HNO_3-$HCLO_4$ Media and Determination of Stability Constants of the Nitrato Complexes.* Turkish Journal of Chemistry, Vol. 20, pp 111-117.

69. **Uetake N.,** 1989, *Precipitation formation of zirconium-dibutyl phosphate complex in PUREX process.* Journal of Nuclear Science and Technology, Vol. 26, Issue 3, pp 329-338.

70. **Purolite Corporation,** 2014. *Products.* Available at: http://www.purolite.com/products. Accessed September 2014.

71. **Dowex Corporation,** 2014. *Published Literature.* Available at: http://msdssearch.dow.com/PublishedLiteratureDOWCOM/dh_0062/0901b80380062619.pdf?filepath=liquidseps/pdfs/noreg/177-01812.pdf&fromPage=GetDoc. Accessed September 2014.

72. **Valenta M. M., Parker K. E. and Pierce E. M.,** 2010, *Tc-99 Ion Exchange Resin Testing.* Available at: http://www.pnl.gov/main/publications/external/technical_reports/PNNL-19681.pdf. Accessed Septemebr 2014.

73. **Freundlich H. M. F.,** 1906, *Über die Adsorption in Lösungen.* Zeitschrift für Physikalische Chemie, Vol. 57, pp 385-470.

74. **Langmuir I.,** 1917, *The evaporation, condensation and reflection of molecules and the mechanism of adsorption.* Journal of the Franklin Institute, Vol. 183, Issue 1, pp 101–102.

75. **Giles C. H. and Smith D.,** 1974, *A General Treatment and Classification of the Solute Adsorption Isotherm.* Journal of Colloid and Interface Science, Vol. 47, Issue 3, pp 755-765.

76. **Alyüz B. and Veli S.,** 2009, *Kinetics and equilibrium studies for the removal of nickel and zinc from aqueous solutions by ion exchange resins.* Journal of Hazardous Materials, Vol. 167, Issue 1-3, pp 482–488.

77. **Skoog D. A., Holler F. J. and Crouch S. R.,** 2007, *Inductively Coupled Plasma Mass Spectrometry*. In Principles of Instrumental Analysis. 6th Edition, Belmont, Thomson Brooks Cole, pp 291-298.

78. **Skoog D. A., Holler F. J. and Crouch S. R.,** *An Introduction to Infrared Spectrometry.* Principles of Instrumental Analysis. 6th Edition, Belmont, Thomson Brooks Cole, pp 430-451.

79. **Skoog D. A., Holler F. J. and Crouch S. R.,** 2007, Chapter 4, *Selecting and Analytical Method.* In Principles of Instrumental Analysis. 6th Edition, Belmont, Thomson Brooks Cole, pp 17-21.

80. **Miller J. N. and Miller J. C.,** 2005. *Statistics and Chemometrics for Analytical Chemistry.* 5th Edition, Harlow, Pearson Education Limited, pp. 107-146.

81. **Taylor R.J., Dennis I.S. and May I.,** 2001, *Hydroxamic Acids – Novel reagents for Advanced Purex Processes.* Available at: http://www.iaea.org/inis/collection/NCLCollectionStore/_Public/32/034/32034000.pdf, Accessed October 2013.

82. **Lin W., Kung S. and Dai S.,** 2014, *Development of Novel Sorbents for Uranium Extraction from Seawater.* Available at: http://www.iaea.org/inis/collection/NCLCollectionStore/_Public/45/068/45068212.pdf, Accessed March 2013.

83. **May I. Taylor R.J. and Brown G.,** 1998, *'The Formation of Hydrophilic Np(iv) Complexes and their Potential Application in Nuclear Fuel Reprocessing.* Journal of Alloys and Compounds, Vol. 650. pp 271-273.

84. **Vernon F.,** 1982, *Chelating Ion Exchangers – The Synthesis and Uses of Poly(Hydroxamic Acid) Resins.* Pure and Applied Chemistry, Vol. 54, Issue 11, pp 2151-2158.

85. **Mendes F. D. and Martin A. H.,** 2004, *Selective Sorption of Nickel and Cobalt from Sulfate Solutions Using Chelating Resins.* International Journal of Mineral Processing, Vol. 74, pp 359-371.

86. **Barbalace K. L.,** 1995, *Periodic Table of Elements Sorted by Ionic Radius.* Available at: http://environmentalchemistry.com/yogi/periodic/ionicradius.html. Accessed October 2015.

87. **Huheey J. E., Keiter E. A. and Keiter R. L.,** 1993, *Inorganic Chemistry: Principles of Structure and Reactivity.* 4th Edition, New York, Harper Collins, pp 232-236.

88. **Shannon R. D.,** 1976, *Revised Effective Ionic Radii and Systematic Studies of Interatomic Distances in Halides and Chalcogenides.* Acta Crystallographica Section A, Vol. 32, Issue 5, pp 751-767.

89. **McElroy W. D. and Glass B.,** 1951, *Phosphorus Metabolism.* Baltimore, John Hopkins University Press, p 27.

90. **Deepatana A. and Valix M.,** 2006, *Recovery of Co and Ni from Organic Acid Complexes: Adsorption Mechenisims of Metal-Organic Complexes onto Aminophosphate Chelate Resin.* Journal of Hazardous Materials, Vol. 137, Issue 2, pp 925-933.

91. **Serjeant E. P. and Dempsey B.,** 1979, *IUPAC Chemical Data Series No. 23. Ionization Constants of Organic Acids in Solution.* 23rd Edition, Oxford, Pergamon Press, pp 1-138.

92. **Cotton F. A. and Wilkingson G.,** 1980, *Advanced Inorganic Chemistry. A Comprehensive Text.* 4th Edition, New York, John Wiley & Sons Inc., p 878.

93. **O'Neil M. J.,** 2001, *The Merck Index: An Encyclopedia of Chemicals, Drugs and Biologicals.* 12th Edition, New Jersey, Whitehouse Station, pp 10226-10233.

94. **Alvarez S., Ferrer X., Sarmiento C., Fernandez N. and Garcia C.,** 1996, *Analysis of Operational Variables in Ion Exchange Kinetics of Cadmium with Synthetic Resins.* Ciencia, Vol. 4, Issue 2, pp 125-140.

95. **Al-Rashed S. M., and Al-Gaid A. A.,** 2012, *Kinetic and Thermodynamic Studies on the Adsorption Behavior of Rhodamine B dye on Duolite C-20 Resin.* Journal of Saudi Chemistry, Vol. 16, Issue 2, pp 209-215.

96. **Dose E. V., Jacobson S. and Guiochen G.,** 1991, *Determination of Isotherms from Chromatographic Peak Shapes.* Analytical Chemistry, Vol. 63, Issue 8, pp 833-839.

97. **Gelencser A., Kiss G., Krivacsy Z. and Varga-Puchony Z.,** 1995, *A simple method for the determination of capacity factor on solid-phase extraction cartridges.* Journal of Chromatogrpahy A, Vol. 693, Issue 2, pp 217-225.

98. **Liska I., Krupcik J. and Leclercq P. A.,** 1989, *The use of solid sorbents for direct accumulation of organic compounds from water matrices–a review of solid-phase extraction techniques.* Journal of High Resolution Chromatography, Vol. 12, Issue 9, pp 577-636.

99. **Merck Sharp & Dohme Corp.,** 2009, *Organophosphates (Toxicity).* Available at: http://www.merckmanuals.com/vet/toxicology/insecticide_and_acaricide_organic_toxicity/organophosphates_toxicity.html, Accessed March 2015.

100. **Tsung-Ming Shiha J.R. and McDonough J. H.,** 1999, *Organophosphorus Nerve Agents-Induced Seizures and Efficacy of Atropine Sulfate as Anticonvulsant Treatment.* 1, Pharmacology Biochemistry and Behavior, Vol. 64, Issue 1, pp 147-153.